DISSECTING ROLES FOR THE MACROMOLECULAR MACHINERY

INVOLVED IN NEUROTRANSMITTER RELEASE

APPROVED BY SUPERVISORY COMMITTEE

Jose Rizo-Rey, Ph.D., Advisor

Daniel Rosenbaum, Ph.D., Committee Chair

Luke Rice, Ph.D.

Hongtao Yu, Ph.D.

DEDICATION

To my family, friends, and colleagues who all helped to make this work possible

DISSECTING ROLES FOR THE MACROMOLECULAR MACHINERY INVOLVED IN NEUROTRANSMITTER RELEASE

by

ERIC ANDREW PRINSLOW

DISSERTATION

Presented to the Faculty of the Graduate School of Biomedical Sciences

The University of Texas Southwestern Medical Center at Dallas

In Partial Fulfillment of the Requirements

For the Degree of

DOCTOR OF PHILOSOPHY

The University of Texas Southwestern Medical Center at Dallas

Dallas, Texas

May, 2019

DISSECTING ROLES FOR THE MACROMOLECULAR MACHINERY INVOLVED IN NEUROTRANSMITTER RELEASE

PUBLICATION NO. _____

ERIC ANDREW PRINSLOW, Ph.D.

The University of Texas Southwestern Medical Center at Dallas, 2019

Supervising Professor: JOSE RIZO-REY, Ph.D.

Neurotransmitter release is a tightly regulated process that involves synaptic vesicle docking at presynaptic active zones, priming of the vesicles to a release-ready state, and calcium evoked fusion of the vesicle and plasma membranes. The probability of release is modulated by plastic changes that depend on synaptic activity; these changes shape the properties of neural networks and underlie multiple forms of information processing in the brain. Elucidating the mechanisms of neurotransmitter release and its regulation is thus critical for understanding brain function and establishing fundamental principles of neuronal

communication. I have investigated the mechanism by which neurotransmitters send messages between neurons as a specific model system to study the general mechanism of intracellular membrane fusion. In one project, I investigated whether trans-SNARE complexes can be disassembled by NSF-αSNAP. I showed that trans-SNARE complex formation in the presence of NSF-αSNAP requires both Munc18-1 and Munc13-1, and is facilitated by synaptotagmin-1. I proposed a model whereby Munc18-1 and Munc13-1 are critical for mediating vesicle priming as well as precluding de-priming by preventing trans-SNARE complex disassembly. Complexin-1 also impaired de-priming, while synaptotagmin-1 may have assisted in priming and hindered de-priming. Additionally, I used various biophysical approaches including ITC and NMR to shed light into how Complexin has dual roles in fusion. One of my projects investigated the inhibitory role of Complexin and solved a controversy over conflicting ITC data. Another project focused on the Complexin N-terminal and C-terminal domains to try and develop a complete model of how Complexin functions that incorporates all of its known interactions and activating/inhibiting properties. I observed cooperative interactions between Complexin, the SNARE complex, and lipids by forming SNARE complexes anchored on nanodiscs and liposomes. Such cooperative binding of Complexin to membranes and SNAREs may be critical for releasing the inhibition caused by the accessory helix, although the molecular mechanism of action has yet to be determined. Overall, these experiments highlight the importance of interactions between numerous accessory proteins and the trans-SNARE for proper regulation of SNARE complex formation, and therefore fusion.

Acknowledgements

First and foremost, I would like to thank my parents for everything that they have done for me the past 28 years. Your never-ending love and support throughout my entire life has been the backbone to my success both as a person and as a scientist. Thanks for always being there for me every step of the way.

Additionally, I owe endless gratitude to my wife, the now Dr. Elisabeth Geyer. Thank you for being my day to day rock, for always keeping me grounded, and for putting a smile on my face at the end of each and every day. Without a doubt I would not be as sane or happy as I am today without you here by my side throughout this journey. Who'd a thought that our grad school interview at Johns Hopkins University would lead us to where we are today. I guess that is what grad school will do to ya. Also, a very important shout-out to Abigail, my beloved yorkiepoo of three years who is always sure to make me laugh when I get home and walk in the door. Little puppy, you underestimate what relief a simple walk around the block or a quick game of fetch can be from a long day pondering about science.

Obviously much of this work is attributed to my mentor, Jose Rizo-Rey. He and I go back before grad school to my days at Austin College as an undergrad. I worked in his lab as a SURF student the summer before my senior year, and he passed on to me his passion for NMR and biophysics from the very first day. Thank you for all of your tireless effort, for teaching me the reigns of biophysics, and for always encouraging me to think critically.

I would also like to thank the members of the Rizo-Rey lab, past and present, for their camaraderie the past 6 years. Science is a team effort and I am greatly appreciative for all of the guidance everyone provided me as a young scientist. I would like to give a special thanks

to Bradley Quade and Rashmi Voleti, my fellow classmates in the lab. We have gone through a lot together including core course, qualifying exams, WIPS, symposiums, and of course the memorable ICMRBS trip in Kyoto, Japan. I always laugh at the thought of our numerous arguments and debates about a plethora of topics, some scientific and some not. My most infamous memory involves deciding whether it makes sense it dissolve a compound in 22 liters of buffer to make a working stock (20/20 hindsight, the answer is no). I will forever cherish these memories and friendships that will last a lifetime.

Last but not least, I would like to thank my dissertation committee for all of their feedback and guidance throughout the entirety of my time at UT Southwestern as a graduate student. Thank you for all your tips about how to be a better scientist.

Table of contents

Prior publications

- Brewer, K. D., T. Bacaj, A. Cavalli, C. Camilloni, J. D. Swarbrick, J. Liu, A. Zhou, P. Zhou, N. Barlow, J. Xu, A. B. Seven, **E. A. Prinslow**, R. Voleti, D. Haussinger, A. M. Bonvin, D. R. Tomchick, M. Vendruscolo, B. Graham, T. C. Sudhof, and J. Rizo. 2015. "Dynamic binding mode of a Synaptotagmin-1-SNARE complex in solution." Nat Struct Mol Biol 22 (7):555-64. doi: 10.1038/nsmb.3035.

- **Prinslow, E. A.**, C. A. Brautigam, and J. Rizo. 2017. "Reconciling isothermal titration calorimetry analyses of interactions between complexin and truncated SNARE complexes." Elife 6. doi: 10.7554/eLife.30286.

- **Prinslow, E. A.**, Karolina P. Stepien, Yun-Zu Pan, Junjie Xu and Josep Rizo. (Corrections submitted December 2018). "Multiple factors protect neuronal trans-SNARE complexes against disassembly by NSF and αSNAP." Elife.

List of figures

Chapter 1

Chapter 2

Chapter 3

Chapter 4

List of Tables

Chapter 3

List of abbreviations

Å- Angstrom

AAA- ATPases associated with diverse cellular activities

AH- accessory α-helix

ATP- adenosine triphosphate

ATPγS- adenosine 5'-(3-thiotriphosphate)

β-OG- octyl-beta-D-glucopyranoside

B.C.- before Christ

BODIPY- boron-dipyrromethene

C. elegans- *Caenorhabditis elegans*

CD- circular dichroism

CaMb- calmodulin binding sequence

CH- central α-helix

CNS- central nervous system

Cpx- Complexin

CTD- C-terminal domain

Cy- Cyanine

D_2O- deuterium oxide

DAG- diacylglycerol

DOPS- 1,2-dioleoyl-sn-glycero-3-phospho-L-serine

DHPE- 1,2-dihexadecanoyl-sn-Glycero-3-phosphoethanolamine

DKO- double knockout

D. melanogaster- Drosophila melanogaster

DPC- dodecylphosphocholine

DTT- dithiothreitol

E. coli- Escherichia coli

EDTA- ethylenediaminetetraacetic acid

EGTA- ethylene glycol-bis(β-aminoethyl)-N,N,N,N'-tetraacetic acid

EM- electron microscopy

FEI- Field Electron and Ion

FL- full-length

FRET- fluorescence resonance energy transfer

GABA- gamma-aminobutyric acid

Gdn-HCl- guanidinium hydrochloride

GE- General Electric

GST- glutathione S-transferase

GTP- guanosine triphosphate

HEPES- 4-(2-hydroxyethyl)-2-piperazineethanesulfonic acid

His_6- polyhistidine

HOPS- homotypic fusion and protein sorting

HSQC- heteronuclear single quantum coherence

IANBD- (N,N'-Dimethyl-N-(Iodoacetyl)-N'-(7-Nitrobenz-2-Oxa-1,3-Diazol-4 yl)Ethylenediamine

IPTG- Isopropyl β-d-1-thiogalactopyranoside

ITC- isothermal titration calorimetry

k_b- Boltzmann constant

K_D- dissociation constant

KO- knockout

mcc- mini core complex

mccf- mini core complex full

MHz- Megahertz

MSP- membrane scaffold protein

Munc- Mammalian Unc

NaPi- sodium phosphate

NBD- nitrobenzoxadiazole

Ni-NTA- Nickel nitrilotriacetic acid

NSF- N-ethyl maleimide sensitive factor

NMJ- neuromuscular junction

NMR- nuclear magnetic resonance

NT- neurotransmitter

NTD- N-terminal domain

NYV- new yeast V-SNARE

O.D.- optical density

PIP_2- phosphatidylinositol 4,5-bisphosphate

P/L- protein-to-lipid

PBS- phosphate buffered saline

POPC- 1-palmitoyl-2-oleoyl-glycero-3-phosphocholine

POPE- 1-palmitoyl-2-oleoyl-sn-glycero-2-phosphoethanolamine

PSD- postsynaptic density

Q-SNARE- glutamine SNARE

R-SNARE- arginine SNARE

Rab- Ras-associated binding protein

Ras- Rat sarcoma

RIM- Rab Interacting Molecule

RRP- readily-releasable pool

S- Svedberg

Sec- Secretory

SM- Sec1/Munc18-1

SNARE- soluble N-ethyl maleimide sensitive factor attachment protein receptor

SNAP- soluble N-ethyl maleimide sensitive factor attachment protein

SNAP-25 – Synaptosomal-associated protein of 25 kDa

SUMO- small ubiquitin-like modifier

Syb- Synaptobrevin

Syt- Synaptotagmin

Syx- Syntaxin

TCEP- tris(2-carboxyethyl)phosphine

TEV- tobacco etch virus

TM- transmembrane

TMR- tetramethylrhodamine

T-SNARE- target SNARE

Tris- tris(hydroxymethyl)aminomethane

Unc- Uncoordinated

UV-vis- Ultraviolet-visible

V-SNARE- vesicle SNARE

VAM- vacuolar morphogenesis

VAMP- vesicle-associated membrane protein

VPS- vacuolar protein sorting

wt- wild-type

Chapter 1- General introduction

1.1 Neuronal signal transduction

Brief history

The human brain is the most complex organ in the entire body and performs many vital functions that are essential for life. Even the great ancient philosopher Hippocrates appreciated the significance of the brain back in the fourth century B.C stating, "Men ought to know that from nothing else but the brain comes joys, delights, laughter and sports, and sorrows, griefs, despondency, and lamentations. In these ways I am of the opinion that the brain exercises the greatest power in the man." Although much is known about how the brain works in the modern era, it took centuries worth of research and discoveries to understand all that we know about the brain today.

The history of how the brain works dates back to the end of the eighteenth century with Luigi Galvani's discovery of animal electricity. He observed muscle contractions in frog legs using a metal hook simultaneously attached to a frog and an iron railing (Galvani 1791). His rival, Alessandro Volta, later realized that the source of the animal electricity in Galvani's experiments was from the interaction of two different metals, one in the hook and the other in the railing, not from the animal itself (Volta 1792). This contraction of the leg following electrical stimulation is regarded as the first experiment demonstrating communication in the brain, known as synaptic transmission.

More than 70 years later, Willy Kühne and Wilhelm Krause presented some of the earliest descriptions of structures in the brain called neuromuscular junctions, showing distinct separation between nerve endings and muscle fibers (Kuhne 1862, Wilhelm 1863).

They suggested that communication between nerve and muscle is an electrical process, an idea that was later validated by Emil du Bois-Reymond, the father of electrophysiology.

Santiago Ramón y Cajal was able to study the morphology of individual brain cells, called neurons, by applying a silver chromate solution developed by Camillo Golgi in 1873 to brain tissue. By staining only a small subset of cells in the brain, Cajal noted the distinct features of all the different components of neurons. His documentation of the numerous different components found in the brain led to the conclusion that neurons are not continuous and must communicate by contact (Cajal 1937). This neuron doctrine, originally coined by Waldeyer in 1891, states that neurons are developmentally, structurally, functionally, and pathologically discrete entities (Waldeyer-Hartz 1891). Physiologist Charles Sherrington then conceived the term synapse in 1897 to define the site at which neurons make a functional contact with another cell (Sherrington 1897). At the same time Sherrington was studying synapses, John Newport Langley provided the first definitive evidence that neuronal signal transduction occurred by chemical means through studies with autonomic ganglia (Langley 1905). Although this is a mere brief history of the earliest works on neuronal signal transduction, it lays the crucial groundwork that defines modern neuroanatomy.

Neuroanatomy

Neurons are specialized cells in the brain that relay information through electrical and chemical signals. There are over 100 billion neurons in the brain, each forming more than 500 connections, creating a vast convoluted network of 10^{14}-10^{15} intercellular junctions (Sudhof 2004). They consist of three main parts: the stoma, the axon, and dendrites (Figure

1.1). The stoma, or cell body, is the spherical central part of the neuron that contains numerous organelles needed for cell function, such as the nucleus, endoplasmic reticulum, Golgi apparatus, and mitochondria. Extending outward from the stoma is a projection called the axon, which acts as a telegraph wire to send information over large distances. The specific site where a presynaptic axon comes into contact with another neuron is called the synapse. Postsynaptic neurons receive information through structures called dendrites, which function as antennae to collect the signal released from the presynaptic axon into the synaptic cleft, the space between the presynaptic axon and postsynaptic dendrite. Neurons communicate with one another through chemical signals called neurotransmitters that are packaged into small membrane compartments called synaptic vesicles.

Synaptic vesicle composition

Synaptic vesicles are about 40 nm in diameter and encapsulate a chemical signal called neurotransmitter used to communicate with the postsynaptic neuron (Sudhof 2004). Synaptic vesicles store nonpeptide neurotransmitters such as acetylcholine, glutamate, GABA, and glycine (Jahn et al. 1990). They were first discovered in 1955 by Sanford Palay and George Palade (Palay et al. 1955), and linked to chemical transmission in 1962 by Bernard Katz (Katz 1962). Due to their small size, they contain a limited number of lipid and protein molecules. Each vesicle contains about 10,000 phospholipid molecules (Jahn et al. 1993) and 600 transmembrane domains (Takamori et al. 2006). Over 400 different proteins were found to be associated with synaptic vesicles, 80 of which are integral membrane proteins (Takamori et al. 2006). These proteins include both transport proteins,

used for uptake of neurotransmitters, and trafficking proteins, which will be discussed in detail in section 1.3. Most importantly, they can rapidly be recycled and refilled without synthesizing new proteins, a critical time saving process since the distance from nerve terminals to the cell body can be quite far. The process by which synaptic vesicles repeatedly release and reload their contents is referred to as the synaptic vesicle cycle.

The synaptic vesicle cycle

The active zone is a small area within the presynaptic plasma membrane in a synapse and is the site where neurotransmitter release occurs. Simply put, the basic feature of a synapse is a close separation of the plasma membranes from two neurons. The distance between two neurons in contact with one another is typically 20-50 nm wide (Bear et al. 2001), and the space between them is referred to as the synaptic cleft. The presynaptic side contains clusters of neurotransmitter filled synaptic vesicles, while the post synaptic side contains numerous neurotransmitter receptors. Although there is an abundance of synaptic vesicles outside the active zone (200-500) in a common reserve pool, only a small number (5-10) are found attached to the active zone at a synapse (Peters et al. 1991).

The trafficking of synaptic vesicles in the nerve terminal can be summarized in 10 stages described below (Figure 1.2). Synaptic vesicles must first be filled with neurotransmitters, a process that requires ATP through the use of a proton pump that creates an electrochemical gradient across the synaptic vesicle membrane by acidifying the interior of the vesicle. This gradient allows transport proteins to load the synaptic vesicles with neurotransmitters. Once filled, the synaptic vesicles move toward the active zone via

diffusion with the help of recruitment proteins. The vesicles must then be physically linked to the plasma membrane through a step known as tethering. After tethering, the synaptic vesicles go through a priming/docking process that requires many proteins, leaving the synaptic vesicles in a meta-stable or release-ready state. Upon the advent of an action potential, calcium enters the presynaptic cell and rapidly stimulates fusion in less than 0.1 ms (Sabatini et al. 1999). This type of fusion event is known as synchronous-evoked release. Other types of fusion include asynchronous-evoked release, which involves vesicle fusion that outlasts the action potential by one second or more, and spontaneous release, which involves vesicle fusion that is independent of an action potential and is proportional to intracellular calcium levels (Kavalali 2015). I will mainly focus on the regulation of synchronous-evoked release for the majority of this discussion.

Subsequently, synaptic vesicles are recycled through endocytosis involving clathrin coated pits. Coated vesicles bud from the plasma membrane, release their clathrin coats, reacidify, and either refill immediately or travel to the endosome to be sorted and cleaned up before reentering the synaptic vesicle cycle. This entire process takes a mere 60 seconds from start to finish, with the vast majority of time required for neurotransmitter uptake and recycling. Despite the specifics of synaptic vesicle exocytosis that make it incredibly fast, this trafficking process shares the same fundamental properties and mechanisms as all other intracellular fusion events.

1.2 Membrane fusion

A key feature of neurotransmitter release is that it involves fusion of the membrane of synaptic vesicles with the presynaptic plasma membrane, a process that is tightly controlled by calcium. However, membrane fusion is not unique to this system. It is a general process that all cells use to communicate and deliver molecules. Other examples of membrane fusion events include organelle inheritance during mitosis (Chen et al. 2001), delivery of cargo proteins and lipids from one compartment to another (Rothman 1994), viral fusion (Peng et al. 2010), and extracellular fusion of cells (Primakoff et al. 2007). Fusion in viruses is accomplished by single proteins that mediate the entire process, while protein complexes are required for intracellular fusion events. Variations on the latter share common features, such as the use of Rab GTPases, tethering complexes, AAA ATPases, SM proteins, and SNAREs, but are catalyzed by different homologs that are usually specific to a certain type of fusion event (Gerst 2003).

Membrane fusion is a universal process that varies vastly in the space time continuum. For yeast vacuoles, the area of membrane contact is 10,000 times larger than that of synaptic vesicles (Jahn et al. 2003). Consequently, the time of fusion, minutes for vacuoles and milliseconds for synaptic vesicles, is 10,000 times longer. Regardless of the type of membrane fusion event at hand, both theoretical and experimental studies have indicated that all membrane fusion events proceed through a stalk intermediate (Cohen et al. 2004a).

According to the stalk hypothesis, a specific order of events ultimately leads to membrane fusion: membrane contact, membrane merging, and opening of an aqueous fusion

pore (Chernomordik et al. 2008) (Figure 1.3). This model is supported by X-ray diffraction data that shows the stalk intermediate in numerous different lipid environments (Aeffner et al. 2012). Fusion between two membrane bilayers does not happen simply by membrane contact because opposing electrostatic forces need to be overcome before two proximal leaflets can interact (Dennison et al. 2006). These forces can be surpassed by small molecules or proteins that perturb the boundary between the hydrophilic water and the hydrophobic lipids. Using only pulling forces, it would be expected that membranes could only be brought into close proximity without fusion (Figure 1.3B). However, a combination of both pulling and pushing forces would be expected to apply the force much more efficiently to the membrane (Figure 1.3A). Additionally, membrane bending may also be caused by proteins that insert into the bilayer and induce curvature. The numerous protein machinery described in section 1.3 is responsible for applying these forces to efficiently disrupt and fuse membranes.

1.3 Regulation of synaptic vesicle exocytosis

Overview

Synaptic vesicle exocytosis is more tightly regulated and more localized than any other known membrane fusion event. Calcium triggered fusion occurs faster than most enzymatic reactions, suggesting that calcium only completes the fusion reaction of a pre-formed and primed macromolecular assembly. The focus on this chapter will be on a small number of proteins that have been demonstrated to be critical for formation and regulation of this macromolecular assembly, from the earliest stages of attachment of a synaptic vesicle to

the active zone, to formation of the primed complex itself, to the ultimate step of recognizing calcium and triggering fusion. These regulatory elements are essential to both trigger and inhibit fusion since synaptic vesicle exocytosis is reliably unreliable. As mentioned earlier, 5-10 vesicles can be found docked to the active zone at one time. However, only a single synaptic vesicle fuses for every 5-10 calcium signals. This perhaps strange mechanism is surprisingly advantageous because it provides the synapse lots of room for regulation and modulation of vast synaptic networks. There are more than 1000 different proteins that operate in the presynaptic nerve terminal, and over 100 of them are hypothesized to play a role in synaptic vesicle exocytosis (Sudhof 2004). The rest of this section will take a look at the critical components that constitute the core presynaptic fusion machinery.

SNARE proteins

The soluble N-ethyl maleimide sensitive factor attachment protein receptors (SNAREs) are characterized by sequences of 65 residues called SNARE motifs that have a high propensity to form coiled coils (Jahn et al. 2006). The neuronal SNARE proteins that moderate neurotransmitter release are Syntaxin-1, Synaptosomal-associated protein of 25 kDa (SNAP-25), and Synaptobrevin-2 (also called VAMP-2 or vesicle-associated membrane protein). Syntaxin-1 and Synaptobrevin each contain a single SNARE motif followed by a transmembrane (TM) helix and are found anchored to the plasma and vesicle membrane, respectively (Figure 1.4A,B). Syntaxin-1 also contains an N-terminal three-helix bundle called the H_{abc} domain (Fernandez et al. 1998), as well as a small N-terminal sequence known as the N-peptide (Khvotchev et al. 2007). I will discuss in more detail in a later

section the importance of how the H_{abc} domain binds to its own SNARE motif to form a closed conformation that inhibits SNARE complex formation. SNAP-25 contains two SNARE motifs and is attached to the plasma membrane through palmitoylation of 4 cysteine residues. Together, these 4 SNARE motifs from 3 different SNARE proteins form a four-helix bundle known as the SNARE complex that is critical for membrane fusion (Figure 1.4C) (Sollner et al. 1993a, Poirier et al. 1998, Sutton et al. 1998). Alternative notation for the SNARE proteins include referring to Synaptobrevin as a v-SNARE due to its localization on the synaptic vesicle and Syntaxin-1/SNAP-25 as t-SNAREs since they are found on the target plasma membrane (Sollner et al. 1993b). They can also be referred to as Q-SNAREs (Syntaxin and SNAP-25) and R-SNAREs (Synaptobrevin) since the conserved polar layer in the middle of the SNARE complex is formed by three glutamines and one arginine residue (Fasshauer et al. 1998).

The SNARE complex is a leucine-zipper like structure (Sutton et al. 1998) that folds into a helical bundle from the N-terminus to the C-terminus (Figure 1.4C). Numerous studies have shown that the SNARE complex zippers in a stepwise like fashion (Figure 1.4D), and that the overall energy from SNARE complex formation, ranging from 30 k_bT from experiments using atomic force microscopy to 68 k_bT from experiments using optical tweezers, could be sufficient to induce membrane fusion (Gao et al. 2012, Li et al. 2007, Liu et al. 2009). Energetically speaking, 40-100 k_bT has been theorized to induce membrane fusion (Cohen et al. 2004b), so technically one or two SNARE complexes may be sufficient to cause fusion. However, it is still not well understood how the SNARE complex applies these forces to the membrane, since most of this energy is used to form the helical bundle.

Depending on the experimental conditions, the SNAREs alone may be sufficient to induce fusion (Figure 1.4E), or they may simply bring the two membranes into close proximity without fusion (Figure 1.4F). As mentioned earlier in section 1.2, pulling forces alone cannot induce fusion, so additional components of the release machinery may be absolutely necessary to help apply these forces more efficiently to membranes by utilizing pushing forces that generate a torque to bend and further destabilize the membranes. This suggests that other accessory or regulatory proteins may have a direct role in fusion.

One could argue that the SNARE proteins are fundamentally the most important proteins required for membrane fusion events. This is because they can tether vesicles together and bring two opposing membranes into close proximity (Hanson et al. 1997) through formation of a trans-SNARE complex between two membranes that is capable of inducing membrane fusion, or at least lipid mixing, without any other proteins (Weber et al. 1998, Weber et al. 2000). Although the timescale of this event is nowhere near biologically relevant, the simple fact that the SNARE proteins alone can induce membrane fusion suggests that the role of other essential proteins, discussed below, is to regulate formation of the SNARE complex and to lower the energy barrier for fusion so that membrane fusion can occur on a much faster timescale. This elegant mechanism allows the cell to precisely control when and where membrane fusion occurs through regulation of the number of SNARE complexes that are primed and ready for fast evoked release to match the ever changing needs of the cell. Section 1.4 will describe a model that illustrates the interplay between the SNAREs and other key components of the release machinery that I will now outline.

NSF and SNAPs

Although the SNARE proteins are now considered to be at the forefront of membrane fusion, they were not originally hypothesized to be at the center of neurotransmitter release. That award actually goes to the enzyme N-ethyl maleimide sensitive factor (NSF), originally discovered in 1988 by James Rothman (Malhotra et al. 1988) and found to associate with soluble NSF attachment proteins (SNAPs) and the SNAREs one year later (Weidman et al. 1989).

The traditional role of NSF and SNAP proteins are to disassemble fully zippered cis SNARE complexes that reside on the plasma membrane after fusion to recycle the protein machinery for subsequent rounds of neurotransmitter release (Sollner et al. 1993a, Mayer et al. 1996, Banerjee et al. 1996, Hayashi et al. 1995). This process requires ATP hydrolysis by NSF, a member of the ATPases associated with diverse cellular activities (AAA) family of proteins. NSF contains an N-terminal domain and two nucleotide binding domains (called D1 and D2) (Figure 1.5A,B,C). The N-terminal domain binds to SNAPs, which in turn bind to the SNARE complex and serve as adaptors. Collectively, NSF, SNAP, and the neuronal SNARE complex form a macromolecular complex called the 20S complex; a structure of this amazing supercomplex was solved in 2015 by the laboratories of Axel Brunger and Yifan Cheng (Zhao et al. 2015).

In the cryo-EM structure of the 20S complex, the D1 and D2 domains of NSF assemble into hexamers, while 4 SNAP molecules are observed simultaneously binding to the SNARE four-helix bundle and the N-domains of NSF (Figure 1.5C,D,E,F). This structure shows how the hexameric symmetry of NSF transitions to the four-fold symmetry

of the SNARE complex. Interestingly, it reveals that the twist of the SNAP molecules is opposite to that of the SNARE complex, suggesting that the SNARE complex is disassembled by an unwinding mechanism through ATP hydrolysis and structural changes in NSF.

The interaction between αSNAP, which is ubiquitously expressed and used in this study, and the SNARE complex is primarily electrostatic through positively charged residues on αSNAP and negatively charged residues on the surface on the SNARE complex. Additionally, it is important to point out that αSNAP also contains an N-terminal hydrophobic loop that is expected to interact with membrane. This loop causes a dramatic increase in the rate of disassembly of membrane-anchored cis-SNARE complexes compared to soluble SNARE complexes (Winter et al. 2009). In the 20S structure, this hydrophobic loop is close to the C-terminus of the SNARE complex (Figure 1.5E).

The roles of NSF-αSNAP have been well studied in yeast vacuolar fusion. One important conclusion to mention is that NSF-αSNAP (Sec18 and Sec17 respectively in yeast) can disassemble trans-SNARE complexes (Xu et al. 2010), which prevents fusion induced by the SNAREs alone. However, strong synergy between Sec18, Sec17, and the HOPS tethering complex was surprisingly shown to stimulate fusion and overcome the innate disassembly of trans-SNARE complexes (Mima et al. 2008). This synergy arises from the fact that NSF-αSNAP can also disassemble off pathway t-SNARE complexes (Ungermann et al. 1998, Hayashi et al. 1995). Syntaxin-1 and SNAP-25 can form a three-helix bundle that is assumed to serve as an acceptor complex for Synaptobrevin even though well-formed three-helix complexes have been challenging to form and poorly studied. However, SNARE

motifs tend to prefer formation of four-helix bundles, resulting in in the formation of both 1:1 t-SNARE complexes and 2:1 t-SNARE complexes where the fourth helix is filled by a second Syntaxin molecule (Xiao et al. 2001). The latter is considered an off pathway complex that acts as a kinetic trap by hindering ternary complex formation because of incorrect stoichiometry (Rizo et al. 2012b). It is well established in the field that NSF-αSNAP break apart these different types of Syntaxin-1 SNARE complexes (Hayashi et al. 1995), requiring the system to begin SNARE complex formation from a better regulated started point. Additionally, it remains to be determined whether or not NSF and αSNAP can actively participate in membrane fusion by themselves.

In stark contrast to the disassembly of trans-SNARE complexes observed in yeast vacuolar fusion, some experiments suggest that that NSF-αSNAP cannot disassemble neuronal trans-SNARE complexes (Weber et al. 2000). In chapter 2, I will challenge this finding and show that they do in fact also disassemble neuronal trans-SNARE complexes (Yavuz et al. 2018), and that the other protein machinery is absolutely critical to protect primed SNARE complexes from disassembly before fusion.

Munc18-1

One critical component of the release machinery is Munc18-1, a member of the Sec1/Munc18-1 (SM) family of proteins. SM proteins have been shown to be essential for many types of intracellular membrane trafficking events, as evident by the complete elimination of neurotransmitter release in Munc18-1 knockout mice (Verhage et al. 2000). As eluded to earlier, this dramatic effect is because of numerous interactions between

Munc18-1 and neuronal SNAREs, especially Syntaxin-1 (Hata et al. 1993). Mun18-1 binds very tightly to Syntaxin-1 in a closed conformation (Dulubova et al. 1999), a four-helix bundle formed between the three helices from the H_{abc} domain (Fernandez et al. 1998) and a single helix from the SNARE motif of Syntaxin-1. A crystal structure showed that Munc18-1 is arch shaped with a cavity containing closed Syntaxin-1 (Figure 1.6A) (Misura et al. 2000). Extensive contacts are observed between both the H_{abc} domain and the N-peptide with Munc18-1. Although Munc18-1 is also suggested to interact with four-helix SNARE complex (Dulubova et al. 2007), it remains unclear at the moment exactly how this interaction occurs.

The previous interaction between Munc18-1 and Syntaxin-1 requires Syntaxin-1 to be in a closed conformation. However, Syntaxin-1 can also exist in an open state (Dulubova et al. 1999); the transition between these two states requires the MUN domain of Munc13-1, which will be discussed in a later section (Ma et al. 2011). More recently, two seminal crystal structures were solved showing the yeast SM protein Vps33 bound to the Syntaxin-1 homolog Vam3 and the Synaptobrevin homolog Nyv1 (Baker et al. 2015). An overlay of these two structures shows that both SNARE motifs are in close proximity and in register, suggesting a templating role for Munc18-1 in SNARE complex formation (Figure 1.6B). This idea is further supported by the fact that the location of the Syntaxin-1 SNARE motif in the closed formation bound to Munc18-1 is similar to that in the open state, highlighting the importance of both states of Syntaxin-1. The open state allows for SNARE complex formation and suggests that the role of the Syntaxin-1 N-peptide is to act as a pivot point to prevent the release of Munc18-1 when Syntaxin-1 undergoes a conformation change from a

closed to an open state (Dulubova et al. 1999). Since the Syntaxin involved in yeast vacuolar fusion does not contain an N-peptide, nor does it adopt a closed conformation (Dulubova et al. 2001), it is thought that this interaction between Munc18-1 and closed Syntaxin-1 is a novel aspect of neuronal membrane fusion that provides a highly regulated starting point by initially inhibiting SNARE complex formation (Burkhardt et al. 2008).

Altogether, the data described above argue against the t-SNARE complex serving as the beginning state for neuronal membrane fusion. Instead, a more highly regulated system initiates from an inhibited conformation with closed Syntaxin-1 bound to Munc18-1. This starting point is highly advantageous because Syntaxin-1/SNAP-25 complexes are heterogeneous in nature and are unlikely to exist in the cell in large quantities because they are disassembled by NSF-αSNAP (Ma et al. 2013, Hayashi et al. 1995). With this in mind, Munc18-1 and therefore Munc13-1 become essential components for neuronal exocytosis because they orchestrate SNARE complex assembly in an NSF-αSNAP resistant manner. Additionally, both Munc18-1 and Munc13-1 prevent the formation of antiparallel SNARE complexes, which improves the fidelity of SNARE complex assembly (Lai et al. 2017). Current data shows that SNAP-25 cannot bind to a tripartite complex between Munc18-1, Syntaxin-1, and Synaptobrevin, and it remains to be solved the order in which the SNARE proteins are templated by Munc18-1. Possibly the most urgent question to address is whether or not Munc18-1 and Munc13-1 remain bound to the SNARE complex after assembly. The latest evidence suggests that this binding could prevent disassembly of trans-SNARE complexes by NSF-αSNAP, which suggests that Munc18-1 and Munc13-1 may have additional, direct roles in membrane fusion. Although this proposal still requires validation,

it remains clear that the roles of Munc18-1 and Munc13-1 are related and essential for proper formation of the primed state of synaptic vesicles.

Munc13-1

As described in the previous section, a crucial role for SM proteins, like Munc18-1, and tethering proteins, like Munc13-1, is to orchestrate SNARE complex assembly in cellular conditions that favor SNARE complex disassembly. Munc13s are large, 200 kDa proteins that are found localized to presynaptic active zones and are essential for tethering, docking/priming, and fusion. They have low homology to an array of tethering complexes, suggesting that these proteins may provide a physical attachment between synaptic vesicles and the plasma membrane (Pei et al. 2009). Similar to the Munc18-1 knockout mouse, a double knockout of Munc13-1 and -2 also results in a total loss of evoked release (Varoqueaux et al. 2002). Munc13-1 is frequently referenced as the master regulator of release because of its numerous roles in regulating fusion through its multidomain architecture (Figure 1.7A).

The largest domain of Munc13-1, the MUN domain, has been shown to expedite the transition from the closed Syntaxin-1/Munc18-1 complex, to an open state where Syntaxin-1 is bound to Munc18-1 and can template SNARE complex formation (Ma et al. 2011). This finding actually correlates with an LE Syntaxin mutant that was found to rescue release in *C. elegans unc13* nulls by helping to destabilize the closed conformation and causing it to open (Dulubova et al. 1999, Richmond et al. 2001). The closed conformation of Syntaxin-1 thus acts as an energy barrier that prevents against SNARE complex formation until the MUN

domain is able to stimulate opening of this inhibited state, making Munc13-1 critical for neuronal membrane fusion.

Besides its MUN domain, Munc13-1 has a handful of other domains that are essential for its function. The C_2A domain is located at the very N-terminus of Mun13-1 and servers as a hub for protein-protein interactions. It can form a homodimer that inhibits neurotransmitter release (Lu et al. 2006, Deng et al. 2011) (Figure 1.7F), as well as a heterodimer with the zinc finger domain of αRIMS (Betz et al. 2001, Dulubova et al. 2005) (Figure 1.7G), which are large Rab3 effector proteins that are important for both the docking and priming stages of membrane fusion by bringing Munc13-1 to the active zone (Schoch et al. 2002, Koushika et al. 2001). Located between the C_2A and C_1 domains is a linker region spanning over 300 residues that contains a calmodulin binding sequence (CaMb) (Figure 1.7E). Deletion of this linker region (151-520) has mild effects on release, while deletion of the entire N-terminal region of Munc13-1 (1-520) causes a 50% decrease in evoked release. However, deletion of only the C_2A domain (1-150) causes a severe impairment of release (Camacho et al. 2017). It is hypothesized that this linker region inhibits release by preventing the MUN domain from interacting with the SNAREs, and that this inhibition could be relieved from either calmodulin binding to the CaMb sequence or binding events involving the C_2A domain. However, much of this is speculative and remains to be determined.

The C_1 domain of Munc13-1 is responsible for binding to DAG-phorbol esters (Rhee et al. 2002, Basu et al. 2007), which increases the fusion competency of synaptic vesicles at high concentrations of DAG (Figure 1.7B). DAG, or diacylglycerol, is a second messenger

signaling lipid that is the result of hydrolysis of the phospholipid phosphatidylinositol 4,5-bisphosphate (PIP_2). Immediately adjacent to C_1 is the C_2B domain, which binds to both calcium (Ca^{2+}) and PIP_2 (Shin et al. 2010) (Figure 1.7C). To date, the largest structure obtained of Munc13-1 involves a fragment spanning the C_1, C_2B, and MUN domains known as C_1C_2BMUN (Xu et al. 2017). This structure revealed that the DAG-binding interface of the C_1 domain and the Ca^{2+}-PIP_2-binding interface of the C_2B domain are near each other in three-dimensional space and face the same direction (Figure 1.7D), suggesting a binding mode to the plasma membrane that is dependent on DAG, Ca^{2+}, and PIP_2. However, these two domains also form a polybasic region that is capable of interacting with the plasma membrane in a different binding mode without DAG, Ca^{2+}, and PIP_2. Additionally, the C_2C domain of Munc13-1 is known to bind membranes in a Ca^{2+} independent manner, and that the $C_1C_2BMUNC_2C$ fragment is capable of bridging Synaptobrevin containing liposomes with Syntaxin-1/SNAP-25 liposomes containing DAG and PIP_2 (Liu et al. 2016).

All of this information on Munc13-1 has led to a model that involves two membrane bridging modes (Figure 1.8). In the first state, the polybasic region of C_1 and C_2B binds to the plasma membrane, while the C_2C domain binds to the synaptic vesicle. This state is expected to allow for the formation of the primed, meta-stable state of the release machinery while simultaneously inhibiting fusion because of the large distance between the synaptic vesicle and the plasma membrane. The second binding mode promotes fusion and is favored in the presence of DAG, Ca^{2+}, and PIP_2 because of a decreased distance between the two membranes due to a tilt that allows for binding of the C_1/C_2B interface, which could potentially stimulate SNARE complex formation. This model is supported by the fact that

Ca^{2+} is required for fusion *in vitro* when Munc18-1, the Munc13-1 $C_1C_2BMUNC_2C$ fragment, and NSF-αSNAP are included in the reaction (Liu et al. 2016). Additionally, deletion of only the C_1 or the C_2B domain causes an enhancement in evoked release, while deletion of both domains leads to a severe impairment of evoked release (Michelassi et al. 2017). Although the previous two sections have established the critical importance for both Munc18-1 and Munc13-1 in promoting efficient neurotransmitter release, additional proteins with specialized roles, such as Synaptotagmin-1 and Complexin-1, are also important for proper regulation of membrane fusion.

Synaptotagmin-1

Synaptotagmins are regulatory proteins that are important calcium sensors for the three different types of neurotransmitter release mentioned earlier in section 1.1. A knockout of only Synaptotagmin-1 (Syt1) has a severe impairment in synchronous release and a simultaneous increase in asynchronous release (Geppert et al. 1994). A subsequent knockdown of Synaptotagmin-7 (Syt7) in the background of the Syt1 knockout has a severe reduction in both synchronous and asynchronous release (Bacaj et al. 2013). This evidence suggests that Syt1 is the primary sensor for synchronous release, while Syt7 is the primary sensor for asynchronous release (Sudhof 2013). Although many works have suggested an interplay between the two types of release, including a recent study that focused on the importance of membrane affinity in determining the role of Synaptotagmin in neuronal membrane fusion (Voleti et al. 2017), the remainder of this section will concentrate on the role of Syt1 in fast evoked release as a direct result of an action potential.

Like the v-SNARE Synaptobrevin, Syt1 is also found anchored to the synaptic vesicle by a single trans-membrane helix, followed by two C_2 domains that compose the cytoplasmic region (Sudhof 2002) (Figure 1.9A). These two C_2 domains have traditional β-sandwich structures with three and two Ca^{2+} ions bound, respectively, through coordination with aspartate residues located in loops at the top (Sutton et al. 1995, Shao et al. 1998, Fernandez et al. 2001) (Figure 1.9B). Although calcium binding does not promote any substantial conformational changes of either C_2 domain, it does significantly change the electrostatic potential of the calcium binding region (Fernandez et al. 2001, Shao et al. 1997, Ubach et al. 1998). This change in electrostatic potential allows these loops to bind negatively charged phospholipid membranes in a calcium dependent manner via hydrophobic and basic residues that surround calcium binding site (Chapman et al. 1998, Zhang et al. 1998). Mutations that perturb the calcium binding affinity of Syt1 for membranes correlate with simultaneous changes in neurotransmitter release (Fernandez-Chacon et al. 2001, Rhee et al. 2005), and additional experiments have shown that the C_2B domain is the predominant player in Syt1 (Shin et al. 2009), while the C_2A domain is the predominant player in Syt7 (Bacaj et al. 2013). Although these results must be taken with a grain of salt since dominant negative effects were observed with C_2B mutants (Wu et al. 2017), they promote a model for Syt1 that involves membrane bridging and SNARE complex binding.

The Syt1 C_2B domain also contains two arginine residues on the bottom (R398 and R399) that allow it to simultaneously bridge the synaptic vesicle and plasma membranes within 4 nm of each other (Arac et al. 2006, Xue et al. 2008a, Seven et al. 2013) (Figure 1.9B). One current model proposes that Syt1 inhibits fusion in the absence of calcium

because of repulsion between membranes due to the negatively charged calcium binding loops (Figure 1.9C, left panel), and that this hindrance is relieved upon calcium binding that allows for membrane bridging (Figure 1.9C, center) and fusion (Figure 1.9C, right panel). Syt1 may even directly participate in fusion by actively lowering the energy barrier needed to fuse membranes by facilitating membrane curvature (Arac et al. 2006, Martens et al. 2007). Numerous reconstitution experiments support this bridging model (Kyoung et al. 2011, Mahal et al. 2002, Tucker et al. 2004, Lee et al. 2010, Xue et al. 2008a), but what remains unclear at the moment is how Syt1 and the SNARE complex cooperate in membrane fusion.

Various groups have demonstrated interactions between Syt1 and the individual SNAREs, t-SNARE complexes, and even the ternary SNARE complex (Rizo et al. 2015, Chapman 2008). One possible reason for the plethora of these interactions may lie in the promiscuity of these highly charged proteins. Syt1 C_2B also contains a polybasic region on its side that has been shown to interact with both PIP_2 (Bai et al. 2004, Li et al. 2006), a negatively charged phospholipid, and the SNARE complex, which is highly negatively charged on the surface. Most of these studies have reported interactions in the absence of membranes, which may hinder the ability to rationalize all of the established *in vitro* interactions. The most inclusive model to date incorporates information from three different Syt1-SNARE complex structures (Brewer et al. 2015, Zhou et al. 2015, Zhou et al. 2017) (Figure 1.9C), but even this is unable to explain how Syt1 is able to induce membrane fusion. In order to wrap our heads around these perplexing results, we must also investigate the interplay between Synaptotagmins, SNAREs, membranes, and Complexins.

Complexin-1

The final regulatory protein that I will introduce are Complexins, which are small soluble proteins that are mostly unstructured in solution (Pabst et al. 2000), but bind tightly to SNARE complexes by forming helical elements (McMahon et al. 1995, Chen et al. 2002). Numerous studies analyzing knockouts or knockdowns of the major Complexin isoforms, either Complexin-1 (Cpx1) and Complexin-2 (Cpx2), or Cpx1, Cpx2, and Complexin-3 (Cpx3), clearly show a severe impairment in evoked neurotransmitter release (Reim et al. 2001, Xue et al. 2008b, Maximov et al. 2009). The effects on spontaneous release are variable and likely depend on compensatory effects from Cpx3 (Yang et al. 2013). A decrease in vesicle priming is also observed from studies using sucrose-induced release (Xue et al. 2010b, Yang et al. 2010). Although not as drastic as the results from Munc18-1 or Munc13-1/Muinc13-2 knockouts mentioned earlier, which suggest that Cpx1 is not essential for docking and priming, they do propose a role for Cpx1 in stabilizing the primed state. I will discuss my results about a novel role for Cpx1 that protects trans-SNARE complexes from being de-primed in Chapter 2.

Cpx1 has been shown to have dual roles in neurotransmitter release, with numerous studies reporting both inhibitory and activating functions. Outside of the activating role described above, an inhibitory role for Cpx1 was introduced based on both physiological and reconstitutions experiments that showed an interplay with Syt1 (Tang et al. 2006, Giraudo et al. 2006, Schaub et al. 2006) (see below). Additionally, an increase in spontaneous release was shown in both *D. melanogaster* and *C. elegans* in the absence of Cpx1, further supporting the inhibitory role for Cpx1 (Huntwork et al. 2007, Martin et al. 2011, Hobson et

al. 2011). Although challenging to comprehend, these apparently contradictory roles are actually not that surprising for a protein whose regulatory function is a finely tuned balance between activating and inhibiting abilities that seems to vary in different organisms.

Cpx1 contains 4 domains (Figure 1.10A). At the center of the protein is a central α-helix (CH) that inserts in an antiparallel orientation into the groove between Syntaxin-1 and Synaptobrevin on the SNARE complex (Chen et al. 2002) (Figure 1.10B). This central helix is essential for all aspects of Cpx1 function (Xue et al. 2007), likely because it stabilizes the SNARE complex and positions the other domains of Cpx1 in an optimal location for proper function. Preceding the central helix is an accessory α-helix (AH) that contributes toward the inhibiting function of Cpx1 (see below), although this helix was not shown to contact the SNAREs (Chen et al. 2002). The N-terminus contains an N-terminal helix (NTD) that has been shown to play an activating role in fusion likely through interactions with membranes and the SNARE complex (Xue et al. 2010b, Lai et al. 2016, Zdanowicz et al. 2017). Lastly, the C-terminus also contains a C-terminal helix (CTD) that is important for membrane binding to the synaptic vesicle (Seiler et al. 2009, Snead et al. 2014, Gong et al. 2016), which has been suggested to play an inhibitory role (Wragg et al. 2013). I will discuss my recent work on Cpx1 in Chapters 2, 3, and 4.

Multiple different models have been proposed to explain how Cpx1 inhibits fusion, the two most prominent being the electrostatic/steric hindrance model (Trimbuch et al. 2014) (Figure 1.10D), and the insertion model (Figure 1.10C) (Giraudo et al. 2009, Xue et al. 2007, Kummel et al. 2011), which I will discuss in detail in Chapter 3. The insertion model requires the accessory helix to insert into the C-terminus of partially zippered SNARE

complexes, and many biophysical experiments claim to support this model (Krishnakumar et al. 2011, Li et al. 2011, Krishnakumar et al. 2015), although NMR data has provided very strong evidence against this proposal (Trimbuch et al. 2014). Alternatively, replacing the accessory helix with an engineered helical element still allowed Cpx1 to inhibit spontaneous release in *C. elegans*, strongly supporting the electrostatic/steric hindrance model (Radoff et al. 2014), which advocates that inhibition results from steric clashes between the accessory helix and the membrane near the site of fusion (Figure 1.10D).

This idea is supported by recent structural studies involving Syt1 and the SNARE complex, which was discussed in the previous section (Brewer et al. 2015, Zhou et al. 2017) (Figure 1.9D). Syt1 is hypothesized to release this inhibition based on earlier works showing that a soluble fragment of Syt1 containing both C_2 domains, referred to as C_2AB, is able to displace a fragment of Cpx1 containing only the central and accessory helices from SNARE complexes attached to membranes (Dai et al. 2007, Tang et al. 2006). Interestingly, C_2AB could not displace full-length Cpx1, likely due to additional interactions with the SNAREs and membranes (Xu et al. 2013). All three of these components were shown to simultaneously bind in solution, suggesting an interplay that is important for switching from an inhibited to a fusogenic state. Although lots is known about these proteins, there is still much to learn in order to incorporate Cpx1 and Syt1 into a molecular model for neurotransmitter release.

1.4 Current model of neurotransmitter release

The previous sections of this chapter have collectively described decades worth of research on the protein machinery behind neurotransmitter release. Amazingly, all of these proteins somehow function together to control and regulate a highly complicated process. The first step of neurotransmitter release involves tethering, or creating a physical link between the synaptic vesicle and the plasma membrane (Figure 1.11). This occurs before SNARE complex assembly and leaves the vesicle at a larger distance away from the plasma membrane. After tethering, docking/priming occur, which leaves the trans-SNARE complex in a primed, meta-stable state that is almost ready to induce fusion. Docking leaves the synaptic vesicle in very close proximity to the plasma membrane (<5 nm). This state is very close to fusion, but is arrested until the arrival of a calcium signal. After an action potential causes a rapid influx of calcium into the presynaptic cell and induces fusion, neurotransmitters enter the synaptic cleft and bind to receptors on the postsynaptic cell.

Section 1.3 described in detail a plethora of information on a handful of proteins known to be essential for regulating neuronal membrane fusion. A seminal study in 2013 (Ma et al. 2013) proposed a mechanism that incorporates eight of these proteins into a model for neurotransmitter release (Figure 1.12). Most importantly, this model emphasizes that Syntaxin-1-SNAP-25 t-SNARE complexes are not the starting point for SNARE complex assembly. Instead, the presence of NSF/αSNAP forces the system to begin with Syntaxin-1-Munc18 complexes (Figure 1.12). This closed state of Syntaxin-1 is opened by the MUN domain of Munc13-1, where the SNARE complex can begin to assemble with Munc18-1 acting as a template to properly form fusogenic complexes. Partially assembled trans-

SNARE complexes that cannot be disassembled by NSF/αSNAP are assumed to be at the heart of the primed-state, where the protein machinery is assembled but fusion has not occurred. Although Syt1 is known to trigger fast synaptic vesicle fusion, its exact mechanism of action remains elusive.

Protein-protein interactions are clearly essential for proper regulation of this process, but cooperativity amongst numerous protein-lipid interactions is also an often overlooked feature of this system. By studying membrane fusion events in different systems, we will learn both what is unique to each transportation process and what is conserved across millions of years of evolution in the not so distant future. Perhaps one day we will understand at the atomic level how all of these proteins work together to control the human brain, a computing masterpiece that lies at the center of life itself.

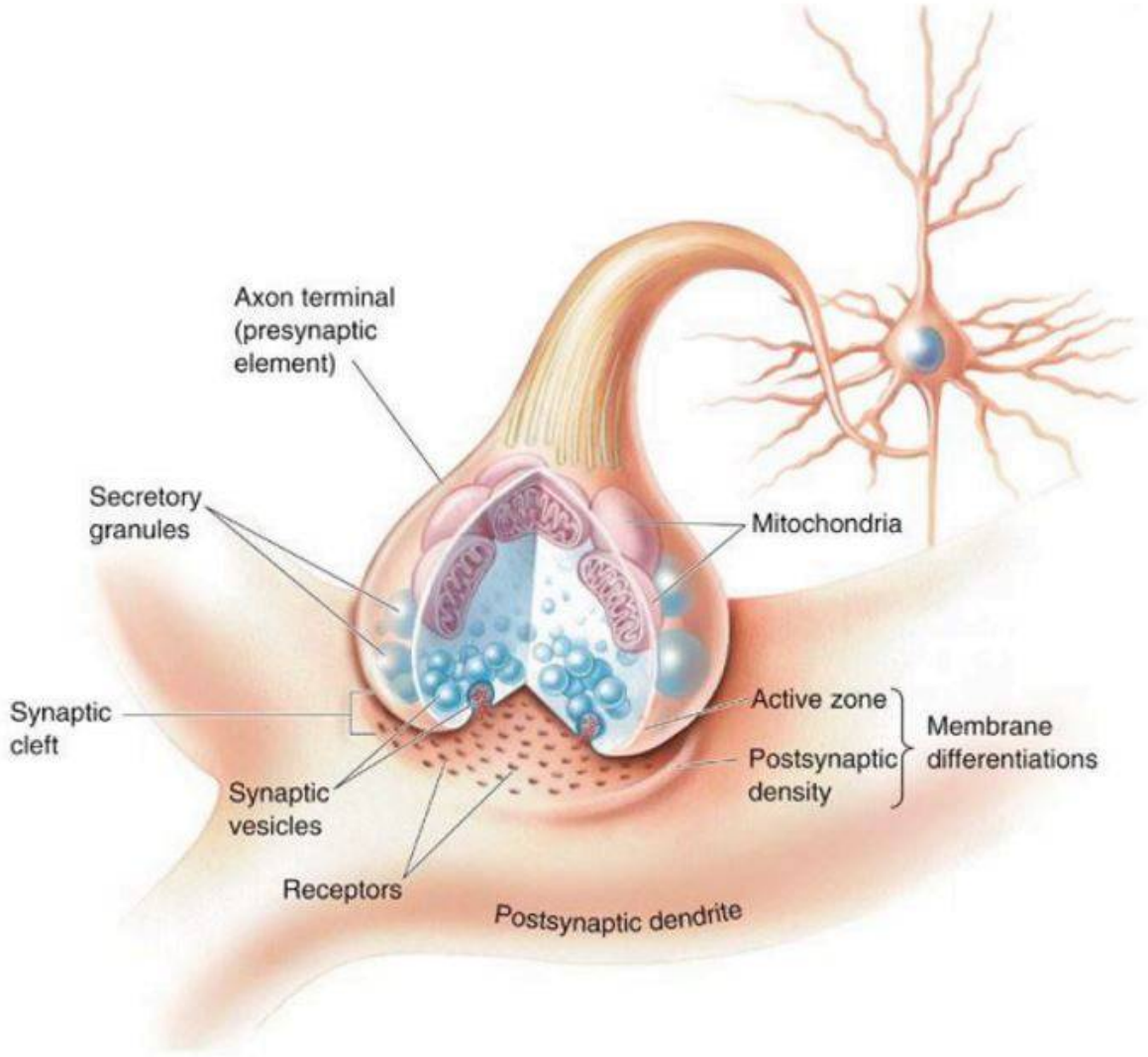

Figure 1.1. Diagram of a neuron. Schematic of how presynaptic axons form synapses with postsynaptic dendrites of other neurons. An action potential causes neurotransmitter molecules to be released from synaptic vesicles into the synaptic cleft, where they bind to specific receptors and propagate the electrical/chemical signal. Figure adapted from Bear, Connors, and Paradiso 2001.

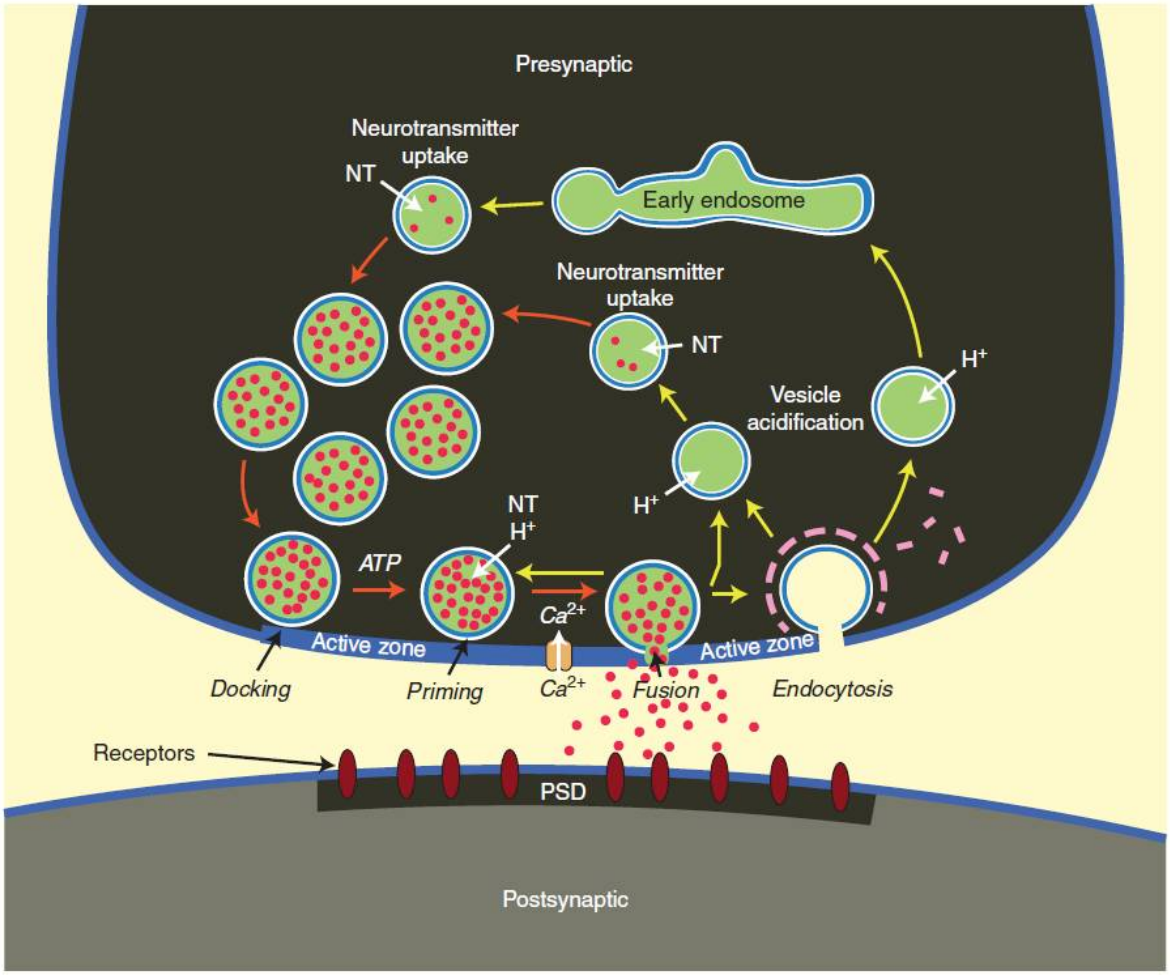

Figure 1.2. The synaptic vesicle cycle. Schematic of a presynaptic nerve terminal in contact with a postsynaptic neuron. Red arrows indicate exocytosis and yellow arrows indicate endocytosis. Synaptic vesicles (green circles) are first filled with neurotransmitters (NT; red dots) before they are tethered or attached to the active zone and docked/primed by an ATP-dependent process that renders the vesicles competent to respond to a Ca^{2+}-signal. When an action potential depolarizes the presynaptic membrane, Ca^{2+}-channels open and induce fusion. Released neurotransmitters then bind to receptors associated with the postsynaptic density (PSD). After fusion, synaptic vesicles recycle via three pathways: local refilling with neurotransmitters without undocking ("kiss-and-stay"), local recycling with undocking ("kiss-and-run"), and full recycling of vesicles with passage through an endosomal intermediate. Figure adapted from Sudhof and Rizo 2011.

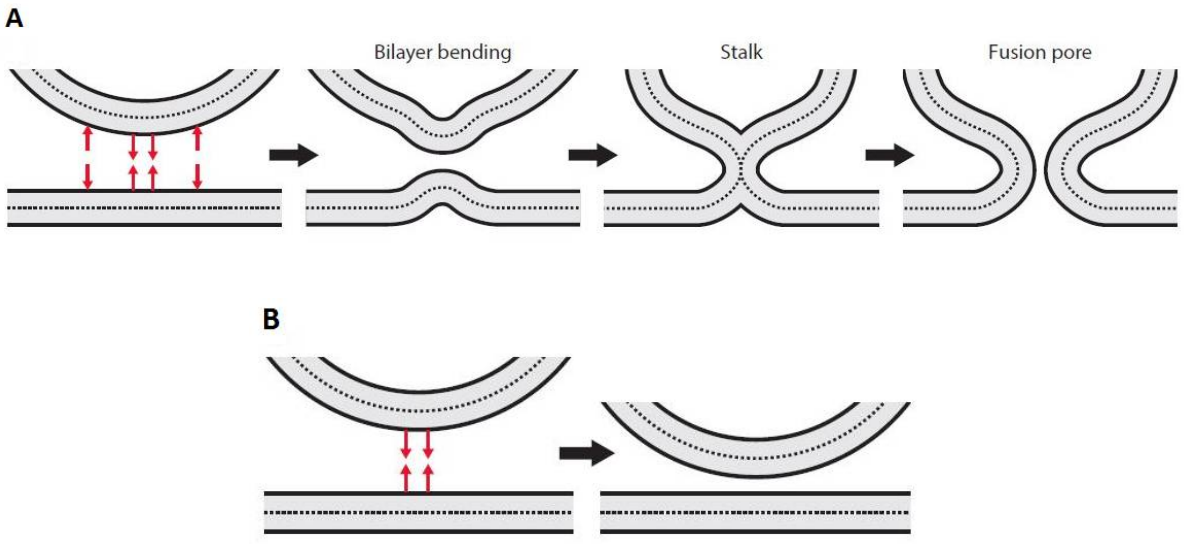

Figure 1.3. The stalk model. (A) Schematic of the stalk model of membrane fusion. When two membranes are in close proximity to one another, bending forces destabilize the bilayers and lead to a stalk intermediate where the proximal leaflets have merged. The fusion pore is formed only after fusion of the distal leaflets. Red arrows illustrate that both pulling forces (arrows point toward each other) and pushing forces (arrows point away from each other) may be required for fusion. (B) Schematic illustrating that pulling forces alone may bring the membranes into close contact without inducing fusion. Figure adapted from Rizo and Xu 2015.

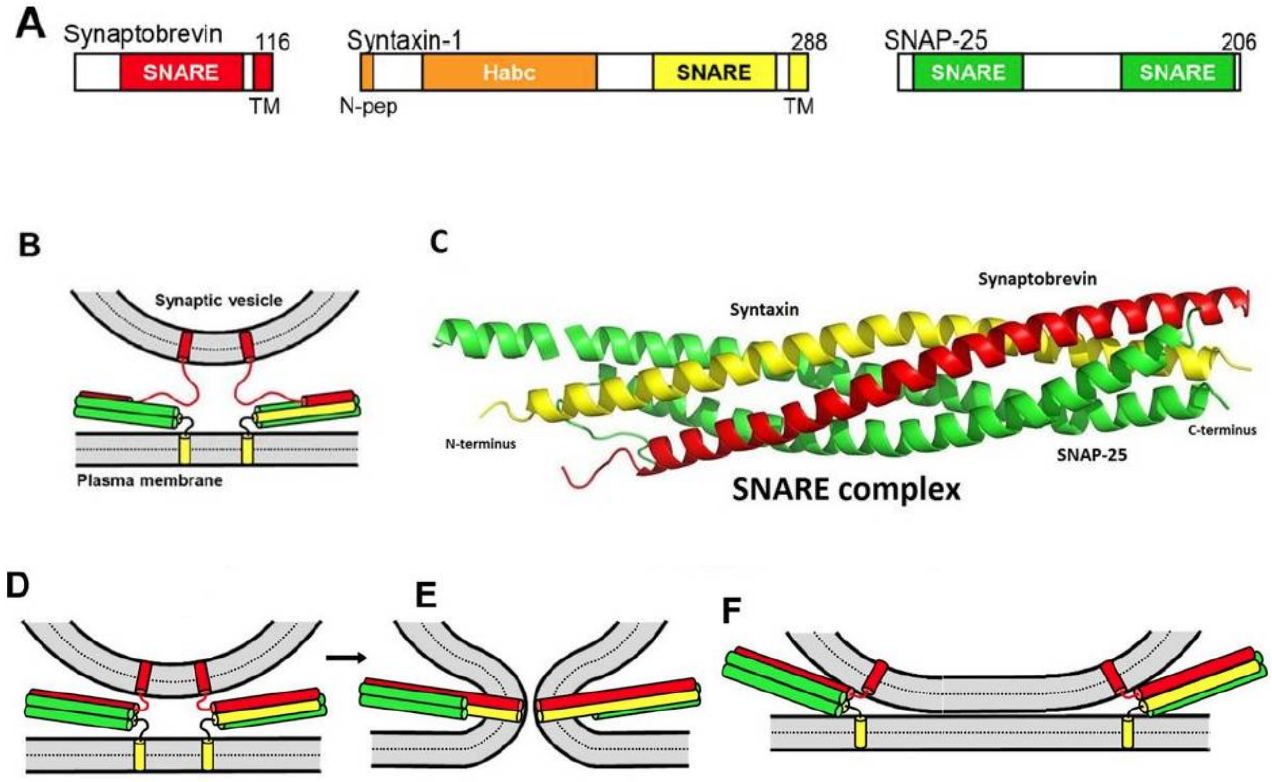

Figure 1.4. Models of SNARE-dependent fusion. (A) Domain diagrams of Synaptobrevin, Syntaxin-1, and SNAP-25. SNARE indicates SNARE motif, N-pep indicates the N-peptide of Syntaxin-1, and TM indicates transmembrane helix. Numbers on the right above the diagrams indicate the length of the protein. (B) Schematic illustrating Synaptobrevin anchored to a synaptic vesicle and Syntaxin-1 anchored on the plasma membrane. The 3 SNARE proteins can form partially assembled trans-SNARE complexes between two membranes. Here, the trans-SNARE complex is shown to be roughly halfway zippered based on the C-terminal half of Synaptobrevin remaining unstructured (C) Ribbon diagram representing the three-dimensional structure of the neuronal SNARE complex (PDB accession code 1SFC). (D-E) These diagrams illustrate the widespread model where the SNARE complex is initially formed at the N-terminus (B), zippers toward the C-terminus (D), and causes membrane fusion as continuous helices are formed by the SNARE motifs and TM regions of Syntaxin-1 and Synaptobrevin, as well as the short linkers between them (E). SNARE complex assembly can also lead to extended membrane-membrane interfaces without fusion (F). Figure adapted from Rizo 2018.

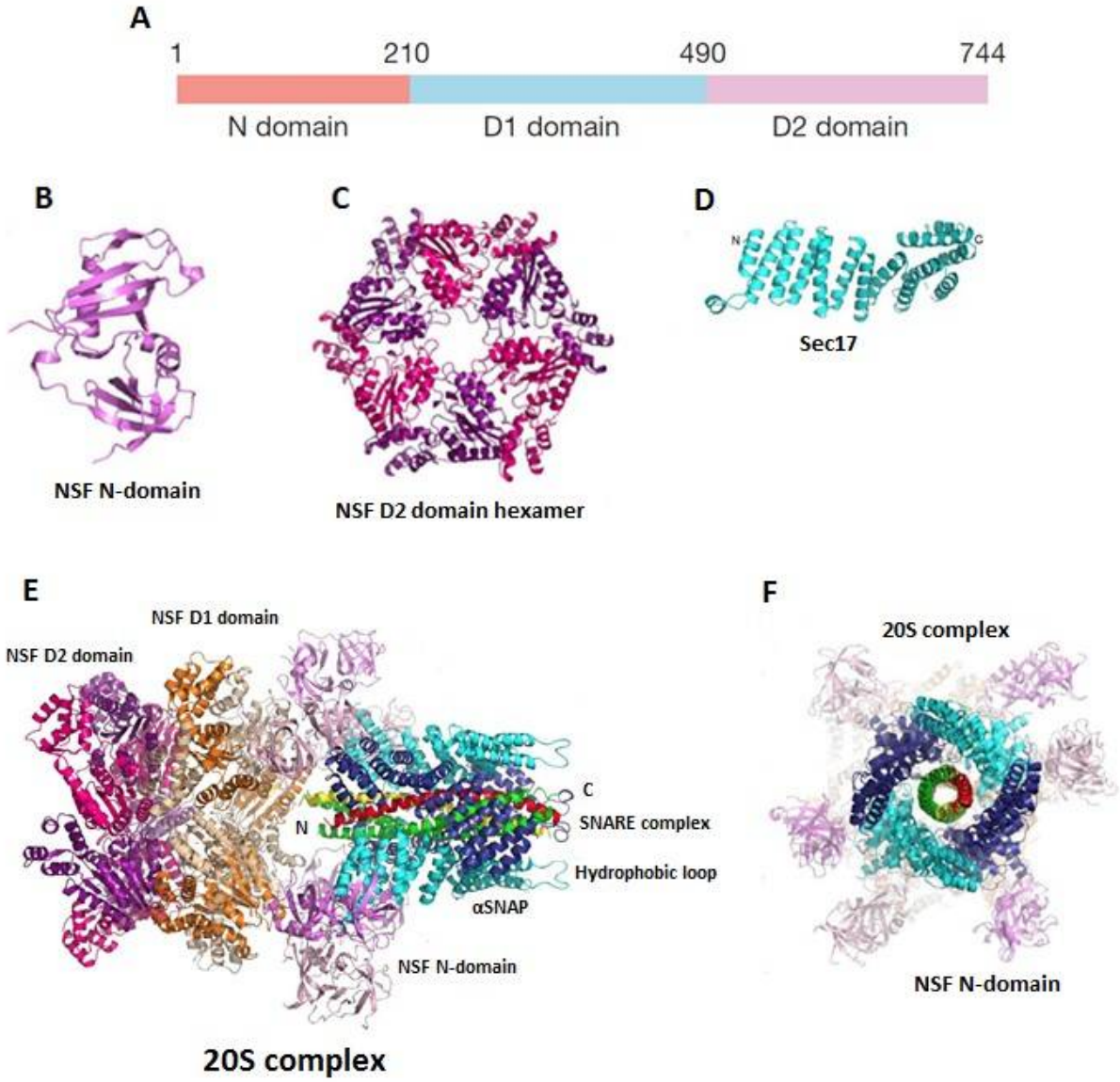

Figure 1.5. Structures of NSF, SNAP/Sec17 and the 20S complex. (A) Domain diagram of NSF, followed by ribbon diagrams showing the three-dimensional structures of (B) the N-terminal domain of NSF, (C) the NSF D2 domain hexamer, (D) Sec17, and (E,F) the 20S complex. The PDB accession codes are 1QDN, 1NSF, 1QQE, and 3J96, respectively. In (D) and (E), N and C indicate the N- and C-termini of Sec17 and the SNARE four-helix bundle, respectively. Panels (E,F) show two different views of the 20S complex rotated approximately 90°. In (F), the C-terminus of the SNARE four-helix bundle is facing the front. For alternate subunits of NSF, the N-terminal domain is shown in violet or pink, the D1 domain in orange or wheat, and the D2 domain in magenta or purple. Alternate αSNAP subunits are shown in cyan or deep blue. The N-terminal hydrophobic loop of one of the αSNAP subunits is indicated in (E). Figure adapted from Zhou et al. 2015 and Rizo 2018.

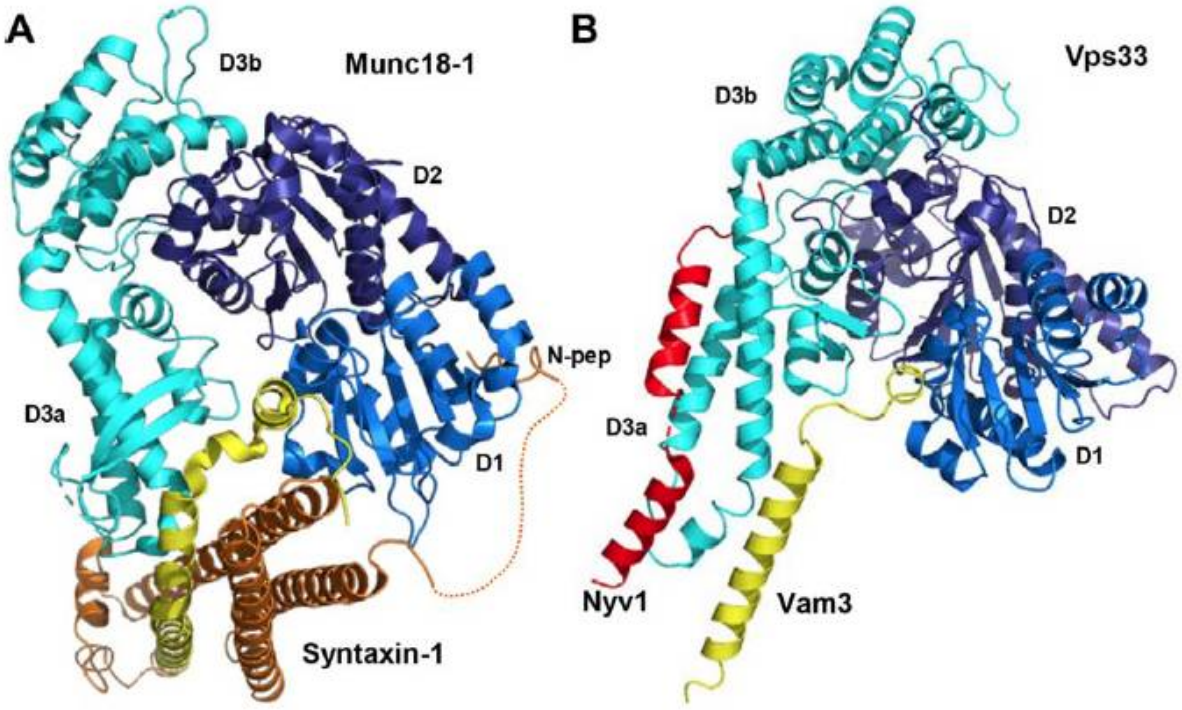

Figure 1.6. Structures of SM protein-SNARE complexes. (A) Ribbon diagram of the three-dimensional structure of Munc18-1 bound to closed Syntaxin-1 (PDB accession code 3C98). The domains of Munc18-1 are colored in blue (D1), deep blue (D2), and cyan (D3a and D3b). Syntaxin-1 is colored in orange (N-terminal region) and yellow (SNARE motif). The dashed curve represents the flexible sequence linking the N-peptide (N-pep) to the H_{abc} domain of Syntaxin-1. (B) Superposition of the crystal structures of Vps33 (blue, deep blue and cyan) bound to the SNARE motifs of the Synaptobrevin homolog Nyv1 (red) and the Syntaxin-1 homolog Vam3 (yellow) (PDB accession codes 5BUZ and 5BV0, respectively). Figure adapted from Rizo 2018.

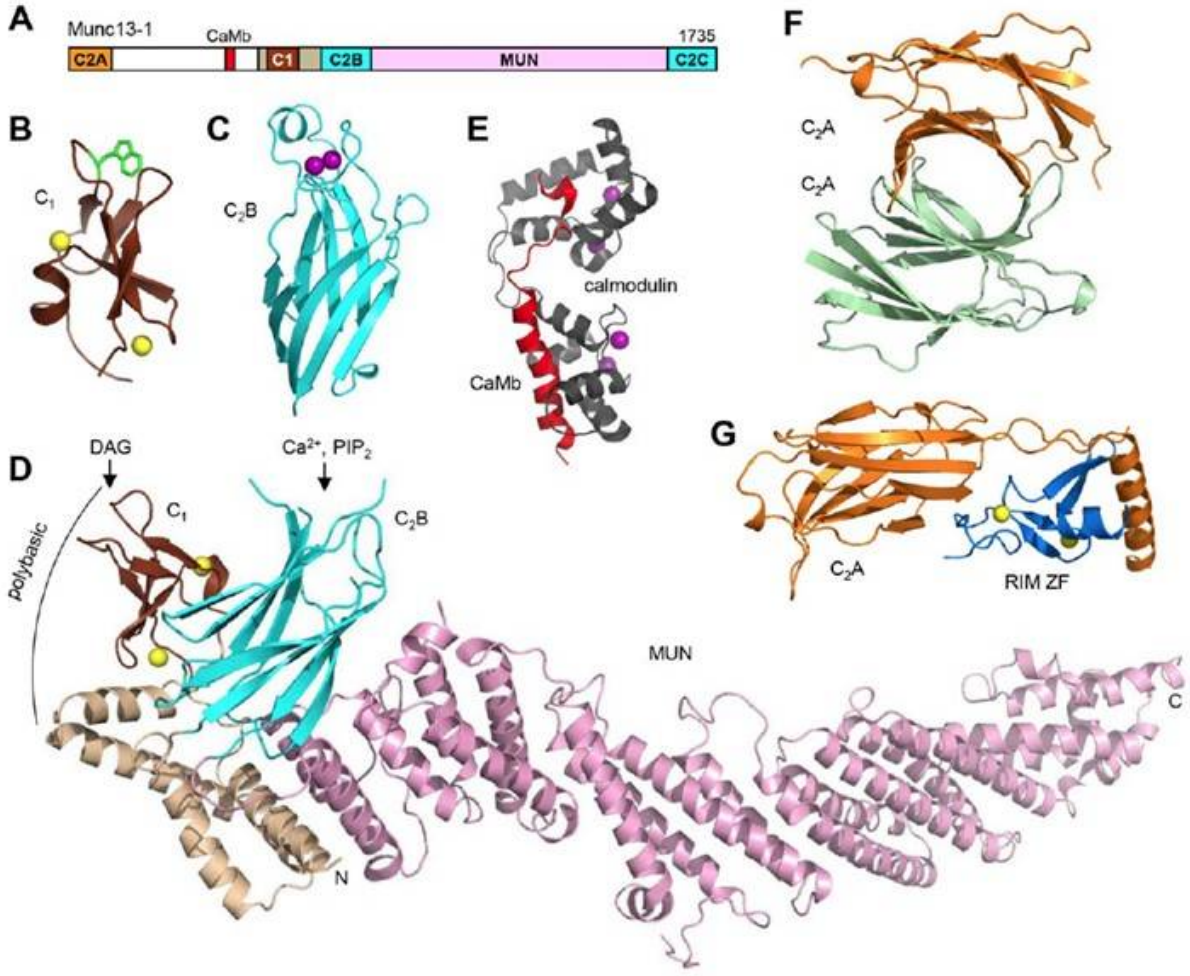

Figure 1.7. Structures involving Munc13-1. (A) Domain diagram of Munc13-1. The calmodulin-binding sequence is labeled CaMb. The number on the right above the diagram indicates the length of the protein. (B-G) Ribbon diagrams of the three-dimensional structures of the C_1 domain (B), the Ca^{2+}-bound C_2B domain, (C) and the C_1C_2BMUN fragment of Munc13-1 (D), as well as calmodulin (black) bound to the Munc13-1 CaMb sequence (red) (E), the Munc13-1 C_2A domain homodimer (F) and the heterodimer of the Munc13-1 C_2A domain (orange) with the RIM2α ZF domain (blue) (G). The PDB accession codes are 1Y8F, 3KWU, 5UE8, 2KDU, 2CJT and 2CJS, respectively. Ca^{2+} ions are shown as purple spheres and zinc ions are shown as yellow spheres. In (D), the locations of the DAG/phorbol ester-binding site in the C_1 domain, the Ca^{2+}/PIP_2-binding site in the C_2B domain, and a polybasic region formed by the C_1 domain, the C_2B domain and the linker sequence between them are indicated. Figure adapted from Rizo 2018.

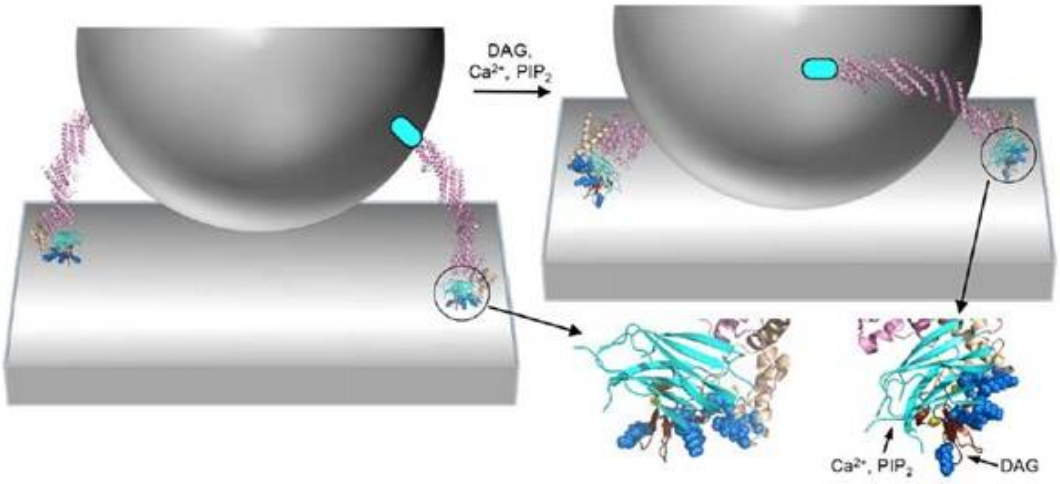

Figure 1.8. Membrane bridging models by Munc13-1. Three-dimensional diagram illustrating how Munc13-1 can bridge the synaptic vesicle and plasma membranes in two different orientations. The model includes a synaptic vesicle, plasma membrane and a ribbon diagram representing the structure of the Munc13-1 C_1C_2BMUN fragment attached to a cyan ellipse that represents the C_2C domain. Below the right diagram are close-up views of the Munc13-1 C_1-C_2B region. The residues that form the polybasic region are shown as blue spheres. On the right, the DAG- and Ca^{2+}/PIP_2-binding sites are indicated. Figure adapted from Rizo 2018.

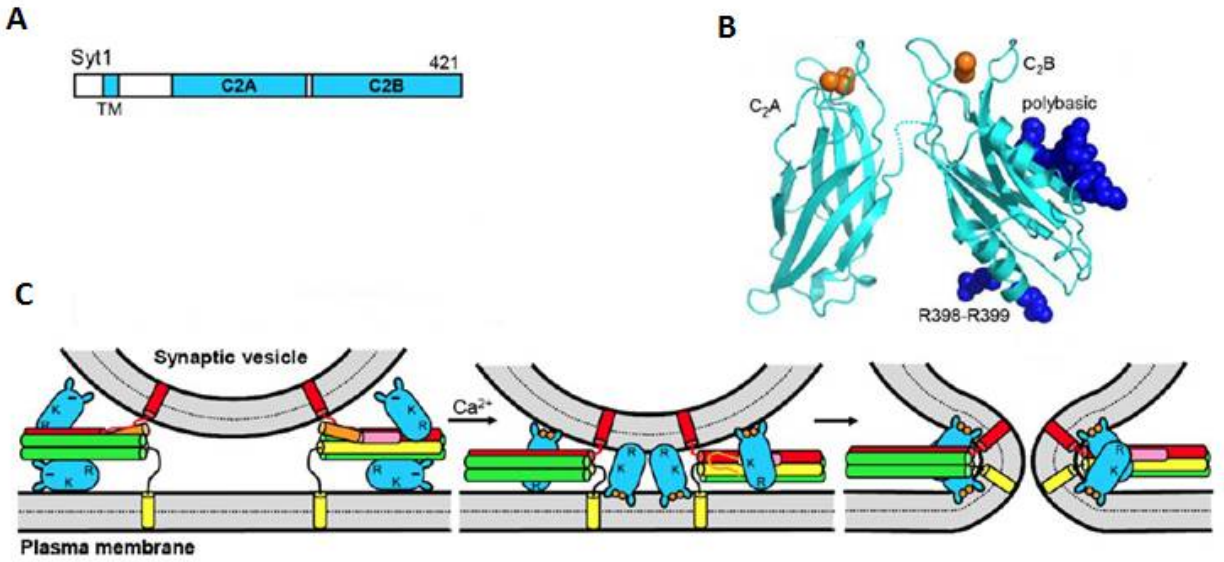

Figure 1.9. Structure and function of Syt1. (A) Domain diagram of Syt1. The number on the right above the diagram indicates the length of the protein. (B) Ribbon diagrams of the three-dimensional structures of the Ca^{2+}-bound Syt1 C_2A and C_2B domains (PDB accession codes 1BYN and 1K5W, respectively). Ca^{2+} ions are shown as orange spheres. The side chains of R398-R399 and the polybasic region of the C_2B domain are shown as deep blue spheres. (C) Model that attempts to integrate the three structures of Syt1-SNARE complex assemblies. The Syt1 C_2B domain is represented by cyan ellipses with protuberances that represent the Ca^{2+}-binding loops and Ca^{2+} ions are represented by orange circles. R indicates the location of R398-R399, and K the location of the polybasic region. Cpx1 is shown in orange (accessory helix) and pink (central helix). Before calcium influx, the C_2B domain is expected to have electrostatic repulsion with the vesicle membrane. Steric hindrance between the vesicle and the Cpx1 accessory helix also contributes to hinder membrane fusion (left). Ca^{2+} binding to the Syt1 C_2B domain allows for simultaneous binding of the C_2B domain polybasic region to the SNARE complex, the Ca^{2+}-binding loops to the vesicle, and the R398-R399 region to the plasma membrane (middle). During this stage, the SNARE complex zippers and the Cpx1 accessory helix melts because of steric hindrance. The position of Syt1 can further rearrange to facilitate membrane bending and fusion (right). Figure adapted from Rizo 2018.

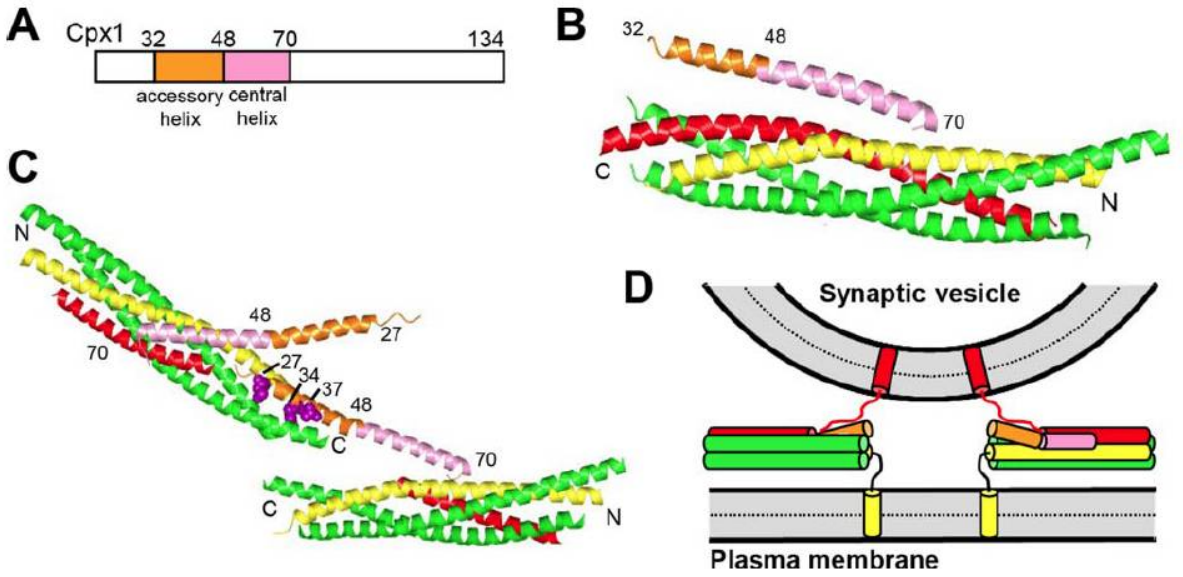

Figure 1.10. Structure and function of Complexins. (A) Domain diagram of Cpx1. Numbers above the diagram indicate the domain boundaries and the length of the protein. (B) Ribbon diagram showing the three-dimensional structure of the Cpx1(26–83)/SNARE complex (PDB accession code 1KIL). (C) Ribbon diagram illustrating the three-dimensional structure of the complex between Cpx1(26–83) bearing the superclamp mutation and a SNARE complex that was truncated at the synaptobrevin C-terminus 160 (PDB accession code 3RK3). The three mutated residues are shown as purple spheres. In (B,C), N and C indicate the N- and C-termini of the SNARE complex. Selected residue numbers of Cpx1 are indicated. (D) Model illustrating how the accessory helix can hinder membrane fusion due to steric and/or electrostatic hindrance with the vesicle. Cpx1(26–83) is color coded as in panel (A), syntaxin-1 is yellow, synaptobrevin red and SNAP-25 green. Figure adapted from Rizo 2018.

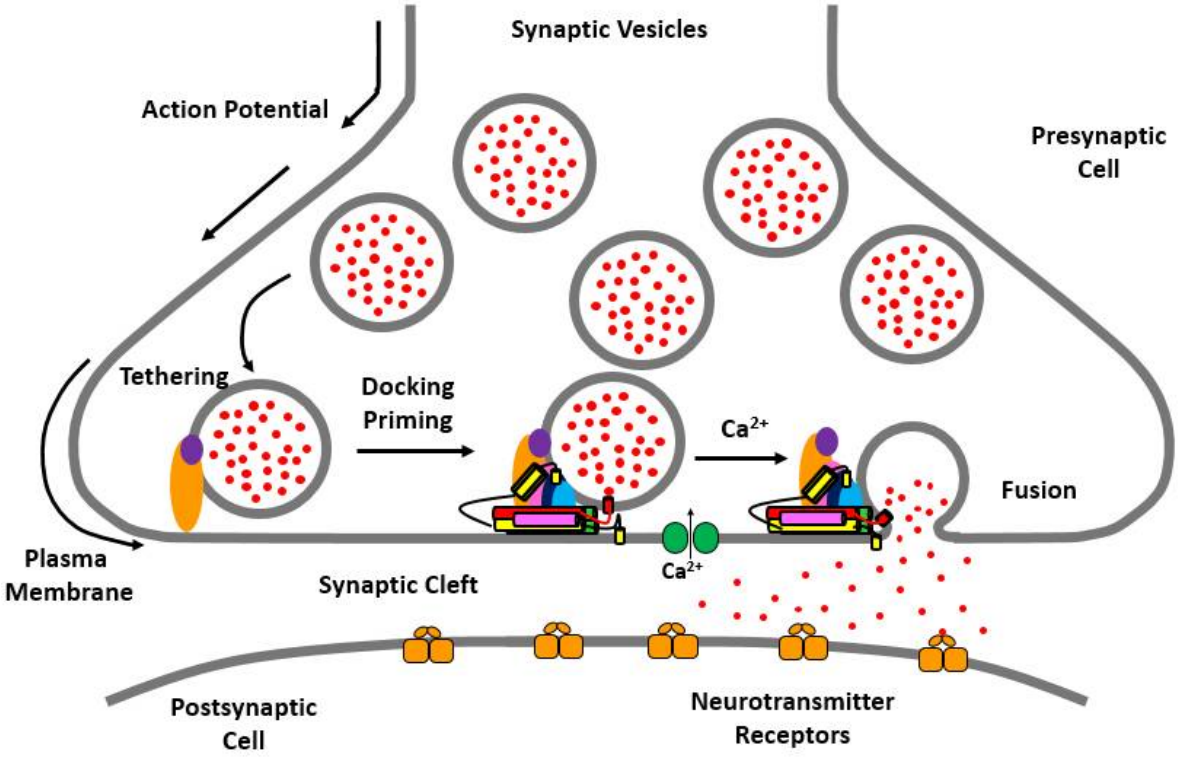

Figure 1.11. Diagram of neurotransmitter release. Model depicting how a synaptic vesicle travels to the active zone and fuses with the plasma membrane through 3 main steps: tethering, docking/priming, and fusion. Tethering, or a physical link between the synaptic vesicle and the plasma membrane, leaves the vesicle at a larger distance away from the plasma membrane. Docking and priming prep the trans-SNARE complex to a primed, meta-stable state that is almost ready to induce fusion. This state is in very close proximity to the plasma membrane (<5 nm), but arrested until the arrival of a calcium signal. After an action potential causes a rapid influx of calcium into the presynaptic cell and induces fusion, neurotransmitters enter the synaptic cleft and bind to receptors on the postsynaptic cell.

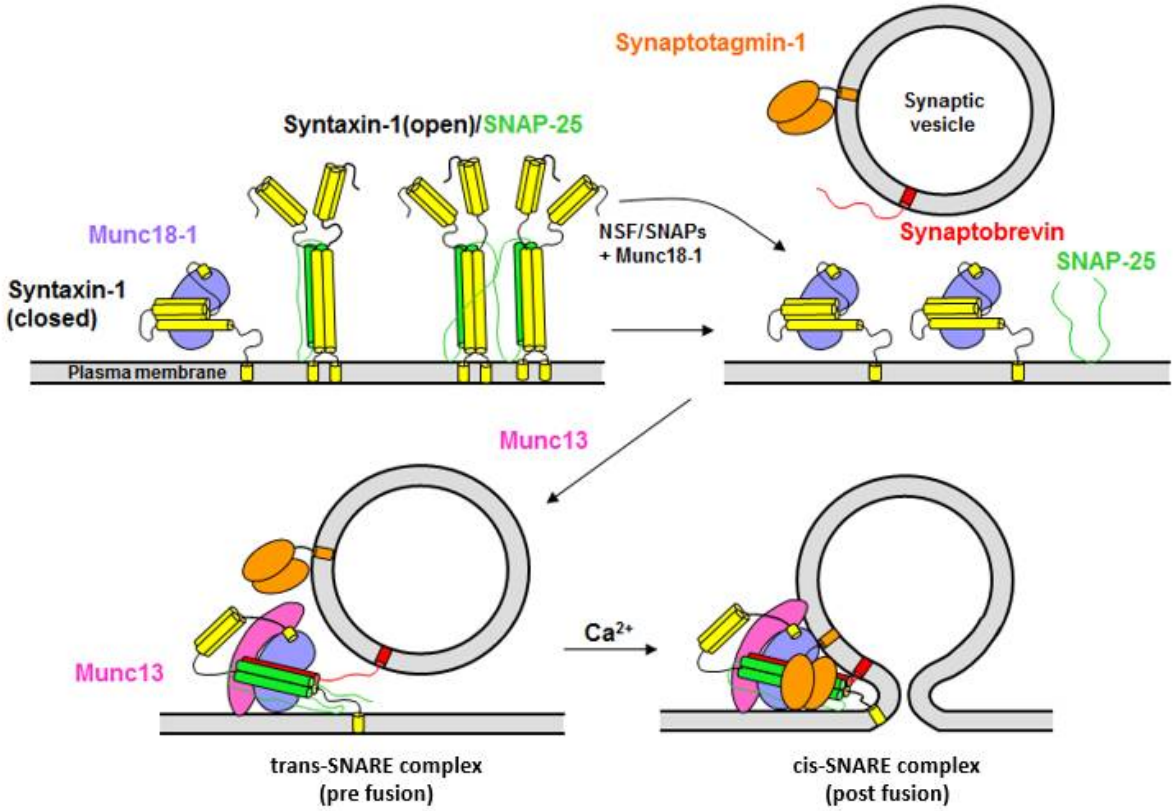

Figure 1.12. Model of synaptic vesicle fusion integrating the function of eight major components of the release machinery. In the top left, syntaxin-1 (yellow) is shown in a closed conformation bound to Munc18-1 and in an open conformation bound to SNAP-25. Syntaxin-1-SNAP-25 heterodimers are converted to syntaxin-1-Munc18-1 complexes with the help of NSF/αSNAP (top right). Munc13-1 then helps to open syntaxin-1, leading to a partially assembled trans-SNARE complex that may remain bound to Munc18-1 and Munc13-1 (bottom left). This potentially primed state that cannot be disassembled by NSF-αSNAP serves as the substrate for synaptotagmin-1-Ca^{2+} to trigger fast synaptic vesicle fusion (bottom right). Figure adapted from Ma et al. 2013.

Chapter 2- Multiple factors protect neuronal trans-SNARE complexes against disassembly by NSF and αSNAP

*This section was reproduced from: **Prinslow, E. A.**, Karolina P. Stepien, Yun-Zu Pan, Junjie Xu and Josep Rizo. (Corrections submitted December 2018). "Multiple factors protect neuronal trans-SNARE complexes against disassembly by NSF and αSNAP." eLife.

2.1 Abstract

Neurotransmitter release requires formation of trans-SNARE complexes between the synaptic vesicle and plasma membranes, which likely underlies synaptic vesicle priming to a release-ready state. It is unknown whether Munc18-1, Munc13-1, complexin-1 and synaptotagmin-1 are important for priming because they mediate trans-SNARE complex assembly and/or because they prevent trans-SNARE complex disassembly by NSF-αSNAP, which can lead to de-priming. Here we show that trans-SNARE complex formation in the presence of NSF-αSNAP requires both Munc18-1 and Munc13-1, as proposed previously, and is facilitated by synaptotagmin-1. Our data also show that Munc18-1, Munc13-1 and complexin-1 protect trans-SNARE complexes from disassembly by NSF-αSNAP, and suggest that synaptotagmin-1 enhances such protection. We propose a model whereby Munc18-1 and Munc13-1 are critical not only for mediating vesicle priming but also for precluding de-priming by preventing trans-SNARE complex disassembly; in this model, complexin-1 also impairs de-priming, while synaptotagmin-1 may assist in priming and hinder de-priming.

2.2 Introduction

The release of neurotransmitters by Ca^{2+}-triggered synaptic vesicle exocytosis is a central event for interneuronal communication and involves multiple steps. Synaptic vesicles first dock at specialized sites on the plasma membrane called active zones, undergo one or more priming reactions that leave the vesicles ready for release, and fuse with the plasma membrane upon Ca^{2+} influx evoked by an action potential (Sudhof 2013). Extensive research has shown that these steps are exquisitely regulated by a sophisticated protein machinery and has led to defined models for the functions of key components from this machinery (Brunger et al. 2018, Jahn et al. 2012, Rizo 2018, Sudhof et al. 2009). The soluble N-ethylmaleimide sensitive factor attachment protein receptors (SNAREs) synaptobrevin, syntaxin-1 and SNAP-25 form a parallel four-helix bundle called the SNARE complex that brings the synaptic vesicle and plasma membranes together and is key for membrane fusion (Hanson et al. 1997, Poirier et al. 1998, Sollner et al. 1993a, Sutton et al. 1998). N-ethylmaleimide sensitive factor (NSF) and soluble NSF attachment proteins (SNAPs; no relation to SNAP-25) disassemble SNARE complexes after release to recycle the SNAREs for another round of fusion (Banerjee et al. 1996, Mayer et al. 1996, Sollner et al. 1993a). Munc18-1 and Munc13s orchestrate SNARE complex assembly in an NSF-SNAP-resistant manner (Ma et al. 2013) that improves the fidelity of parallel assembly (Lai et al. 2017). The underlying mechanism involves binding of Munc18-1 to a self-inhibited ‘closed conformation’ of syntaxin-1 (Dulubova et al. 1999, Misura et al. 2000) and to synaptobrevin, thus forming a template to assemble the SNARE complex (Baker et al. 2015, Parisotto et al. 2014, Sitarska et al. 2017), while Munc13s bridge the vesicle and plasma membranes (Liu et al. 2016) and

help to open syntaxin-1 (Ma et al. 2011, Richmond et al. 2001, Yang et al. 2015b). Synaptotagmin-1 acts as the major Ca^{2+} sensor that triggers release through interactions with phospholipids (Fernandez-Chacon et al. 2001) and the SNARE complex (Brewer et al. 2015, Zhou et al. 2015, Zhou et al. 2017), in a tight interplay with complexins (Giraudo et al. 2006, Schaub et al. 2006, Tang et al. 2006).

Despite these and other crucial advances, fundamental questions remain about how trans-SNARE complexes that bridge the vesicle and plasma membranes are formed, about the interplay between Munc18-1, Munc13-1, NSF and αSNAP in promoting trans-SNARE complex assembly or disassembly, and about the nature of the primed state(s) of the release machinery in the readily-releasable pool (RRP) of vesicles. The primed state is believed to include trans-SNARE complexes that are partially formed, with the N-terminal half assembled and at least part of the C-terminal, membrane proximal portion unassembled [e.g. (Sorensen et al. 2006, Walter et al. 2010)], but it is unclear which other components are bound to the SNAREs in this state. Reconstitution assays showing that the fusion between synaptobrevin-containing liposomes and syntaxin-1-SNAP-25-containing liposomes observed in the presence of synaptotagmin-1 and Ca^{2+} is abolished by NSF-αSNAP, but occurs efficiently upon further addition of Munc18-1 and a Munc13-1 fragment, led to the notion that Munc18-1 and Munc13-1 mediate a pathway for trans-SNARE complex assembly that is resistant to NSF-αSNAP (Liu et al. 2016, Ma et al. 2013), explaining the essential nature of Munc18-1 and Munc13s for vesicle priming (Aravamudan et al. 1999, Richmond et al. 2001, Varoqueaux et al. 2002, Verhage et al. 2000). This interpretation arose in part because NSF-αSNAP disassemble not only cis-SNARE complexes but also syntaxin-1-

SNAP-25 heterodimers (Hayashi et al. 1995), thus preventing trans-SNARE complex formation by the SNAREs alone, and because of evidence suggesting that NSF-αSNAP cannot disassemble trans-SNARE complexes (Weber et al. 2000). However, studies of yeast vacuolar fusion showed that the NSF-αSNAP homologues Sec18-Sec17 disassemble trans-SNARE complexes and that disassembly is prevented by HOPS, a tethering complex that includes the Munc18-1 homologue Vps33 and coordinates SNARE complex formation (Mima et al. 2008, Xu et al. 2010). Moreover, recent reports showed that at least a fraction of neuronal trans-SNARE complexes can be disassembled by NSF-αSNAP in vitro (Yavuz et al. 2018) and that Munc18-1 and Munc13-1 are critical to prevent de-priming of readily-releasable synaptic vesicles in neurons, but such requirement can be bypassed by the NSF inactivating agent N-ethylmaleimide (He et al. 2017).

These findings suggest that the cytoplasmic environment of a presynaptic terminal favors disassembly of all kinds of SNARE complexes and hence that the trans-SNARE complexes formed after priming must be protected against disassembly by NSF-αSNAP. However, the mechanisms underlying such protection are unknown. The results of He et al. 2017 indicate that Munc18-1 and Munc13-1 play key roles in such protection, in addition to mediating an NSF-αSNAP-resistant pathway of trans-SNARE complex assembly, but this hypothesis has not been tested, and Munc18-1 and Munc13-1 are often assumed to be dispensable after mediating assembly. Moreover, it is plausible that protection against disassembly by NSF-αSNAP depends also on other proteins such as synaptotagmin-1 and complexins, which bind to SNARE complexes and have also been proposed to facilitate trans-SNARE complex formation (Diao et al. 2013, Li et al. 2017). In this context, while

initial studies suggested that synaptic vesicle priming is not altered in neurons from synaptotagmin-1 knockout (KO) mice (Geppert et al. 1994) and in complexin-1/2 double knockout (DKO) mice (Reim et al. 2001), subsequent analyses revealed that absence of these proteins does decrease the RRP of vesicles (Bacaj et al. 2015, Chang et al. 2018, Xue et al. 2010b, Yang et al. 2010). Such decreases were not as dramatic as those observed in Munc18-1 KO mice (Verhage et al. 2000) and Munc13-1/2 DKO mice (Varoqueaux et al. 2002), where priming is totally abrogated, but do suggest that synaptotagmin-1 and complexins are involved in priming or perhaps in maintenance of the RRP. Thus, while it is known that the existence of an RRP of vesicles depends on Munc18-1, Munc13-1, synaptotagmin-1 and complexins, it is still unclear to what extent the roles of these various factors arise because they mediate priming by facilitating trans-SNARE complex assembly via a NSF-SNAP-resistant pathway and/or because they stabilize primed vesicles by protecting against trans-SNARE complex disassembly by NSF-SNAPs.

The study presented herein was designed to address these questions and understand the interplay between these proteins in trans-SNARE complex assembly and disassembly, using a fluorescence resonance energy transfer (FRET) assay. Our data show that trans-SNARE complex assembly in the presence of NSF-αSNAP requires Munc18-1 and Munc13-1, as expected from our previous reconstitution experiments (Ma et al. 2013), but does not require complexin-1. Moreover, we find that Munc18-1 and Munc13-1 synergistically protect trans-SNARE complexes against disassembly by NSF-αSNAP, which is strongly enhanced by Ca^{2+}, and that trans-SNARE complexes are also protected against disassembly by complexin-1. Synaptotagmin-1 facilitates NSF-αSNAP-resistant trans-SNARE complex

assembly and may contribute to stabilizing trans-SNARE complexes, but its effects are less marked. These results support a model whereby Munc18-1 and Munc13-1 play key roles not only in priming synaptic vesicles to a readily-releasable state, but also in protecting them against de-priming by NSF-SNAPs, while synaptotagmin-1 plays a less critical role in both priming and maintenance of the RRP, and complexin-1 does not mediate priming but stabilizes primed vesicles.

2.3 Materials and methods

Recombinant proteins

The following constructs were used for protein expression in *E. coli* BL21 (DE3) cells: Full-length rat syntaxin-1A, rat syntaxin 2-253, full-length rat SNAP-25A (C84S, C85S, C90S, C92S), full-length rat synaptobrevin, rat synaptobrevin 49-93, rat synaptotagmin-1 57-421 (C74S, C75A, C77S, C79I, C82L, C277S) (a kind gift from Thomas Sollner), rat synaptotagmin-1 C_2AB (131-421 C277A), full-length rat complexin, full-length Chinese hamster NSF (a kind gift from Minglei Zhao), full-length *Bos Taurus* αSNAP, full length rat Munc18-1, and a rat Munc13-1 fragment spanning the C_1C_2BMUNC_2C regions (529-1725 Δ1408-1452). Expression and purification of the corresponding proteins were performed as previously reported (Chen et al. 2006, Chen et al. 2002, Dulubova et al. 1999, Liang et al. 2013, Liu et al. 2017, Ma et al. 2011, Ma et al. 2013, Xu et al. 2013, Zhao et al. 2015) with the modifications described below. His_6-full-length syntaxin-1A was induced with 0.4 mM IPTG and expressed overnight at 25°C. Purification was done using Ni-NTA resin (Thermo Fisher) in 20 mM Tris pH 7.4, 500 mM NaCl, 8 mM imidazole, 2% Triton X-

100, and 6M urea followed by elution in 20 mM Tris pH 7.4, 500 mM NaCl, 400 mM imidazole, and 0.1% DPC. The His_6 tag was removed using thrombin cleavage, followed by size exclusion chromatography on a Superdex 200 column (GE 10/300) in 20 mM Tris pH 7.4, 125 mM NaCl, 1 mM TCEP, 0.2% DPC (Liang et al. 2013). GST-syntaxin-1A 2-253 was induced with 0.4 mM IPTG and expressed overnight at 25°C. Purification was done using glutathione sepharose resin (GE) followed by thrombin cleavage of the GST-tag and anion exchange chromatography on a HiTrap Q column (GE) in 25 mM Tris pH 7.4, 1mM TCEP using a linear gradient from 0 mM to 1000 mM NaCl. GST-Syb49-93 was induced with 0.4 mM IPTG and expressed overnight at 23°C. Purification was done using glutathione sepharose resin (GE) followed by cleavage of the GST-tag and size exclusion chromatography on a Superdex 75 column (GE 16/60) in 20 mM Tris pH 7.4, 125 mM NaCl. His_6-full-length complexin-1 was induced with 0.5 mM IPTG and expressed for 4 hours at 37°C. Purification was done using Ni-NTA resin followed by TEV cleavage of the His_6-tag and size exclusion chromatography on a Superdex 75 column (GE 16/60) in 20 mM Tris pH 7.4, 125 mM NaCl, 1 mM TCEP. His_6-full-length NSF was induced with 0.4 mM IPTG and expressed overnight at 20°C. Purification was done in 5 steps (Zhao et al. 2015): i) Ni-NTA affinity chromatography; ii) size exclusion chromatography of hexameric NSF on a Superdex S200 column (GE 16/60) in 50 mM Tris pH 8.0, 100 mM NaCl, 1 mM ATP, 1 mM EDTA, 1 mM DTT, and 10% glycerol; iii) TEV cleavage of the His_6-tag and monomerization with apyrase during 36 hr dialysis with nucleotide-free buffer; iv) three rounds of size exclusion chromatography to separate monomeric and hexameric NSF (re-injecting the latter) on a Superdex S200 column (GE 16/60) in 50 mM NaPi pH 8.0, 100 mM NaCl, 0.5 mM TCEP;

and v) reassembly of the NSF monomers and size exclusion chromatography of reassembled hexameric NSF on a Superdex S200 column (GE 16/60) in 50 mM Tris pH 8.0, 100 mM NaCl, 1 mM ATP, 1 mM EDTA, 1 mM DTT, and 10% glycerol. For experiments requiring the use of a non-hydrolyzable analog of ATP, reassembly of monomeric NSF was done in the presence of ATPγS followed by size exclusion chromatography of the hexamer in a similar buffer as before substituting ATPγS for ATP. His_6-Munc13-1 C_1C_2BMUNC_2C (529-1725 Δ1408-1452) was induced with 0.5 mM IPTG and expressed overnight at 16°C. Purification was done using Ni-NTA resin (Thermo Fisher) followed by thrombin cleavage of the His_6-tag and anion exchange chromatography on a HiTrap Q column (GE) in 20 mM Tris pH 8.0, 10% glycerol, 1 mM TCEP using a linear gradient from 0 to 500 mM NaCl.

Mutant proteins

All mutations were performed using QuickChange site-directed mutagenesis (Stratagene). These include the S186C mutation in full length syntaxin-1A (C145A, C271A, C272A) and in syntaxin-1A 2-253 (C145A), the M71D,L78D mutation in full-length SNAP-25A (C84S, C85S, C90S, C92S), the L26C mutation in full-length synaptobrevin (C103A), and the F27S,F28S and K122E,K163E mutations in αSNAP. For synaptobrevin L26C, the construct was cloned into a pet28A vector with an N-terminal His_6 tag for soluble expression. All mutant proteins were purified as the wild type proteins.

Labeling proteins with Alexa Fluor 488 and tetramethylrhodamine

Single cysteine mutants were labeled with Alexa Fluor 488 (Alexa488, for full length synaptobrevin L26C) or with tetramethylrhodamine (TMR, for full-length syntaxin-1A S186C and syntaxin-1A 2-253 S186C) using maleimide reactions (Thermo Fisher). Full length synaptobrevin L26C was first buffered exchanged to 20 mM Tris pH 7.4, 150 mM NaCl, 1 mM TCEP, 1% octyl β-glucopyranoside (β-OG) using a PD Miditrap G25 column to provide buffer conditions that allow the reactive thiol group to be sufficiently nucleophilic so that they exclusively react with the dye. Buffered exchanged proteins at a concentration of 75 μM were incubated with a 20-fold excess of dye for 2 hours at room temperature. Unreacted dye was separated from the labeled protein through cation exchange chromatography on a HiTrap SP column (GE) in 25 mM NaAc pH 5.5, 1 mM TCEP, 1% β-OG using a linear gradient from 0 to 1000 mM NaCl. Full length Syntaxin S186C and Syntaxin 2-253 S186C were tagged with tetramethylrhodamine (Thermo Fisher) using a similar protocol. After labeling full length syntaxin-1A S186C, unreacted dye was separated from the labeled protein though anion exchange chromatography on a HiTrap Q column (GE) in 20 mM Tris pH 7.4, 1 mM TCEP, 0.1% DPC using a linear gradient from 0 to 1000 mM NaCl. After labeling syntaxin-1A 2-253 L26C, unreacted dye was separated from the labeled protein using multiple PD Miditrap G25 columns. The concentration of fluorescently tagged proteins was determined using UV-vis absorbance and a Bradford assay.

Simultaneous lipid mixing and content mixing assays

Assays that simultaneously monitor lipid and content mixing were performed as described in detail in (Liu et al. 2017). Briefly, V-liposomes with full length synaptobrevin contained 39% POPC, 19% DOPS, 19% POPE, 20% cholesterol, 1.5% NBD-PE, and 1.5% Marina Blue DHPE. T-liposomes with full-length syntaxin-1A and full-length SNAP25 (WT or M71D,L78D mutant) contained 38% POPC, 18% DOPS, 20% POPE, 20% cholesterol, 2% PIP2, and 2% DAG. Dried lipid mixtures were re-suspended in 25 mM HEPES pH 7.4, 150 KCl, 1 mM TCEP, 10% glycerol, 2% β-OG. Purified SNARE proteins and fluorescently labeled content mixing molecules were added to the lipid mixtures to make the syntaxin-1:SNAP25:lipid ratio 1:5:800 and Phycoerythrin-Biotin (4 μM) for T-liposomes, and the synaptobrevin:lipid ratio 1:500 and Cy5-Streptavidin (8 μM) for V-liposomes. The mixtures were incubated at room temperature and dialyzed against the reaction buffer (25 mM HEPES pH 7.4, 150 mM KCl, 1 mM TCEP, 10% glycerol) with 2g/L Amberlite XAD-2 beads (Sigma) 3 times at 4 °C. Proteoliposomes were purified by floatation on a three-layer histodenz gradient (35%, 25%, and 0%) and harvested from the topmost interface. To simultaneously measure lipid mixing from de-quenching of Marina Blue lipids and content mixing from the development of FRET between Phycoerythrin-Biotin trapped in T-liposomes and Cy5-streptavidin trapped in V-liposomes, T-liposomes (0.25 mM lipid) were mixed with V-liposomes (0.125 mM lipid) in a total volume of 200 μL. Acceptor T-liposomes were first incubated with 0.8 μM NSF, 2 μM αSNAP, 2.5 mM $MgCl_2$, 2 mM ATP, 0.1 mM EGTA, and 1 μM Munc18-1 at 37 °C for 25 minutes. They were then mixed with donor V-liposomes, 0.5 μM Munc13-1 $C_1C_2BMUNC_2C$, and 1 μM excess SNAP25.

All experiments were performed at 30 °C and 0.6 mM Ca^{2+} was added at 300 s. The fluorescence signal from Marina Blue (excitation at 370 nm, emission at 465 nm) and Cy5 (excitation at 565 nm, emission at 670 nm) were recorded to monitor lipid and content mixing, respectively. At the end of the reaction, 1% β-OG was added to solubilize the liposomes and the lipid mixing data were normalized to the maximum fluorescence signal. Most experiments were performed in the presence of 5 μM streptavidin, and control experiments without streptavidin were performed to measure the maximum Cy5 fluorescence after detergent addition for normalization of the content mixing data.

FRET assays to monitor trans-SNARE complex assembly and disassembly

Reconstituted liposomes were made similarly to those used for the lipid and content mixing assay. V-liposomes with full-length synaptobrevin L26C-Alexa488 contained 42% POPC, 19% DOPS, 19% POPE, and 20% cholesterol. VSyt1-liposomes with Synaptotagmin 57-421 and full length synaptobrevin L26C-Alexa488 contained 43% POPC, 6.8% DOPS, 30.2% POPE, and 20% cholesterol. T-liposomes with full-length syntaxin-1A S186C-TMR and full length SNAP25-A M71D, L78D mutant contained 38% POPC, 18% DOPS, 20% POPE, 20% cholesterol, 2% PIP2, and 2% DAG (note that for selected experiments WT SNAP-25 was used instead of the mutant). Dried lipid mixtures were re-suspended in 25 mM HEPES pH 7.4, 150 KCl, 1 mM TCEP, 2% β-OG. Purified SNARE proteins were added to the lipid mixtures to make the syntaxin-1:SNAP25:lipid ratio 1:5:800 for T-liposomes, the synaptobrevin:lipid ratio 1:10,000 for V-liposomes, and the synaptotagmin-1:synaptobrevin:lipid ratio 1:0.1:1,000 for VSyt1-liposomes. The mixtures were incubated at

room temperature and dialyzed against the reaction buffer (25 mM HEPES pH 7.4, 150 mM KCl, 1 mM TCEP) with 2g/L Amberlite XAD-2 beads (Sigma) 3 times at 4 °C. All FRET experiments were performed at 37 °C on a PTI Quantamaster 400 spectrofluorometer (T-format) with all slits set to 1.25 mm. A GG495 longpass filter (Edmund optics) was used to filter scattered light. SNARE complex formation was measured by the development of FRET between Alexa488-Synaptobrevin on V- or VSyt1-liposomes and TMR-syntaxin-1 on T-liposomes or TMR-syntaxin-1(2-253). For kinetic traces, the fluorescence signal at 518 nm (excitation at 468 nm) was recorded to monitor the Alexa488 donor fluorescence intensity. The signal of donor V-or VSyt1-liposomes (0.0625 mM lipid) in reaction buffer containing 0.1 mM EGTA, 2.5 mM $MgCl_2$, 2 mM ATP and various additions was first recorded for 180s to check for signal stability and then either acceptor T-liposomes (0.25 mM lipid) or soluble acceptor TMR-syntaxin-1 2-253 (300 nM) were added. The initial additions included the following in different combinations as specified in the Figures and their legends: 10 μM Syb49-93, 2 μM complexin-1, 1 μM synaptotagmin-1 C_2AB, 0.6 mM Ca^{2+}, 1 μM Munc18-1, and 0.3 μM Munc13-1 $C_1C_2BMUNC_2C$. For experiments where disassembly was tested after recording an assembly reaction (Figures 2.4, 2.6B-D), 2 μM αSNAP and 0.4 μM NSF were added at the indicated time points. For experiments designed to test the assembly of cis- or trans-SNARE complexes in the presence of NSF-αSNAP (Figures 2.3, 2.6A), 0.1 mM EGTA, 2.5 mM $MgCl_2$, 2 mM ATP, 2 μM αSNAP and 0.4 μM NSF were mixed with the V- or VSyt1-liposomes from the start, together with the corresponding additional proteins. For some experiments, Ca^{2+} (0.6 mM) was added at the time points indicated in the Figures. Data points were collected (1 s acquisition) every 20 seconds for 30 minutes for reactions where

saturation was reached, and for longer times for slower reactions. Only a small amount of photobleaching of the donor was observed under these conditions in control experiments with donor alone. Pre-formed trans-SNARE complexes were made by incubating V-liposomes, T-liposomes, SNAP25m (or WT SNAP-25 when specifically stated), Synaptobrevin 49-93, and 0.1 mM EGTA together for 5 hours at 37 °C. For samples with VSyt1 liposomes or with WT SNAP-25, these reagents were mixed together for 24 hours at 4 °C. Various combinations of the proteins listed above, as well as 2.5 mM $MgCl_2$ and 2 mM ATP, were added to the pre-formed trans-SNARE complex and incubated for 5 minutes at 37 °C. An emission scan was then collected (excitation 468 nm, emission from 490 nm to 700 nm) to detect how much trans-SNARE complex was formed. Two μM αSNAP and 0.4 μM NSF were then added to each reaction and allowed to incubate for 5 minutes at 37 °C to disassemble the trans-SNARE complex. A second wavelength scan was then collected to determine how much of the complex was disassembled. All experiments were repeated at least 3 times with a single preparation and the results were verified in multiple experiments with different preparations. For some control experiments, ATPγS (2 mM) was used instead of ATP, or Mg^{2+} was replaced with EDTA (1 mM).

Cryo-electron microscopy

Samples of pre-formed trans-SNARE complexes between V- and T-liposomes were prepared by incubating them with Syb49-93 for five hours at 37 °C as for the assays used to measure protection against disassembly by NSF-αSNAP. Cryo-EM grids were prepared by applying 3 μL of the sample solution to a negatively glow discharged Lacey carbon copper

grid (200-mesh; Electron Microscopy Sciences) and blotted for 4.0 s under 100% humidity at 4 ^{o}C before plunge-freezing in liquid ethane using a Mark IV Vitrobot (FEI). Micrographs were acquired on a Talos Arctica microsope (FEI) operated at 200 kV with a K2 Summit direct electron detector (Gatan). A nominal magnification of 11,000 was used for imaging, and 20 dose-fractionation frames were recorded over a 10 s exposure at a dose rate of 2.1 electrons/Å^2/s for each micrograph. Motion correction was performed using the MotionCorr2 program (Zheng et al., 2017).

2.4 Results

A sensitive assay to monitor trans-SNARE complex assembly and disassembly

In order to investigate the factors that influence trans-SNARE complex assembly and disassembly, membrane fusion must be prevented to avoid the conversion of trans-SNARE complexes into cis complexes that are well known to be disassembled by NSF-αSNAP (Sollner et al. 1993a). To set up a trans-SNARE complex assembly assay without interference from membrane fusion, we used a similar approach to that described recently by Yavuz et al. 2018, which was published during the course of this work and used a mutation at the C-terminus of the synaptobrevin SNARE motif to prevent C-terminal assembly of the SNARE complex. For our assay, we designed a SNAP-25 mutant bearing two single residue substitutions (M71D,L78D) that replace buried hydrophobic residues with negatively charged residues at the C-terminus of the SNARE four-helix bundle (Figure 2.1A), and thus are also expected to strongly hinder C-terminal zippering of the SNARE complex. To verify this expectation, we used a membrane fusion assay that simultaneously measures lipid and

content mixing between synaptobrevin-containing liposomes and syntaxin-1-SNAP-25-containing liposomes in the presence of NSF, αSNAP, Munc18-1 and a fragment containing the C_1, C_2B, MUN and C_2C domains of Munc13-1 (Liu et al. 2016, Liu et al. 2017). This fragment, which we refer to as $C_1C_2BMUNC_2C$, spans the entire highly conserved C-terminal region of Munc13-1 and is sufficient to efficiently rescue neurotransmitter release in Munc13-1/2 DKO neurons (Liu et al. 2016). As expected, we observed highly efficient, Ca^{2+}-dependent membrane fusion in experiments performed with wild type (WT) SNAP-25; however, content mixing was abolished and lipid mixing was very inefficient when SNAP-25m was used in the assays instead of WT SNAP-25 (Figures 2.1B,C), demonstrating that the M71D,L78D mutation in SNAP-25 indeed prevents membrane fusion.

To test for formation of trans-SNARE complexes, we developed a FRET assay based on attachment of donor (Alexa488) and acceptor (tetramethylrhodamine, TMR) fluorescent probes on single-cysteine mutants of full-length synaptobrevin (L26C) and syntaxin-1 (S186C), respectively (all native cysteines were mutated to serine or hydrophobic residues). Residues L26 of synaptobrevin and S186 of syntaxin-1 were chosen to place the fluorescent probes because they closely precede the N-termini of the SNARE motifs in the four-helix bundle (Sutton et al. 1998), i.e. residue 29 of synaptobrevin and 190 of syntaxin-1 (Figure 2.1A). Hence, SNARE complex assembly is not expected to be perturbed by attachment of fluorescent probes to these residues but should bring the fluorescent probes into close proximity for efficient FRET, while disassembly by NSF-αSNAP should eliminate the FRET (Figure 2.2A). Attachment of fluorescent probes to residue 26 of synaptobrevin and 186 of syntaxin-1 is also expected to have no effect on binding of both proteins to NSF-αSNAP,

complexin-1, synaptotagmin-1 or Munc18-1 based on the three-dimensional structural information available on the 20S complex formed by NSF, αSNAP and the SNAREs (Zhao et al. 2015), on the complexin-SNARE complex (Chen et al. 2002), on three synaptotagmin-1-SNARE complexes (Brewer et al. 2015, Zhou et al. 2015, Zhou et al. 2017), on the Munc18-1-closed syntaxin-1 complex (Misura et al. 2000), and on the vacuolar Vps33-Nyv1 complex (Baker et al. 2015), which most likely provides a reliable model for the homologous Munc18-1-synaptobrevin complex (Sitarska et al. 2017). Since in the experiments described below we relied on the donor fluorescence emission to monitor FRET, we tested whether the emission spectrum of liposomes containing Alexa488-synaptobrevin is affected by various proteins used in this study, including Munc18-1, Munc13-1 C_1C_2BMUNC_2C, NSF, αSNAP, complexin-1 and a soluble fragment of synaptotagmin-1 spanning the two C_2 domains that form most of its cytoplasmic region (C_2AB) and include its Ca^{2+}-binding sites (Fernandez et al. 2001, Sutton et al. 1995, Ubach et al. 1998). None of these proteins substantially affected the fluorescence spectrum except for a slight increase in fluorescence caused by Munc13-1 C_1C_2BMUNC_2C (Figure 2.2-figure supplement 1) that did not affect the conclusions derived from our data.

A potential problem with FRET assays to monitor trans-SNARE complex formation is that only a small subset of the SNAREs may form these complexes, leading to low FRET efficiency and hindering quantification of the degree of SNARE complex assembly (or disassembly). To maximize the amount of observable FRET based on the decrease in donor fluorescence emission intensity, we employed liposomes containing Alexa488-labeled synaptobrevin at a low protein-to-lipid (P/L) ratio (1:10,000) (V-liposomes) and used a large

excess of liposomes containing TMR-syntaxin-1 and SNAP-25m at higher P/L ratio (1:800) (T-liposomes) in our FRET assays. Mixing the V- and T-liposomes at a 1:4 ratio led to a very slow decrease in donor fluorescence intensity (Figure 2.2-figure supplement 2A) that shows that trans-SNARE complex assembly is very inefficient under these conditions, most likely because SNARE complex assembly is hindered by formation of syntaxin-1-SNAP-25m heterodimers where synaptobrevin is replaced by a second syntaxin-1 molecule, leading to a 2:1 stoichiometry (Figure 2.2A). To overcome this problem, we used a synaptobrevin peptide spanning residues 49-93 (Syb49-93), which is expected to facilitate SNARE complex formation by displacing the second syntaxin-1 molecule (Pobbati et al. 2006). Indeed, inclusion of Syb49-93 strongly accelerated the rate of decrease in donor fluorescence intensity upon mixing V- and T-liposomes (Figure 2.2-figure supplement 2A). No further decrease in FRET was observed after five hours of incubation at 37 ^{o}C, indicating that this time was sufficient to maximize the formation of trans-SNARE complexes. Cryo-electron microscopy (cryo-EM) images obtained for samples prepared under these conditions revealed well-dispersed liposomes that often exhibited close contacts with one or two other liposomes but did not form large clusters (Figure 2.2-figure supplement 3), as expected because of the use of low synaptobrevin-to-lipid ratios in the V-liposomes.

Comparison of the fluorescence emission spectrum acquired after incubating V- and T-liposomes with Syb49-93 for five hours with a control spectrum obtained by adding the spectra of separate samples of V- and T-liposomes confirmed a clear decrease in donor fluorescence, showing that efficient FRET developed as a result of trans-SNARE complex formation (Figure 2.2B, black and blue curves, respectively). The efficient FRET suggests

that most of the accessible synaptobrevin molecules were incorporated into SNARE complexes, as only half of the Alexa488-labeled synaptobrevin molecules are expected to be accessible on the surface of the liposomes. Further addition of NSF-αSNAP led to a substantial but not complete recovery of the donor fluorescence (Figure 2.2B, red curve). These results show that NSF-αSNAP disassembled a fraction of the trans-SNARE complexes (estimated to be about 50%) while the remaining complexes were resistant to NSF-αSNAP, in agreement with the results of Yavuz et al. (2018). It is worth noting that in these experiments there was a small degree of direct excitation of the large excess of acceptor probes used (see Figure 2.2-figure supplement 4A), even though the excitation wavelength corresponded to the donor. As expected, the acceptor fluorescence increased with respect to the V+T control upon incubating V- and T-liposomes for five hours, due to trans-SNARE complex formation (Figure 2.2B, black and blue curves). However, the acceptor fluorescence exhibited only a small increase upon addition of NSF-αSNAP (Figure 2.2B, red curve). This finding arises because the acceptor fluorescence is considerably affected by NSF-αSNAP, in contrast to the donor fluorescence (see below and Figure 2.5-figure supplements 2,3). Hence, the donor fluorescence provides a more reliable parameter than the acceptor fluorescence to assess the degree of trans-SNARE complex disassembly by NSF-αSNAP.

Disassembly of trans-SNARE complexes required ATP hydrolysis by NSF, as no disassembly was observed when Mg^{2+} was replaced by EDTA in the reaction, or NSF was bound to ATPγS rather than ATP (Figure 2.2C). A similar amount of disassembly was observed in parallel assays performed with WT SNAP-25 instead of SNAP-25m in the presence of ATP and Mg^{2+} (Figure 2.2-figure supplement 4B), showing that the reaction is

not affected by the M71D,L78D mutation. We also examined whether trans-SNARE complex disassembly is affected by a K122E,K163E (KE) mutation in αSNAP that impairs SNARE binding (Zhao et al. 2015) and by an F27S,F28S (FS) mutation in an N-terminal loop of αSNAP that impairs disassembly of membrane-anchored cis-SNARE complexes because it disrupts binding of αSNAP to membranes (Winter et al. 2009). Both αSNAP mutations strongly impaired the recovery of donor fluorescence observed when trans-SNARE complexes were disassembled by NSF in the presence of wild type (WT) αSNAP (compare green and red curves in Figures 2.2D,E), showing that interactions of αSNAP with both the membranes and the SNAREs are critical for trans-SNARE complex disassembly.

Interplay between NSF, αSNAP, Munc18-1, Munc13-1, synaptotagmin-1 and complexin-1 in trans-SNARE complex assembly-disassembly

Our previous reconstitution studies showing that fusion between synaptobrevin-liposomes and syntaxin-1-SNAP-25-liposomes in the presence of NSF-αSNAP requires Munc18-1 and Munc13-1 led us to propose that Munc18-1 and Munc13-1 organize trans-SNARE complex assembly in an NSF-αSNAP resistant manner (Liu et al. 2016, Ma et al. 2013). However, trans-SNARE complex assembly was not directly monitored in these studies and it was unclear whether Munc18-1 and Munc13-1 were dispensable after trans-SNARE complex assembly. The finding that trans-SNARE complexes can be disassembled by NSF-αSNAP raises the question as to whether, in addition to providing an NSF-αSNAP-resistant pathway for trans-SNARE complex assembly, Munc18-1 and Munc13-1 protect assembled trans-SNARE complexes from disassembly by NSF-αSNAP. To address this

question and also investigate the roles of synaptotagmin-1 and complexin-1 in trans-SNARE complex assembly and protection against disassembly, we performed kinetic experiments where we used our FRET assay, monitoring the decrease in donor emission fluorescence associated with trans-SNARE complex assembly in the presence of NSF-αSNAP and various combinations of Munc18-1, Munc13-1 $C_1C_2BMUNC_2C$, the synaptotagmin-1 C_2AB fragment and complexin-1. Ca^{2+} was added after 750 s to test its effects on assembly.

In the presence of Munc18-1 and Munc13-1 $C_1C_2BMUNC_2C$, we observed some slow trans-SNARE complex assembly before Ca^{2+} addition and assembly was dramatically enhanced by Ca^{2+}, while there was almost no assembly in reactions with Munc18-1 alone or Munc13-1 $C_1C_2BMUNC_2C$ alone (Figure 2.3A). Complexin-1 and synaptotagmin-1 C_2AB were unable to support trans-SNARE complex assembly in the presence of NSF-αSNAP even after Ca^{2+} addition, and did not appear to enhance the rate of trans-SNARE complex assembly supported by Munc18-1 and Munc13-1 $C_1C_2BMUNC_2C$ (Figure 2.3B). These results confirm our proposal that Munc18-1 and Munc13-1 organize trans-SNARE complex assembly in an NSF-αSNAP resistant manner based on liposome fusion assays (Liu et al. 2016, Ma et al. 2013) but note that, in these assays, fusion might ensue quickly, in a concerted fashion, upon trans-SNARE complex formation without a chance for disassembly. Because in our FRET assays of trans-SNARE complex formation fusion is prevented by the mutation in SNAP-25m, the efficient decrease in donor fluorescence observed in the presence of Ca^{2+}, Munc18-1 and Munc13-1 $C_1C_2BMUNC_2C$ (Figure 2.3A) suggests that these factors prevent disassembly of trans-SNARE complexes in addition to mediating NSF-αSNAP-resistant assembly.

The slow assembly observed in these experiments before Ca^{2+} addition suggests that Munc18-1 and Munc13-1 $C_1C_2BMUNC_2C$ also protect against disassembly in the absence of Ca^{2+}, but it is unclear whether such protection is as efficient as that occurring in the presence of Ca^{2+} because of the slow rate of Ca^{2+}-independent assembly. To overcome this problem, we performed additional assays where Ca^{2+} was added after two minutes to accelerate assembly, and EGTA was added at different time points afterwards to test whether, upon chelation of Ca^{2+}, NSF-αSNAP disassembled the trans-SNARE complexes that had been formed. Interestingly, EGTA caused some recovery of the donor fluorescence intensity that was more substantial when EGTA was added at the latter time points, when more trans-SNARE complexes were assembled, but the recovery leveled off with time (Figure 2.3C). The donor fluorescence reached a lower level at the latest time point the later EGTA was added, showing that we did not reach equilibrium in these assays. Nevertheless, these data do suggest that Munc18-1 and Munc13-1 protect trans-SNARE complexes from disassembly by NSF-αSNAP in the absence of Ca^{2+}, and that such protection is enhanced in the presence of Ca^{2+}. Using a similar approach, we tested whether the synaptotagmin-1 C_2AB or complexin-1 protect against the disassembly of trans-SNARE complexes observed upon addition of EGTA. Including complexin-1 completely prevented such disassembly, whereas synaptotagmin-1 C_2AB had no effect (Figure 2.3D). Note that complexin-1 seemed to enhance the assembly rate in these assays, in contrast to those of Figure 2.3B; thus, it is unclear from these data whether complexin-1 assists in assembly.

The use of the soluble synaptotagmin-1 C_2AB fragment allowed us to directly compare the assembly and disassembly of trans-SNARE complexes in the absence and

presence of the synaptotagmin-1 C_2 domains with the same V-liposomes, but in vivo synaptotagmin-1 is anchored on synaptic vesicles. To investigate how membrane anchoring of synaptotagmin-1 influences trans-SNARE complex assembly-disassembly, we performed FRET experiments analogous to those described above but using liposomes that contained the same low P/L ratio of Alexa488-labeled synaptobrevin (1:10,000) and synaptotagmin-1 incorporated at a 1:1,000 P/L [comparable to physiological ratios for sybaptotagmin-1; (Takamori et al. 2006)] (referred to below as VSyt1-liposomes). Trans-SNARE complex formation between VSyt1- and T-liposomes was again stimulated strongly by the Syb49-93 peptide (Figure 2.2-figure supplement 2B) and fluorescence spectra acquired after a long incubation with Syb49-93 revealed efficient formation of trans-SNARE complexes, while addition of NSF-αSNAP disassembled about 55% of these complexes (Figure 2.2-figure supplement 4C), similar to the results obtained with V-liposomes (Figure 2.2B).

No trans-SNARE complex assembly between VSyt1- and T-liposomes was observed in kinetic experiments performed in the presence of NSF-αSNAP together with Syb49-93, Syb49-93 plus complexin-1, Munc18-1 alone or Munc13-1 alone (Figure 2.3E). However, considerable trans-SNARE complex assembly was observed in the presence of Munc18-1 and Munc13-1 C_1C_2BMUNC_2C, which was strongly accelerated by Ca^{2+} (Figure 2.3E, red trace). These results show again that Munc18-1 and Munc13-1 C_1C_2BMUNC_2C are critical for trans-SNARE complex assembly in the presence of NSF-αSNAP, as observed in the experiments performed with V- and T-liposomes (Figure 2.3A,B). Interestingly, Ca^{2+}-independent assembly was more efficient with the VSyt1-liposomes than with V-liposomes, suggesting that membrane-anchored synaptotagmin-1 facilitates the NSF-αSNAP-resistant

assembly mediated by Munc18-1 and Munc13-1 $C_1C_2BMUNC_2C$. To test whether, in addition, membrane anchored synaptotagmin-1 helps to protect trans-SNARE complexes once they are formed, we again performed kinetic assays where we added Ca^{2+} shortly after mixing the VSyt1- and T-liposomes, and EGTA was added afterwards at different time points. We again observed partial recovery of the donor fluorescence intensity upon EGTA addition (Figure 2.3F), similar to the results obtained with V- and T-liposomes (Figure 2.3C). These results indicate that membrane-anchored synaptotagmin-1 does not help to protect trans-SNARE complexes against disassembly by NSF-αSNAP once they are formed.

In parallel experiments including complexin-1, no donor fluorescence recovery was observed when EGTA was added, showing again that complexin-1 protects against disassembly, and the overall efficiency of assembly was higher (Figure 2.3F). It is also worth noting that, in our standard assembly assays where Ca^{2+} was added at 750 s, Ca^{2+}-independent assembly was slower in the presence of complexin-1 than in its absence, but did not appear to level off at this time, as did the reaction without complexin-1 (Figure 2.3E, red and blue curves). Indeed, at longer time periods Ca^{2+}-independent assembly was more efficient in the presence of complexin-1 even though it was lower in the beginning (Figure 2.3-figure supplement 1). These results suggest that, in the absence of Ca^{2+}, complexin-1 partially inhibits assembly of trans-SNARE complexes between VSyt1- and T-liposomes but increases the overall assembly efficiency because it protects trans-SNARE complexes against disassembly by NSF-αSNAP, which was further supported by additional experiments described below.

The substantial amount of Ca^{2+}-independent trans-SNARE complex assembly between VSyt1- and T-liposomes observed in our FRET assays in the presence of NSF-αSNAP, Munc18-1 and Munc13-1 $C_1C_2BMUNC_2C$ contrasts with the absence of content mixing that we commonly observed in fusion assays performed with V- or VSyt1-liposomes using a synaptotabrevin-to-lipid ratio of 1:500 and incorporating WT SNAP-25 in the T-liposomes (Figure 2.1C and Liu et al., 2016). To verify the latter result with the same synaptobrevin density used for the trans-SNARE complex assembly assays, we performed fusion assays using VSyt1-liposomes with the same synaptobrevin-to-lipid density (1:10,000). We did not observe any fusion in the absence of Ca^{2+} while lipid and content mixing were efficient but slow upon Ca^{2+} addition (Figure 2.3-figure supplement 2), in contrast with both the substantial Ca^{2+}-independent trans-SNARE complex assembly and the fast Ca^{2+}-dependent assembly observed in our FRET assays (Figure 2.3E). These data clearly show that trans-SNARE complex assembly does not necessarily lead to membrane fusion under these conditions, likely because fusion is controlled not only by the SNAREs but also by Munc18-1, Munc13-1 and synaptotagmin-1.

Multiple factors stabilize trans-SNARE complexes against disassembly by NSF-αSNAP

The kinetic assays of Figure 2.3 show how different factors influence trans-SNARE complex assembly in the presence of NSF-αSNAP and provide some information on which of these factors protect trans-SNARE complexes against disassembly. However, since only a fraction of trans-SNARE complexes formed by SNAREs alone are disassembled by NSF-αSNAP (Figure 2.2B), it is plausible that the absence of disassembly during our kinetic

assays arises from formation of NSF-αSNAP-resistant trans-SNARE complexes, rather than because the various proteins actively protect against disassembly. To gain further insights into whether Munc18-1, Munc13-1, synaptotagmin-1 and complexin-1 can prevent disassembly of trans-SNARE complexes by NSF-αSNAP, we performed similar kinetic assays where trans-SNARE complex assembly between V- and T-liposomes was monitored by FRET in the presence of various combinations of Munc18-1, Munc13-1 C_1C_2BMUNC_2C, synaptotagmin-1 C_2AB and complexin-1, but adding NSF-αSNAP at the end of the reaction, rather than the beginning. For experiments with complexin-1 and synaptotagmin-1 C_2AB, we included the Syb49-93 peptide to facilitate trans-SNARE complex assembly, but the peptide was not included for experiments with Munc18-1 and Munc13-1 C_1C_2BMUNC_2C because these proteins presumably can overcome at least in part the inhibition arising from formation of 2:1 syntaxin-1-SNAP-25 heterodimers (Ma et al. 2011, Ma et al. 2013).

The rate of trans-SNARE complex assembly was similar in assays started in the absence of Ca^{2+} with or without synaptotagmin-1 C_2AB, and the recovery of donor fluorescence upon addition of NSF-SNAP was also comparable (Figure 2.4A, green and black curves), showing that C_2AB does not alter assembly or disassembly in the absence of Ca^{2+}. However, assembly was dramatically accelerated by C_2AB in the presence of Ca^{2+} (Figure 2.4A, blue curve), likely because C_2AB can bridge two membranes together (Arac et al. 2006), and addition of NSF-αSNAP led to only a small amount of donor fluorescence recovery, suggesting that Ca^{2+}-bound C_2AB markedly protected trans-SNARE complexes against disassembly (but see below). Complexin-1 accelerated trans-SNARE complex assembly (Figure 2.4A, red curve), consistent with previous results (Diao et al. 2013), and

appeared to partially prevent disassembly by NSF-αSNAP, but it was difficult to quantitate protection with this approach because of a small amount of photobleaching occurring during acquisition of the kinetic traces. The contrast of these results with those of Figure 2.3B most likely arises because syntaxin-1-SNAP-25m heterodimers constitute the starting point for trans-SNARE complex assembly facilitated by complexin-1 and synaptotagmin-1 C_2AB, but this pathway is blocked in the presence of NSF-αSNAP because they disassemble the heterodimers.

Munc13-1 C_1C_2BMUNC_2C alone or Munc18-1 alone were unable to promote trans-SNARE complex assembly, but together they did mediate trans-SNARE complex assembly that was slow in the absence of Ca^{2+} and was strongly accelerated upon Ca^{2+} addition (Figure 2.4B). Addition of NSF-αSNAP consistently led to a slight further decrease in donor fluorescence intensity (Figure 2.4B, red curve), supporting the notion that that Munc18-1 and Munc13-1 C_1C_2BMUNC_2C protect against trans-SNARE complex disassembly by NSF-αSNAP, and suggesting that in fact they cooperate with NSF-αSNAP in formation of trans-SNARE complexes (see below). This notion is further supported by the observation that trans-SNARE complex assembly was more efficient in the experiments performed with Munc18-1 and Munc13-1 C_1C_2BMUNC_2C when NSF-αSNAP were present from the beginning (Figure 2.3A, red curve). These results most likely arise because, in the former experiments, Munc18-1 must displace the SNAP-25m bound to syntaxin-1 in the T-liposomes to initiate the Munc18-1-closed syntaxin-1 pathway. Such displacement is slow and is accelerated when NSF-αSNAP are added from the beginning because they disassemble the syntaxin-1-SNAP-25m heterodimers, facilitating binding of Munc18-1 to

closed syntaxin-1 and initiating the NSF-αSNAP-resistant pathway of trans-SNARE complex assembly.

We also performed assays where we monitored formation of trans-SNARE complexes between VSyt1- and T-liposomes, including Syb49-93 to facilitate assembly and adding NSF-αSNAP at the end to test for disassembly. We observed similar rates of assembly and similar amounts of disassembly in the absence and presence of Ca^{2+} (Figure 2.4C), which again indicates that synaptotagmin-1 does not protect against disassembly and contrasts with the results obtained with V- and T-liposomes in the presence of synaptotagmin-1 C_2AB (Figure 2.4A; see discussion). Including complexin-1 decreased the assembly rate but enhanced the overall efficiency of assembly and strongly hindered disassembly of trans-SNARE complexes by NSF-αSNAP (Figure 2.4C, red curve), in correlation with the results obtained in kinetic experiments performed with NSF-αSNAP from the beginning (Figures 2.3E,F, Figure 2.3-figure supplement 1). We did not pursue these kinetic experiments further because, although they suggested that Munc18-1, Munc13-1, synaptotagmin-1 and complexin-1 have differential abilities to protect trans-SNARE complexes against disassembly NSF-αSNAP, it is difficult to quantify these abilities from these assays because of the different extent of trans-SNARE complex assembly under the various conditions, because of a small amount of photobleaching occurring during the experiments, and because it is unclear to what extent trans-SNARE complexes that are intrinsically resistant to NSF-αSNAP were formed under the various conditions.

To overcome these problems and have a common benchmark that can give a quantitative idea of the protecting activity of the various proteins, we again followed the

approach of pre-forming trans-SNARE complexes by incubation of V- and T-liposomes (1:4 ratio) in the presence of Syb49-93 for five hours, after which there are no further changes in the fluorescence spectrum [note that Syb49-93 is released from the syntaxin-1-SNAP-25 complexes upon trans-SNARE complex assembly (Yavuz et al. 2018) and hence should not interfere in the measurement of protection against disassembly]. Different aliquots of the same reaction mixture where then incubated with synaptotagmin-1 C_2AB, complexin-1, Munc18-1 and Munc13-1 $C_1C_2BMUNC_2C$ in different combinations, with or without Ca^{2+} whenever C_2AB and/or $C_1C_2BMUNC_2C$ were present. Fluorescence emission spectra of the resulting samples were acquired before and after addition of NSF-αSNAP to quantify the changes in FRET caused by NSF-αSNAP (Figure 2.5A and Figure 2.5-figure supplement 1). We also acquired control fluorescence spectra of separate samples where we preformed trans-SNARE complexes between V-liposomes that contained the donor probe and T-liposomes lacking the acceptor probe (referred to as V*+T), as well as analogous trans-SNARE complexes that contained the acceptor probe but not the donor probe (V+T*); both sets of liposomes were also incubated with various proteins and fluorescence spectra were acquired before and after addition of NSF-αSNAP (Figure 2.5-figure supplements 2,3). The control spectra showed that none of the proteins substantially affect the donor fluorescence, except for a slight but consistent increase caused by Munc13-1 $C_1C_2BMUNC_2C$, while NSF-αSNAP did cause a considerable decrease of the acceptor fluorescence in the V+T* controls that was prevented by Munc18-1. Hence, we focused on the donor fluorescence to quantitate the protection against disassembly.

The fluorescence spectra obtained after incubation of the preformed trans-SNARE complexes with different combinations of Munc18-1, Munc13-1 $C_1C_2BMUNC_2C$, synaptotagmin-1 C_2AB and complexin-1 before addition of NSF-αSNAP were very similar for all samples, indicating that the amount of trans-SNARE complexes was not affected by the incubations. However, substantial differences were observed in the donor emission intensities in the spectra obtained after addition of NSF-αSNAP (Figure 2.5-figure supplement 1), indicating different extents of SNARE complex disassembly. To derive a quantitative idea of how much the different combinations of proteins protect against disassembly, we calculated the ratio *r* between the donor fluorescence intensity after adding NSF-αSNAP and that before addition of NSF-αSNAP. This ratio was 1.30 for control experiments with no additions before disassembly with NSF-αSNAP (Figure 2.5B). This value was variable in experiments performed with different liposome preparations and depended on the extent of trans-SNARE complex assembly achieved, but the relative changes in *r* values obtained in the presence of different factor were comparable for the different preparations.

The *r* values measured showed that Ca^{2+}-free synaptotagmin-1 C_2AB provided no protection but Ca^{2+}-bound C_2AB prevented disassembly considerably. Complexin-1 afforded similar protection as Ca^{2+}-bound C_2AB. In experiments with Munc13-1 $C_1C_2BMUNC_2C$ alone in the absence or presence of Ca^{2+}, *r* was slightly larger than that observed in the control with no additions, which can be attributed to the slight increase in donor fluorescence caused by Munc13-1 $C_1C_2BMUNC_2C$ on the V*+T control (Figure 2.5-figure supplement 2C) and shows that there is no protection against disassembly under these conditions. The *r*

value observed with Munc18-1 alone was slightly smaller than 1.3; although the difference with respect to the controls with no additions was not statistically significant, there was a significant difference between the (smaller) *r* value observed in experiments with Munc18-1 and Munc13-1 $C_1C_2BMUNC_2C$ in the absence of Ca^{2+} and the control with no additions. A dramatic decrease in *r* was observed when Ca^{2+} was included with Munc18-1 and Munc13-1 $C_1C_2BMUNC_2C$. Adding complexin-1 or of C_2AB together with Munc18-1 and Munc13-1 $C_1C_2BMUNC_2C$, with or without Ca^{2+}, also decreased the corresponding *r* values, and the smallest *r* was observed in experiments that included all these components (Figure 2.5B), showing almost complete protection under these conditions (Figure 2.5A). Overall, these results support the notion that Munc18-1 and Munc13-1 $C_1C_2BMUNC_2C$ can protect trans-SNARE complexes against disassembly to a moderate extent in the absence of Ca^{2+} and that such protection is increased by Ca^{2+}, in correlation with the results of the kinetic assays (Figure 2.3). These data also indicate that synaptotagmin-1 C_2AB and particularly complexin-1 provide additional protection against disassembly.

To investigate how protection of trans-SNARE complexes is influenced by membrane-anchored synaptotagmin-1, we performed additional experiments where we preformed trans-SNARE complexes between VSyt1- and T-liposomes in the presence of Syb49-93, and we incubated the resulting samples with different combinations of Munc18-1, Munc13-1 $C_1C_2BMUNC_2C$, complexin-1 and Ca^{2+} before adding NSF-αSNAP to test for disassembly. Munc18-1, Munc13-1 $C_1C_2BMUNC_2C$, complexin-1 and Ca^{2+} did not significantly alter the fluorescence spectra acquired before addition of NSF-αSNAP, but markedly affected the spectra obtained after such addition (black and red curves,

respectively, in the different panels of Figure 2.5-figure supplement 4). The ratio *r* between the donor fluorescence emission intensities observed after and before addition of NSF-αSNAP without other proteins was 1.46 and, surprisingly, addition of Ca^{2+} did not lead to protection against disassembly (Figure 2.5C), which contrasts with the protection provided by Ca^{2+}-bound synaptotagmin-1 C_2AB in experiments with V-liposomes (Figure 2.5B). Munc18-1 alone again appeared to have a tendency to prevent disassembly, compared to the control with no additions, but the difference was not statistically significant, and Munc13-1 $C_1C_2BMUNC_2C$ alone provided no protection. Together, Munc18-1 and Munc13-1 $C_1C_2BMUNC_2C$ did provide moderate protection in the absence of Ca^{2+} and strong protection in its presence. Interestingly, complexin-1 alone afforded robust protection against disassembly (Figure 2.5C) that appeared to be stronger than that observed with V- and T-liposomes (Figure 2.5B), suggesting that membrane-anchored synaptotagmin-1 can cooperate with complexin-1 in protecting trans-SNARE complexes against disassembly. Maximal protection of the trans-SNARE complexes between VSyt1- and T-liposomes against disassembly by NSF-αSNAP was again observed when all components (Munc18-1, Munc13-1 $C_1C_2BMUNC_2C$, complexin-1 and Ca^{2+}) were included (Figure 2.5C).

Disassembly of cis-SNARE complexes

To further investigate the functional interplay between NSF, αSNAP, Munc18-1, Munc13-1, complexin-1 and synaptotagmin-1 in the SNARE complex assembly-disassembly cycle, we performed kinetic assays where we analyzed the assembly and disassembly of cis-SNARE complexes mixing V-liposomes containing Alexa488-synaptobrevin with SNAP-

25m and a soluble fragment spanning the cytoplasmic region of syntaxin-1 (residues 2-253) labeled with TMR at residue 186. Cis-SNARE complex assembly was efficient in the presence of Syb49-93 but was abolished if NSF-αSNAP were included from the beginning (Figure 2.6A, dark and light gray curves, respectively). Munc18-1 plus Munc13-1 C_1C_2BMUNC_2C or complexin-1 plus synaptotagmin-1 C_2AB, or the four proteins together, were unable to support cis-SNARE complex formation in the presence of NSF-αSNAP even upon addition of Ca^{2+} (Figure 2.6A). These results are in stark contrast to the efficient formation of trans-SNARE complexes observed in the presence of NSF-αSNAP when Munc18-1 and Munc13-1 C_1C_2BMUNC_2C were included (Figure 2.3A) and provide a dramatic demonstration of how the apposition of two membranes tilts the balance in favor of assembly, whereas disassembly dominates on a single membrane.

In experiments performed initially without NSF-αSNAP, cis-SNARE complex assembly was strongly stimulated by complexin-1 or by Ca^{2+}-bound synaptotagmin-1 C_2AB, but most of the donor fluorescence was recovered upon addition of NSF-αSNAP at the end of the reaction due to disassembly of the cis-SNARE complexes (Figure 2.6B). Munc18-1 and the Munc13-1 C_1C_2BMUNC_2C fragment were unable to support cis-SNARE complex assembly even after addition of Ca^{2+} (Figure 2.6C, red curve), and they partially inhibited cis-SNARE complex assembly catalyzed by Syb49-93, without protecting against disassembly upon addition of NSF-αSNAP (Figure 2.6C, gray curve). We also performed additional experiments where we preformed cis-SNARE complexes in the presence of Syb49-93 and tested whether incubation of these complexes with Munc18-1, Munc13-1, synaptotagmin-1 C_2AB, complexin-1 and Ca^{2+} for five minutes protected against

disassembly by NSF-αSNAP, but disassembly was as efficient as a control experiment where the four proteins were not added (Figure 2.6D). This result was somewhat surprising because complexin-1 was previously shown to partially protect against cis-SNARE complex disassembly by NSF-αSNAP (Choi et al. 2016, Winter et al. 2009). To test for potential effects arising from different relative concentrations of complexin-1 versus αSNAP, or perhaps from the mutation in SNAP-25m, we performed additional experiments where we incubated pre-formed cis-SNARE complexes with different concentrations of complexin-1 or we replaced SNAP-25m with WT SNAP-25, but no protection was observed in any of these experiments (Figure 2.6-figure supplement 1). It is plausible that the differences observed with the results of Winter et al. (2009) and Choi et al. (2018) arose because syntaxin-1 did not include the N-terminal region containing the H_{abc} domain in both of these studies, and in the latter NSF-αSNAP might have been less active because of the absence of membranes. Regardless of this possibility, the contrast of these results with those obtained with trans-SNARE complexes shows that the existence of two apposed membranes facilitates the protection of these complexes against disassembly by NSF-αSNAP, while the topology of cis-SNARE complexes disfavors such protection.

2.5 Discussion

Extensive research has yielded a wealth of information on the mechanism of neurotransmitter release, including the notions that assembly of the trans-SNARE complex four-helix bundle between the synaptic vesicle and plasma membranes is crucial for membrane fusion, that NSF-αSNAP disassemble cis-SNARE complexes after fusion to recycle the SNAREs, and that priming of synaptic vesicles to a readily releasable state

involves formation of partially assembled trans-SNARE complexes, which is organized by Munc18-1 and Munc13-1 in an NSF-αSNAP-resistant manner. However, the nature of the primed state of synaptic vesicles remained enigmatic and the recent finding that NSF-αSNAP also disassemble trans-SNARE complexes (Yavuz et al. 2018) raised the question of how trans-SNARE complexes are protected to prevent vesicle de-priming. More generally, it was unclear how the functions of Munc18-1 and Munc13-1, as well as those of other proteins that have been implicated in vesicle priming such as synaptotagmin-1 and complexin-1, are related to roles in promoting trans-SNARE complex assembly and/or in preventing their disassembly by NSF-αSNAP. The results presented here now show that Munc18-1 and Munc13-1 are crucial to form trans-SNARE complexes in the presence of NSF-αSNAP, as expected, and that in addition they protect trans-SNARE complexes against disassembly. Complexin-1 does not appear to play a role in NSF-αSNAP-resistant trans-SNARE complex assembly, but strongly protects against disassembly, while synaptotagmin-1 may play a role in both assembly and protection. These results suggest that Munc18-1, Munc13-1, synaptotagmin-1 and complexin-1 all contribute to maintaining the primed state of synaptic vesicles, perhaps forming macromolecular assemblies with trans-SNARE complexes that constitute the core of the primed state of synaptic vesicles.

Our FRET data showing that trans-SNARE complexes can be disassembled by NSF-αSNAP agree with recent results obtained by Yavuz et al. (2018) using a similar approach, and with earlier studies of yeast vacuolar fusion showing that Sec18-Sec17 disassemble trans-SNARE complexes (Xu et al. 2010). However, our FRET assays and those of Yavuz et al. (2018) also show that a substantial fraction of trans-SNARE complexes is resistant to

disassembly by NSF-αSNAP, which might explain the finding that NSF-αSNAP inhibited lipid mixing between synaptobrevin- and syntaxin-1-SNAP-25 liposomes if added from the beginning but not if added after the liposomes were pre-incubated at low temperature (Weber et al. 2000). NSF-αSNAP resistant, tightly docked liposomes were attributed to the formation of large, flat interfaces between the liposomes (Yavuz et al. 2018). Our cryo-EM images also revealed extended interfaces between liposomes but the interfaces were generally smaller (Figure 2.2-figure supplement 3), perhaps because we used a much lower synaptobrevin-to-lipid ratio. It is unclear whether such extended interfaces are physiologically relevant, as inclusion of other key components of the release machinery favors the formation of point contacts between liposomes over extended interfaces (Gipson et al. 2017). These observations emphasize the difficulty of reconstituting with a few components the steps that lead to synaptic vesicle fusion, particularly the formation of the primed state, because of the metastable, transient nature of this state and because off-pathway, kinetically trapped states can be formed in the absence of some components that are important for vesicle priming [e.g. RIM and CAPS in our assays, see (Rizo et al. 2012b)]. We speculate that the population of trans-SNARE complexes that can be disassembled by NSF-αSNAP in our assays is more closely related to the partially assembled trans-SNARE complexes present in primed synaptic vesicles. This proposal is supported by electrophysiological studies showing that readily-releasable vesicles can be de-primed and that de-priming is prevented by N-ethylmaleimide, an agent that inactivates NSF (He et al. 2017). Although N-ethylmaleimide could potentially alter other proteins in vivo, the correlation with the finding that trans-SNARE complexes can be disassembled by NSF-αSNAP in vitro strongly supports the notion that de-priming is

mediated by NSF. Since NSF-SNAPs can also disassemble syntaxin-1-SNAP-25 heterodimers (Hayashi et al. 1995), there is little doubt that the cytoplasm provides an environment that favors SNARE complex disassembly in general, and hence that trans-SNARE complexes need to be protected to maintain vesicles primed.

The decreases in the RRP of primed vesicles observed in mice lacking Munc18-1, Munc13-1, complexins or synaptotagmin-1/7 (Bacaj et al. 2015, Chang et al. 2018, Rosenmund et al. 2002, Verhage et al. 2000, Xue et al. 2010b, Yang et al. 2010) could arise because they mediate vesicle priming and/or because they protect against de-priming. With the underlying hypothesis that trans-SNARE complex assembly in our in vitro assays recapitulates, at least to some extent the process of vesicle priming, we used different types of assays to dissect the contributions of Munc18-1, Munc13-1, synaptotagmin-1 and complexin-1 to assembling trans-SNARE complexes in the presence of NSF-αSNAP and to protecting these complexes against disassembly once they are formed. Our assays that included NSF-αSNAP from the beginning clearly show that Munc18-1 and Munc13-1 C_1C_2BMUNC_2C are essential to assemble trans-SNARE complexes in the presence of NSF-αSNAP (Figures 2.3A,B,E), as expected from the results of our previous liposome fusion assays (Liu et al. 2016, Ma et al. 2013). The progressive formation of trans-SNARE complexes observed in these assays suggests that Munc18-1 and Munc13-1 C_1C_2BMUNC_2C prevent their disassembly, in addition to mediating assembly, but we could not rule out that the assembled trans-SNARE complexes are NSF-αSNAP resistant and Munc18-1 and/or Munc13-1 C_1C_2BMUNC_2C become dispensable after assembly, particularly in the absence of Ca^{2+}. The experiments where we added EGTA after allowing efficient Ca^{2+}-dependent

assembly show that at least a population of the trans-SNARE complexes formed could be disassembled by NSF-αSNAP, but a substantial amount of complexes remained assembled even after addition of EGTA (Figures 2.3C,F). These data suggest that Munc18-1 and Munc13-1 C_1C_2BMUNC_2C do protect trans-SNARE complexes against disassembly by NSF-αSNAP to some extent, and that Ca^{2+} enhances the protective activity. This conclusion was further supported by experiments where we preformed trans-SNARE complexes in the absence of NSF-αSNAP and monitored disassembled by NSF-αSNAP in the presence of Munc18-1 and Munc13-1 C_1C_2BMUNC_2C (Figures 2.5B,C).

Overall, the crucial nature of Munc18-1 and Munc13-1 C_1C_2BMUNC_2C for trans-SNARE complex assembly provides a clear explanation for the complete abrogation of synaptic vesicle priming observed in mice lacking Munc18-1 or Munc13-1/2 (Varoqueaux et al. 2002), while the finding that Munc18-1 and Munc13-1 C_1C_2BMUNC_2C protect trans-SNARE complexes against disassembly can explain the key importance of Munc18-1 and Munc13-1 to prevent de-priming of the RRP (He et al. 2017). These correlations support the physiological relevance of our in vitro results. It is also worth noting that Ca^{2+} strongly stimulates NSF-αSNAP-resistant trans-SNARE complex assembly mediated by Munc18-1 and Munc13-1 C_1C_2BMUNC_2C (Figures 2.3A,E) and enhances their ability to protect trans-SNARE complexes against disassembly (Figures 2.5B,C). These properties likely underlie at least in part the importance of Ca^{2+} binding to the Munc13 C_2B domain for facilitating release during repetitive stimulation, when there is a strong demand to rapidly refill the RRP to prevent its depletion (Shin et al. 2010).

In contrast to Munc18-1 and Munc13-1 $C_1C_2BMUNC_2C$, synaptotagmin-1 and complexin-1 are not essential to form trans-SNARE complexes in the presence of NSF-αSNAP, but they do enhance the amount of trans-SNARE complexes formed (Figure 2.3). These findings correlate with the observation that deletion of synaptotagmin-1 or complexins leads to decreases in the RRP of vesicles (Bacaj et al. 2015, Chang et al. 2018, Xue et al. 2010b, Yang et al. 2010, Xue et al. 2010a), but not as dramatic as those observed in Munc18-1 KO and Munc13-1/2 DKO neurons. Complexin-1 appeared to inhibit in the initial states of Ca^{2+}-independent trans-SNARE complex assembly between VSyt1- and T-liposomes in the presence of Munc18-1, Munc13-1 $C_1C_2BMUNC_2C$ and NSF-αSNAP, but increased the overall efficiency of assembly at longer time scales (Figures 2.3E, Figure 2.3-figure supplement 1). Moreover, complexin-1 clearly protected against disassembly by NSF-αSNAP in analogous experiments where EGTA was added after efficient Ca^{2+}-dependent assembly (Figures 2.3D,F), and in experiments where NSF-αSNAP were added after trans-SNARE complexes were pre-formed (Figure 2.5B,C). These results suggest that complexin-1 does not assist in synaptic vesicle priming but protects the RRP against de-priming. Conversely, membrane-anchored synaptotagmin-1 clearly accelerated Ca^{2+}-independent trans-SNARE complex assembly (Figures 2.3A,E), suggesting a role in priming, while we obtained mixed results with regard to whether synaptotagmin-1 protects trans-SNARE complexes against disassembly by NSF-αSNAP. Ca^{2+}-bound C_2AB impaired disassembly of pre-formed trans-SNARE complexes (Figure 2.5B), but this result must be examined with caution, as it may arise from excessive accumulation of C_2AB molecules at the membrane-membrane interface (Arac et al. 2006), and membrane-anchored synaptotagmin-1 did not

protect pre-formed trans-SNAREs complexes from disassembly even in the presence of Ca^{2+} (Figure 2.5C). Moreover, membrane-anchored synaptotagmin-1 did not appear to hinder disassembly when EGTA was added after Ca^{2+}-stimulated trans-SNARE complex assembly in the presence of NSF-αSNAP (Figure 2.3D,F). Nevertheless, in the absence of Ca^{2+}, C_2AB appeared to enhance the protection afforded by complexin-1 and by Munc18-1 together with Munc13-1 $C_1C_2BMUNC_2C$ and membrane-anchored synaptotagmin-1 also seemed to increase the protection provided by complexin-1 (Figure 2.5B,C).

In summary, our data suggest that Munc18-1, Munc13-1, complexin-1 and likely synaptotagmin-1 contribute to protect trans-SNARE complexes in primed synaptic vesicles from disassembly by NSF-αSNAP. Although the underlying mechanisms remain to be determined, it is worth noting that almost any protein that interacts with the SNARE four-helix bundle might compete with αSNAP for binding, as αSNAP covers much of the surface of the SNARE four-helix in the cryo-EM structure of the 20S complex formed by NSF, αSNAP and the SNAREs (Zhao et al. 2015) (Figure 2.7A). Indeed, the interactions observed in structural studies of the SNARE complex bound to complexin-1 and/or synaptotagmin-1 (Brewer et al. 2015, Chen et al. 2002, Zhou et al. 2015, Zhou et al. 2017) are incompatible with formation of the 20S complex. Given the high nanomolar affinity of complexin-1 for the SNARE complex (Pabst et al. 2002), it is not surprising that this protein can hinder formation of the 20S complex, preventing disassembly of trans-SNARE complexes. The affinities of the various binding modes that have been observed between synaptotagmin-1 and the SNARE complex are in the micromolar range in solution (Brewer et al. 2015, Zhou et al. 2015, Zhou et al. 2017), but binding could be enhanced by the localization of synaptotagmin-

1 on the vesicle membrane and by cooperativity with complexin-1 binding (Zhou et al. 2017) as well as with interactions of synaptotagmin-1 with one or two membranes (Bai et al. 2004, Brewer et al. 2015). Munc18-1 and Munc13-1 also exhibit weak interactions with SNARE complexes that are strengthened by membranes (Dulubova et al. 2007, Guan et al. 2008, Ma et al. 2011, Shen et al. 2007, Weninger et al. 2008), and could potentially compete with binding of αSNAP to the SNAREs. Munc13-1 $C_1C_2BMUNC_2C$ was recently proposed to bridge the vesicle and plasma membranes (Liu et al. 2016), which could provide an additional mechanism to protect trans-SNARE complexes against disassembly by NSF-αSNAP by imposing steric constraints that hinder formation of the 20S complex. Moreover, Ca^{2+}-binding to the Munc13-1 C_2B domain is expected to change the orientation of Munc13-1 $C_1C_2BMUNC_2C$ with respect to the plasma membrane, bringing the two membranes into closer proximity (Sitarska et al. 2017) and potentially increasing the steric constraints that impair 20S complex assembly. This model can explain why Ca^{2+} increases the ability of Munc13-1 $C_1C_2BMUNC_2C$ (together with Munc18-1) to protect trans-SNARE complexes against disassembly by NSF-αSNAP (Figure 2.5B,C).

It is interesting to note the dramatic effects that the membrane topology has on SNARE complex assembly and on protection against disassembly: Munc18-1 and Munc13-1 $C_1C_2BMUNC_2C$ mediate efficient formation of trans-SNARE complexes but not of cis-SNARE complexes in the presence of NSF-αSNAP (Figures 2.3A, 2.6A), and pre-formed trans-SNARE complexes are protected from disassembly by Munc18-1, Munc13-1 $C_1C_2BMUNC_2C$, complexin-1 and synaptotagmin-1 (Figure 2.5B,C), unlike cis-SNARE complexes (Figure 2.6D). These differences must arise from distinct balances among the

interactions of these proteins with the SNAREs and the membranes. In the cis configuration, up to four αSNAP molecules readily interact with much of the surface of the SNARE four-helix bundle (Zhao et al. 2015) and at the same time a hydrophobic N-terminal loop from all αSNAP molecules, which is known to strongly stimulate disassembly of membrane-anchored cis-SNARE complexes (Winter et al. 2009), can bind simultaneously to the membrane, likely with high cooperativity (Figure 2.7A). Interactions of αSNAP with the SNAREs and the membranes are also important for disassembly of trans-SNARE complexes by NSF-αSNAP (Figure 2.2D,E), but the geometry of the system (Figure 2.7B) is expected to hinder simultaneous binding of all αSNAP molecules to membranes, and incomplete assembly of the SNARE four-helix bundle may also limit the extent of αSNAP-SNARE interactions. Hence, NSF-αSNAP are expected to be less active in disassembling trans- than cis-SNARE complexes. Conversely, the trans-configuration favors the simultaneous binding of Munc13-1 C_1C_2BMUNC_2C to the apposed membranes, which is likely key for its activity in promoting trans-SNARE complex assembly (Liu et al. 2016) and is impossible in the cis-configuration. The protection of trans- but not cis-SNARE complexes by complexin-1 under the conditions of our experiments may arise simply because complexin-1 binds tighter to the former than NSF-αSNAP, while the opposite is true for the latter. This model also explains that under some conditions complexin-1 did hinder disassembly of cis-SNARE complexes (Choi et al. 2018, Winter et al. 2009).

The results of our experiments designed to quantitate the ability of different factors to protect against trans-SNARE complex disassembly by NSF-αSNAP (Figures 2.5B,C) are also expected to depend on the experimental conditions, including the concentrations of the

various proteins, and should thus be examined with caution. For instance, different concentrations of complexin-1 yield different levels of protection against disassembly (Figure 2.5-figure supplement 5). Moreover, other proteins that were not included in this study might also influence the protection of trans-SNARE complexes. As an example, RIMs are intrinsic components of pre-synaptic active zones that bind to the N-terminal region of Munc13-1 containing the C_2A domain (Betz et al. 2001, Dulubova et al. 2005), an interaction that is important for optimal vesicle priming (Camacho et al. 2017) and increases the local concentrations of Munc13-1 at release sites. Thus, more systematic studies of how the components of the release machinery protect trans-SNARE complexes against disassembly in vitro and against de-priming of the RRP in neurons will be required to better understand the nature of the primed state of synaptic vesicles. Based on the available data, we speculate that the core of this primed state is formed by a macromolecular assembly that includes trans-SNARE complexes, Munc18-1, Munc13-1, complexin-1 and synaptotagmin-1.

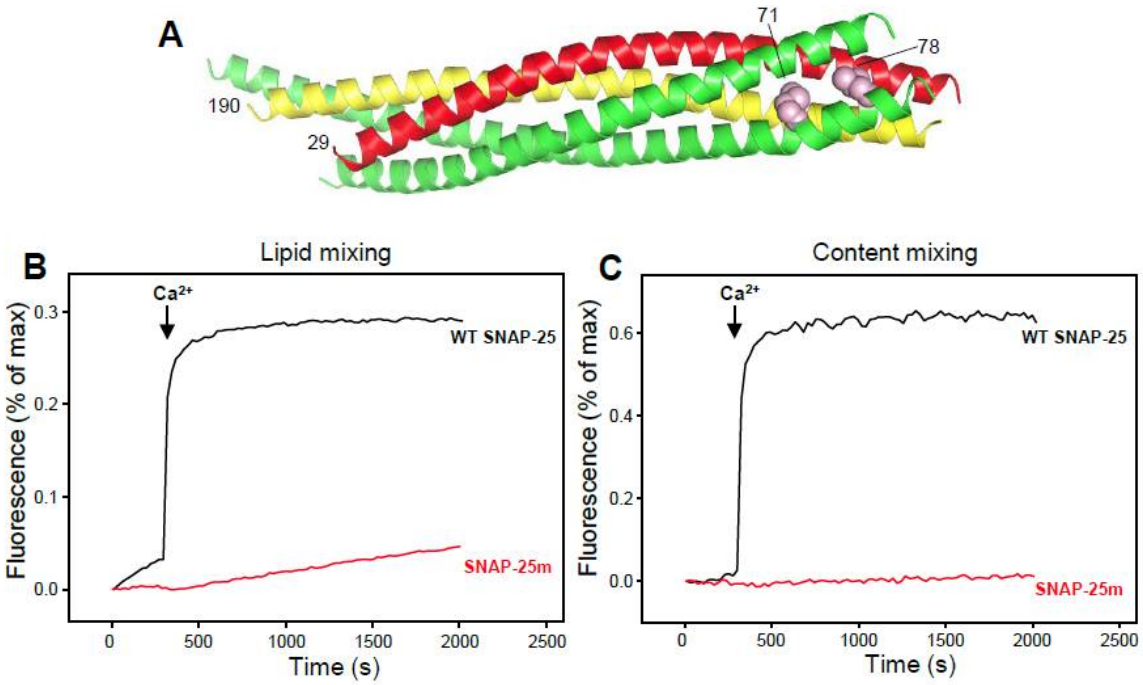

Figure 2.1. Design of a SNAP-25 mutation that abrogates its ability to support membrane fusion. (A) Ribbon diagram of the crystal structure of the SNARE complex (PDB accession code 1SFC) (Sutton et al., 1998). Synaptobrevin is red, syntaxin-1 yellow and SNAP-25 green, with the side chains of the two residues that were mutated to aspartate (M71 and L78) shown as pink spheres. Note that the side chains are pointing toward the hydrophobic interior of the four-helix bundle. Hence, mutating these residues to aspartate is expected to prevent C-terminal zippering of the SNARE complex. The residue numbers of the two mutated residues and of the N-termini of synaptobrevin and syntaxin-1 SNARE motifs are indicated. (B,C) The SNAP-25 M71D,L78D mutation abrogates membrane fusion in reconstitution assays. Lipid mixing (B) between V- and T-liposomes was monitored from the fluorescence de-quenching of Marina Blue lipids and content mixing (C) was monitored from the increase in the fluorescence signal of Cy5-streptavidin trapped in the V-liposomes caused by FRET with PhycoE-biotin trapped in the T-liposomes upon liposome fusion. The assays were performed in the presence of Munc18-1, Munc13-1 C_1C_2BMUNC_2C, NSF and αSNAP with T-liposomes that contained syntaxin-1 and wild type (WT) SNAP-25 or SNAP-25 M71D,L78D mutant (SNAP-25m). Experiments were started in the presence of 100 µM EGTA and 5 µM streptavidin, and Ca^{2+} (600 µM) was added at 300 s.

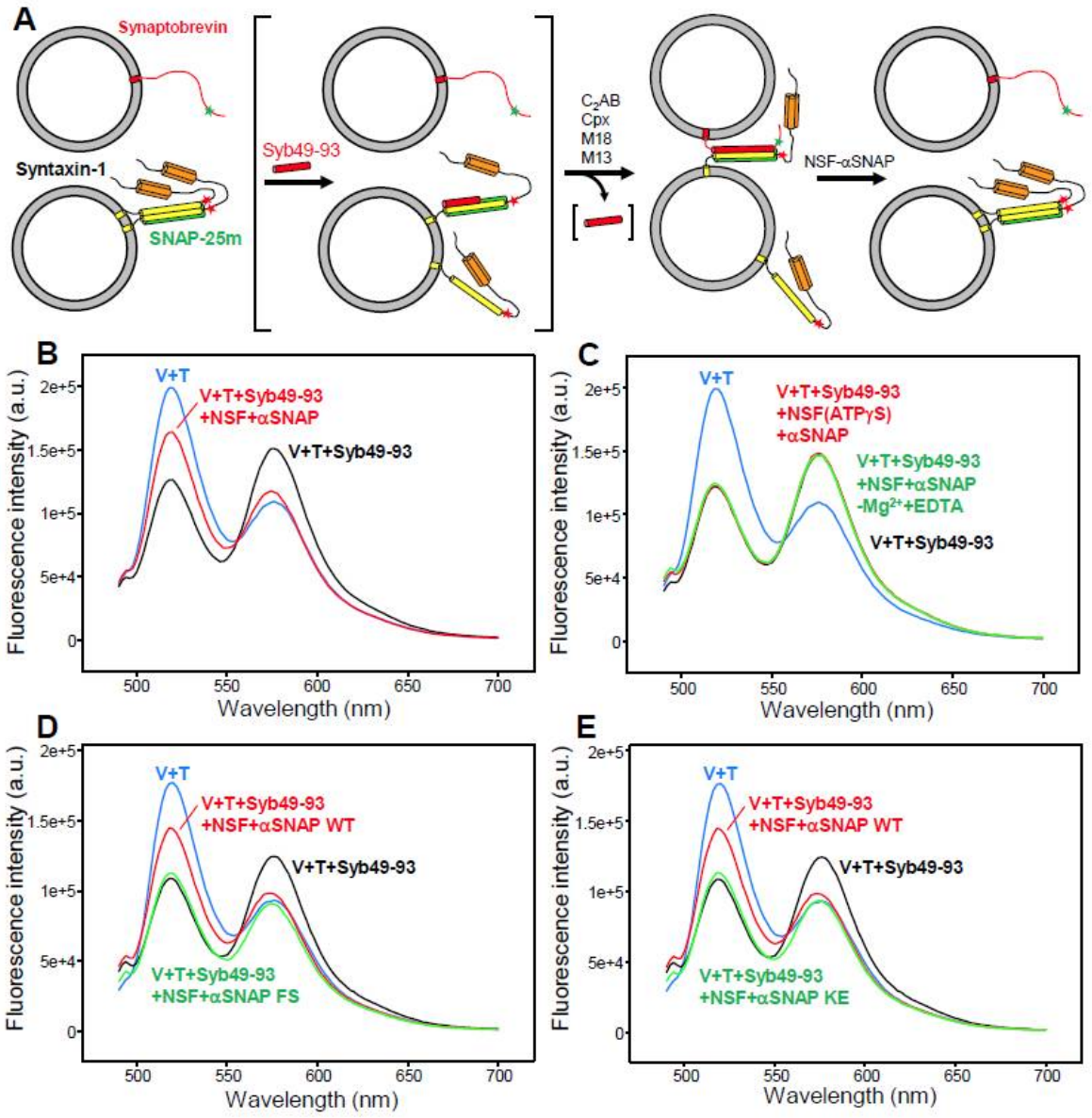

Figure 2.2. An assay to measure assembly of trans-SNARE complexes and disassembly by NSF-αSNAP. (A) Diagram illustrating the assay used to monitor trans-SNARE complex assembly and disassembly. V-liposomes containing synaptobrevin labeled with a FRET donor (Alexa488, green star) at residue 26 are mixed with T-liposomes containing SNAP-25m and syntaxin-1 labeled at residue 186 with a FRET acceptor (TMR, red star) in the presence of different factors. After monitoring the decrease in donor fluorescence intensity resulting from trans-SNARE complex formation under diverse conditions, NSF and αSNAP are added to test for disassembly of trans SNARE complexes. Synaptobrevin is red, SNAP-25m green and syntaxin-1 orange (N-terminal H_{abc} domain) and yellow (SNARE motif). Although an excess of SNAP-25m was used in preparing the syntaxin-1-SNAP-25m

liposomes, the majority of syntaxin-1-SNAP-25m complexes are expected to have a 2:1 stoichiometry such that the second syntaxin-1 SNARE molecule occupies the position of the synaptobevin SNARE motif in the SNARE four-helix bundle (bottom left diagram), hindering SNARE complex formation [see (Rizo and Sudhof, 2012)]. In some of the experiments, trans-SNARE complex assembly was facilitated by inclusion of the Syb49-93 peptide, which spans the C-terminal part of the synaptobrevin SNARE motif and displaces the second syntaxin-1 molecule from the syntaxin-1-SNAP-25m heterodimer, yielding the intermediate shown between brackets. Because Syb49-93 lacks the N-terminal half of the synaptobrevin SNARE motif, it can readily be displaced by full-length synaptobrevin to form trans-SNARE complexes (Pobbati et al., 2006). (B) Fluorescence emission spectra (excitation at 468 nm) of a mixture of V-liposomes containing Alexa488-synaptobrevin and T-liposomes containing TMR-syntaxin-1-SNAP-25m (1:4 V- to T-liposome ratio) that had been incubated for five hours with Syb49-93 (black trace), and of the same sample after adding NSF-αSNAP plus ATP and Mg^{2+} (red trace). The blue curve shows a control spectrum obtained by adding spectra acquired separately for V- and T-liposomes at the same concentrations. (C) Fluorescence emission spectra acquired under conditions similar to those of (B), with V- and T-liposomes that had been incubated with Syb49-93 before (black curve) or after addition of NSF-αSNAP plus ATP and EDTA (green curve) or NSF-αSNAP plus ATPγS and Mg^{2+} (red curve). (D,E) Fluorescence emission spectra acquired under similar conditions to those of (B), except that for the green curve WT αSNAP was replaced with the αSNAP FS (D) or KE (E) mutant. The red, black and blue curves are the same as in panel (B). All spectra were corrected for dilution caused by addition of reagents.

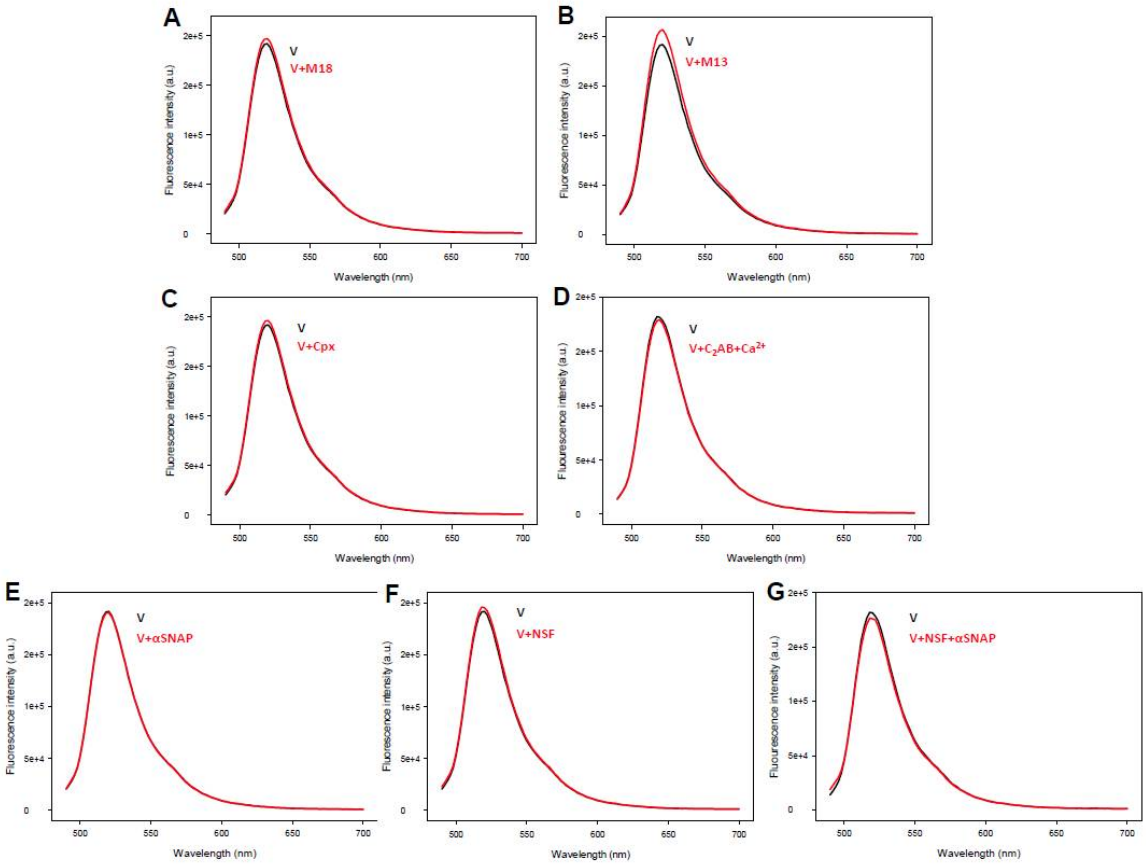

Figure 2.2- Figure supplement 1. Control experiments acquired to assess the effects of various factors on the fluorescence emission spectra of V-liposomes containing Alexa488-synaptobrevin. Spectra were acquired before (V) (black traces) or after (red traces) addition of Munc18-1 (M18), Munc13-1 $C_1C_2BMUNC_2C$ (M13), complexin-1 (Cpx), Ca^{2+}-bound synaptotagmin-1 C_2AB, NSF, αSNAP or NSF+αSNAP.

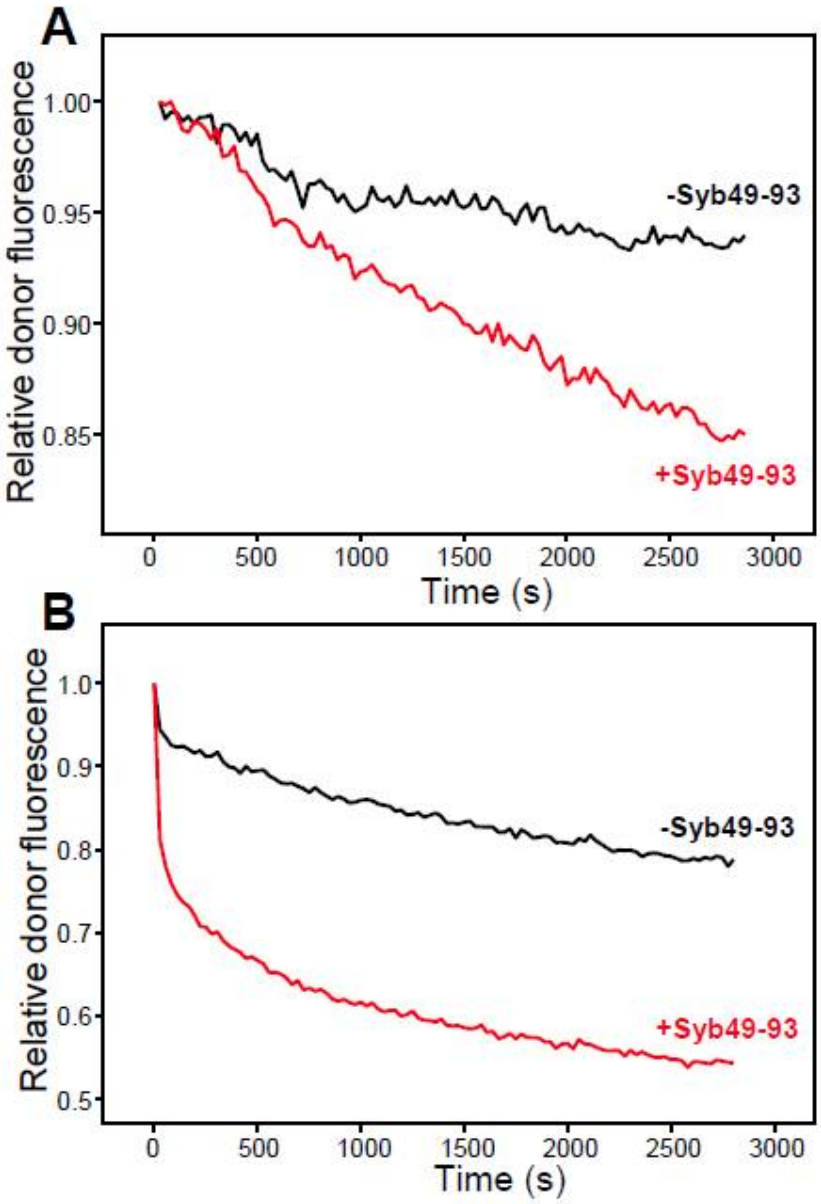

Figure 2.2- Figure supplement 2. Syb49-93 strongly accelerates trans-SNARE complex assembly. (A) Kinetic assays where the donor fluorescence emission intensity was measured to monitor trans-SNARE complex assembly as a function of time upon mixing V- and T-liposomes (1:4 ratio) in the absence (black) and presence (red) of Syb49-93. (B) Analogous experiments performed to monitor trans-SNARE complex assembly between VSyt1- and T-liposomes (1:4 ratio) in the absence (black) and presence (red) of Syb49-93.

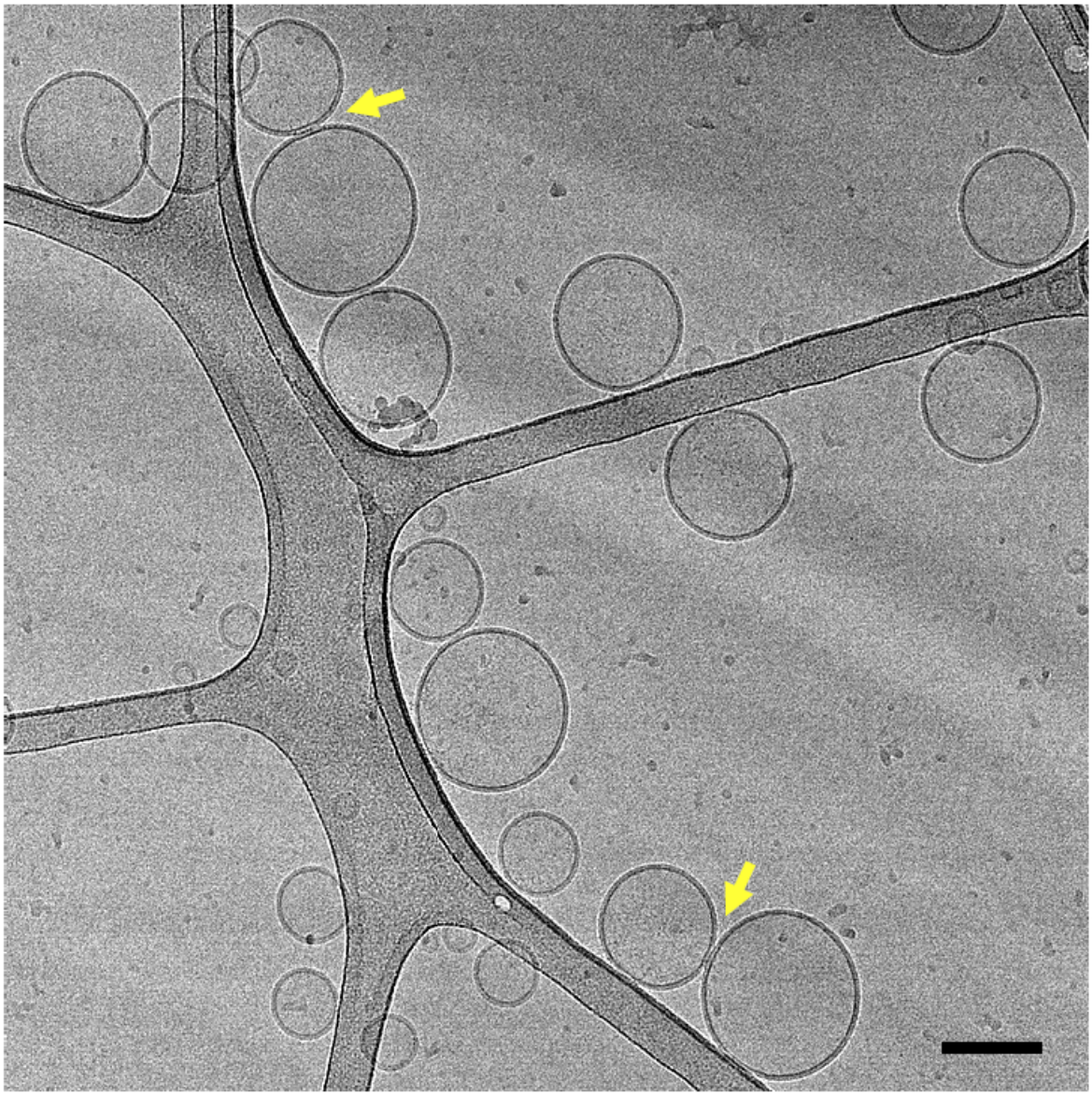

Figure 2.2- Figure supplement 3. Representative cryo-EM image of a mixture of V- and T-liposomes (1:4 ratio) that had been incubated with Syb49-93 for five hours before rapid freezing (scale bar, 100 nm). The yellow arrows point to somewhat extended interfaces between liposomes.

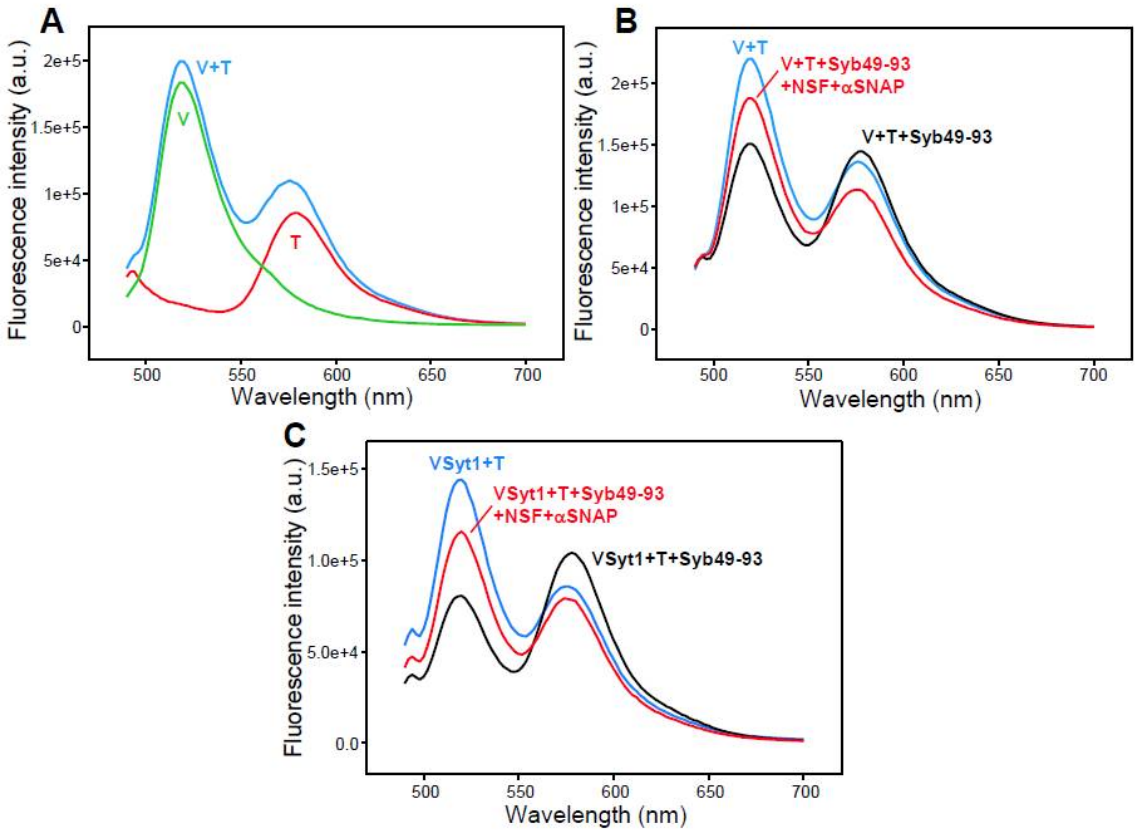

Figure 2.2- Figure supplement 4. Additional supporting fluorescence emission spectra. (A) Fluorescence emission spectra (excitation at 468 nm) of separate samples of V-liposomes containing Alexa488-synaptobrevin (green trace) and T-liposomes containing TMR-syntaxin-1-SNAP-25m (1:4 V- to T-liposome ratio) (red trace) acquired at the same concentrations used for the spectra of Figures 2B-E. The blue curve shows the addition of the red and green curves. (B) Analogous fluorescence emission spectra acquired on a mixture of V-liposomes containing Alexa488-synaptobrevin and T-liposomes containing TMR-syntaxin-1-SNAP-25 WT (1:4 V- to T-liposome ratio) that had been incubated overnight at 4 °C with Syb49-93 before (black trace) and after adding NSF-αSNAP plus ATP and Mg^{2+} (red trace). The blue curve shows a control spectrum obtained by adding spectra acquired separately for V- and T-liposomes at the same concentrations. These experiments are analogous to those shown in Figure 2B but using WT SNAP-25 instead of SNAP-25m, and performing the incubation overnight at low temperature to form trans-SNARE complexes while preventing membrane fusion. (C)) Fluorescence emission spectra of a mixture of VSyt1-liposomes containing Alexa488-synaptobrevin and T-liposomes containing TMR-syntaxin-1-SNAP-25m (1:4 V- to T-liposome ratio) that had been incubated with Syb49-93 overnight at 4 °C (black trace), and of the same sample after adding NSF-αSNAP plus ATP and Mg^{2+} (red trace). The blue curve shows a control spectrum obtained by adding spectra acquired separately for VSyt1- and T-liposomes at the same concentrations. All spectra in (B,C) were corrected for dilution caused by addition of reagents.

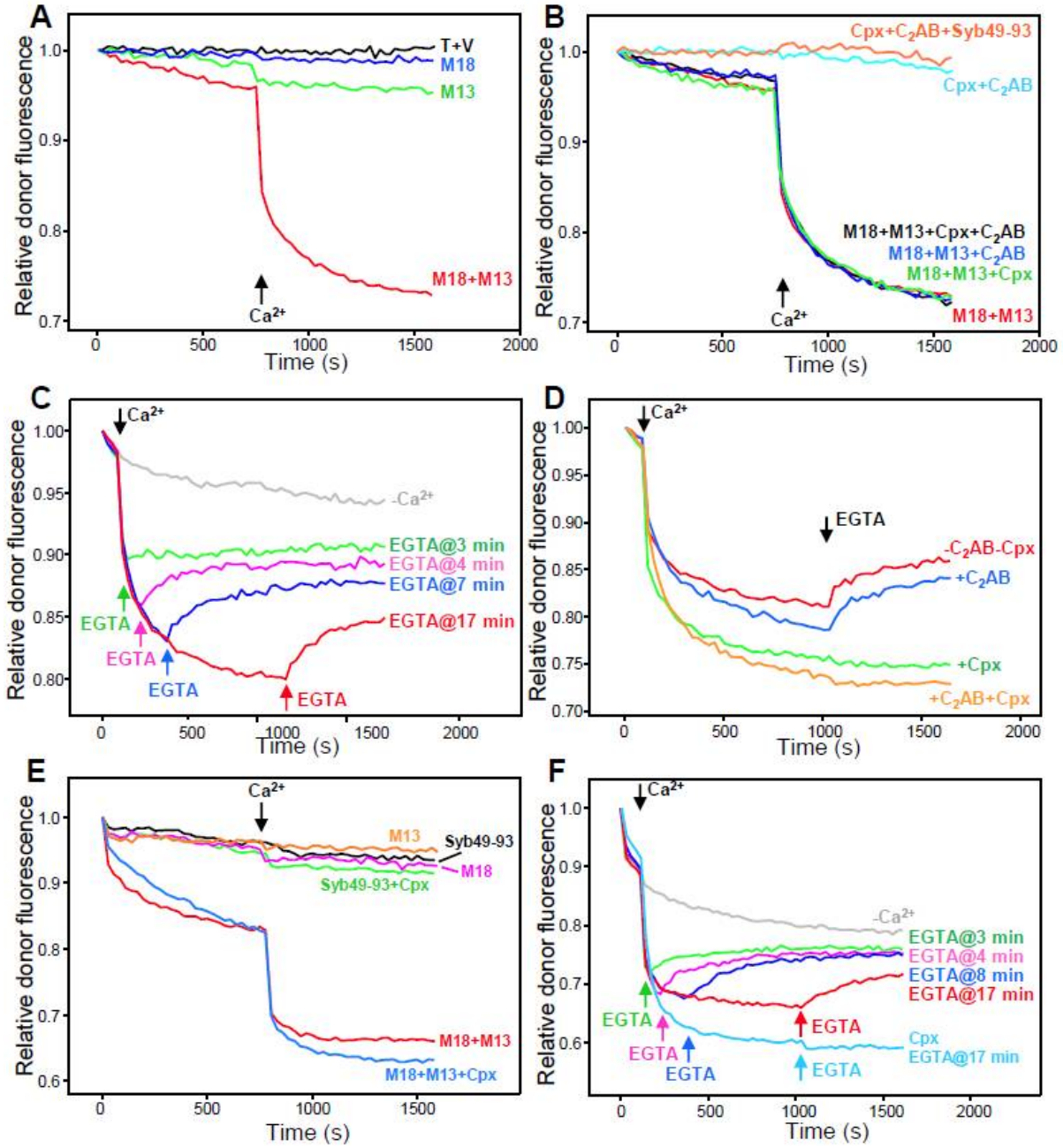

Figure 2.3. Influence of Munc18-1, Munc13-1 $C_1C_2BMUNC_2C$, complexin-1 and synaptotagmin-1 on trans-SNARE complex assembly-disassembly in the presence of NSF-αSNAP. (A,B) Kinetic assays monitoring trans-SNARE complex assembly between V- and T-liposomes (1:4 ratio) in the presence of NSF-αSNAP from the decrease in the donor fluorescence emission intensity. The experiments were performed in the absence of other proteins (V+T) or in the presence of different combinations of Munc18-1 (M18), Munc13-1

$C_1C_2BMUNC_2C$ (M13), complexin-1 (Cpx), synaptotagmin-1 C_2AB and Syb49-93, as indicated by the colors. Experiments were started in 100 µM EGTA and Ca^{2+} (600 µM) was added after 750 s. (C) Analogous kinetic assays performed in the presence of Munc18-1, Munc13-1 $C_1C_2BMUNC_2C$, NSF-αSNAP and 100 µM EGTA, but adding 240 µM Ca^{2+} at 2 minutes to stimulate trans-SNARE complex assembly and adding 500 µM EGTA at different times to chelate the Ca^{2+} and interrogate whether there is trans-SNARE complex disassembly. An experiment that was also started in 100 µM EGTA but without addition of Ca^{2+} or EGTA at later times (gray trace) is shown for comparison. (D) Experiments analogous to those of (C), with addition of 240 µM Ca^{2+} at 2 minutes and 500 µM EGTA at 17 minutes, performed in the absence or presence of complexin-1 and/or synaptotagmin-1 C_2AB. (E) Kinetic assays monitoring trans-SNARE complex assembly between VSyt1- and T-liposomes (1:4 ratio) in the presence of NSF-αSNAP and different combinations of Munc18-1, Munc13-1 $C_1C_2BMUNC_2C$, complexin-1, synaptotagmin-1 C_2AB and Syb49-93, as indicated by the colors. Experiments were started in 100 µM EGTA and Ca^{2+} (600 µM) was added after 750 s. (F) Kinetic assays analogous to those of (E) performed in the presence of Munc18-1, Munc13-1 $C_1C_2BMUNC_2C$, NSF-αSNAP and 100 µM EGTA, but adding 240 µM Ca^{2+} at 2 minutes to stimulate trans-SNARE complex assembly and adding 500 µM EGTA at different times to chelate the Ca^{2+} and interrogate whether there is trans-SNARE complex disassembly. An experiment that was also started in 100 µM EGTA but without addition of Ca^{2+} or EGTA at later times (gray trace) is shown for comparison. The light blue trace shows an additional experiment started in 100 µM EGTA in the presence of complexin-1, with addition of 240 µM Ca^{2+} at 2 minutes and 500 µM EGTA at 17 minutes. For all traces shown in (A-F), fluorescence emission intensities were normalized with the intensity observed in the first point and corrected for the dilution caused by the addition of reagents.

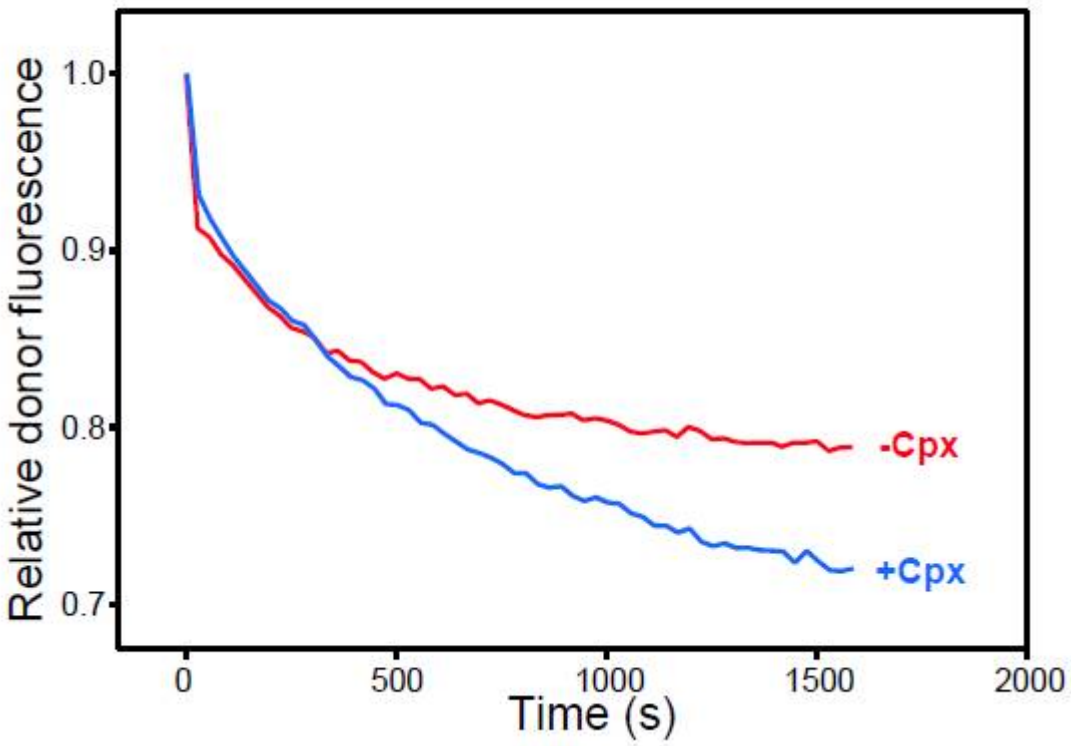

Figure 2.3- Figure supplement 1. Complexin-1 increases the efficiency of Ca^{2+}-independent trans-SNARE complex assembly between VSyt1- and T-liposomes in the presence of NSF-αSNAP. The traces show kinetic assays monitoring trans-SNARE complex assembly between VSyt1- and T-liposomes (1:4 ratio) in the presence of Munc18-1, Munc13-1 C_1C_2BMUNC_2C, NSF-αSNAP and 100 μM EGTA, without (red trace) or with complexin-1 (Cpx) (blue trace). The experiments are analogous to those of Figure 3E (red and blue traces), but without addition of Ca^{2+}.

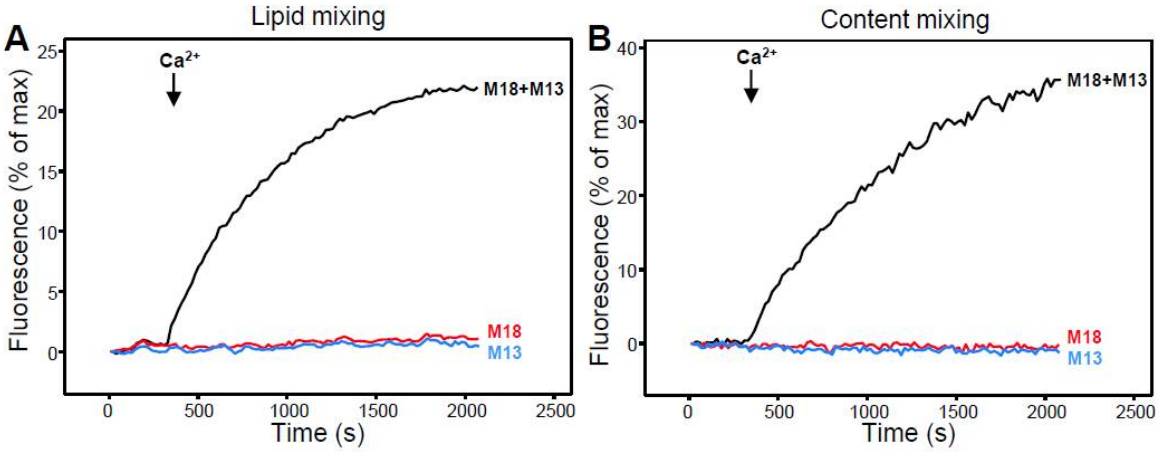

Figure 2.3- Figure supplement 2. Ca^{2+}-dependent fusion between VSyt1- and T-liposomes. (A,B) Lipid mixing (B) between VSyt1-liposomes (synaptobrevin-to-lipid ratio 1:10,000; synaptotagmin-1-to-lipid ratio 1:1,000) and T-liposomes was monitored from the fluorescence de-quenching of Marina Blue lipids and content mixing (C) was monitored from the increase in the fluorescence signal of Cy5-streptavidin trapped in the V-liposomes caused by FRET with PhycoE-biotin trapped in the T-liposomes upon liposome fusion. The assays were performed in the presence of NSF-αSNAP, and Munc18-1 (M18), Munc13-1 $C_1C_2BMUNC_2C$ (M13) or both. Experiments were started in the presence of 100 µM EGTA and 5 µM streptavidin, and Ca^{2+} (600 µM) was added at 300 s.

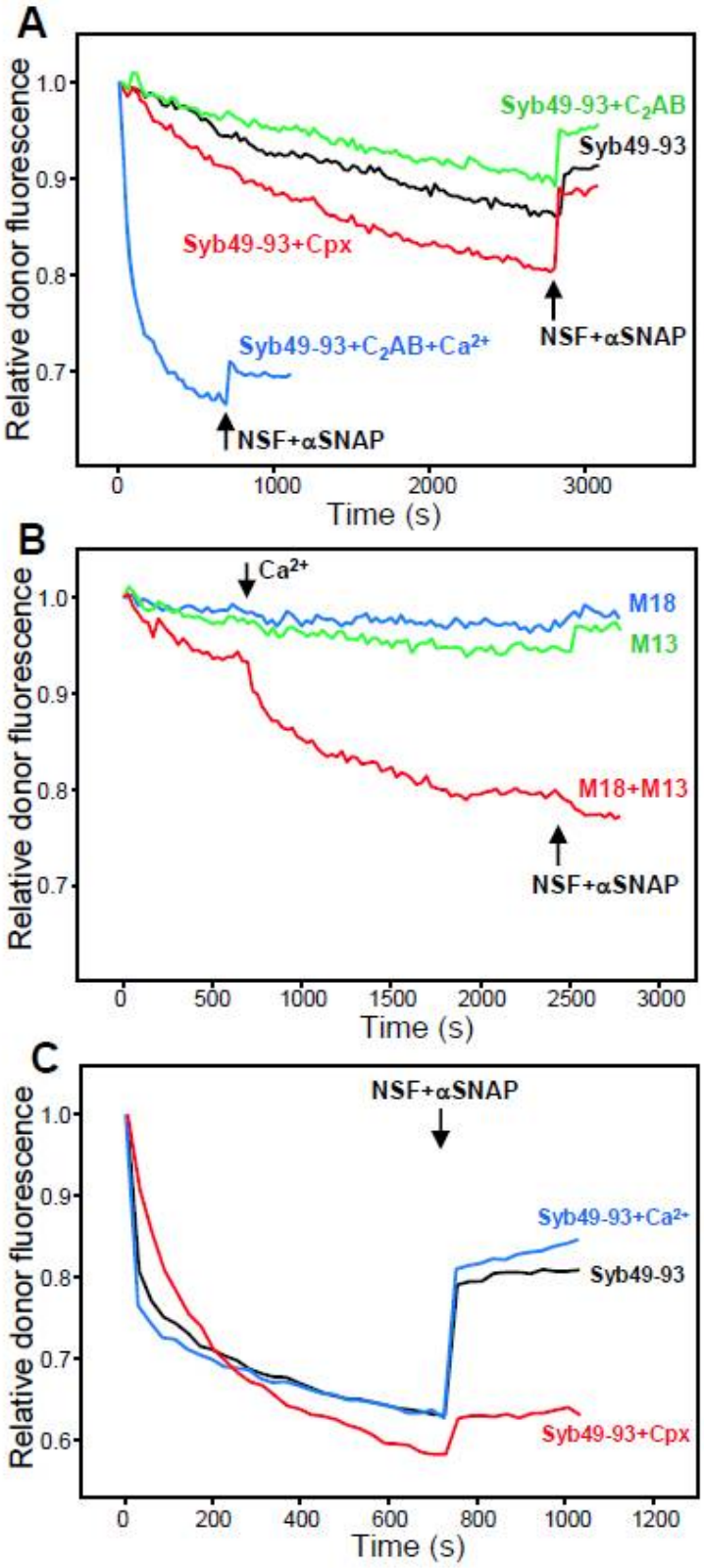
A
Relative donor fluorescence
1.0
0.9
0.8
0.7
Syb49-93+C2AB
Syb49-93
Syb49-93+Cpx
NSF+αSNAP
Syb49-93+C2AB+Ca2+
NSF+αSNAP
0
1000
2000
3000
Time (s)
B
Relative donor fluorescence
Ca2+
M18
M13
M18+M13
NSF+αSNAP
0
500
1000
1500
2000
2500
3000
Time (s)
C
Relative donor fluorescence
NSF+αSNAP
Syb49-93+Ca2+
Syb49-93
Syb49-93+Cpx
0.6
200
400
600
800
1000
1200
Time (s)

Figure 2.4. Influence of Munc18-1, Munc13-1 $C_1C_2BMUNC_2C$, complexin-1 and synaptotagmin-1 on trans-SNARE complex assembly in the absence of NSF-αSNAP and on protection against disassembly upon addition of NSF-αSNAP. (A) Kinetic assays monitoring trans-SNARE complex assembly upon mixing V- and T-liposomes (1:4 ratio) in the presence of Syb49-93 and disassembly upon addition of NSF-αSNAP (indicated by the arrows), from the changes in the donor fluorescence emission intensity. The experiments included Syb49-93 alone (black trace) or together with complexin-1 (Cpx) (red trace), synaptotagmin-1 C_2AB (green trace) and synaptotagmin-1 plus Ca^{2+} (blue trace). (B) Kinetic assays analogous to those of (A) but performed in the absence of Syb49-93 and the presence of Munc18-1 (M18), Munc13-1 $C_1C_2BMUNC_2C$ (M13) or both (blue, green and red traces, respectively). Experiments were started in 100 µM EGTA and Ca^{2+} (600 µM) was added after 700 s. (C) Analogous kinetic assays monitoring trans-SNARE complex assembly between VSyt1- and T-liposomes (1:4 ratio) in the presence of Syb49-93 alone (black trace) or together with Ca^{2+} (blue trace) or complexin-1 (Cpx) (red trace), and addition of NSF-αSNAP at the end (black arrow). For all traces shown in (A-C), fluorescence emission intensities were normalized with the intensity observed in the first point and corrected for the dilution caused by the addition of reagents.

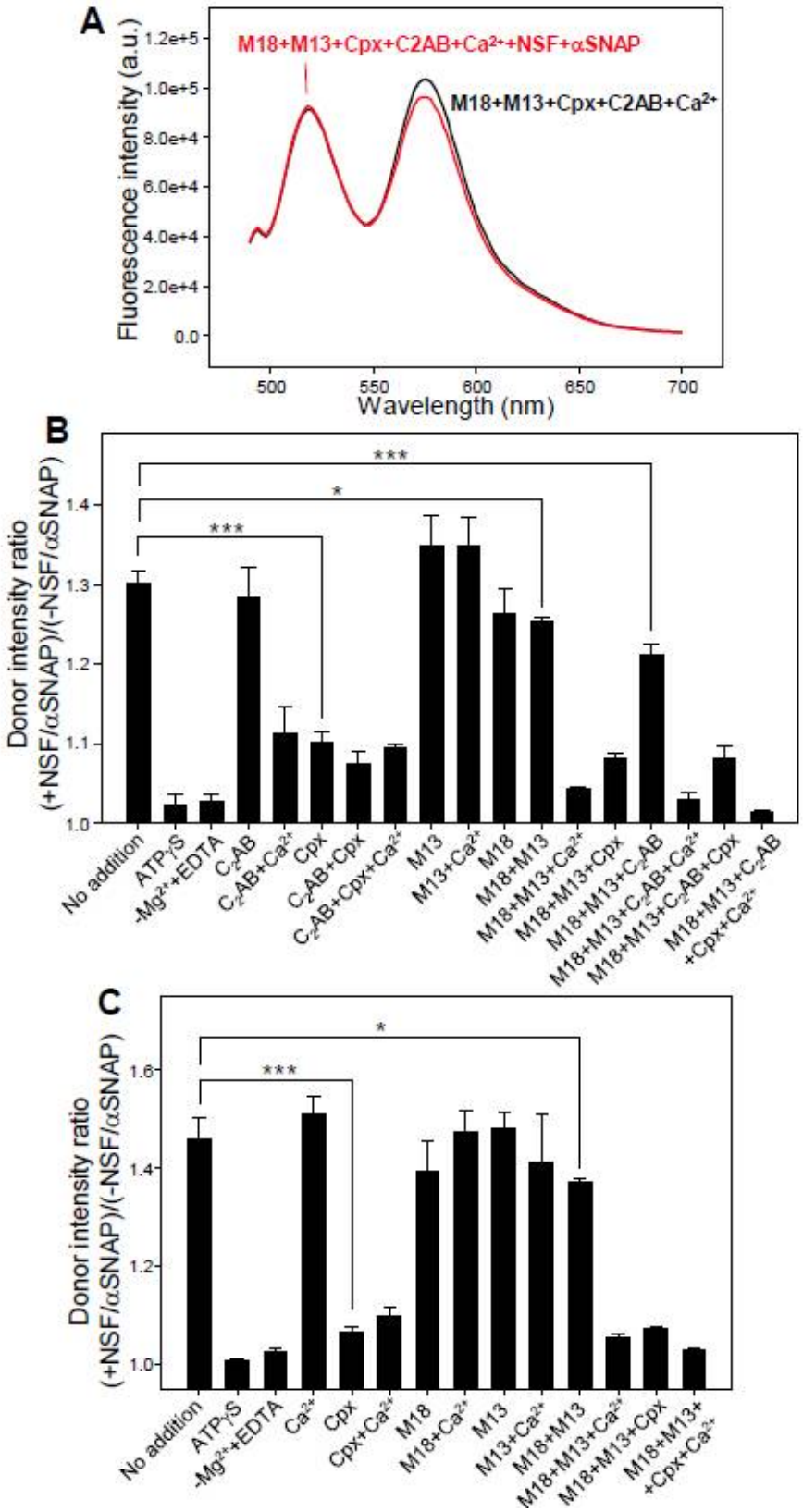
A
M18+M13+Cpx+C2AB+Ca2++NSF+αSNAP
M18+M13+Cpx+C2AB+Ca2+
Fluorescence intensity (a.u.)
1.2e+5
1.0e+5
8.0e+4
6.0e+4
4.0e+4
2.0e+4
0.0
500
550
600
650
700
Wavelength (nm)
B
Donor intensity ratio (+NSF/αSNAP)/(-NSF/αSNAP)
1.4
1.3
1.2
1.1
1.0
***
*
***
No addition
ATPγS
-Mg2++EDTA
C2AB
C2AB+Ca2+
Cpx
C2AB+Cpx
C2AB+Cpx+Ca2+
M13
M13+Ca2+
M18
M18+M13
M18+M13+Ca2+
M18+M13+Cpx
M18+M13+C2AB
M18+M13+C2AB+Ca2+
M18+M13+C2AB+Cpx
M18+M13+C2AB +Cpx+Ca2+
C
Donor intensity ratio (+NSF/αSNAP)/(-NSF/αSNAP)
1.6
1.4
1.2
1.0
*
***
No addition
ATPγS
-Mg2++EDTA
Ca2+
Cpx
Cpx+Ca2+
M18
M18+Ca2+
M13
M13+Ca2+
M18+M13
M18+M13+Ca2+
M18+M13+Cpx
M18+M13+ +Cpx+Ca2+

Figure 2.5. Quantitative analysis of how Munc18-1, Munc13-1 $C_1C_2BMUNC_2C$, complexin-1 and synaptotagmin-1 protect pre-formed trans-SNARE complexes against disassembly by NSF-αSNAP. (A) Fluorescence emission spectra of mixtures of V-liposomes containing Alexa488-synaptobrevin and T-liposomes containing TMR-syntaxin-1-SNAP-25m (1:4 V- to T-liposome ratio) that were incubated for five hours with Syb49-93; Munc18-1, Munc13-1 $C_1C_2BMUNC_2C$, complexin-1, synaptotagmin-1 C_2AB and Ca^{2+} were then added and, after an additional incubation for five minutes, spectra were acquired before (black trace) or after (red trace) addition of NSF-αSNAP. (B) Bar diagram illustrating the ability of Munc18-1, Munc13-1 $C_1C_2BMUNC_2C$, complexin-1, synaptotagmin-1 C_2AB and Ca^{2+} to protect pre-formed trans-SNARE complexes against disassembly by NSF-αSNAP. As in (A), V- and T-liposomes were incubated for five hours with Syb49-93 to preform trans-SNARE complexes and then they were incubated for five minutes with different combinations of Munc18-1 (M18), Munc13-1 $C_1C_2BMUNC_2C$ (M13), complexin-1 (Cpx), synaptotagmin-1 C_2AB (C_2AB) and Ca^{2+}. Fluorescence emission spectra were acquired before and after addition of NSF-αSNAP and the ratio r between the donor fluorescence intensities at 518 nm measured after and before NSF-αSNAP addition was calculated. Representative examples of the spectra acquired under different conditions are shown in Figure 5-figure supplement 1. (C) Bar diagram illustrating the ability of Munc18-1, Munc13-1 $C_1C_2BMUNC_2C$, complexin-1 and Ca^{2+} to protect pre-formed trans-SNARE complexes between VSyt1- and T-liposomes against disassembly by NSF-αSNAP. Similar to (B), VSyt1- and T-liposomes were incubated with Syb49-93 (but for 24 hours at 4 °C) to preform trans-SNARE complexes and then they were incubated for five minutes with different combinations of Munc18-1, Munc13-1 $C_1C_2BMUNC_2C$, complexin-1 (Cpx) and Ca^{2+}. Fluorescence emission spectra were acquired before and after addition of NSF-αSNAP and the ratio r between the donor fluorescence intensities at 518 nm measured after and before NSF-αSNAP addition was calculated. Representative examples of the spectra acquired under different conditions are shown in Figure 5-figure supplement 4. In (B,C), 'No additions' indicates experiments where none of these factors were included before addition of NSF-αSNAP. Control experiments with no additions and replacing ATP with ATPγS or replacing Mg^{2+} with EDTA were also performed. All experiments were performed in triplicate. Values indicate means +/- standard deviations. A few examples of statistical significance are indicated to illustrate which differences among the r values obtained under different conditions are meaningful. Statistical significance and P values were determined by one-way analysis of variance (ANOVA) with Holm-Sidak test (* $P < 0.05$; *** $P < 0.001$).

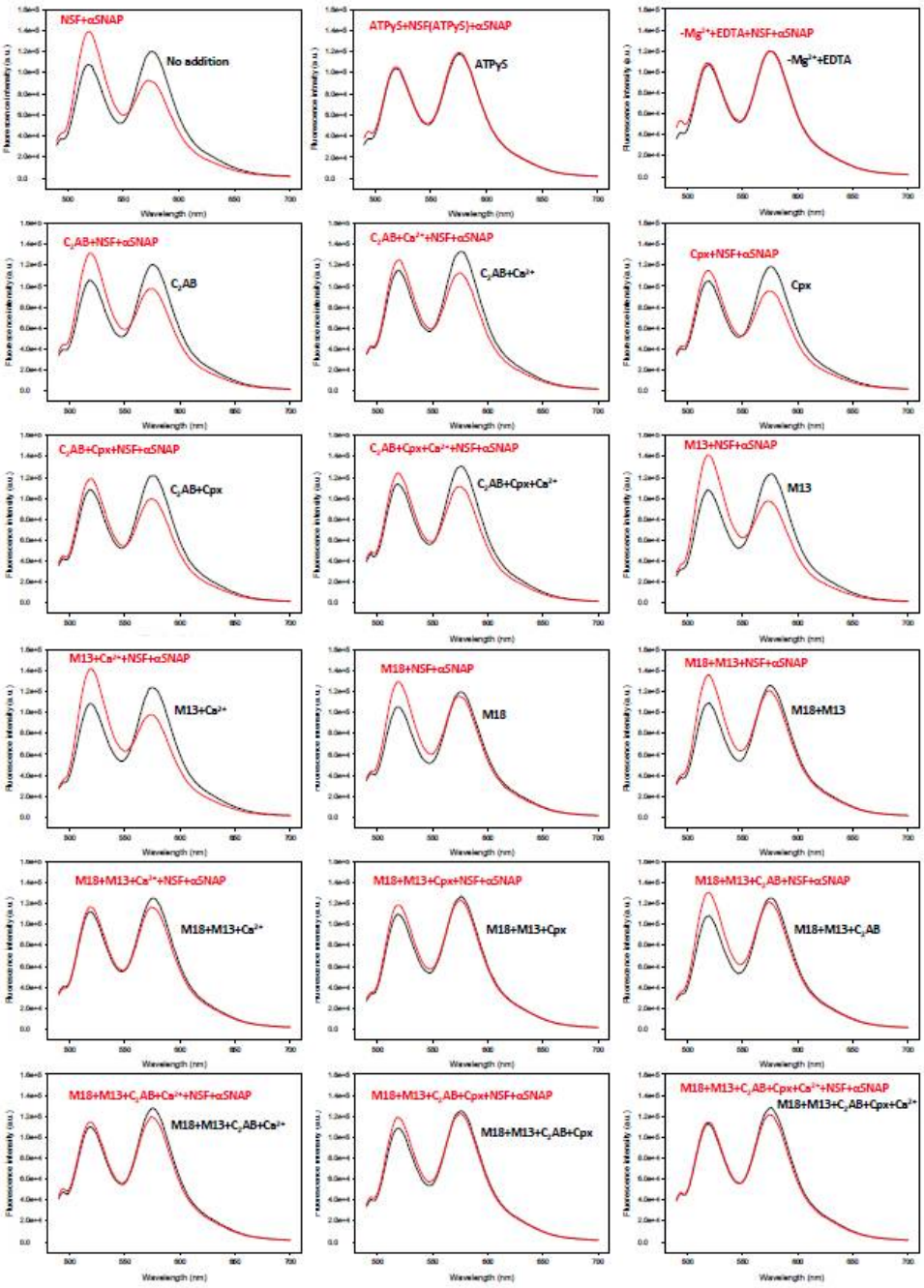

Figure 2.5- Figure supplement 1. Representative fluorescence emission spectra used in the experiments of Figure 5B to obtain a quantitative measurement of how Munc18-1, Munc13-1, complexin-1, synaptotagmin-1 and Ca^{2+} in different combinations protect pre-formed trans-SNARE complexes against disassembly by NSF-αSNAP. Black curves show spectra acquired before addition of NSF-αSNAP, and red curves the spectra obtained after addition of NSF-αSNAP.

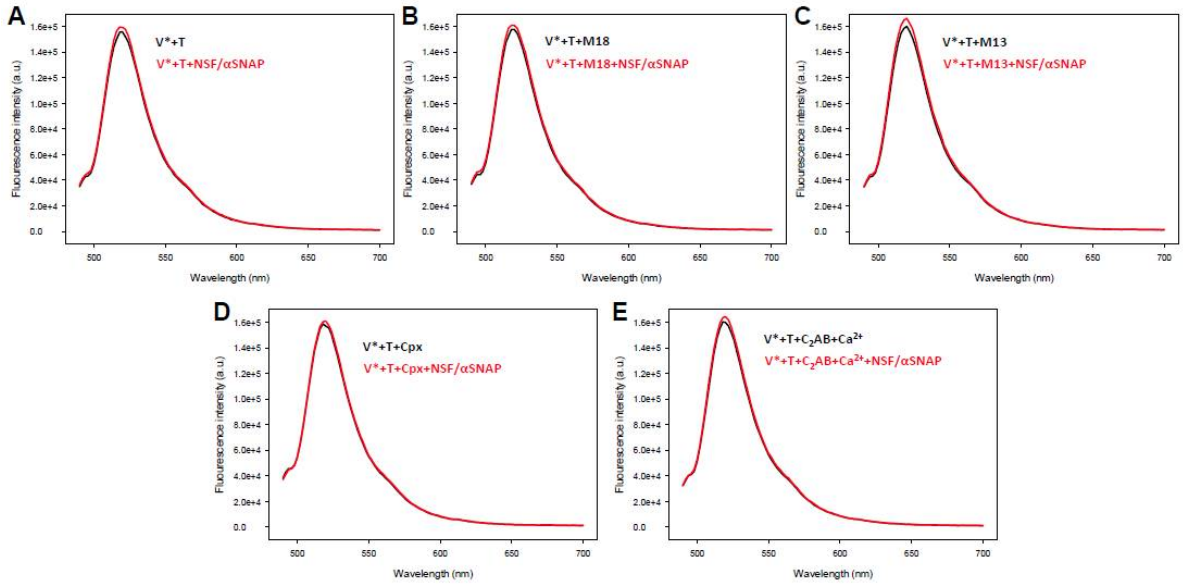

Figure 2.5- Figure supplement 2. Control spectra acquired to assess the effects of various factors on the fluorescence emission spectra of V-liposomes incorporated into trans-SNARE complexes in the absence of FRET. V-liposomes containing Alexa488-synaptobrevin (V*) were incubated for five hours with Syb49-93 and T-liposomes containing syntaxin-1-SNAP-25m (T) (1:4 V- to T-liposome ratio). The mixture was then incubated with Munc18-1 (M18), Munc13-1 $C_1C_2BMUNC_2C$ (M13), complexin-1 (Cpx) or synaptotagmin-1 C_2AB/Ca^{2+} for five minutes, and spectra were acquired before (black traces) or after (red traces) addition of NSF-αSNAP.

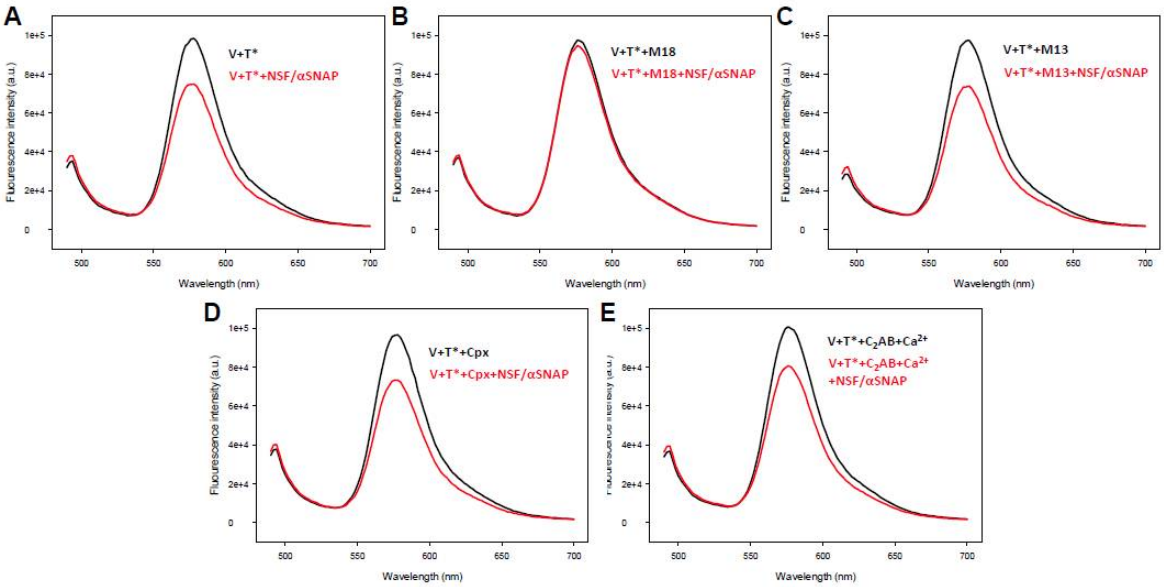

Figure 2.5- Figure supplement 3. Control spectra acquired to assess the effects of various factors on the fluorescence emission spectra of T-liposomes incorporated into trans-SNARE complexes in the absence of FRET. V-liposomes containing synaptobrevin (V) were incubated for five hours with Syb49-93 and T-liposomes containing TMR-syntaxin-1-SNAP-25m (T*) (1:4 V- to T-liposome ratio). The mixture was then incubated with Munc18-1 (M18), Munc13-1 C_1C_2BMUNC_2C (M13), complexin-1 (Cpx) or synaptotagmin-1 C_2AB/Ca^{2+} for five minutes, and spectra were acquired before (black traces) or after (red traces) addition of NSF-αSNAP.

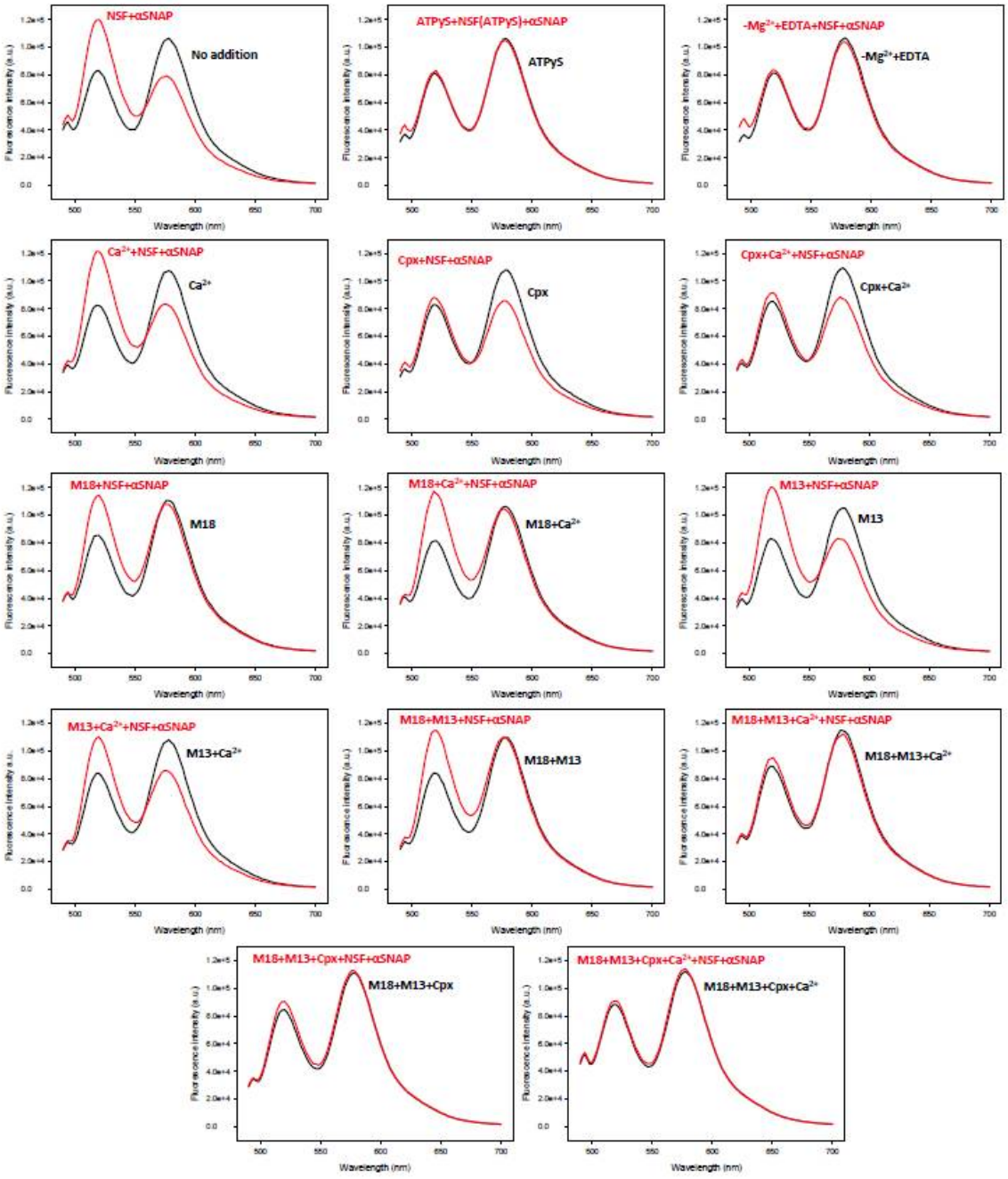

Figure 2.5- Figure supplement 4. Representative fluorescence emission spectra used in the experiments of Figure 5C to obtain a quantitative measurement of how Munc18-1, Munc13-1, complexin-1 and Ca^{2+} in different combinations protect pre-formed trans-SNARE complexes between VSyt1- and T-liposomes against disassembly by NSF-αSNAP. Black curves show spectra acquired before addition of NSF-αSNAP, and red curves the spectra obtained after addition of NSF-αSNAP.

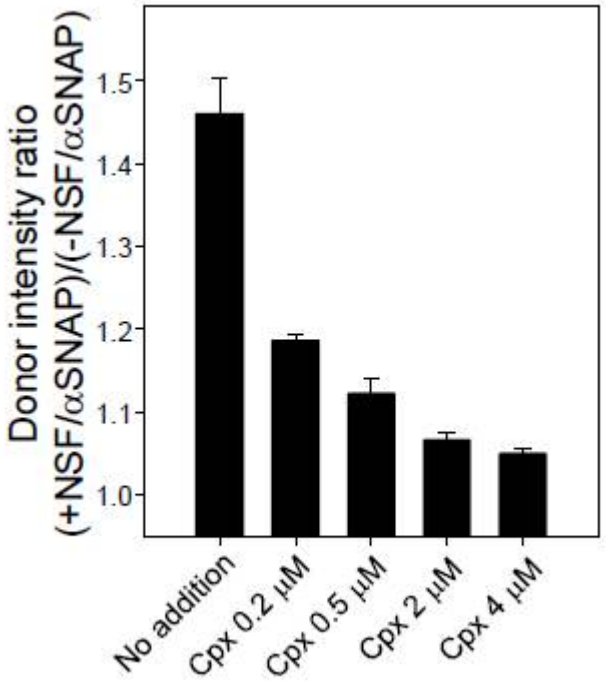

Figure 2.5- Figure supplement 5. Complexin-1 concentration dependence of protection of trans-SNARE complexes against disassembly by NSF-αSNAP. Protection experiments with pre-formed trans-SNARE complexes between VSyt1- and T-liposomes analogous to those of Figure 5C were performed by adding different complexin-1 concentrations, incubating for five minutes and acquiring fluorescence emission spectra before and after addition of NSF-αSNAP. The ratio r between the donor fluorescence intensities at 518 nm measured after and before NSF-αSNAP addition was calculated. All experiments were performed in triplicate. Values indicate means +/- standard deviations.

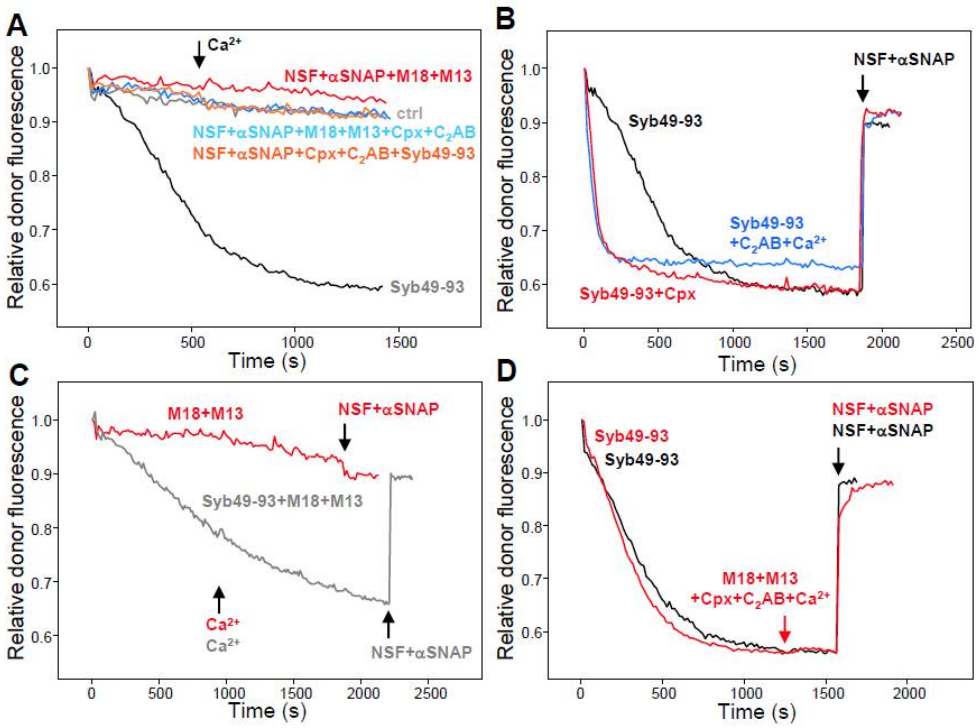

Figure 2.6. Munc18-1, Munc13-1 $C_1C_2BMUNC_2C$, complexin-1 and synaptotagmin-1 C_2AB do not protect cis-SNARE complexes against disassembly by NSF-αSNAP. (A) Kinetic assays monitoring changes in the donor fluorescence emission intensity due to cis-SNARE complex formation upon mixing V-liposomes containing Alexa488-synaptobrevin with an excess of TMR-labeled syntaxin-1(2-253) and SNAP-25m in the presence of NSF-αSNAP with no additions (ctrl) (light gray trace) or with different combinations of Munc18-1 (M18), Munc13-1 $C_1C_2BMUNC_2C$ (M13), complexin-1 (Cpx) and synaptotagmin-1 C_2AB as indicated. Ca^{2+} was added at 550 s. For comparison purposes, the dark gray trace shows a cis-SNARE complex assembly reaction performed in the presence of Syb49-93 and absence of NSF-αSNAP. (B) Kinetic assays of cis-SNARE complex assembly analogous to those of (A), but performed in the absence of NSF-αSNAP and the presence of Syb49-93 alone (black trace) or together with complexin-1 (Cpx) (red trace) or synaptotagmin-1 C_2AB plus Ca^{2+} (blue trace). NSF-αSNAP were added when the reactions reached a plateau (black arrow) to monitor cis-SNARE complex disassembly. (C) Kinetic assays analogous to those in (B), but in the presence of Munc18-1 (M18) and Munc13-1 $C_1C_2BMUNC_2C$ (M13) without (dark gray trace) or with (red trace) Syb49-93. Ca^{2+} was added after 950 s. (D) Kinetic assays where cis-SNARE complex formation was initially catalyzed by Syb49-93 and, after reaching a plateau, Munc18-1, Munc13-1 $C_1C_2BMUNC_2C$, complexin-1, synaptotagmin-1 C_2AB and Ca^{2+} were added (red arrow); after five minutes, NSF-αSNAP were added to test for disassembly (red trace). The black trace shows a control experiment where the four proteins were not included before adding NSF-αSNAP. For all traces of (A-D), fluorescence emission intensities were normalized with the intensity observed in the first point and corrected for the dilution caused by the addition of reagents.

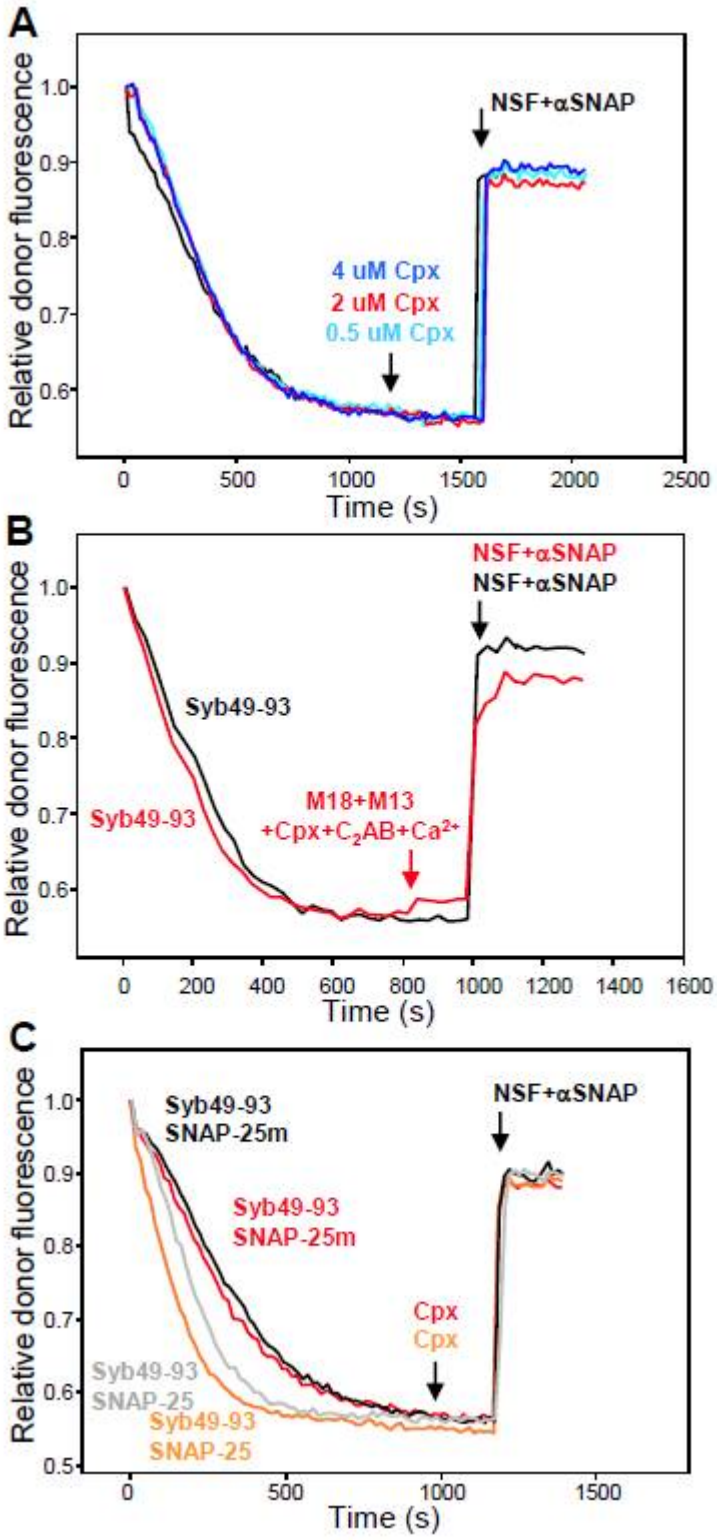
A
Relative donor fluorescence
1.0
0.9
0.8
0.7
0.6
NSF+αSNAP
4 uM Cpx
2 uM Cpx
0.5 uM Cpx
0
500
1000
1500
2000
2500
Time (s)
B
Relative donor fluorescence
1.0
0.9
0.8
0.7
0.6
NSF+αSNAP
NSF+αSNAP
Syb49-93
Syb49-93
M18+M13
+Cpx+C2AB+Ca2+
0
200
400
600
800
1000
1200
1400
1600
Time (s)
C
Relative donor fluorescence
1.0
0.9
0.8
0.7
0.6
0.5
Syb49-93
SNAP-25m
NSF+αSNAP
Syb49-93
SNAP-25m
Cpx
Cpx
Syb49-93
SNAP-25
Syb49-93
SNAP-25
0
500
1000
1500
Time (s)

Figure 2.6- Figure supplement 1. Munc18-1, Munc13-1 C_1C_2BMUNC_2C, complexin-1 and synaptotagmin-1 C_2AB do not protect cis-SNARE complexes against disassembly by NSF-αSNAP. (A) Kinetic assays where cis-SNARE complex formation was catalyzed by Syb49-93, as in Figure 6D, and different concentrations of complexin-1 (Cpx) were added five minutes before disassembly with NSF-αSNAP. (B) Kinetic assays analogous to those of Figure 6D, but using WT SNAP-25 instead of SNAP-25m to ensure that the mutation in SNAP-25m did not affect the disassembly of cis-SNARE complexes by NSF-αSNAP in the presence of Munc18-1, Munc13-1 C_1C_2BMUNC_2C, complexin-1, synaptotagmin-1 C_2AB and Ca^{2+}. (C) Kinetic assays analogous to those of panels (A), but adding 1 μM complexin-1 five minutes before disassembly with NSF-αSNAP (red and orange traces). In these experiments, the concentrations of NSF and αSNAP were 0.1 μM and 0.5 μM, respectively, which were lower than those of our standard conditions (0.5 μM and 2 μM, respectively) to test whether complexin-1 might hinder disassembly at a higher molar ratio with respect to αSNAP. The experiments were performed with SNAP-25m (black and red traces) or WT SNAP-25 (gray and orange traces). The black and gray traces are controls where complexin-1 was not added. For all traces of (A-C), fluorescence emission intensities were normalized with the intensity observed in the first point and corrected for the dilution caused by the addition of reagents to make the data comparable.

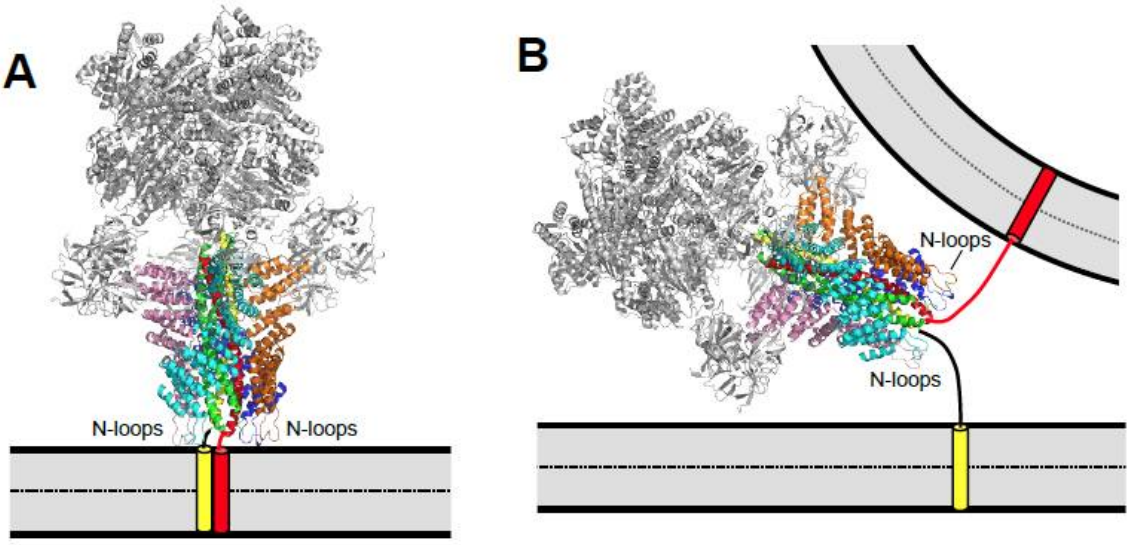

Figure 2.7. Models illustrating the different geometric constraints of cis- and trans-SNARE complex disassembly. (A,B) Models showing ribbon diagrams of the cryo-electron microscopy structure of the 20S complex (PDB accession code 3J96) (Zhao et al., 2015) assembled on a cis-SNARE complex on one membrane (A) or on a trans-SNARE complex between two membranes (B). Synaptobrevin is in red, syntaxin-1 in yellow, SNAP-25 in green, NSF in gray and the four molecules of αSNAP in cyan, orange, blue and pink. The positions of the αSNAP N-terminal hydrophobic loops (N-loops) are indicated. The orientation of the 20S complex in (A) was chosen to favor simultaneous interactions of the N-loops of the four αSNAP molecules with the membrane. In (B), the orientation of the 20S complex is arbitrary and is meant to illustrate the difficulty of simultaneous interactions of the N-loops from the four αSNAP molecules with membranes in the trans configuration. Note that, at the same time, the apposition of both membranes may enhance the affinity of Munc18-1, Munc13-1, synaptotagmin-1 and complexin-1 for SNARE complexes in the trans configuration due to simultaneous interactions with the membranes that are not possible or less favorable in the cis configuration.

Chapter 3- Reconciling isothermal titration calorimetry analyses of interactions between complexin and truncated SNARE complexes

*This section was reproduced from: **Prinslow, E. A.**, C. A. Brautigam, and J. Rizo. 2017. "Reconciling isothermal titration calorimetry analyses of interactions between complexin and truncated SNARE complexes." Elife 6. doi: 10.7554/eLife.30286.

3.1 Abstract

Neurotransmitter release depends on the SNARE complex formed by syntaxin-1, synaptobrevin and SNAP-25, as well as on complexins, which bind to the SNARE complex and play active and inhibitory roles. A crystal structure of a Complexin-I fragment bearing a so-called 'superclamp' mutation bound to a truncated SNARE complex lacking the C-terminus of the synaptobrevin SNARE motif (SNAREΔ60) suggested that an 'accessory' α-helix of Complexin-I inhibits release by inserting into the C-terminus of the SNARE complex. Previously, isothermal titration calorimetry (ITC) experiments performed in different laboratories yielded apparently discrepant results in support or against the existence of such binding mode in solution (Trimbuch et al. 2014, Krishnakumar et al. 2015). Here, ITC experiments performed to solve these discrepancies now show that the region containing the Complexin-I accessory helix and preceding N-terminal sequences does interact with SNAREΔ60, but the interaction requires the polybasic juxtamembrane region of syntaxin-1 and is not affected by the superclamp mutation within the experimental error of these experiments.

3.2 Introduction

The release of neurotransmitters by Ca^{2+}-triggered synaptic vesicle exocytosis is governed by a sophisticated protein machinery that includes the neuronal soluble N-ethylmaleimide sensitive factor attachment protein receptors (SNAREs) synaptobrevin, syntaxin-1 and SNAP-25 as central components (Sudhof et al. 2009, Rizo et al. 2015). These proteins form a tight SNARE complex that consists of a four-helix bundle and plays a key role in membrane fusion by bringing the synaptic vesicle and plasma membranes together (Sollner et al. 1993a, Sutton et al. 1998, Weber et al. 1998). The exquisite regulation of release also depends on multiple specialized proteins, including Complexins among others. These small soluble proteins bind tightly to the SNARE complex (McMahon et al. 1995) and play both active and inhibitory roles in release (Reim et al. 2001, Huntwork et al. 2007, Hobson et al. 2011, Martin et al. 2011), but the underlying mechanisms remain unclear.

A crystal structure of the SNARE complex bound to a fragment spanning residues 26–83 of Complexin-I [CpxI(26-83)] showed that binding involves a central α-helix of CpxI, while a preceding accessory α-helix does not contact the SNAREs (Figure 3.1A,B). Electrophysiological studies indicated that the accessory helix mediates at least in part the inhibitory role of CpxI, leading to a model whereby the accessory helix inhibits release by replacing part of the synaptobrevin SNARE motif in a partially assembled SNARE complex, thus preventing C-terminal assembly of the complex (Xue et al. 2007, Maximov et al. 2009). Cell-cell fusion assays supported this model and led to the design of several CpxI mutants with increased or decreased inhibitory activity in these assays, including a superclamp' mutant where three charged residues were replaced with hydrophobic residues (D27L, E34F,

R37A) to enhance the putative binding to the partially assembled SNARE complex (Giraudo et al. 2009).

A crystal structure of a SNARE complex with synaptobrevin truncated at residue 60 (SNAREΔ60) bound to CpxI(26-83) bearing the superclamp mutation [scCpxI(26-83)] later revealed a zig-zag array where the central helix binds to one SNAREΔ60 complex and the accessory helix binds to another SNAREΔ60 complex (Figure 3.1C), suggesting that such an array inhibits neurotransmitter release before Ca^{2+} influx (Kummel et al. 2011). The validity of the scCpxI accessory helix-SNAREΔ60 interaction observed in the structure was supported by isothermal titration calorimetry (ITC) results that we discuss in detail below (Kummel et al. 2011). However, no interaction between the accessory helix of WT CpxI(26-83) or scCpxI(26-83) with C-terminally truncated SNARE complexes was observed by analogous ITC experiments and extensive NMR analyses in a separate study (Trimbuch et al. 2014). Moreover, electrophysiological experiments performed in the same study did not detect significant functional effects for the superclamp mutation in CpxI, and led to a model whereby the accessory helix inhibits release because it causes electrostatic and/or steric hindrance with the membranes at the site of fusion (Figure 3.1D) (Trimbuch et al. 2014). Note that, in a previous study, the superclamp CpxI mutant was claimed to inhibit spontaneous release more efficiently than WT CpxI (Yang et al. 2010), but the data were not inconsistent with the results of (Trimbuch et al. 2014). Rescue assays with mammalian CpxI in Drosophila Complexin nulls did reveal a stronger inhibition of spontaneous release for superclamp CpxI than for WT CpxI (Cho et al. 2014), supporting the hydrophobic interaction observed in the crystal structure of (Kummel et al. 2011). Conversely, the finding that the

accessory helix can be functionally replaced by an unrelated, uncharged α-helix in *C. elegans* supported the notion that the inhibitory role of this helix does not involve protein-protein interactions (Radoff et al. 2014), suggesting that steric hindrance with the membranes may be sufficient for this role.

The above results and other studies have led to considerably different views on the available data and the merits of the proposed models, which is natural in ongoing investigations of a highly complex molecular mechanism that is still poorly understood. However, it was worrisome and confusing to the field that different results were obtained in the Rothman and Rizo laboratories in ITC experiments that presumably were performed under analogous conditions with the same protein sequences (Kummel et al. 2011, Trimbuch et al. 2014, Krishnakumar et al. 2015). Here we describe our efforts to identify the source of the discrepancies and present new data showing that there is indeed an interaction between SNAREΔ60 and residues 1–47 of CpxI, although this interaction is not affected by the superclamp mutation in CpxI and requires the polybasic juxtamembrane region of syntaxin-1.

3.3 Materials and methods

Protein expression and purification

Expression vectors for GST-PreScission human synaptobrevinΔ60 (residues 29–60; SybΔ60), GST-TEV rat syntaxin-1A (residues 191–253), His_6-SUMO human SNAP25A-N terminal SNARE motif (residues 7–82; SNAP25N), His_6-SUMO human SNAP25A-C terminal SNARE motif (residues 141–203; SNAP25C), His_6-SUMO human CpxI (residues 48–134), His_6-thrombin human CpxI (residues 1–134), and His_6-thrombin human scCpxI

(residues 1–134 D27L, E34F, R37A) were described previously by the Rothman laboratory (Kummel et al. 2011). Additionally, vectors for His_6-rat syntaxin-1A (residues 188–259) and His6-rat syntaxin-1A (residues 188–265) were also prepared by the Rothman laboratory using standard recombinant DNA techniques. All fusion proteins were expressed in *E. coli* BL21 (DE3) cells by induction with 0.5 mM IPTG at an $O.D_{600}$ of 0.6 for 4 hr at 37°C. Proteins were purified as described (Kummel et al. 2011, Trimbuch et al. 2014). Briefly, cells were harvested and re-suspended in PBS pH 7.4 containing 1 mM TCEP and supplemented with Sigma protease inhibitors. Cleared lysates were applied to either glutathione sepharose resin (GE) or Ni-NTA resin (Thermo Fisher), washed with PBS pH 7.4, and eluted in PBS pH 7.4, 400 mM imidazole. Affinity tags were cleaved with the indicated protease overnight at 4°C. After affinity tag cleavage, all proteins were further purified using size exclusion chromatography on a Superdex S75 column (GE 16/60) equilibrated with 20 mM Tris pH 7.4, 125 mM NaCl, 1 mM TCEP. The expression of Syx 188–265 led to the majority of the protein being expressed in inclusion bodies. Since this fragment does not contain any tertiary structure, a denaturing protocol was used to extract the protein from the pellet after lysis and centrifugation. After extraction in 50 mM Tris pH 7.4, 1M NaCl, and 6 M Gdn-HCl, the protein was applied to Ni-NTA resin, washed with PBS pH 7.4, 1 M NaCl, eluted in PBS pH 7.4, 1 M NaCl, 400 mM imidazole, and dialyzed into buffer containing 20 mM Tris pH 7.4, 1M NaCl. Removal of the affinity tag was performed concomitantly with dialysis for syntaxin-1(188–265), while syntaxin-1(188–265) with an intact His_6-tag was immediately flash frozen after elution from the Ni-NTA column in PBS pH 7.4, 1 M NaCl, 400 mM imidazole.

Isothermal titration calorimetry

ITC experiments were performed using a Microcal ITC200 (Malvern) at 25°C. SNAREΔ60 complexes were prepared by mixing SNAP25N, SNAP25C, SybΔ60 and the corresponding syntaxin-1A fragment in equimolar ratios and incubating overnight at 4°C. Assembled complexes were purified the next day using size exclusion chromatography with a Superdex S75 column (GE 16/60). All proteins were dialyzed (2 L for 4 hr followed by 4 L overnight) in a buffer containing PBS (pH 7.4, 137 mM NaCl, 3 mM KCl, 10 mM phosphate buffer, 0.25 mM TCEP) before the experiments. Protein concentrations were measured by UV absorbance at 280 nm. All experiments were performed at least in duplicate for each combination of CpxI protein and SNAREΔ60 complex to check the reproducibility of the data. For direct titrations (Figure 3.2), CpxI(48-134), CpxI or scCpxI (150 µM) was directly titrated into the chamber containing 8 µM SNAREΔ60-Sx253, SNAREΔ60-Sx259, SNAREµ60-Sx265 or His_6-SNAREΔ60-Sx265. The data were baseline corrected and integrated with NITPIC, fitted with a nonlinear least squares routine using a single-site binding model with ITCsy and plotted with GUSSI (Brautigam et al. 2016). The 'A + B < ->AB' model was used for the fitting, and apparent concentration errors for the cell contents were compensated for by refining an incompetent fraction parameter. The 68.3% confidence intervals were obtained using the error surface projection method. Global analysis with ITCsy was performed for each set of experiments carried out with the same protein fragments to derive the K_Ds described in Table 3.1. For blocking assays, CpxI(48-134), CpxI or scCpxI (300–500 µM) was titrated into the chamber containing 17–21 µM SNAREΔ60-Sx253,

SNAREΔ60-Sx259, SNAREΔ60-Sx265 or His_6-SNAREΔ60-Sx265 and 4.9 equivalents of CpxI(48-134).

3.4 Results and discussion

The ITC experiments that yielded apparently discrepant results involved blocking assays where SNAREΔ60 was saturated with a CpxI fragment lacking the accessory helix and the mixture was titrated with full-length CpxI or CpxI(26-83), both of which contain the accessory helix. The observation of heat release in the assays performed with WT CpxI, and of an increase in the heat release when the superclamp mutation was introduced in the accessory helix, supported the notion that the interaction of the CpxI accessory helix with SNAREΔ60 observed in the zigzag crystal structure occurs in solution (Kummel et al. 2011, Krishnakumar et al. 2015). These conclusions relied on the assumption that the excess of the blocking CpxI fragment used in the competition assays [CpxI (48-134)] completely saturates the SNAREΔ60 complex, which was supported by direct titrations of SNAREΔ60 with CpxI(48-134) that yielded a K_D of 457 nM (Krishnakumar et al. 2015). However, another study that used similar conditions to those described in (Kummel et al. 2011), blocking SNAREΔ60 with a 1.5-fold excess of a CpxI(47-134) fragment, observed similar heat release upon titration with WT or superclamp mutant CpxI(26-83) (Trimbuch et al. 2014). Because direct titrations of SNAREΔ60 with CpxI(47-134) yielded a K_D of 2.4 μM, this study concluded that the heat release observed in the blocking assays arises from incomplete saturation of SNAREΔ60 by CpxI(47-134) rather than from an interaction of the accessory helix with SNAREΔ60. Note that the relatively weak affinity reflected by this K_D is not

surprising because the truncation of synaptobrevin in SNAREΔ60 removes multiple residues that contact the central CpxI helix in the crystal structure of CpxI(26-83) bound to the SNARE complex (Chen et al. 2002).

To elucidate the reasons for these discrepancies, the Rothman laboratory shared the expression vectors used in Kummel et al. 2011 and Krishnakumar et. al 2015 with the Rizo laboratory, so that we could rule out the possibility that the distinct results obtained in Trimbuch et. al. 2014 arose from differences in the protein fragments used. In addition, E. Prinslow from the Rizo laboratory visited the Rothman laboratory. In the resulting discussions, the Rothman laboratory explained an experimental detail that had not been reported in Kummel et. al 2011 and Krishnakumar et. al 2015: in the blocking assays monitored by ITC, sufficient excess of CpxI fragment [CpxI(48-134)] to block SNAREΔ60 was added so that minimal heat release was observed in control experiments where blocked SNAREΔ60 was titrated with CpxI(48-134) itself. Hence, the (larger) heat release observed in the titrations with CpxI or scCpxI could not arise from incomplete saturation of SNAREΔ60 by CpxI(48-134). Moreover, the conversations between the two laboratories and protein analyses by SDS PAGE revealed that there were differences in the syntaxin-1 fragments used to assemble SNAREΔ60. The Rizo laboratory used a fragment spanning residues 191–253 of syntaxin-1 (Trimbuch et al. 2014), as reported in Kummel et. al 2011 and Krishnakumar et. al 2015. However, the Rothman laboratory explained that, for the ITC experiments reported in these two papers, SNAREΔ60 complexes were actually formed with syntaxin-1 fragments spanning residues 188–259 or 188–265, and containing an N-terminal His_6-tag. Note that syntaxin-1(191–253) spans most of the SNARE motif except for a few C-

terminal residues, which helps to improve the solubility of SNARE complexes (Chen et al. 2002), syntaxin-1(188–259) includes the entire SNARE motif, and syntaxin-1(188–265) contains in addition the juxtamembrane region of syntaxin-1, which includes five positively charged residues.

To investigate how the differences in the syntaxin-1 fragments might affect the ITC results, we performed a systematic analysis using SNAREΔ60 containing syntaxin-1(191–253), syntaxin-1(188–259) or syntaxin-1(188–265) with or without a His_6-tag (below referred to as SNAREΔ60-Sx253, SNAREΔ60-Sx259, SNAREΔ60-Sx265 or His_6-SNAREΔ60-Sx265, respectively). The analysis involved direct titrations of the various SNAREΔ60 complexes with CpxI(48-134), full-length CpxI or full-length scCpxI mutant, and blocking assays using these complexes. All proteins were expressed using vectors provided by the Rothman laboratory. Representative data are shown in Figures 3.2 and 3.3, and Table 3.1 describes the K_Ds measured in the direct titrations. All direct titrations performed with the 12 different combinations of SNAREΔ60 complexes and CpxI proteins yielded K_D values around 2 μM, with no marked differences considering the confidence intervals of the measurements. The consistency of these results underlines the reliability of the data and shows that the affinity of CpxI for SNAREΔ60 is not substantially altered by the presence of residues 1–47 of CpxI or by the differences in the syntaxin-1 fragments used to assemble SNAREΔ60.

The systematic blocking assays were performed using the approach designed by the Rothman laboratory, blocking the various SNAREΔ60 complexes with a large (4.9-fold) excess of CpxI(48-134), and titrating with CpxI(48-134) itself, CpxI or scCpxI. Because the

use of different total protein concentrations might have yielded some variability in the heat release observed in the previously published blocking assays, all experiments of this systematic analysis used similar total protein concentrations. In all the control experiments where the blocked SNAREΔ60 complexes were titrated with CpxI(48-134) itself, only a very small amount of heat release was observed (Figure 3.3A–D), which can be attributed to a small amount of remaining free SNAREΔ60. Assuming a K_D of 2 μM, this small amount is estimated to be about 2.5% of the total SNAREΔ60 complex, which is consistent with the small heat release observed. Comparable, very small heat release was observed in experiments where blocked SNAREΔ60-Sx253 or SNAREΔ60-Sx259 complexes were titrated with full-length CpxI or scCpxI (Figure 3.3E,F,I,K), indicating that there is no interaction of residues 1–47 of CpxI with these complexes. However, the heat release was higher when full-length CpxI or scCpxI were titrated into blocked SNAREΔ60-Sx265 (Figure 3.3G,L), showing that residues 1–47 of CpxI do interact with SNAREΔ60 when the complex includes the juxtamembrane region in syntaxin-1. Reliable K_Ds cannot be derived from these data because of the difficulty in accurately defining the baselines in the respective isotherms, but it appears that the interaction is weak based on the small amount of heat release (Figure 3.3G,L) and the fact that the presence of the juxtamembrane region did not lead to an overt increase in the measured affinities in the direct titrations (Figure 3.2, Table 3.1). We also note that even higher heat release was observed in blocking experiments where His_6-SNAREΔ60-Sx265 was titrated with CpxI or scCpxI (Figure 3.3H,M), showing that the His_6-tag can alter the results and hence should be removed.

Overall, these results show that there is an interaction between the C-terminus of SNAREΔ60-Sx265 and residues 1–47 of CpxI, although the nature of the interaction remains unclear. It seems highly unlikely that the CpxI accessory helix-SNAREΔ60 interaction observed in the zigzag crystal structure (Figure 3.1C) underlies the heat release observed in the blocking assays performed with the SNAREΔ60-Sx265 and His_6-SNAREΔ60-Sx265 complexes because the heat release was not markedly altered by the superclamp mutation (Figure 3.3G,H,L,M; see also the superposition of data obtained for WT CpxI and scCpxI shown in Figure 3.3—figure supplement 1). Note that the superclamp mutation replaces three charged residues of WT CpxI with hydrophobic side chains that in the zigzag crystal structure pack against the hydrophobic groove left in SNAREΔ60 by the synaptobrevin truncation (Figure 3.1C) (Kummel et al. 2011); therefore the presence of three charged residues in WT CpxI is expected to strongly disrupt this interaction. Because the observation of heat release in the blocking assays requires the polybasic juxtamembrane region of syntaxin-1 within SNAREΔ60-Sx265, it is most likely that the interaction underlying this heat release involves binding of the juxtamembrane region to acidic side chains within residues 1–47 of CpxI, which include the accessory helix and preceding N-terminal sequence (Figure 3.1A). This type of interaction could occur between CpxI and the blocked SNAREΔ60-Sx265 complex, or between the juxtamembrane region of one SNAREΔ60-Sx265 complex and residues 1–47 of a CpxI molecule that is bound via its central helix to another SNAREΔ60-Sx265 complex. In this ‘trans’ configuration, CpxI would bridge two SNAREΔ60-Sx265 complexes, which might or might not lead to a zigzag arrangement similar to that observed in the crystal structure of scCpxI(26-83) bound to SNAREΔ60 (note

that the SNAREΔ60 complex in the crystal structure did not include the syntaxin-1 juxtamembrane region). Both interactions of CpxI (one involving the central helix and the other involving residues 1–47) could also be established in 'cis' with a single SNAREΔ60-Sx265 complex. In any case, the two interactions do not appear to act cooperatively, as residues 1–47 of CpxI or the syntaxin-1 juxtamembrane region do not markedly increase the affinity of SNAREΔ60 for CpxI (Figure 3.2; Table 3.1). Thus, the heat released by the interaction involving the syntaxin-1 juxtamembrane region with residues 1–47 of CpxI is most likely masked in the direct titrations by the much stronger heat arising from the binding of the CpxI central helix.

The functional significance of the interaction of the syntaxin-1 juxtamembrane region with CpxI might be questioned because it appears to be rather weak, but the interaction could be dramatically enhanced by the high local protein concentrations resulting from localization on a membrane. Indeed, this interaction could underlie a conformational change induced by CpxI in the C-terminus of membrane-anchored SNARE complexes that was recently observed by single-molecule fluorescence resonance energy transfer experiments (Choi et al. 2016). However, it is also worth noting that our experiments were performed in solution and, in vivo, the syntaxin-1 juxtamembrane region is expected to interact with negatively charged phospholipids present in the plasma membrane such as PS and PIP_2 (Khuong et al. 2013). Hence, further research will be required to test whether the interaction of the syntaxin-1 juxtamembrane region with CpxI can occur in the presence of such lipids and whether the interaction is physiologically relevant.

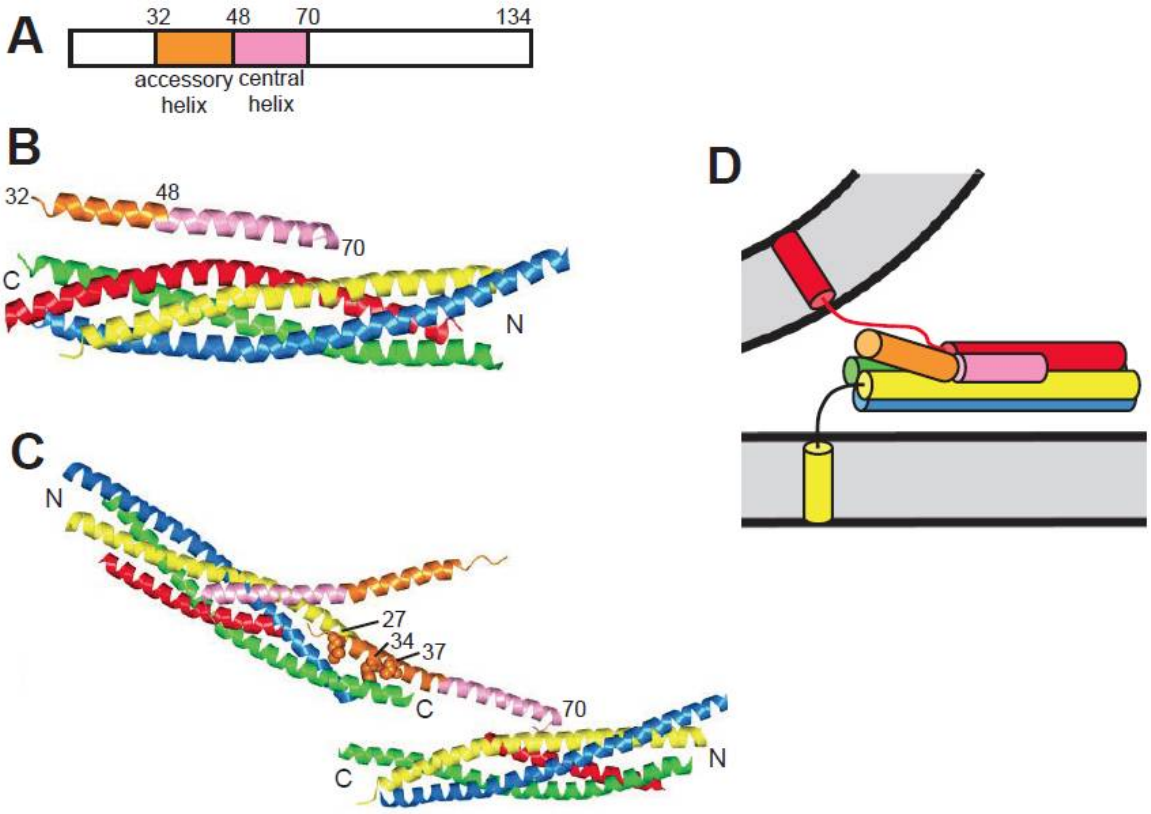

Figure 3.1. Models of the inhibitory function of Complexin. (A) Domain diagram of CpxI. Selected residue numbers are indicated above the diagram. (B) Ribbon diagram of the crystal structure of the SNARE complex bound to CpxI(26-83) (PDB code 1KIL) (Chen et al. 2002). Synaptobrevin is colored in red, syntaxin-1 in yellow, SNAP-25 in blue and green (N-terminal and C-terminal SNARE motifs, respectively), and CpxI(26-83) in orange (accessory helix) and pink (central helix). N and C indicate the N- and C-termini of the SNARE motifs. Selected residue numbers of CpxI(26-83) are indicated. (C) Ribbon diagram of the crystal structure of the SNAREΔ60 complex bound to the CpxI(26-83) superclamp mutant (PDB code 3RK3) (Kummel et al. 2011). Two complexes are shown to illustrate the zigzag array present in the crystals. Selected residue numbers are indicated for one of the scCpxI(26-83) molecules, which binds to one SNAREΔ60 complex through the central helix and to another SNAREΔ60 complex through the accessory helix. The three mutated residues in the accessory helix are shown as spheres and their residue numbers are indicated. (D) Model postulating that the Complexin accessory helix inhibits neurotransmitter release because of steric repulsion with the vesicle membrane. The model is based on the crystal structure shown in (A), but assumes that the C-terminus of the synaptobrevin SNARE motif is not assembled into the SNARE complex. This figure is based on Figure 1 of (Trimbuch et al. 2014), with modifications.

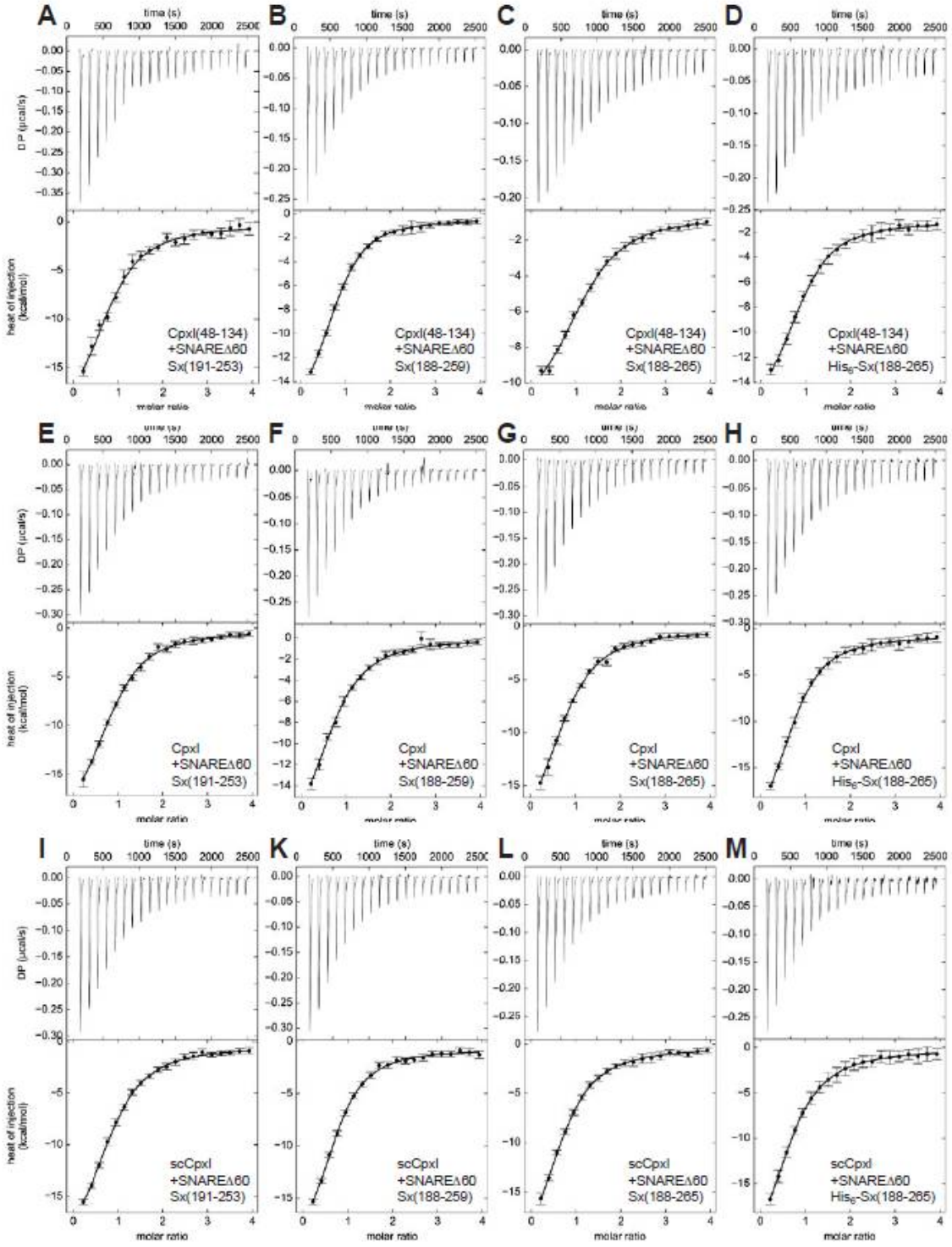

Figure 3.2. ITC analysis of CpxI-SNAREΔ60 interactions by direct titration. The various panels show direct titrations of SNAREΔ60 containing syntaxin-1 (191–253) (A,E,I),

syntaxin-1(188–259) (B,F,K), syntaxin-1(188–265) (C,G,L) or His_6-syntaxin-1(188–265) (D,H,M) with CpxI(48-134) (A–D), CpxI (E–H) or scCpxI (I–M), monitored by ITC. The upper panels show the baseline- and singular-value-decomposition-corrected thermograms for the respective experiments. The circles in the lower panels are the integrated heats of injection, with the error bars representing estimated errors for these values (Keller et al. 2012). The lines in these panels represent the respective fits of the data to a single binding site 'A + B <->AB' model.

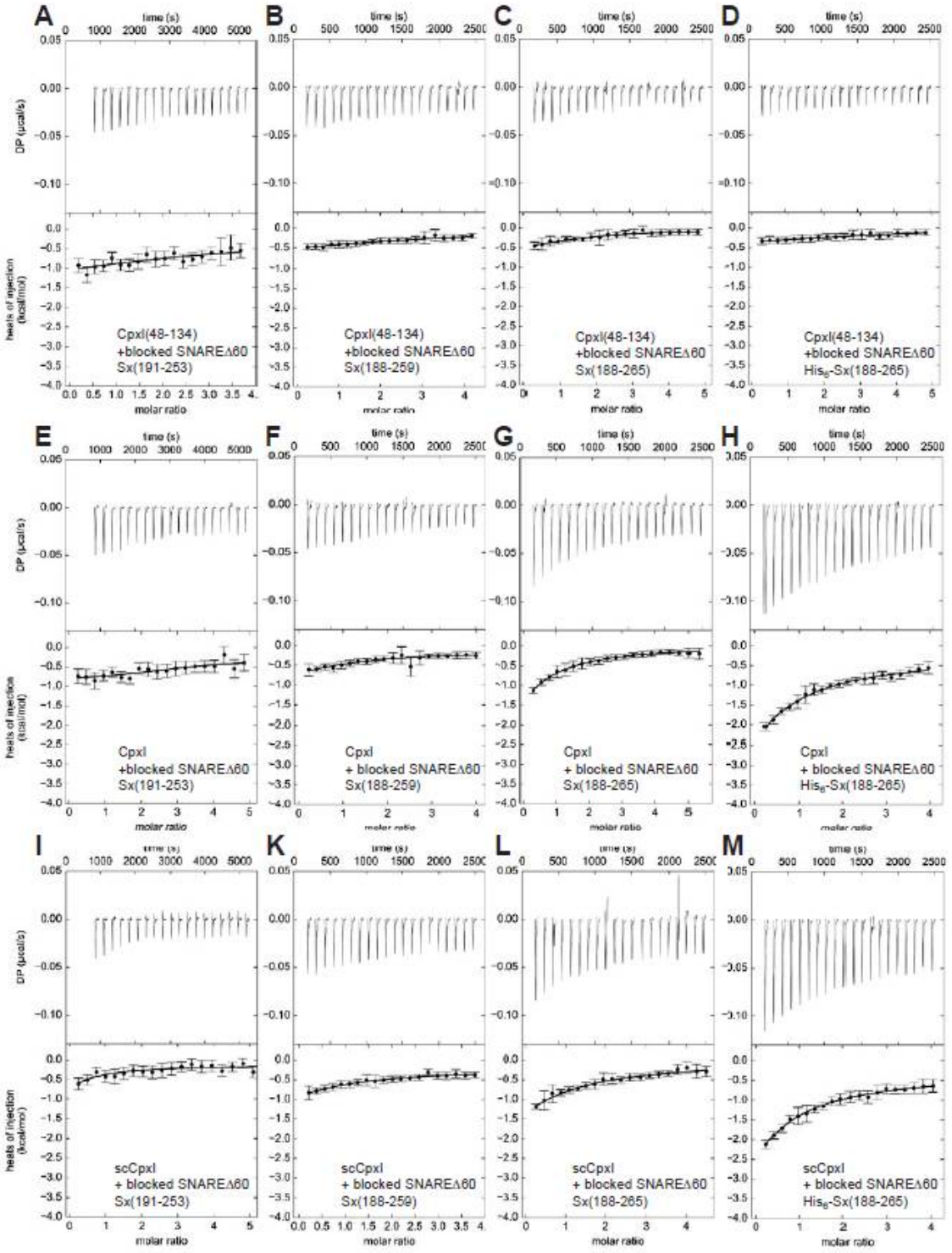

Figure 3.3. ITC analysis of CpxI-SNAREΔ60 interactions through blocking assays. The various panels show blocking assays monitored by ITC where SNAREΔ60 complex blocked

with 4.9 equivalents of CpxI(48-134) and containing syntaxin-1(191–253) (A,E,I), syntaxin-1(188–259) (B,F,K), syntaxin-1(188–265) (C,G,L) or His_6-syntaxin-1(188–265) (D,H,M) was titrated with CpxI(48-134) itself (A–D), CpxI (E–H) or scCpxI (I–M). The upper panels show the baseline- and singular-value-decomposition-corrected thermograms for the respective experiments. The circles in the lower panels are the integrated heats of injection, with the error bars representing estimated errors for these values (Keller et al. 2012). The lines in these panels represent the respective fits of the data to a single binding site 'A + B < ->AB' model, but note that no meaningful thermodynamic parameters can be derived from these data sets.

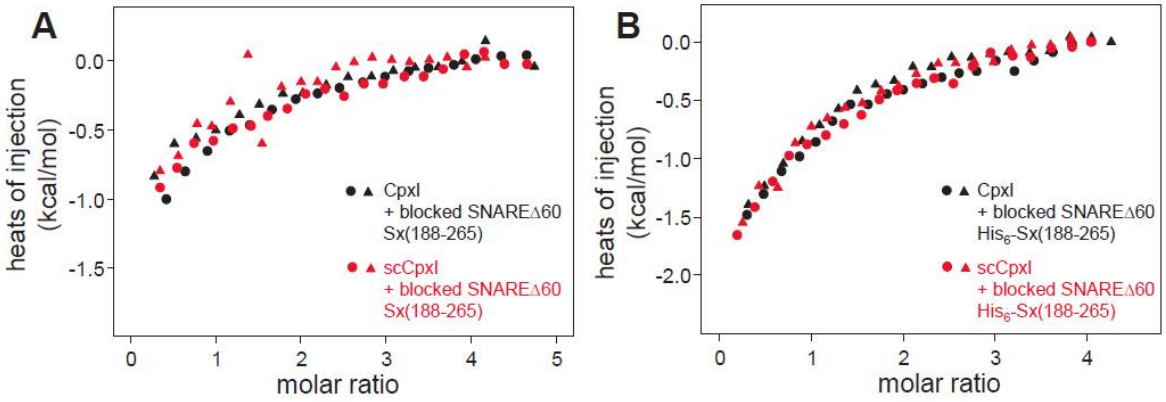

Figure 3.3- Figure Supplement 1. The superclamp mutation does not alter the heat release observed in the blocking assays. The plots show superpositions of ITC data obtained in blocking assays such as those described in Figure 3.3, including two separate experiments performed with WT CpxI and two separate experiments performed with scCpxI, titrated into blocked SNAREΔ60-Sx265 (A) or His_6-SNAREΔ60-Sx265 (B) complexes. To facilitate comparison of the four data sets shown in each panel, a constant value resulting from the average of the last five data points was subtracted from each data point of a given dataset. Note that, as a consequence, the baseline at the end of the titration is closer to zero than observed in the plots of Figure 3.3G,H,L,M, where the baseline was determined by the data fitting procedure. The data superpositions show that the superclamp mutation does not markedly influence the heat release observed in experiments performed with blocked SNAREΔ60-Sx265 (A) or His_6-SNAREΔ60-Sx265 (B) complexes.

	SNAREΔ60-Sx253	SNAREΔ60-Sx259	SNAREΔ60-Sx265	His_6-SNAREΔ60-Sx265
CpxI(48-134)	2.0 [1.4–2.8]	1.4 [1.2–1.7]	2.0 [1.6–2.5]	1.8 [1.5–2.1]
CpxI	1.9 [1.6–2.3]	2.5 [2.0–3.1]	2.4 [2.0–3.0]	2.2 [1.8–2.6]
scCpxI	2.0 [1.8–2.4]	2.2 [1.7–2.5]	2.2 [1.9–2.6]	2.2 [1.9–2.5]

Table 3.1. Summary of the K_Ds (in µM units) between Cpx1 proteins and SNAREΔ60 complexes containing different syntaxin-1 fragments measured by ITC. At least two independent experiments were performed for each combination of CpxI protein and SNAREΔ60 complex. K_Ds were derived from global fit of the independent experiments performed for each combination. For all K_Ds, 68.3% confidence intervals calculated using the error-surface projection method are indicated between brackets.

Chapter 4- Investigating interactions between Complexin, the SNARE complex, and lipids

4.1 Abstract

Complexins are small soluble proteins that bind to the SNARE complex through a central α-helix preceded by an accessory α-helix. Absence of Complexin causes a reduction in evoked release, while different effects are observed in spontaneous release. However, it is presently unclear how the Complexin N- and C-termini regulate fusion. Current efforts are directed at testing a model supported by reconstitution experiments and determining the structures of macromolecular complexes involved in neurotransmitter release. The goal of this project is to develop a complete model as to how Complexin functions so that I can understand how and why this protein is so important for calcium evoked release, since there currently is no model of Complexin that is able to incorporate all of its known interactions and activating/inhibiting properties. Importantly, I am forming SNARE complexes anchored on nanodiscs and liposomes in order to incorporate the essential membrane mimetic environment into a reconstituted system. My results suggest that membranes and the SNARE complex cooperate in binding to the Complexin termini. Such cooperative binding of Complexin to membranes and SNAREs may be critical for releasing the inhibition caused by the accessory helix, although the molecular mechanism of action has yet to be determined.

4.2 Introduction

Complexins (also referred to Synaphins) are one of the most well studied accessory proteins that regulate neurotransmitter release. They are small (14 kDa) hydrophilic proteins that were initially discovered as soluble proteins bound to neuronal SNARE complexes in membrane extracts (McMahon et al. 1995, Ishizuka et al. 1995, Takahashi et al. 1995). The domain architecture for Complexin-1 (Cpx1) is relatively simple. At its core is a central α-helix (CH) preceded by an accessory α-helix (AH) (Figure 4.1). The CH is known to interact with the ternary SNARE complex (Pabst et al. 2000, Pabst et al. 2002, Chen et al. 2002) and has been shown to be essential for its function (Xue et al. 2007). As discussed in Chapter 3, numerous groups have proposed different models describing the inhibitory function of the AH (Kummel et al. 2011, Trimbuch et al. 2014). A plethora of functional studies have been completed on Cpx1 using various truncations and mutants (see section 1.3). However, much less is known about the function of either the N-terminal domain (NTD) or the C-terminal domain (CTD).

Flanking the AH and CH of Cpx1 are two termini: the NTD, which consists of the first 30 amino acids, and the CTD, which consists of the final 65 residues (Figure 4.1). The NTD is relatively conserved (Martin et al. 2011) and can form a positively charged amphipathic α-helix (Xue et al. 2010b). Although various effects have been observed when deleting the NTD in different species (Martin et al. 2011, Cho et al. 2014, Hobson et al. 2011), the NTD was shown to be essential for full rescue of evoked and spontaneous release. Either deletion of the first 8 amino acids or a double mutation in the NTD (M5E, K6E) prevented this rescue, suggesting an activating role for the NTD in fusion (Xue et al. 2010b,

Xue et al. 2009, Xue et al. 2007). One of these same studies proposed that the NTD of Cpx1 interacts with C-terminus of the SNARE complex (Xue et al. 2010b), suggesting that this interaction could stabilize the SNARE complex and lower the energy barrier for membrane fusion. Additionally, they introduced the idea that the NTD could release the inhibitory function of the AH, which may switch the state of the release machinery from inhibiting to activating and explain the dual roles for Cpx1 to regulate neurotransmitter release in both a positive and negative manner (Giraudo et al. 2006, Schaub et al. 2006, Yoon et al. 2008, Malsam et al. 2009). Most recently, the Cpx1 NTD was shown to independently activate synaptic vesicle fusion through interactions with membranes that were enhanced by cooperative binding with the neuronal SNARE complex (Lai et al. 2016).

Less variable effects have been observed with the Cpx1 CTD. It is generally assumed that this domain provides some type of an inhibitory activity on neurotransmitter release (Martin et al. 2011, Wragg et al. 2013, Buhl et al. 2013). Like the NTD, the Cpx1 CTD also contains an amphipathic region that has been shown to preferentially interact with membranes of high curvature (Malsam et al. 2009, Seiler et al. 2009, Wragg et al. 2017, Gong et al. 2016). However, the CTD has been reported to activate fusion under some conditions (Kaeser-Woo et al. 2012), and the extent to which the CTD domain directly inhibits or activates fusion could simply be from Cpx1 localizing to fusion sites because of its membrane interactions.

Many studies have been completed on Cpx1 over the past 20 years, and yet no cohesive model exists that is able to synthesize the multitude of results together. One reason for this discrepancy could be from different functional effects in different biological

environments. Cpx1 sequences are conserved in some unicellular organisms and in all metazoans; Cp1x constructs from *Nematostella vectensis*, a cnidarian sea anemone that has evolved divergently than mammals, functionally replace mouse Cpx1 in evoked release (Yang et al. 2015a). However, it is unable to clamp spontaneous fusion. This phenotype is reminiscent of many published results on Cpx1, where varying results are reported in different species (human vs. mouse vs. fly vs. worm). Additional complexity is added to this conundrum when one considers the inconsistencies between *in vivo* and *in vitro* data. Since all Complexins have both inhibitory and activating functions, the field must continue to examine the function of Cpx1 with caution in order to determine how subtle differences in sequence and structure correlate to diverse functional results in varying species.

4.3 Materials and methods

Recombinant protein expression and purification

The following constructs were used for protein expression in *E. coli* BL21 (DE3) cells: Full-length rat syntaxin-1A, rat syntaxin-1A (2-253, 191-253, and 188-259), full-length rat SNAP-25A (C84S, C85S, C90S, C92S), human SNAP-25A (11-82 and 141-203), full-length rat synaptobrevin, rat synaptobrevin (29-93), rat synaptotagmin-1 57-421 (C74S, C75A, C77S, C79I, C82L, C277S), full-length rat complexin-1 (2-134), rat complexin (2-83 and 26-83), full-length Chinese hamster NSF, full-length Bos Taurus αSNAP, full length rat Munc18-1, a rat Munc13-1 fragment spanning the C_1C_2BMUNC_2C regions (529-1725 Δ1408-1452), the MUN domain of rat Munc13-1 (859-1516 Δ1408-1452), and a synthetic apolipoprotein fragment (MSP1E3D1). Expression and purification of the corresponding

proteins were performed as previously reported (Chen et al. 2006, Chen et al. 2002, Dulubova et al. 1999, Liang et al. 2013, Liu et al. 2017, Ma et al. 2011, Ma et al. 2013, Xu et al. 2013, Zhao et al. 2015) with the modifications described below. His_6-full-length syntaxin-1A was induced with 0.4 mM IPTG and expressed overnight at 25°C. Purification was done using Ni-NTA resin (Thermo Fisher) in 20 mM Tris pH 7.4, 500 mM NaCl, 8 mM imidazole, 2% Triton X-100, and 6M urea followed by elution in 20 mM Tris pH 7.4, 500 mM NaCl, 400 mM imidazole, and 0.1% DPC. The His_6 tag was removed using thrombin cleavage, followed by size exclusion chromatography on a Superdex 200 column (GE 10/300) in 20 mM Tris pH 7.4, 125 mM NaCl, 1 mM TCEP, 0.2% DPC (Liang et al. 2013). GST-syntaxin-1A 2-253 and GST-syntaxin-1A 188-259 were induced with 0.4 mM IPTG and expressed overnight at 25°C. Purification was done using glutathione sepharose resin (GE) followed by thrombin cleavage of the GST-tag and anion exchange chromatography on a HiTrap Q column (GE) in 25 mM Tris pH 7.4, 1mM TCEP using a linear gradient from 0 mM to 1000 mM NaCl. His_6-full-length complexin-1, His_6-Cpx1 2-83, His_6-Cpx1 26-83, His_6-Syx-1A 191-253, His_6-Syb 29-93, His_6-SNAP25 SN1 11-82, and His_6-SNAP25 SN3 141-203 were induced with 0.5 mM IPTG and expressed for 4 hours at 37°C. Purification was done using Ni-NTA resin followed by TEV cleavage of the His_6-tag and size exclusion chromatography on a Superdex 75 column (GE 16/60) in 20 mM Tris pH 7.4, 125 mM NaCl, 1 mM TCEP. His_6-full-length NSF was induced with 0.4 mM IPTG and expressed overnight at 20°C. Purification was done in 5 steps (Zhao et al. 2015): i) Ni-NTA affinity chromatography; ii) size exclusion chromatography of hexameric NSF on a Superdex S200 column (GE 16/60) in 50 mM Tris pH 8.0, 100 mM NaCl, 1 mM ATP, 1 mM EDTA, 1 mM

DTT, and 10% glycerol; iii) TEV cleavage of the His6-tag and monomerization with apyrase during 36 hr dialysis with nucleotide-free buffer; iv) three rounds of size exclusion chromatography to separate monomeric and hexameric NSF (re-injecting the latter) on a Superdex S200 column (GE 16/60) in 50 mM NaPi pH 8.0, 100 mM NaCl, 0.5 mM TCEP; and v) reassembly of the NSF monomers and size exclusion chromatography of reassembled hexameric NSF on a Superdex S200 column (GE 16/60) in 50 mM Tris pH 8.0, 100 mM NaCl, 1 mM ATP, 1 mM EDTA, 1 mM DTT, and 10% glycerol. His_6-Munc13-1 $C_1C_2BMUNC_2C$ (529-1725 Δ1408-1452) was induced with 0.5 mM IPTG and expressed overnight at 16°C. Purification was done using Ni-NTA resin (Thermo Fisher) followed by thrombin cleavage of the His6-tag and anion exchange chromatography on a HiTrap Q column (GE) in 20 mM Tris pH 8.0, 10% glycerol, 1 mM TCEP using a linear gradient from 0 to 500 mM NaCl. GST-MUN 859-1516 Δ1408-1452 was induced with 0.5 mM IPTG and expressed overnight at 16°C. Purification was done using glutathione sepharose resin (GE) followed by thrombin cleavage of the GST-tag and anion exchange chromatography on a HiTrap Q column (GE) in 20 mM Tris pH 8.0, 10% glycerol, 1 mM TCEP using a linear gradient from 0 to 1000 mM NaCl. Following anion exchange chromatography, size exclusion chromatography was performed on a Superdex S200 column (GE 16/60) in 10 mM Tris pH 8.0, 150 mM NaCl, 10% glycerol, 1 mM TCEP. His_6-MSP1E3D1 was induced with 1 mM IPTG and expressed for 4 hours at 37 °C. Purification was done using Ni-NTA resin (Thermo Fisher) followed by overnight dialysis in 20 mM Tris pH 7.4, 100 mM NaCl, 0.5 mM EDTA.

Proteins used for NMR studies (Cpx1 2-134, Cpx1 2-83, and Cpx1 26-83) were grown at 37 °C in M9 minimal media with 6.8 g/L Na_2HPO_4, 3.0 g/L KH_2PO_4, 0.5 g/L NaCl, 1 g/L NH_4Cl, 2 mM $MgSO_4$, 100 µM $CalCl_2$, and 4 g/L glucose. Uniform ^{15}N labeling was achieved using $^{15}NH_4Cl$ as the sole nitrogen source. Cells were induced and purified as described above.

Mutant proteins

All mutations were performed using QuickChange site-directed mutagenesis (Stratagene). These include the D326K mutation in full length rat Munc18-1, the M5E, K6E double mutation in full-length rat complexin-1, and the single point mutations M5C, S115C, or V61C in full-length rat complexin-1. All mutant proteins were purified the same as wild type.

Labeling proteins with IANBD and BODIPY fluorophores

Single cysteine mutants were labeled with either IANBD or BODIPY for full length Cpx1 2-134 (M5C, S115C, or V61C) using iodoacetamide or maleimide reactions (Thermo Fisher). Proteins at a concentration of roughly 75 µM were incubated with a 20-fold excess of dye for 2 hours at room temperature. Unreacted dye was separated from the labeled protein through size exclusion chromatography on a Superdex S200 column (GE 10/300) in 25 mM Tris pH 7.4, 125 mM NaCl. The concentration of fluorescently tagged proteins was determined using UV-vis absorbance and a Bradford assay.

SNARE complex assembly

Soluble SNARE complexes (mcc) were formed with SNAP25 SN1 (11-82), SNAP25 SN3 (141-203), Syb (29-93), and Syx (191-253). In some cases, Syx (188-259) was used where indicated. Complex assembly was accomplished by incubating a mixture of the purified fragments in equimolar ratios overnight and removing unassembled fragments by concentration-dilution cycles with a 30-kDa cutoff.

Circular dichroism spectroscopy

CD wavelength scans were recorded in PBS (pH 7.4, 137 mM NaCl, 3 mM KCl, 10 mM phosphate buffer, 0.25 mM TCEP) at a concentration of 0.1 mg/mL in a 1 mm cuvette using a Jasco-815 CD spectrophotometer. Ellipticity in millidegrees was converted to mean residue molar ellipticity to compare the CD spectra of different Cpx1 constructs.

Isothermal titration calorimetry

ITC experiments were performed using a VP-ITC system (MicroCal) at 20°C. Formed SNARE complexes (see above) and Cpx1 fragments were dialyzed (2 L for 4 hr (x2) followed by 2 L overnight) in a buffer containing 25 mM HEPES pH 7.5, 125 mM NaCl, 0.3 mM TCEP. Protein concentrations were measured by UV absorbance at 280 nm. Different Cpx1 fragments at 90 µM (Cpx1 2-134, 2-83, or 26-83) were titrated into the chamber containing 9 µM SNARE complex (mcc). The data were baseline corrected and integrated with NITPIC, fitted with a nonlinear least squares routine using a single-site binding model with ITCsy and plotted with GUSSI (Brautigam et al. 2016). The ‘A + B < ->AB’ model

was used for the fitting, and apparent concentration errors for the cell contents were compensated for by refining an incompetent fraction parameter. The 68.3% confidence intervals were obtained using the error surface projection method.

Nuclear magnetic resonance spectroscopy

^{1}H-^{15}N HSQC spectra were acquired at 20 °C on Agilent DD2 spectrometers operating at either 600 MHz or 800 MHz. Samples contained 20 μM uniformly ^{15}N-labeled protein in a buffer containing 20 mM Tris pH 7.2, 125 mM NaCl, 5% D_2O. All data were processed with NMRpipe (Delaglio et al. 1995) and analyzed with NMRView (Johnson et al. 1994).

Formation of nanodiscs

Nanodiscs with and without the cis-SNARE complex (formed with full-length synaptobrevin) were prepared as described below. Full-length rat synaptobrevin was added to a mixture of MSP1E3D1 and lipid (Syb:MSP:lipid ratio of 1:3:360) with n-octyl-β-D-glucopyranoside (βOG) and sodium cholate at final concentrations of 1%. Lipid composition was 85% POPC, 15% DOPS. The mixture was vortexed and incubated overnight at 4 °C with the remaining SNARE proteins (Syx 2-253 and SNAP-25 FL). The nanodiscs were formed by passing the mixture over a 4-cm-high column using Extracti-Gel D resin (Pierce) to remove the detergent. The nanodiscs were then run on a Superdex S200 column (GE 16/60) in 20 mM Tris pH 7.4, 125 mM NaCl, 0.3 mM TCEP.

Formation of proteoliposomes

Proteoliposomes with and without the cis-SNARE complex (formed with full-length synaptobrevin) were prepared as described below using a standard method of reconstitution. Full-length synaptobrevin was added to a mixture of soluble SNARE proteins (Syx 2-253 and SNAP-25 FL) and lipid using a TM protein:lipid ratio of 1:1,000 with βOG at a final concentrations of 1%. Lipid composition was 85% POPC, 15% DOPS for most experiments using proteoliposomes, except when T-lipids (40% POPC, 18% DOPS, 20%POPE, 20% cholesterol, 2% PIP_2) or V-lipids (42% POPC, 18% DOPS, 20% POPE, 20% cholesterol) are indicated. The mixture was incubated at room temperature and dialyzed against 20 mM Tris pH 7.4, 125 mM NaCl, 0.5 mM TCEP with 2g/L Amberlite XAD-2 beads (Sigma) 3 times at 4 °C overnight.

NBD fluorescence assays

NBD fluorescence experiments were performed at room temperature on a PTI Quantamaster 400 spectrofluorometer (T-format) with all slits set to 1.50 mm. Emission scans were obtained from 500-700 nm using an excitation wavelength of 466 nm in a buffer containing 20 mM Tris pH 7.4, 125 mM NaCl.

Fluorescence anisotropy

Fluorescence anisotropy experiments were performed at room temperature on a PTI Quantamaster 400 spectrofluorometer (T-format) with all slits set to 2.50 mm. Time-based scans were obtained for 60 seconds (0.2 points/s) at 515 nm using an excitation wavelength

of 480 nm in a buffer containing 20 mM Tris pH 7.4, 125 mM NaCl, 0.5 mM TCEP. Vertically and horizontally polarized fluorescence intensities were collected simultaneously and fluorescence anisotropy, r was calculated with the formula: $r = (I_{VV} – G\ I_{VH})/(I_{VV} + 2\ G\ I_{VH})$. G is an instrumental correction factor and I_{VV} and I_{VH} are fluorescence intensities excited with vertically polarized light. Data was corrected for scattering with samples containing no fluorescently tagged protein.

Reconstituted content mixing assays

Assays that monitor content mixing were performed as described in detail in (Liu et al., 2017). VS-liposomes with Synaptotagmin 57-421 and full length synaptobrevin contained 42% POPC, 6.8% DOPS, 31.2% POPE, and 20% cholesterol. T-liposomes with full-length syntaxin-1A and full-length SNAP25 contained 38% POPC, 18% DOPS, 20% POPE, 20% cholesterol, 2% PIP2, and 2% DAG. Dried lipid mixtures were re-suspended in 25 mM HEPES pH 7.4, 150 KCl, 1 mM TCEP, 10% glycerol, 2% βOG. Purified SNARE proteins and fluorescently labeled content mixing molecules were added to the lipid mixtures to make the syntaxin-1:SNAP25:lipid ratio 1:5:800 and Phycoerythrin-Biotin (4 μM) for T-liposomes, and the synaptotagmin-1:synaptobrevin:lipid ratio 1:2:1,000 and Cy5-Streptavidin (8 μM) for VS-liposomes. The mixtures were incubated at room temperature and dialyzed against the reaction buffer (25 mM HEPES pH 7.4, 150 mM KCl, 1 mM TCEP, 10% glycerol) with 2g/L Amberlite XAD-2 beads (Sigma) 3 times at 4 °C. Proteoliposomes were purified by floatation on a three-layer histodenz gradient (35%, 25%, and 0%) and harvested from the topmost interface. To measure content mixing from the development of FRET

between Phycoerythrin-Biotin trapped in T-liposomes and Cy5-streptavidin trapped in VS-liposomes, T-liposomes (0.25 mM lipid) were mixed with VS-liposomes (0.125 mM lipid) in a total volume of 200 µL. Acceptor T-liposomes were first incubated with 0.8 µM NSF, 2 µM αSNAP, 2.5 mM $MgCl_2$, 2 mM ATP, 0.1 mM EGTA, and 1 µM Munc18-1 at 37 °C for 25 minutes. They were then mixed with donor VS-liposomes, 0.5 µM Munc13-1 C_1C_2BMUNC_2C, and 1 µM excess SNAP25. All experiments were performed at 30 °C and 0.6 mM Ca^{2+} was added at 300 s. The fluorescence signal from Cy5-streptavidin (excitation at 565 nm, emission at 670 nm) was recorded to monitor content mixing. Experiments were performed in the presence of 5 µM streptavidin to prevent false signal from leaky liposomes.

4.4 Results

The Complexin-1 termini do not interact with the SNARE complex or other accessory proteins in solution

To investigate the secondary structure of the Cpx1 termini in solution, I performed circular dichroism (CD) spectroscopy on three Cpx1 fragments: the full-length (FL) construct (Cpx1 2-134), a fragment lacking the CTD (Cpx1 2-83), and a fragment lacking both termini (Cpx1 26-83). As expected, Cpx1 26-83 had the most alpha helical content as evident by the large minima in mean residue ellipticity at 208 nm and 222 nm (Figure 4.2). Cpx1 2-83 and Cpx1 2-134 had smaller minima at both of these locations, indicating that both termini of Cpx1 contain random coils and do not form helices when alone in solution.

Next, I looked to see if the termini of Cpx1 interact with the SNARE complex in solution using the mini-core complex (mcc), which only contains the 4 SNARE motifs from

Syntaxin-1, Synaptobrevin, and SNAP-25. Titrations of the same three Cpx1 fragments (Cpx1 2-134, Cpx1 2-83, and Cpx1 26-83) into the mcc showed very similar affinities of about 10 nM (Figure 4.3), which nicely correlates with previously published data (Pabst et al. 2002) and suggests that the termini of Cpx1 do not interact with the SNARE complex in solution. However, it cannot be ruled out that a weak interaction between the termini of Cpx1 and the SNARE complex is masked by the strong heats coming from binding of the Cpx1 CH.

To expand on the previous results, I collected ^{1}H-^{15}N heteronuclear single quantum coherence (HSQC) spectra with different ^{15}N Cpx1 fragments in the presence and absence of unlabeled mcc. HSQC spectra provide protein fingerprints (one crosspeak for each non-proline residue in the protein) that are highly sensitive to even very weak protein interactions (Rizo et al. 2012a). A ratio of crosspeak intensities that equals one indicates no broadening, while a ratio less than one indicates a binding event that causes signal broadening in the presence of the mcc. Assignments for Cpx1 crosspeaks were obtained from Pabst et. al 2000 with modifications (unpublished) from Junjie Xu since Cpx1 from a pET vector instead of a pGEX vector was used, which causes a slight change in the chemical environment of N-terminal residues due to cloning artifacts from the pGEX vector. Broadened crosspeaks for the region of Cpx1 containing the AH and CH (residues 32-70) were observed for all 3 Cpx1 fragments due to binding of the Cpx1 CH (Figure 4.4). Crosspeaks from the Cpx1 CH broaden due to direct binding to the SNARE complex, while crosspeaks from the Cpx1 AH broaden due to helix stabilization effects that propagate beyond the binding region, even though the Cpx1 AH does not directly bind to the SNARE complex (Chen et al. 2002).

Broadening of the Cpx1 termini was not observed when the mcc was added to ^{15}N Cpx1 2-134 (Figure 4.4A, left), as evident by intensity ratios for both the NTD (2-31) and CTD (69-134) that remain around one (Figure 4.4B, left). Similar results were seen for ^{15}N Cpx1 2-83, where the NTD signal intensity remained at one, and for ^{15}N Cpx1 26-83, where almost complete broadening was observed since no termini were present in this fragment (Figure 4.4A,B center and right, respectively). These results further support the idea that the termini of Cpx1 do not interact with the SNARE complex in solution when only the SNARE complex is present. Although it is plausible that the interaction between the Cpx1 termini and the SNARE complex is very weak, it seems most likely that such interactions do not exist in solution.

Since the termini of Cpx1 did not interact with the mcc, I next tested whether Cpx1 interacted with other components of the release machinery in solution, such as Munc18-1, the MUN domain of Munc13-1, and the mini-core complex full (mccf). The mccf uses a slightly longer Syx-1 fragment (188-259) than the mcc, which was formed using Syx-1 191-253. This longer Syx-1 fragment includes the entire Syx-1 SNARE motif and is not truncated to assure that Cpx1 does not recognize the fully zippered C-terminal end of the SNARE complex. Similar ^{1}H-^{15}N HSQC spectra using ^{15}N Cpx1 2-134 showed that only the crosspeaks for the AH and CH broadened in the presence of the mccf, and that addition of Munc18-1 or the MUN domain of Munc13-1 lead to no significant changes in the HSQC spectra (Figure 4.5). Overall, the data suggest that the Cpx1 termini do not bind to the SNARE complex, Munc18-1, or the MUN domain of Munc13-1 in solution. However, a major limitation to all of the experiments described in this chapter thus far has been the lack

of a lipid bilayer, as membrane mimetics may be necessary to provide sufficient cooperativity to stabilize these weak interactions.

The Complexin-1 termini interact with lipids and the cis-SNARE complex

In order to study Cpx1 interactions with the SNARE complex in a more physiologically relevant environment, I reconstituted the SNARE complex into nanodiscs by using Syb full-length (Syb FL), which contains a C-terminal transmembrane helix that anchors the cis-SNARE complex to the lipid bilayer. Nanodiscs are flat, disc-shaped phospholipid bilayers surround by a membrane scaffold protein (MSP) (Denisov et al. 2004). For this study, nanodiscs were made using the MSP1E3D1 engineered scaffold fragment to form nanodiscs with a 13 nm diameter. Reconstituted nanodiscs were injected over a Superdex S200 (16/60) column to select for nanodiscs containing the cis-SNARE complex (Figure 4.6). ^{1}H-^{15}N HSQC spectra were first collected using ^{15}N Cpx1 2-134 to look at binding to empty nanodiscs where only a small number of crosspeaks were observed to broaden (Figure 4.7A). These crosspeaks all localized to the Cpx1 CTD, which suggests that this domain binds to membranes even in the absence of the SNARE complex or other accessory proteins (Figure 4.7B). Previously published data from other labs is in agreement with these results, and the most current model in the field hypothesizes that the role of the Cpx1 CTD is to localize this protein to the site of fusion by binding to membranes so that its other domains can engage with the SNARE complex for proper function (Seiler et al. 2009, Snead et al. 2014, Gong et al. 2016, Wragg et al. 2013).

Unlike the CTD, the NTD was unable to bind to empty nanodiscs, although it was able to bind to nanodiscs containing the cis-SNARE complex (Figure 4.8A,B). Neither of these binding events were observed with the mcc in solution (Figure 4.4A,B, left). A double mutation in two NTD residues to glutamic acid (M5E, K6E) completely abrogated this binding event, while simultaneously preserving binding of the Cpx1 CH (Figure 4.9A,B) (Xue et al. 2010b). Since Cpx1 lacks tertiary structure, only chemical shifts for the mutated and neighboring residues were altered, while most of the crosspeaks remained unchanged. Assignments for these mutated residues were not experimentally obtained since the only well dispersed amino acid in the NTD that changed chemical shifts was residue A8. My results suggest that membranes and the SNARE complex cooperate in binding to the Cpx1 NTD. Such cooperative binding to membranes and SNAREs may be critical for releasing the inhibition caused by the AH, although this remains speculative at the moment.

To further explore the interaction between Cpx1 and membranes, I attached an environmentally sensitive fluorescent probe, (N,N'-Dimethyl-N-(Iodoacetyl)-N'-(7-Nitrobenz-2-Oxa-1,3-Diazol-4-yl)Ethylenediamine (IANBD), to both Cpx1 termini (Figure 4.10A). This probe is highly quenched when exposed to a polar solution, but significantly de-quenched in the nonpolar environment of a membrane bilayer. Fluorescence emission spectra were acquired when the probe was placed at the NTD (K6C) and at the CTD (S115C) for the protein alone, with empty liposomes, and with the cis-SNARE complex anchored to liposomes. The fluorescence data show that the Cpx1 CTD bound well to membranes in the absence of the cis-SNARE complex, as evident from the large fold increase in maximum fluorescence intensity (Figure 4.10B, right). This signal was further increased when the cis-

SNARE complex was attached to liposomes, but the additional gain in signal was not as large. In contrast to the CTD, the Cpx1 NTD bound weakly to membranes, but showed a significantly larger change in maximum fluorescence intensity when the SNARE complex was attached to the liposomes (Figure 4.10B, left). In conjunction with the NMR data, my findings further support a cooperative interaction between the Cpx1 NTD, membranes, and the SNARE complex.

Since I observed an interaction between Cpx1 and liposomes, I determined the apparent affinity of the Cpx1 termini for liposomes made with different lipid compositions. The previous experiments used a simplistic lipid composition (85% POCP, 15% DOPS) for preliminary results to look at the relative changes in lipid affinity with and without the presence of the cis-SNARE complex. To investigate the apparent affinity of each Cpx1 terminus for different types of liposomes, I titrated different concentrations of liposomes into a fixed amount of Cpx1 labeled at both the NTD (K6C) and CTD (S115C) with the environmentally sensitive IANBD probe using fluorescence emission scans (Figure 4.10A). The data were fit to a single site binding model using SigmaPlot to obtain relative affinities for each terminus. No preference for lipid composition was observed for either termini, suggesting that Cpx1 preferentially binds to the negatively charged DOPS lipids (Figure 4.11). The Cpx1 CTD had an apparent affinity 2x greater than the NTD, but the affinities for both termini were relatively weak. However, one must consider the cooperativity between multiple lipid molecules for binding to either termini, which could significantly enhance the strength of these interactions, especially since binding of the Cpx1 CH to the SNARE complex should dramatically increase the local concentration of Cpx1.

The data collected so far suggest that Cpx1 can simultaneously interact with SNARE complexes and lipids. To see how these cooperative interactions influence the affinity of Cpx1 for the SNARE complex, I examined binding between Cpx1 2-134 and 4 different forms of the SNARE complex using fluorescence anisotropy: the soluble mcc in solution, the cis-SNARE complex attached to liposomes, the cis-SNARE complex attached to nanodiscs, and a trans-SNARE complex formed between one nanodisc and one liposome. I titrated different concentrations of the SNARE complex into a fixed amount of Cpx1 labeled with a BODIPY fluorescent probe at a position that does not interfere with SNARE complex binding (V61C) and monitored fluorescence anisotropy using time-based emission (Chen et al. 2002). The data were fit to a single site binding model using SigmaPlot to obtain affinities for the different complexes (Figure 4.12). I obtained an affinity of about 50 nM between Cpx1 FL and the mcc, which is in approximate agreement with my ITC data and previously published literature (Pabst et al. 2002), especially considering that fluorescent probes were used to obtain this value and that only 6 data points were used to fit the binding curve. Stronger affinities were observed when the SNARE complex was anchored either to liposomes or nanodiscs, most likely due to cooperative interactions between the Cpx1 termini, SNARE complex, and lipids, in addition to binding of the CH to the SNARE complex itself. However, a weaker affinity was obtained for the trans-SNARE complex, suggesting that the trans configuration may not zippered as far as the cis state (Gao et al. 2012, Zorman et al. 2014). This conclusion remains speculative since the trans-SNARE complexes used in this assay may not have been fully formed. Since it is now known how to efficiently form trans-SNAE complexes (Chapter 2), it would be beneficial to revisit these

experiments to verify if the affinity of Cpx1 for the trans-SNARE complex truly is weaker than for the cis-SNARE complex. In order to determine the exact role of Cpx1 in membrane fusion, studies need to be completed using functional assays in the presence of other components of the release machinery.

Reconstituting Complexin-1 function with content mixing assays

A recent model for synaptic membrane fusion incorporated the function of 8 key components of the release machinery: the 3 SNARE proteins (Syntaxin-1, Synaptobrevin, and SNAP-25), NSF, αSNAP, Munc18-1, Munc13-1, and Syt1 (Figure 1.12) (Ma et al. 2013). However, Cpx1 was not included in these recent reconstitution experiments (Ma et al. 2013, Liu et al. 2016), and it remains to be determined how Cpx1 interacts with other components of the release machinery to regulate fusion at the molecular level. By incorporating different fragments of Cpx1 into a reconstituted fusion assay that monitors content mixing, I sought to determine how the different domains of Cpx1 both inhibit and activate fusion under numerous conditions.

At the most basic level, I was able to reconstitute calcium independent content mixing by combining T-liposomes, which contain Syx-1/SNAP-25, with VS-liposomes, which contain Syb/Syt1 (Figure 4.13, black). Moderately fast content mixing was observed because Syb must displace a second Syx helix from the 2:1 complex on T-liposomes in order to form the trans-SNARE complex. This process was accelerated because of Syt1 full-length (Syt1-FL), which tethers/docks membranes in the absence of calcium at a close enough distance to allow for the trans-SNARE complex to form. Syt1-FL is a transmembrane protein anchored

to the synaptic vesicle that can simultaneously interact with PIP_2 and t-SNARE complexes on the plasma membrane, allowing it to tether in the absence of calcium (Kim et al. 2012). Because of this, no effect was seen upon Ca^{2+} addition at 5 minutes. Titration of different concentrations of Cpx1 lead to a decrease in content mixing both in the presence and absence of calcium (Figure 4.13). This result is a bit perplexing because previous work in the field has shown that calcium binding to Syt1 is able to displace Cpx1 and release its inhibitory function (Dai et al. 2007, Tang et al. 2006). However, I most likely only observed the inhibitory function of Cpx1 in this assay because the system lacked other critical components of the release machinery that regulate on-pathway SNARE complex formation (Ma et al. 2013).

By including NSF, αSNAP, Munc18-1, and a $C_1C_2BMUNC_2C$ fragment of Munc13-1 in these reconstitution experiments (referred to as the complete system), SNARE complex formation goes through the correct pathway, which starts with Munc18-1 binding to closed Syx-1 (Figure 1.12). In this system, fusion was calcium dependent because of calcium sensing by the C_2B domain of Munc13-1, which releases an inhibitory mechanism that exists in the primed state before calcium addition (Figure 4.14, black) (Liu et al. 2016). Titration of different concentrations of Cpx1 again lead to a decrease in content mixing for calcium dependent fusion (Figure 4.14). This result is also puzzling because, if anything, Cpx1 should inhibit fusion before the addition of calcium, and stimulate fusion upon its addition. Calcium independent content mixing was non-existent in this assay, so it was impossible to detect an inhibitory function of Cpx1 before calcium addition.

In order to modify the complete reconstitution system so that some amount of content mixing occurred in the absence of calcium, I used a Munc18-1 mutation (D326K) to bypass the requirement of Munc13-1 for content mixing (Sitarska et al. 2017). Munc18-1 D326K lead to substantial calcium independent content mixing that was accelerated by the membrane-membrane bridging capabilities of Munc13-1 C_1C_2BMUNC_2C (Figure 4.15, green and black curves). The addition of 4 μM Cpx1 to these experiments significantly decreased the amount of calcium independent content mixing. Interestingly, calcium addition appeared to relieve the system from this inhibition, as similar levels of content mixing were reached when comparing samples that contained the Munc18-1 D36K mutant ± Cpx1 (Figure 4.15, green and yellow curves). This is the first time I observed inhibitory and possible activating functions for Cpx1 in a single functional assay. Whether or not this removal of inhibition corresponds to the activating function of Cpx1 remains to be determined. Literature suggests that Cpx1 should stimulate fusion (Xue et al. 2010b), but this activity may be difficult to detect in a reconstituted system that is already very active.

Lastly, I wanted to observe how different Cpx1 fragments behave in the complete reconstitution system with the Munc18-1 D326K mutant. As observed previously, significant calcium independent content mixing was observed without Cpx1, and this activity was dramatically reduced in the presence of 4 μM Cpx1 FL (Figure 4.16, black and red curves, respectively). Cpx1 fragments lacking either the CTD (Cpx1 2-83) or both termini (Cpx1 26-83) were unable to inhibit calcium independent content mixing as well as Cpx1 FL (Figure 4.16, green and blue curves, respectively). This result suggests that in addition to the AH, the Cpx1 CTD is needed for proper inhibition of fusion. Although this is in agreement

with some data in the field (Wragg et al. 2013, Martin et al. 2011, Buhl et al. 2013), it is in disagreement with others (Xue et al. 2007, Kaeser-Woo et al. 2012). The enigma of Cpx1 still remains to be solved as to how all of its domains cooperatively interact with lipids, SNAREs, and other proteins to regulate fusion at the molecular level.

4.5 Discussion

Complexins are small proteins that are known to interact with the SNARE complex. The heart of this interaction involves binding of the CH to the SNARE complex in an antiparallel orientation (Chen et al. 2002). Despite having secondary structure, the AH does not make any contact with the SNARE complex in this structure. Experiments in this study showed that the Cpx1 termini do not interact with the SNARE complex in solution (Figures 4.3 and 4.4). Binding was observed for both termini when liposomes were included in the experiments, and this interaction was strengthened when the cis-SNARE complex was anchored to the liposomes (Figures 4.7-4.12). Interestingly, binding was only observed for the CTD when nanodiscs were included in the experiments, suggesting that both Cpx1 termini may sense curvature (Seiler et al. 2009, Snead et al. 2014, Gong et al. 2016). Cpx1 has a high affinity for the SNARE complex in solution (about 10 nM, Figure 4.3), and this affinity was further increased by cooperative interactions between both termini with lipids. Binding of Cpx1 to the SNARE complex should dramatically increase the local concentration of Cpx1, so these individual weak interactions may in fact be substantially stronger together (Figures 4.10-4.12). Reconstituted content mixing assays demonstrated that the Cpx1 CTD is necessary for inhibition of calcium independent fusion (Figures 4.13-4.16). This inhibition

of fusion was relieved in the presence of Syt1-FL and Ca^{2+}, but no additional stimulation was observed by Cpx1. Although these results do not definitively show how the different domains of Cpx1 cooperate to simultaneously inhibit and activate fusion, they do suggest a model where the CTD binds to liposomes to localize to the site of fusion (and possibly inhibit), the CH binds to the SNARE complex, the AH prevents full zippering of the trans-SNARE complex (and therefore inhibits fusion) through steric/electrostatic repulsion, and the NTD may potentially release this inhibition through cooperative interactions with both the C-terminus of the SNARE complex and membranes (Figure 4.17).

A recent publication proposed that Cpx1 inhibits fusion through interactions between the Cpx1 NTD and the linker region of the SNARE complex that prevents full zippering (Shon et al. 2018). Ca^{2+} relieves this inhibition by binding to Syt1, which dislodges the Cpx1 NTD from the SNARE complex, and allows the linker domain to fully zipper. Since both Cpx1 termini interact with membranes, perhaps they are in close proximity to each other if they insert into the same membrane. However, much still remains to be determined about where exactly the termini of Cpx1 exert their function.

Currently, a comprehensive model for neurotransmitter release that includes Cpx1 does not exist because the available data cannot be rationalized into a cohesive explanation for its functional activity. The answer to this conundrum can perhaps be explained by the idea that Cpx1 has evolved differently in different species to optimize its activity at synapses. For example, the primary function of Cpx1 at invertebrate neuromuscular junctions (NMJ) is to inhibit spontaneous fusion (Schuske et al. 2004, Trimbuch et al. 2016). Invertebrates only have excitatory inputs and too much activity is undesirable because it hinders the dynamic

range of a neuron's ability to regulate function. Conversely, vertebrates have a central nervous system (CNS) that receives many large inputs from both excitatory and inhibitory synapses (Trimbuch et al. 2016). Here, a predominantly activating function for Cpx1 is exhibited to increase the efficiency of neuronal communication by stimulating evoked action potentials. This elegant model explains numerous bouts of Cpx1 data and simply suggests that while the core function of Cpx1 remains conserved across centuries of evolution, subtle structural differences elicit critical differences in diverse species to optimize the regulation of neuronal membrane fusion. After all, the entire process of synaptic vesicle fusion is efficiently inefficient to match the ever changing needs of the cell.

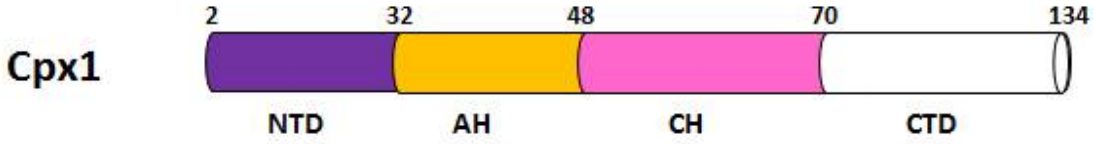

Figure 4.1. Domain architecture of Complexin-1. Schematic of the domain architecture of Cpx1. The N-terminal domain (NTD, 2-31) is shown in purple, accessory α-helix (AH, 32-47) in orange, central α-helix (CH, 48-69) in pink, and C-terminal domain (CTD, 70-134) in white.

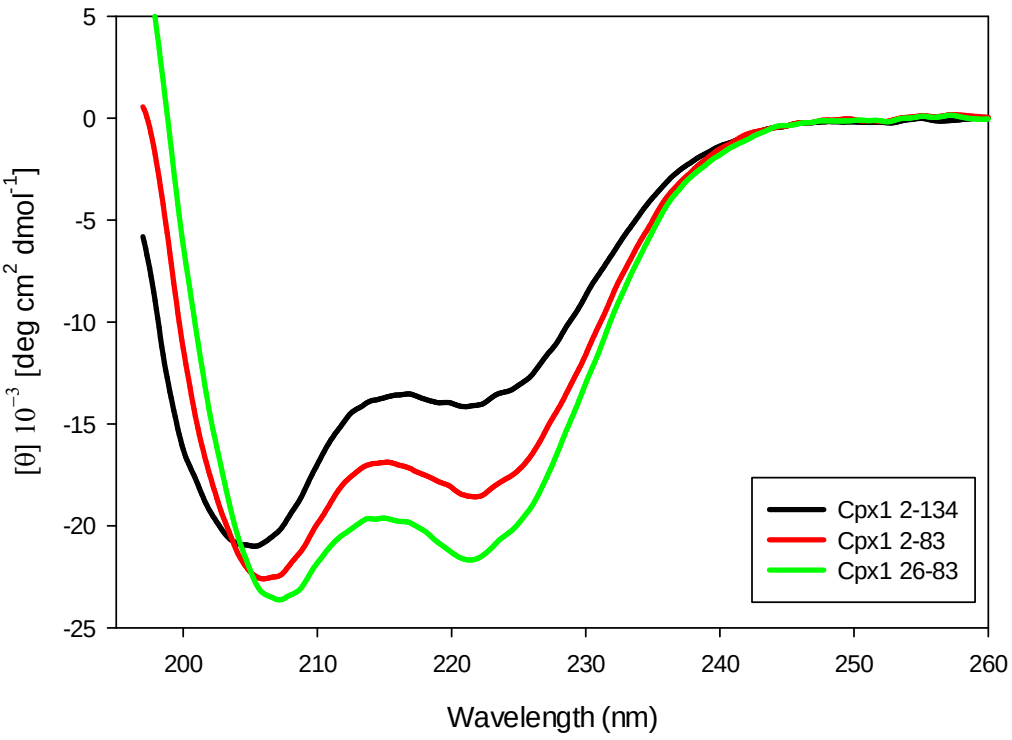

Figure 4.2. CD spectra of different Complexin-1 fragments show that both termini are random coils in solution. The CD spectra show that as the termini of Cpx1 are truncated (black data corresponds to Cpx1 2-34, red data corresponds to Cpx1 2-83 lacking the CTD, and green data corresponds to Cpx1 26-83 lacking both termini), the alpha helical content of Cpx1 increases as seen by an increase in mean residue ellipticity minima at 208 nm and 222 nm.

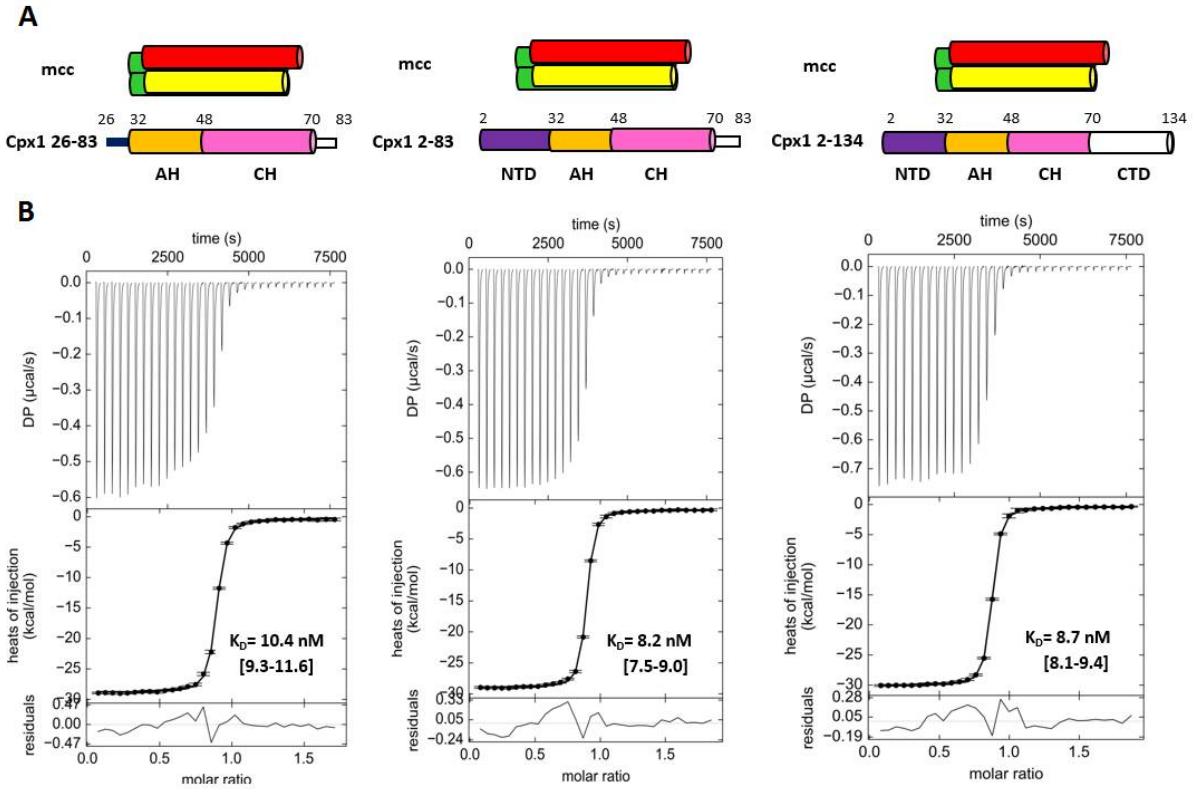

Figure 4.3. Titrations with different Complexin-1 fragments monitored by ITC reveal no interaction between the termini and the SNARE complex in solution. (A) Schematics of the mcc with Syntaxin-1 in yellow, Synaptobrevin in red, and SNAP-25 in green, as well as different Cpx1 constructs with Cpx1 NTD in purple, AH in orange, CH in pink, and CTD in white. (B) The various panels show titrations of the mcc with different Cpx1 fragments (Cpx1 26-83 left, Cpx1 2-83 center, and Cpx1 2-134 right) monitored by ITC. The upper panels show the baseline- and singular-value-decomposition-corrected thermograms for the respective experiments. The circles in the lower panels are the integrated heats of injection, with the error bars representing estimated errors for these values (Keller et al. 2012). The lines in these panels represent the respective fits of the data to a single binding site 'A + B <->AB' model. K_Ds were derived from global fit of the independent experiments performed for each combination. For all K_Ds, 68.3% confidence intervals calculated using the error-surface projection method are indicated between brackets. All three Cpx1 fragments have similar affinities for the mcc in solution, suggesting that the termini of Cpx1 do not interact with the SNARE complex.

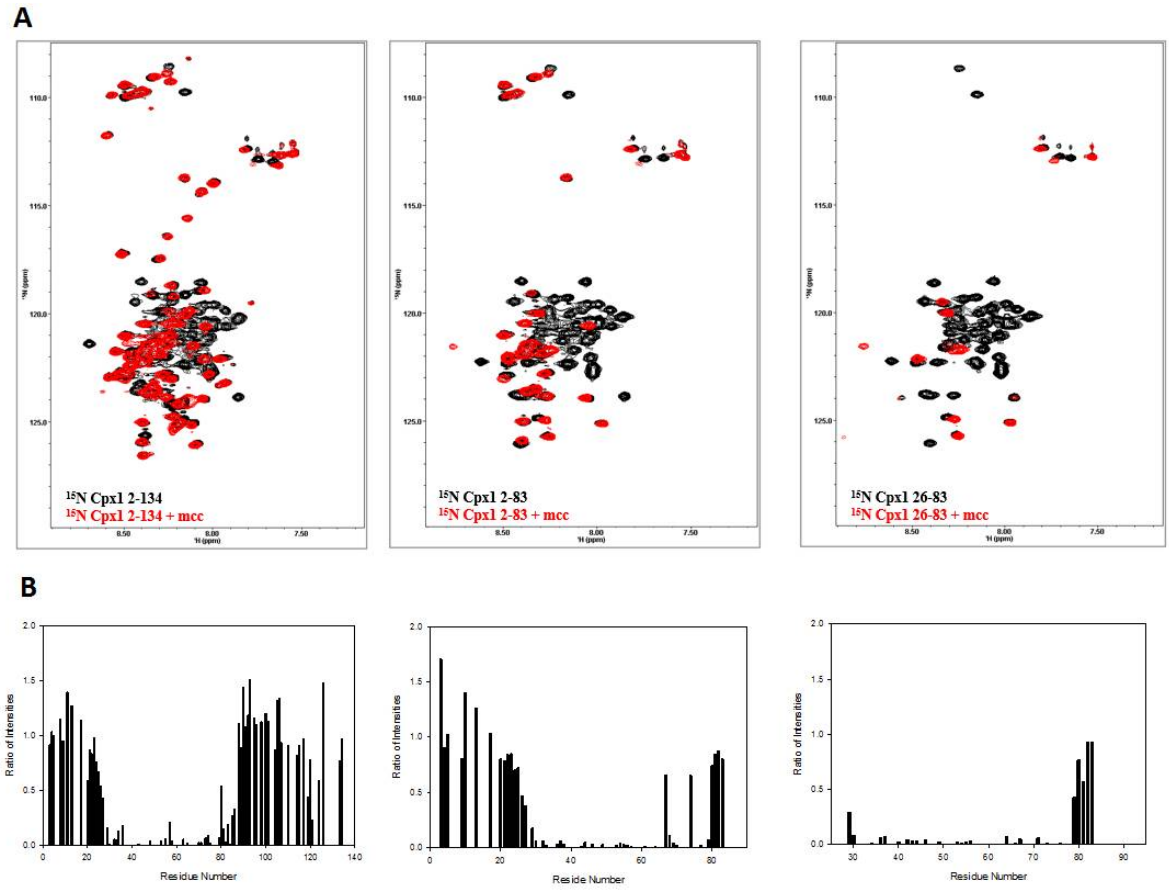

Figure 4.4. ^{1}H-^{15}N HSQC spectra show no interaction between the Complexin-1 termini and the SNARE complex in solution. (A) ^{1}H-^{15}N HSQC spectra of three different ^{15}N Cpx1 fragments: Cpx1 2-134 left, Cpx1 2-83 center, and Cpx1 26-83 right. Black contours were collected with only the indicated Cpx1 fragment (20 µM), and red contours were collected in the presence of the mcc (30 µM). (B) Bar diagrams showing a ratio of crosspeak intensity from ^{1}H-^{15}N HSQC spectra of Cpx1 as a function of residue number. This ratio was obtained by dividing the crosspeak signal intensity of the Cpx1 fragment alone by the crosspeak signal in the presence of the mcc. Only crosspeaks corresponding to the AH and CH (residues 32-70) of Cpx1 broaden due to binding of the CH.

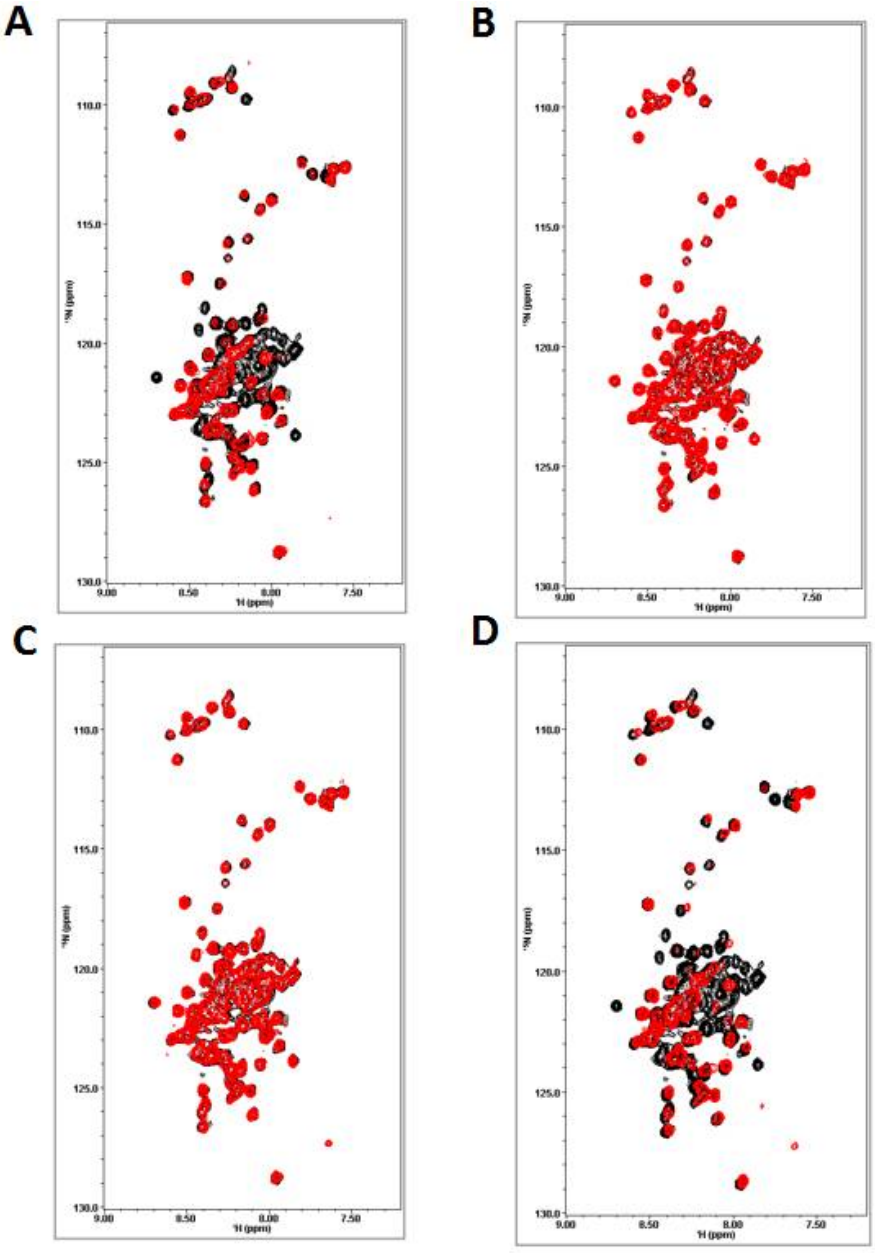

Figure 4.5. ^{1}H-^{15}N HSQC spectra show no interaction between Complexin-1 and other components of the release machinery in solution. ^{1}H-^{15}N HSQC spectra of ^{15}N Cpx1 2-134 alone in solution (15 µM, black contours) in the presence of (A) the mccf (15 µM, red contours), (B) the mccf and the MUN domain of Munc13-1 (15 µM each, red contours), (C) the mccf and Munc18-1 (15 µM each, red contours), and (D) the mccf, MUN domain of Munc13-1, and Munc18-1 (15 µM each, red contours). A lack of significant changes in the crosspeaks for the Cpx1 termini indicates no interaction with any of these components in solution, other than Cpx1 CH binding to the SNARE complex.

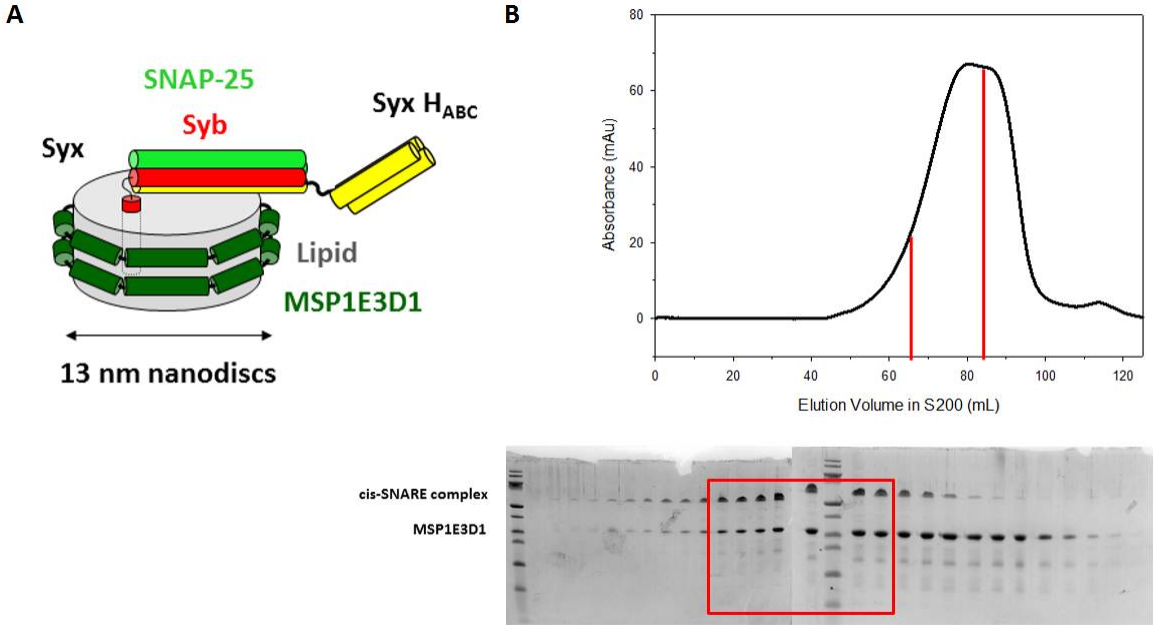

Figure 4.6. Formation of nanodiscs containing the cis-SNARE complex. (A) Schematic of the cis-SNARE complex anchored to nanodiscs with a 13 nm diameter. The lipid bilayer is shown in gray, scaffold protein (MSP1E3D1) in dark green, Syntaxin-1 in yellow, Synaptobrevin in red, and SNAP-25 in light green. (B) Gel filtration chromatogram showing the elution profile of nanodiscs containing the cis-SNARE complex (top). SDS-PAGE gel showing the elutions from gel filtration to determine which fractions contain the cis-SNARE complex anchored to nanodiscs (bottom). Fractions boxed in red (and red lines in the chromatogram) contain the desired product with a band intensity of 1:1 for the cis-SNARE complex:MSP1E3D1. Since the cis-SNARE complex is roughly twice as large as MSP1E3D1, a nanodisc with two copies of MSP1E3D1 and one cis-SNARE complex should have roughly equal band intensities for the two components.

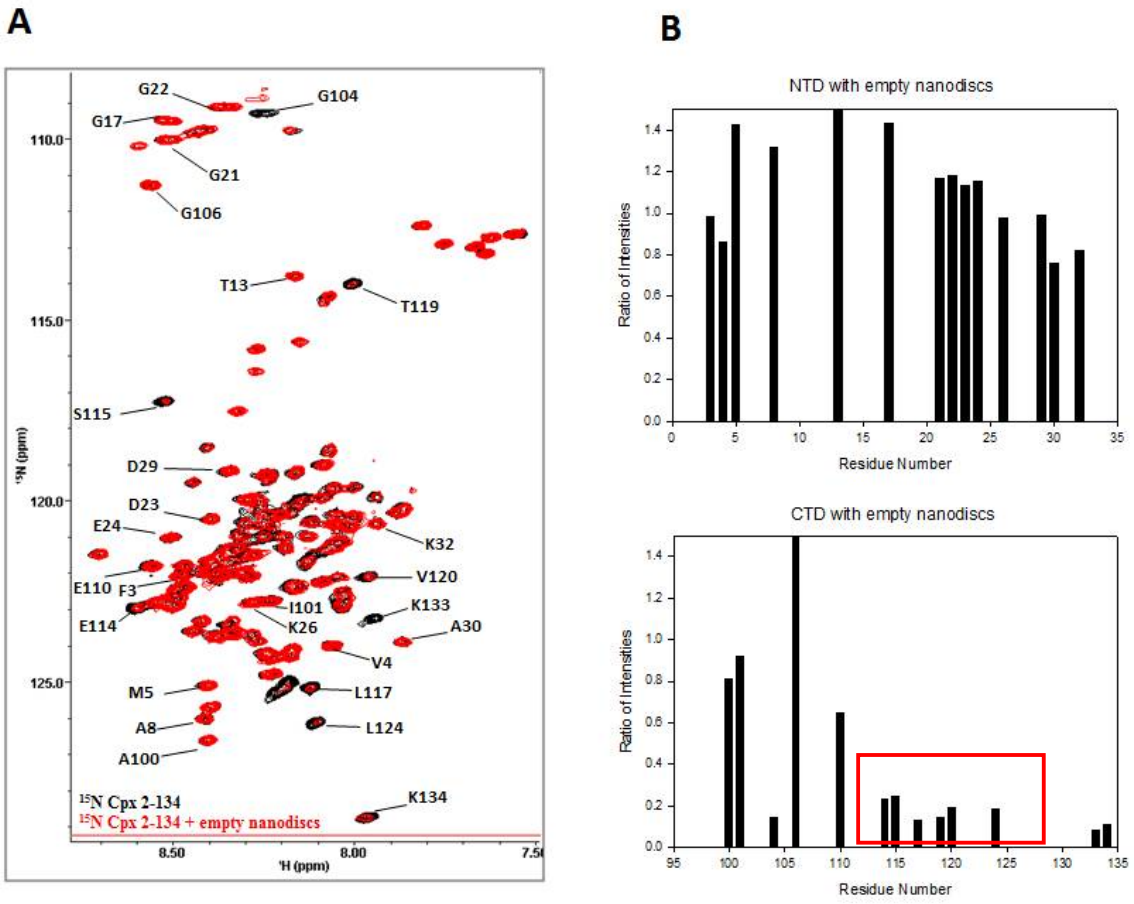

Figure 4.7. ^{1}H-^{15}N HSQC spectra demonstrate an interaction between the Complexin-1 C-terminus and nanodiscs. (A) ^{1}H-^{15}N HSQC spectra of ^{15}N Cpx1 2-134 alone in solution (15 µM, black contours) and in the presence of empty nanodiscs (15 µM, red contours). (B) Bar diagrams showing a ratio of crosspeak intensity from ^{1}H-^{15}N HSQC spectra of Cpx1 as a function of residue number. This ratio was obtained by dividing the crosspeak signal intensity of the Cpx1 fragment alone by the crosspeak signal in the presence of empty nanodiscs. The top panel contains data for the Cpx1 NTD, while the bottom panel contains data for the Cpx1 CTD. Only crosspeaks corresponding to a small region of the Cpx1 CTD (residues 112-130) broaden due to binding (red box).

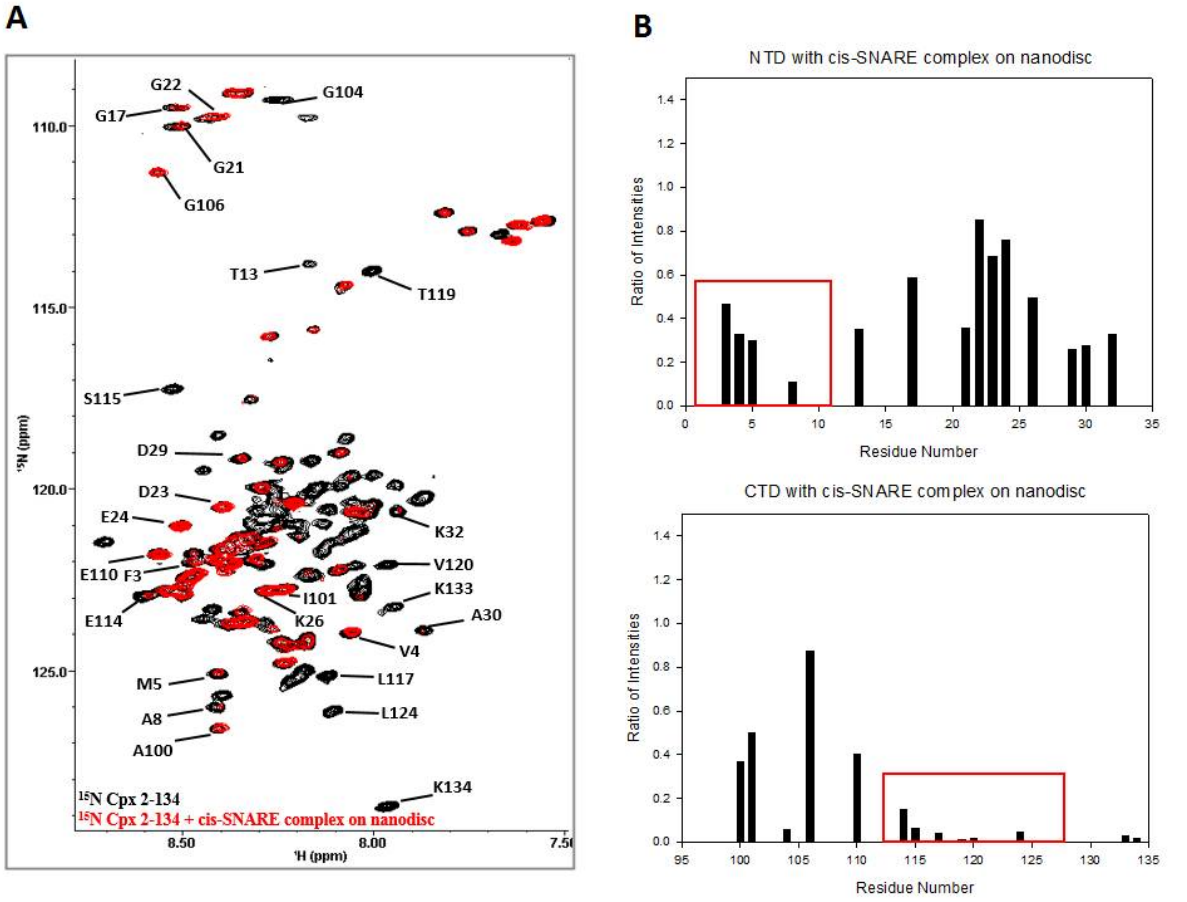

Figure 4.8. ^{1}H-^{15}N HSQC spectra demonstrate an interaction between both Complexin-termini and the cis-SNARE complex attached to nanodiscs. (A) ^{1}H-^{15}N HSQC spectra of ^{15}N Cpx1 2-134 alone in solution (15 µM, black contours) and in the presence of cis-SNARE complex nanodiscs (15 µM, red contours). (B) Bar diagrams showing a ratio of crosspeak intensity from ^{1}H-^{15}N HSQC spectra of Cpx1 as a function of residue number. This ratio was obtained by dividing the crosspeak signal intensity of the Cpx1 fragment alone by the crosspeak signal in the presence of cis-SNARE complex nanodiscs. The top panel contains data for the Cpx1 NTD, while the bottom panel contains data for the Cpx1 CTD. Crosspeaks corresponding to a small region in both the NTD and CTD (residues 1-12 and 112-130, respectively) broaden due to binding (red boxes).

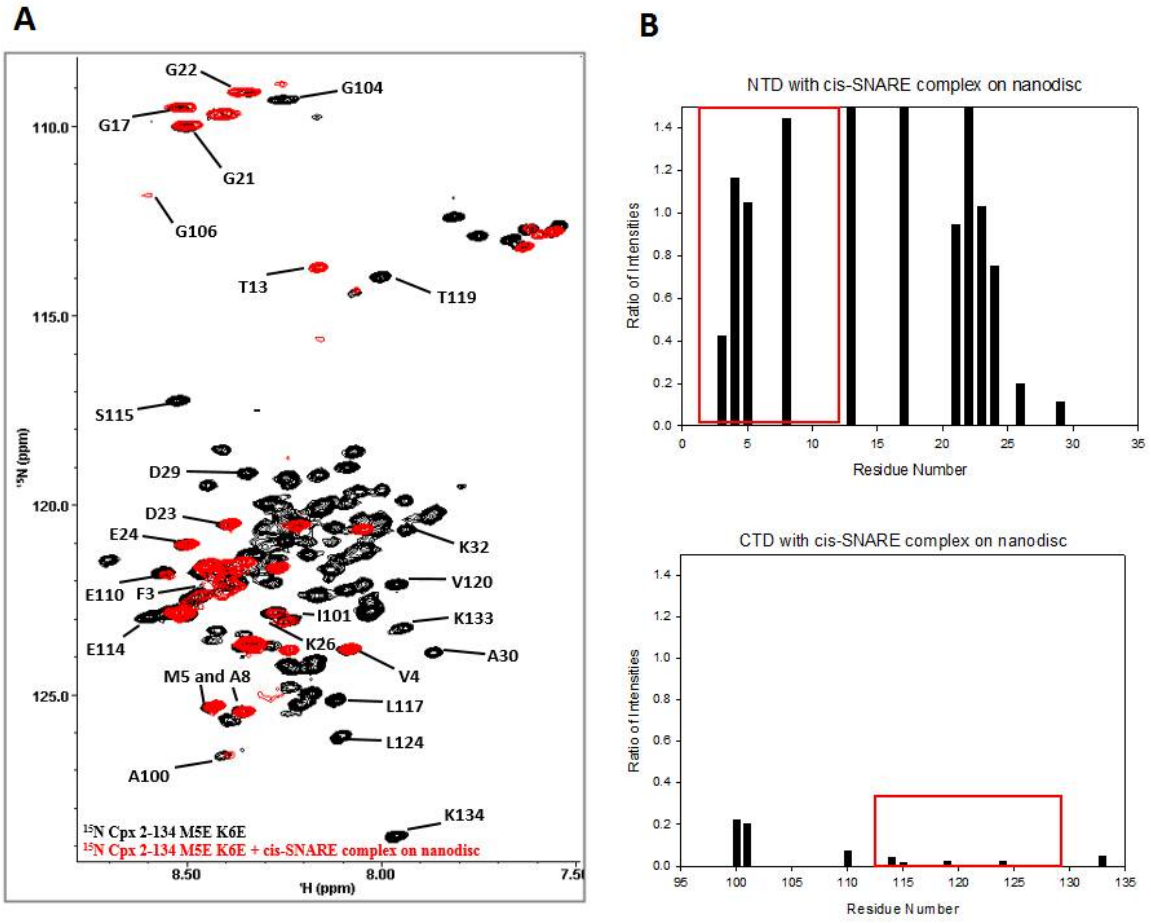

Figure 4.9. ^{1}H-^{15}N HSQC spectra with a Complexin-1 mutant show impaired binding of the N-terminus to cis-SNARE complex nanodiscs. (A) ^{1}H-^{15}N HSQC spectra of ^{15}N Cpx1 2-134 M5E, K6E alone in solution (20 µM, black contours) and in the presence of cis-SNARE complex nanodiscs (30 µM, red contours). (B) Bar diagrams showing a ratio of crosspeak intensity from ^{1}H-^{15}N HSQC spectra of Cpx1 as a function of residue number. This ratio was obtained by dividing the crosspeak signal intensity of the Cpx1 M5E, K6E fragment alone by the crosspeak signal in the presence of cis-SNARE complex nanodiscs. The top panel contains data for the Cpx1 M5E, K6E NTD, while the bottom panel contains data for the Cpx1 M5E, K6E CTD. Crosspeaks corresponding to a small region in the CTD (residues 112-130) still broaden due to binding (red box, bottom), but residues in the NTD (1-12) no longer broaden because of impaired binding (red box, top).

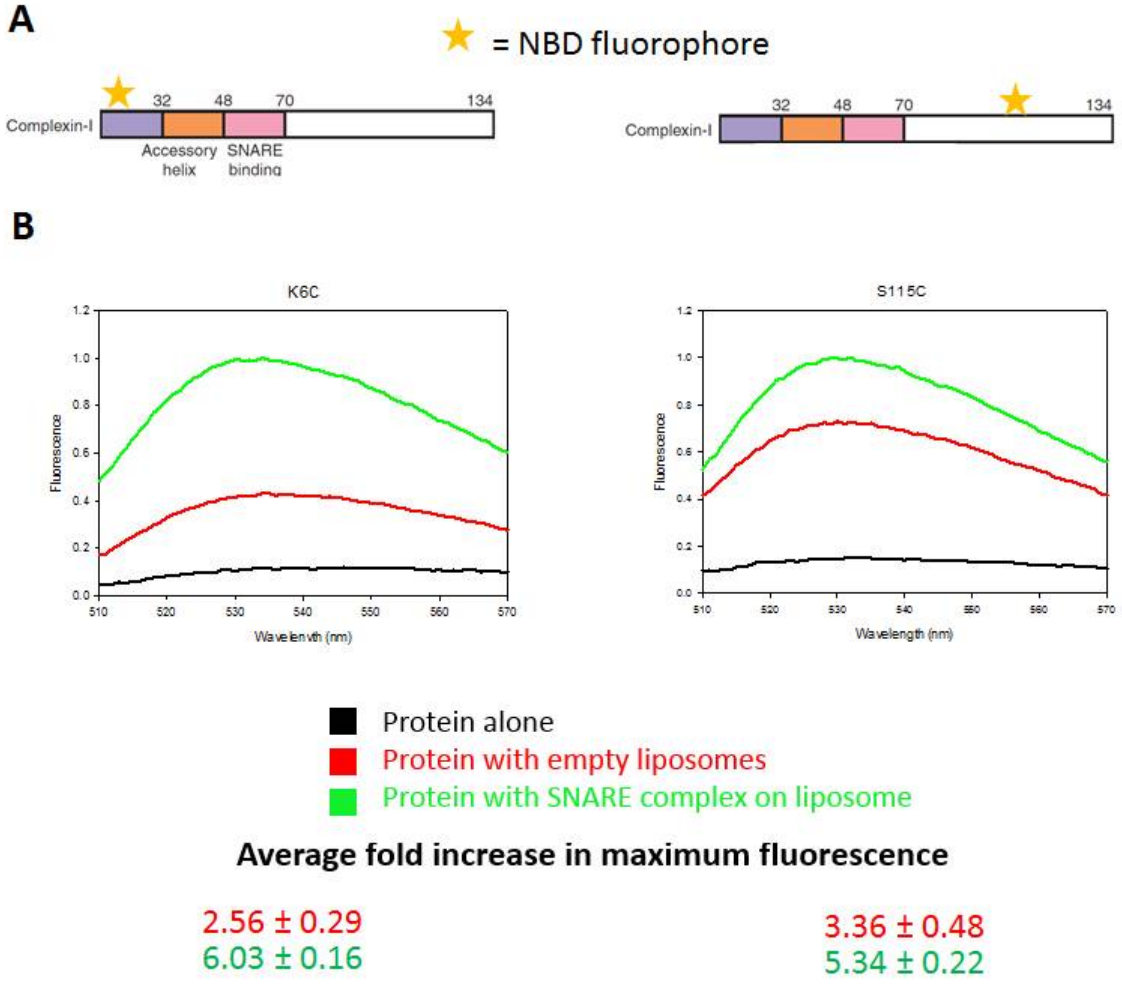

Figure 4.10. Fluorescence binding experiments reveal a cooperative interaction between Compleixn-1, liposomes, and the SNARE complex. (A) Schematic showing the location of the IANBD fluorescent probe (gold star) either at position K6C (left) or S115C (right). The Cpx1 NTD is shown in purple, AH in orange, CH in pink, and CTD in white. (B) Fluorescence emission spectra of IANBD-Cpx1 under 3 different conditions: fluorescent protein alone (100 nM, black), fluorescent protein in the presence of empty liposomes (800 µM, red), and fluorescent protein in the presence of cis-SNARE complex liposomes (800 µM, green). Data with the tag at the NTD (K6C) is on the left, and data with the tag at the CTD (S115C) is on the right. The average fold increase was calculated by dividing the indicated signal intensity by the signal intensity of the protein alone.

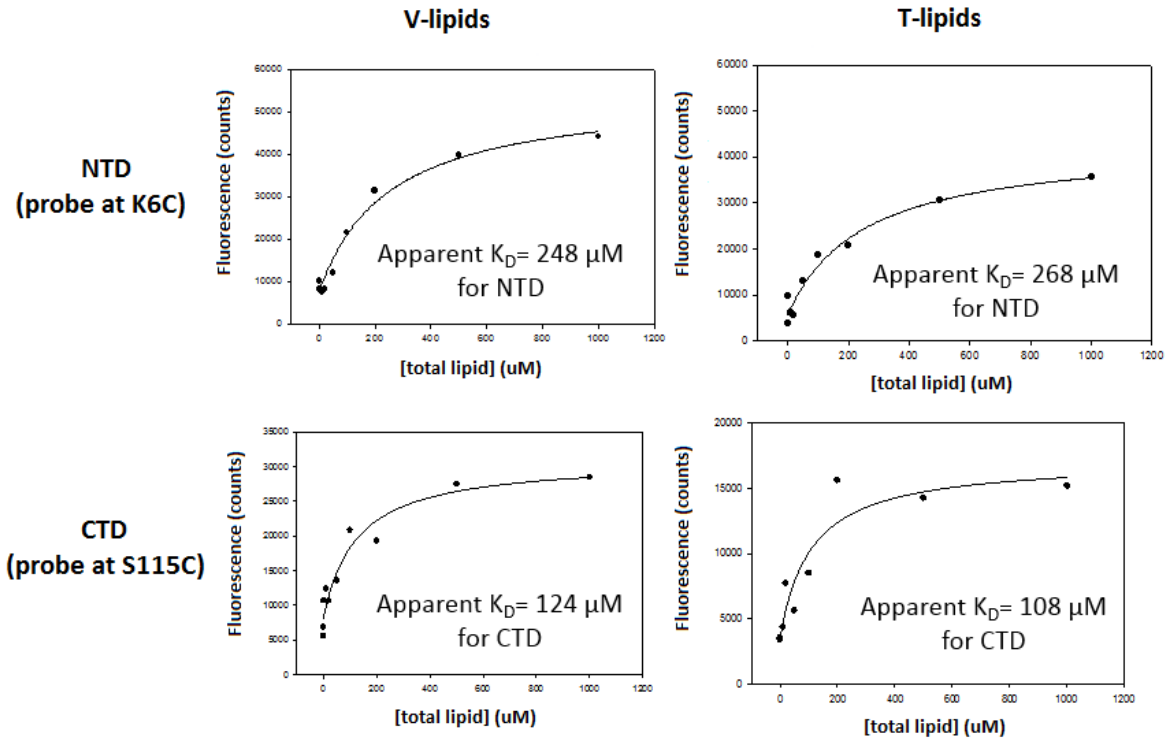

Figure 4.11. Titrations of liposomes with different lipid compositions demonstrate that both Complexin-1 termini interact with liposomes. Titration curves obtained from fluorescence emission scans showing the change in fluoresce signal of Cpx1 tagged with IANBD (50 nM) at two different locations, the NTD (K6C, top), and CTD (S115C, bottom) as a function of total lipid concentration (V-lipid composition left and T-lipid composition right). Data were fit to a single site binding model using SigmaPlot. The apparent affinities show that the CTD binds to liposomes 2 fold tighter than the NTD. No preference for lipid composition was observed for either termini, so accounting for selective binding to the available negatively charged DOPS on the outer leaflet of the liposomes (~10%), the apparent affinities are roughly 25 µM for the NTD and 10 µM for the CTD.

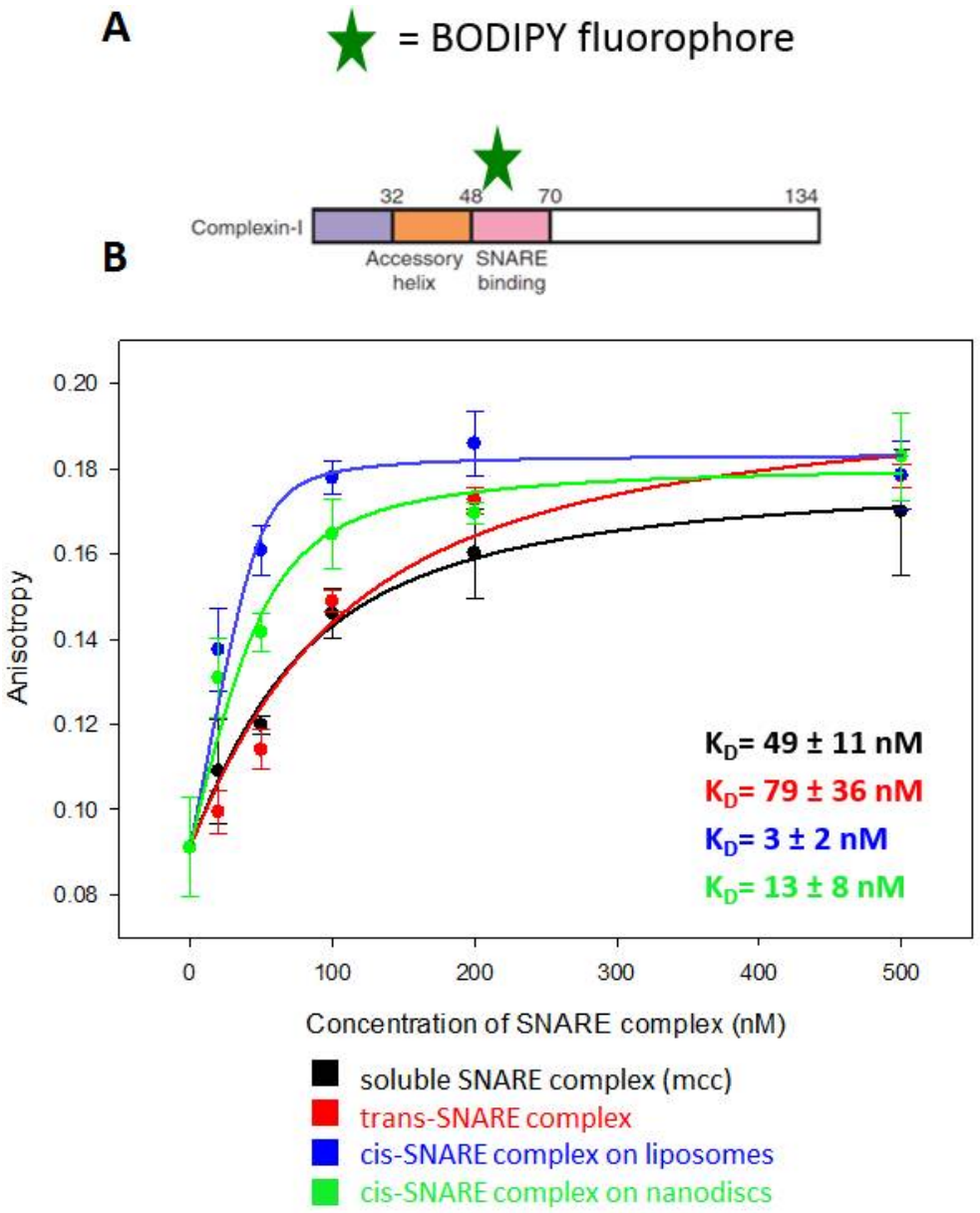

Figure 4.12. Titrations with different types of SNARE complexes show how the presence of membranes increases the affinity of Complexin-1 for the SNARE complex. (A) Schematic showing the location of the BODIPY fluorescent probe (green star) at position V61C. The Cpx1 NTD is shown in purple, AH in orange, CH in pink, and CTD in white. (B) Titrations of BODIPY-Cpx1 (50 nM) with 4 different types of SNARE complexes monitored by fluorescence anisotropy with time-based emission: soluble SNARE complex (mcc, black), cis-SNARE complexes on liposomes (blue), cis-SNARE complexes on nanodiscs (green), and trans-SNARE complexes between one nanodisc and one liposome. Data were fit to a single site binding model using SigmaPlot.

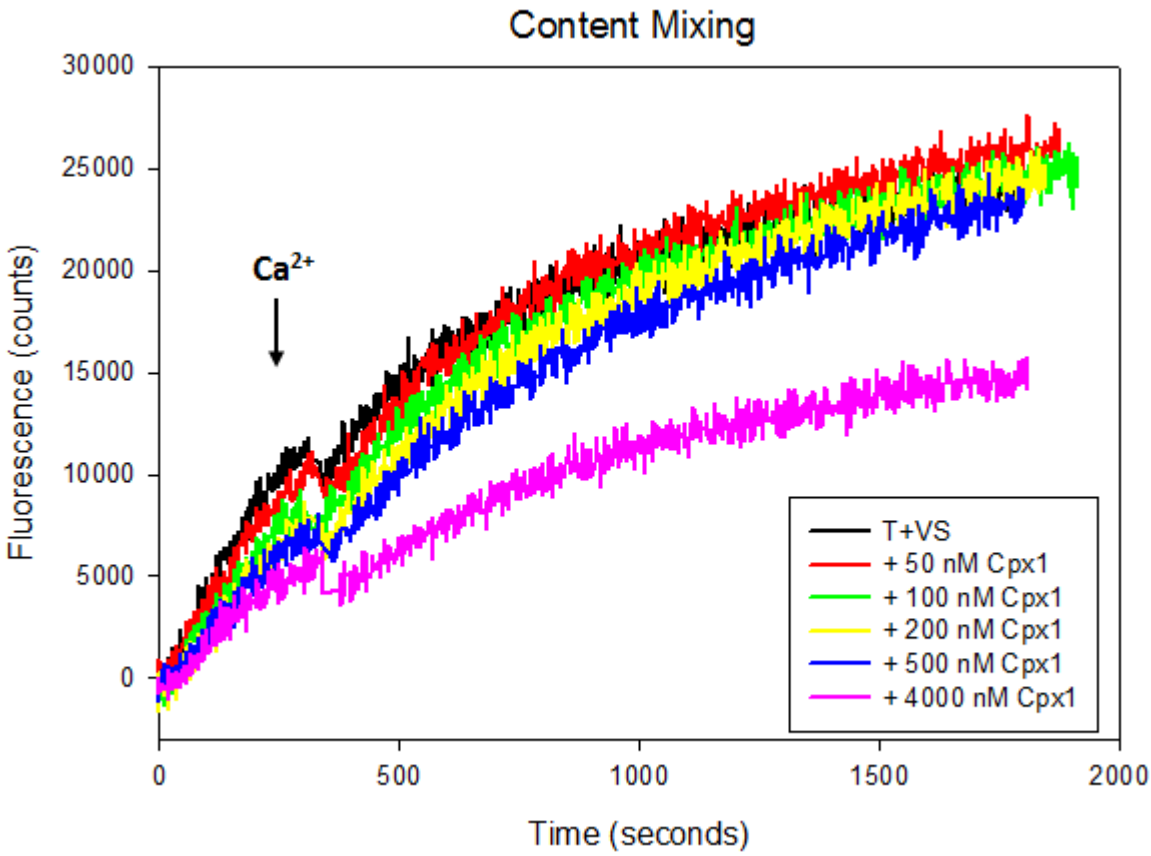

Figure 4.13. Content mixing assay using reconstituted liposomes shows that Complexin-1 inhibits both calcium independent and dependent fusion in a minimal system. Acceptor emission from the development of FRET between content mixing markers is shown as a function of time. Six different reaction conditions are shown with different amounts of Cpx1. All reactions contain T-liposomes and VS-liposomes.

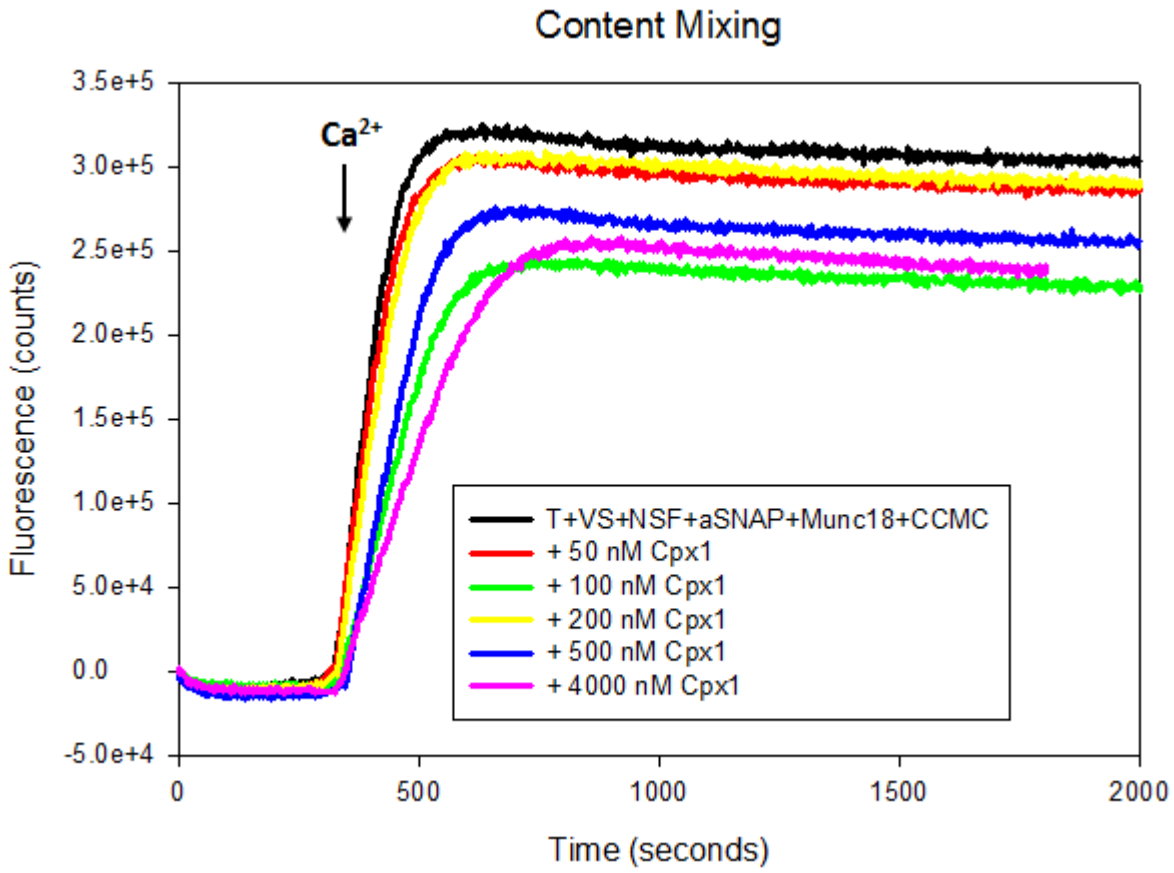

Figure 4.14. Content mixing assay using reconstituted liposomes shows that Complexin-1 inhibits calcium dependent fusion in a complete system. Acceptor emission from the development of FRET between content mixing markers is shown as a function of time. Six different reaction conditions are shown with different amounts of Cpx1. All reactions contain T-liposomes, VS-liposomes, NSF, αSNAP, Munc18-1, and the C_1C_2BMUNC_2C fragment of Munc13-1.

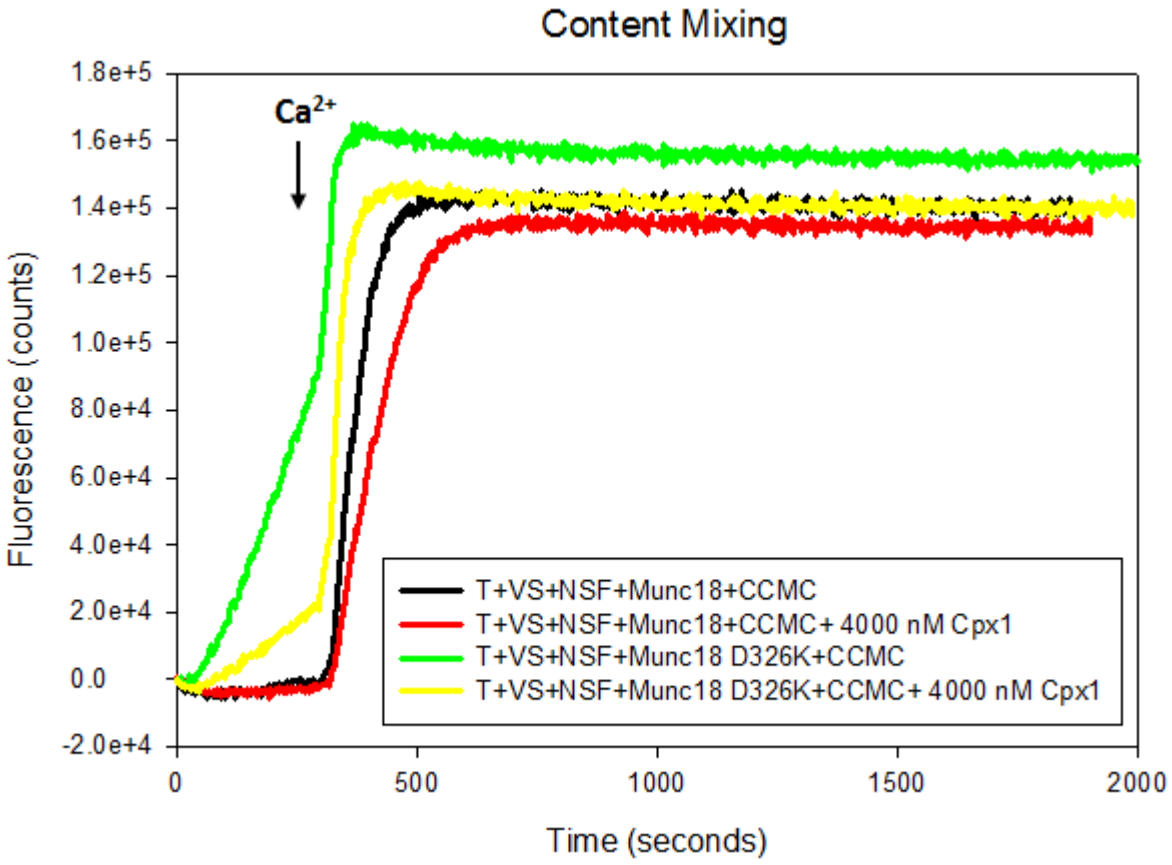

Figure 4.15. Content mixing assay using reconstituted liposomes and a Munc18-1 D326K mutant shows that Complexin-1 inhibits calcium independent fusion, and that this inhibition is removed upon calcium addition in a complete system. Acceptor emission from the development of FRET between content mixing markers is shown as a function of time. 4 different reaction conditions are shown using either Munc18-1 wt (black and red curves) or Munc18-1 D326K (green and yellow curves) in both the absence and presence of 4 μM Cpx1. All reactions contain T-liposomes, VS-liposomes, NSF, αSNAP, Munc18-1 (either wt or D326K), and the C_1C_2BMUNC_2C fragment of Munc13-1.

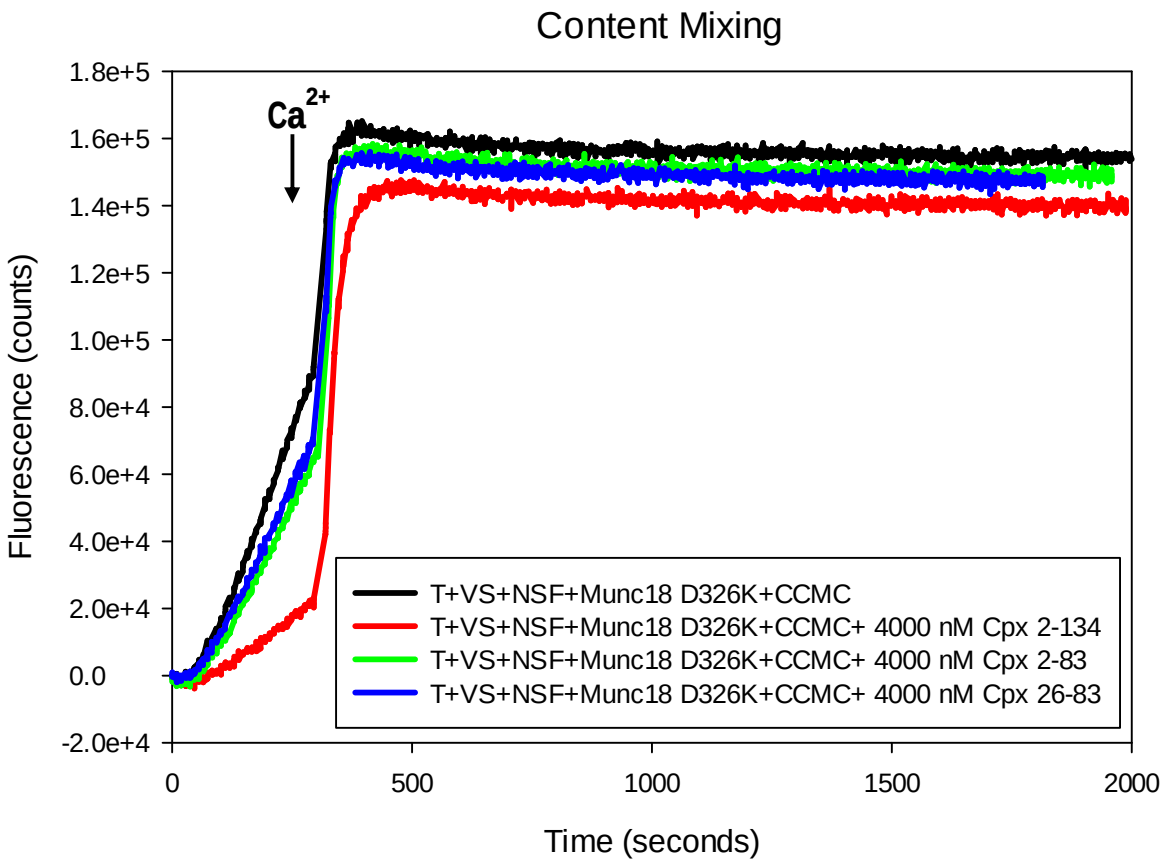

Figure 4.16. Content mixing assay using reconstituted liposomes and a Munc18-1 D326K mutant shows that the Complexin-1 C-terminus is required for inhibition of calcium independent fusion in a complete system. Acceptor emission from the development of FRET between content mixing markers is shown as a function of time. 4 different reaction conditions are shown using Munc18-1 D326K with 3 different Cpx1 fragments: no Cpx1 (black), Cpx1 2-134 (red), Cpx1 2-83 (green), and Cpx1 26-83 (blue). All reactions contain T-liposomes, VS-liposomes, NSF, αSNAP, Munc18-1 D326K, and the C_1C_2BMUNC_2C fragment of Munc13-1.

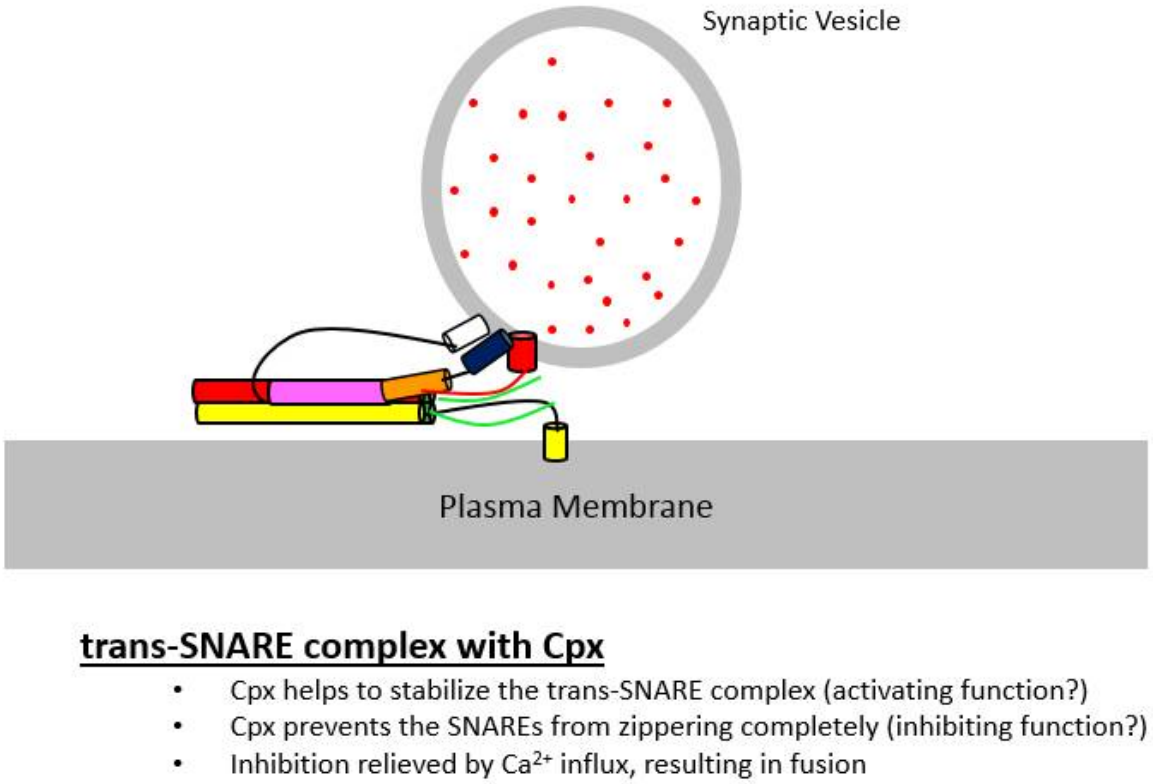

Figure 4.17. Model for Complexin-1 function. Schematic illustrating the many interactions between Cpx1 and the trans-SNARE complex. Syntaxin-1 is shown in yellow, Synaptobrevin in red, and SNAP-25 in green. The Cpx1 NTD is shown in purple, AH in orange, CH in pink, and CTD in white. In the presence of Cpx1, a single population of trans-SNARE complex exists before fusion, suggesting that Cpx1 stabilizes the trans-SNARE complexes while simultaneously hindering full SNARE zippering and fusion. These functional effects are accomplished the CH binding to the SNARE complex, the AH preventing full zippering of the trans-SNARE complex (and therefore inhibiting fusion) through steric/electrostatic repulsion, the CTD binding to liposomes to localize to the site of fusion (and possibly inhibiting), and the NTD potentially releasing this inhibition through cooperative interactions with both the C-terminus of the SNARE complex and membranes. Although speculative, this model could explain the dual roles for Cpx1 in inhibiting and activating fusion. Upon Ca^{2+} influx, this inhibition is relieved and fusion is stimulated.

Chapter 5- Conclusions and future directions

Synaptic vesicle fusion is a tightly regulated process that occurs on the sub-millisecond timescale. A highly conserved protein machinery is responsible for organizing this system beginning with tethering of synaptic vesicles to the plasma membrane, followed by priming/docking steps that leave the fusion machinery in a meta-stable state. Upon Ca^{2+} influx, formation of a fusion pore rapidly releases neurotransmitters into the synaptic cleft. At the heart of this operation lies the SNARE complex and numerous accessory proteins such as Munc13-1, Munc18-1, Complexin-1, and Synaptotagmin-1, which have independent and cooperative roles to coordinate this process. However, neurotransmission is severely impaired if any of these regulatory elements are removed from the system, suggesting that these proteins may not be accessory, but rather essential components of the release machinery itself. This work sought to analyze different stages of this pathway in order to attempt to bridge a cohesive molecular mechanism for neuronal membrane fusion.

In Chapter 2, I presented a recent publication that looked at how multiple factors protect neuronal trans-SNARE complexes against disassembly by NSF-αSNAP. Previously, it was known that NSF-αSNAP disassemble off-pathway SNARE intermediates, as well as the cis-SNARE complex after fusion is complete. Here, I showed that trans-SNARE complexes are also able to be disassembled by NSF-αSNAP, and that other components of the release machinery must be present to protect against such disassembly. Most importantly, I demonstrated using 'on-pathway' SNARE complex formation assays that include Munc18-1, Munc13-1, and NSF-αSNAP from the very beginning of the reaction that the trans-SNARE complex can be assembled in an NSF-αSNAP resistant manner. Syt1

greatly accelerated this process, notably in the absence of Ca^{2+}. Using this approach, SNARE-complex formation did not lead to fusion until the arrival of Ca^{2+}, which may represent the primed-state of membrane fusion.

Many studies have been completed on the SNARE complex since the discovery of these proteins almost 30 years ago. However, very few structural/functional studies have included membrane mimetics. By performing FRET analyses using trans-SNARE complexes anchored to liposomes, I successfully completed the first study involving accessory protein interactions with trans-SNARE complexes in their native lipid environment. This challenging work has provided insight into new roles for accessory proteins that have commonly been assumed to be dispensable after SNARE complex formation. I showed that these proteins are crucial not only for SNARE complex assembly, but also for protection against de-priming. These results help to support the 'on-pathway' mechanism of fusogenic SNARE complex formation. Future experiments can hopefully make use of these assays to probe new protein-protein interactions that could further affect the stability of trans-SNARE complexes. Additionally, this FRET assay can be applied to a single molecule system to look at interactions involving individual SNARE complexes.

In Chapter 3, I presented another publication that looked at reconciling isothermal titration calorimetry analyses of interactions between complexin and truncated SNARE complexes. Previously, ITC experiments performed in different laboratories yielded apparently discrepant results in support or against an insertion model for Cpx1 inhibition. I performed numerous ITC experiments to solve these discrepancies and showed that the region containing the Cpx1 AH and preceding NTD interacted with the truncated SNARE

complex. However, this interaction required the polybasic juxtamembrane region of Syx-1 and was not affected by the Cpx1 superclamp mutation.

Interactions between two proteins are often studied in a minimal context alone in solution. Results from these binding studies may or may not accurately report on biologically relevant interactions, especially when truncated protein fragments are used. In Chapter 3, I discovered that the source of discrepancy involving ITC experiments was different SNARE fragments. The addition of 12 residues to a Syx-1 construct changed the heats detected in blocking ITC experiments. These additional heats were attributed to ionic interactions from the addition of polybasic residues in the Syx-1 fragment used with acidic residues in Cpx1. However, these ITC results must still be interpreted with caution, as truncated proteins were still used to perform these experiments in solution. The Syx-1 juxtamembrane region is expected to interact with negatively charged phospholipids *in vivo*, so the functional significance of these results needs to be questioned until additional experiments are performed. Further elucidation of the model for Cpx1 inhibition will come by performing analogous experiments using full-length proteins and membrane mimetics.

In Chapter 4, I presented a combination of experiments with Cpx1 to try and decipher its molecular mechanism of action. *In vivo*, absence of Cpx1 causes a reduction in evoked release, while different effects are observed in spontaneous release. It is currently unclear how the Cpx1 NTD and CTD contribute to regulating fusion. In solution, I did not observe any binding between the Cpx1 termini and the SNARE complex. Since the CH is known to tightly interact with the SNARE complex, I formed SNARE complexes anchored to either liposomes or nanodiscs to study Cpx1 interactions in their physiologically relevant

membrane environment. Here, I successfully detected binding between Cpx1, the SNARE complex, and lipids. The Cpx1 CTD was also necessary for inhibition of calcium independent fusion in reconstituted content mixing assays. These results suggest that the membranes and the SNARE complex cooperate in binding to the Cpx1 termini. Such cooperative binding of Cpx1 to membranes and SNAREs may be critical for releasing the inhibition caused by the accessory helix, although the molecular mechanism of action has yet to be determined.

Cumulatively, these results urgently stress the need to perform *in vitro* binding studies with membrane mimetics and full-length proteins, especially when numerous interacting partners are present. However, the use of fluorescent probes can perturb or prevent binding interactions if the probes are engineered near the binding site. Functional assays that detect both lipid mixing and content mixing are exceptionally useful for measuring the activities of accessory proteins, as described in Chapter 4. The current system used to complete these studies involved bulk fluorescence measurements collected in solution. Although useful, this setup can be drastically improved through the use of supported lipid bilayers with TIRF microscopy or even amperometry. Analyses of single fusion events will be able to extract more information out of *in vitro* experiments, such as distinguishing between docking, hemifusion, and true fusion. Studies using amperometry will have the highest time resolution and sensitivity and are currently at the forefront of development. Additionally, advancements in structural studies, whether through the use of x-ray crystallography, NMR, or cryo-EM, are sure to provide invaluable structural insights into complex states of this system, such as which proteins are bound to the SNARE complex

in the primed, meta-stable state. I am optimistic that the field will continue to discover how synaptic vesicle fusion is regulated to control neurotransmission in the brain by pursuing incredibly challenging studies that will one day synthesize a cohesive mechanism of action.

BIBLIOGRAPHY

Aeffner, S., T. Reusch, B. Weinhausen, and T. Salditt. 2012. "Energetics of stalk intermediates in membrane fusion are controlled by lipid composition." *Proc Natl Acad Sci U S A* 109 (25):E1609-18. doi: 10.1073/pnas.1119442109.

Arac, D., X. Chen, H. A. Khant, J. Ubach, S. J. Ludtke, M. Kikkawa, A. E. Johnson, W. Chiu, T. C. Sudhof, and J. Rizo. 2006. "Close membrane-membrane proximity induced by Ca(2+)-dependent multivalent binding of synaptotagmin-1 to phospholipids." *Nat Struct Mol Biol* 13 (3):209-17. doi: 10.1038/nsmb1056.

Aravamudan, B., T. Fergestad, W. S. Davis, C. K. Rodesch, and K. Broadie. 1999. "Drosophila UNC-13 is essential for synaptic transmission." *Nat Neurosci* 2 (11):965-71. doi: 10.1038/14764.

Bacaj, T., D. Wu, J. Burre, R. C. Malenka, X. Liu, and T. C. Sudhof. 2015. "Synaptotagmin-1 and -7 Are Redundantly Essential for Maintaining the Capacity of the Readily-Releasable Pool of Synaptic Vesicles." *PLoS Biol* 13 (10):e1002267. doi: 10.1371/journal.pbio.1002267.

Bacaj, T., D. Wu, X. Yang, W. Morishita, P. Zhou, W. Xu, R. C. Malenka, and T. C. Sudhof. 2013. "Synaptotagmin-1 and synaptotagmin-7 trigger synchronous and asynchronous phases of neurotransmitter release." *Neuron* 80 (4):947-59. doi: 10.1016/j.neuron.2013.10.026.

Bai, J., W. C. Tucker, and E. R. Chapman. 2004. "PIP2 increases the speed of response of synaptotagmin and steers its membrane-penetration activity toward the plasma membrane." *Nat Struct Mol Biol* 11 (1):36-44. doi: 10.1038/nsmb709.

Baker, R. W., P. D. Jeffrey, M. Zick, B. P. Phillips, W. T. Wickner, and F. M. Hughson. 2015. "A direct role for the Sec1/Munc18-family protein Vps33 as a template for SNARE assembly." *Science* 349 (6252):1111-4. doi: 10.1126/science.aac7906.

Banerjee, A., V. A. Barry, B. R. DasGupta, and T. F. Martin. 1996. "N-Ethylmaleimide-sensitive factor acts at a prefusion ATP-dependent step in Ca2+-activated exocytosis." *J Biol Chem* 271 (34):20223-6.

Basu, J., A. Betz, N. Brose, and C. Rosenmund. 2007. "Munc13-1 C1 domain activation lowers the energy barrier for synaptic vesicle fusion." *J Neurosci* 27 (5):1200-10. doi: 10.1523/JNEUROSCI.4908-06.2007.

Bear, Mark F., Barry W. Connors, and Michael A. Paradiso. 2001. *Neuroscience: Exploring the Brain*. Baltimore, Maryland: Lippincott Williams & Wilkins.

Betz, A., P. Thakur, H. J. Junge, U. Ashery, J. S. Rhee, V. Scheuss, C. Rosenmund, J. Rettig, and N. Brose. 2001. "Functional interaction of the active zone proteins Munc13-1 and RIM1 in synaptic vesicle priming." *Neuron* 30 (1):183-96.

Brautigam, C. A., H. Zhao, C. Vargas, S. Keller, and P. Schuck. 2016. "Integration and global analysis of isothermal titration calorimetry data for studying macromolecular interactions." *Nat Protoc* 11 (5):882-94. doi: 10.1038/nprot.2016.044.

Brewer, K. D., T. Bacaj, A. Cavalli, C. Camilloni, J. D. Swarbrick, J. Liu, A. Zhou, P. Zhou, N. Barlow, J. Xu, A. B. Seven, E. A. Prinslow, R. Voleti, D. Haussinger, A. M. Bonvin, D. R. Tomchick, M. Vendruscolo, B. Graham, T. C. Sudhof, and J. Rizo. 2015. "Dynamic binding mode of a Synaptotagmin-1-SNARE complex in solution." *Nat Struct Mol Biol* 22 (7):555-64. doi: 10.1038/nsmb.3035.

Brunger, A. T., U. B. Choi, Y. Lai, J. Leitz, and Q. Zhou. 2018. "Molecular Mechanisms of Fast Neurotransmitter Release." *Annu Rev Biophys* 47:469-497. doi: 10.1146/annurev-biophys-070816-034117.

Buhl, L. K., R. A. Jorquera, Y. Akbergenova, S. Huntwork-Rodriguez, D. Volfson, and J. T. Littleton. 2013. "Differential regulation of evoked and spontaneous neurotransmitter release by C-terminal modifications of complexin." *Mol Cell Neurosci* 52:161-72. doi: 10.1016/j.mcn.2012.11.009.

Burkhardt, P., D. A. Hattendorf, W. I. Weis, and D. Fasshauer. 2008. "Munc18a controls SNARE assembly through its interaction with the syntaxin N-peptide." *EMBO J* 27 (7):923-33. doi: 10.1038/emboj.2008.37.

Cajal, Santiago Ramon y. 1937. "Recollections of My Life." *Am. Philos. Soc. Mem.* 8.

Camacho, M., J. Basu, T. Trimbuch, S. Chang, C. Pulido-Lozano, S. S. Chang, I. Duluvova, M. Abo-Rady, J. Rizo, and C. Rosenmund. 2017. "Heterodimerization of Munc13 C2A domain with RIM regulates synaptic vesicle docking and priming." *Nat Commun* 8:15293. doi: 10.1038/ncomms15293.

Chang, S., T. Trimbuch, and C. Rosenmund. 2018. "Synaptotagmin-1 drives synchronous Ca(2+)-triggered fusion by C2B-domain-mediated synaptic-vesicle-membrane attachment." *Nat Neurosci* 21 (1):33-40. doi: 10.1038/s41593-017-0037-5.

Chapman, E. R. 2008. "How does synaptotagmin trigger neurotransmitter release?" *Annu Rev Biochem* 77:615-41. doi: 10.1146/annurev.biochem.77.062005.101135.

Chapman, E. R., and A. F. Davis. 1998. "Direct interaction of a Ca2+-binding loop of synaptotagmin with lipid bilayers." *J Biol Chem* 273 (22):13995-4001.

Chen, X., D. Arac, T. M. Wang, C. J. Gilpin, J. Zimmerberg, and J. Rizo. 2006. "SNARE-mediated lipid mixing depends on the physical state of the vesicles." *Biophys J* 90 (6):2062-74. doi: 10.1529/biophysj.105.071415.

Chen, X., D. R. Tomchick, E. Kovrigin, D. Arac, M. Machius, T. C. Sudhof, and J. Rizo. 2002. "Three-dimensional structure of the complexin/SNARE complex." *Neuron* 33 (3):397-409.

Chen, Y. A., and R. H. Scheller. 2001. "SNARE-mediated membrane fusion." *Nat Rev Mol Cell Biol* 2 (2):98-106. doi: 10.1038/35052017.

Chernomordik, L. V., and M. M. Kozlov. 2008. "Mechanics of membrane fusion." *Nat Struct Mol Biol* 15 (7):675-83. doi: 10.1038/nsmb.1455.

Cho, R. W., D. Kummel, F. Li, S. W. Baguley, J. Coleman, J. E. Rothman, and J. T. Littleton. 2014. "Genetic analysis of the Complexin trans-clamping model for cross-linking SNARE complexes in vivo." *Proc Natl Acad Sci U S A* 111 (28):10317-22. doi: 10.1073/pnas.1409311111.

Choi, U. B., M. Zhao, K. I. White, R. A. Pfuetzner, L. Esquivies, Q. Zhou, and A. T. Brunger. 2018. "NSF-mediated disassembly of on- and off-pathway SNARE complexes and inhibition by complexin." *Elife* 7. doi: 10.7554/eLife.36497.

Choi, U. B., M. Zhao, Y. Zhang, Y. Lai, and A. T. Brunger. 2016. "Complexin induces a conformational change at the membrane-proximal C-terminal end of the SNARE complex." *Elife* 5. doi: 10.7554/eLife.16886.

Cohen, F. S., and G. B. Melikyan. 2004a. "The Energetics of Membrane Fusion from Binding, through Hemifusion, Pore Formation, and Pore Enlargement." *The Journal of Membrane Biology* 199 (1):1-14. doi: 10.1007/s00232-004-0669-8.

Cohen, F. S., and G. B. Melikyan. 2004b. "The energetics of membrane fusion from binding, through hemifusion, pore formation, and pore enlargement." *J Membr Biol* 199 (1):1-14.

Dai, H., N. Shen, D. Arac, and J. Rizo. 2007. "A quaternary SNARE-synaptotagmin-Ca2+-phospholipid complex in neurotransmitter release." *J Mol Biol* 367 (3):848-63. doi: 10.1016/j.jmb.2007.01.040.

Delaglio, F., S. Grzesiek, G. W. Vuister, G. Zhu, J. Pfeifer, and A. Bax. 1995. "NMRPipe: a multidimensional spectral processing system based on UNIX pipes." *J Biomol NMR* 6 (3):277-93.

Deng, L., P. S. Kaeser, W. Xu, and T. C. Sudhof. 2011. "RIM proteins activate vesicle priming by reversing autoinhibitory homodimerization of Munc13." *Neuron* 69 (2):317-31. doi: 10.1016/j.neuron.2011.01.005.

Denisov, I. G., Y. V. Grinkova, A. A. Lazarides, and S. G. Sligar. 2004. "Directed self-assembly of monodisperse phospholipid bilayer Nanodiscs with controlled size." *J Am Chem Soc* 126 (11):3477-87. doi: 10.1021/ja0393574.

Dennison, S. M., M. E. Bowen, A. T. Brunger, and B. R. Lentz. 2006. "Neuronal SNAREs do not trigger fusion between synthetic membranes but do promote PEG-mediated membrane fusion." *Biophys J* 90 (5):1661-75. doi: 10.1529/biophysj.105.069617.

Diao, J., D. J. Cipriano, M. Zhao, Y. Zhang, S. Shah, M. S. Padolina, R. A. Pfuetzner, and A. T. Brunger. 2013. "Complexin-1 enhances the on-rate of vesicle docking via simultaneous SNARE and membrane interactions." *J Am Chem Soc* 135 (41):15274-7. doi: 10.1021/ja407392n.

Dulubova, I., M. Khvotchev, S. Liu, I. Huryeva, T. C. Sudhof, and J. Rizo. 2007. "Munc18-1 binds directly to the neuronal SNARE complex." *Proc Natl Acad Sci U S A* 104 (8):2697-702. doi: 10.1073/pnas.0611318104.

Dulubova, I., X. Lou, J. Lu, I. Huryeva, A. Alam, R. Schneggenburger, T. C. Sudhof, and J. Rizo. 2005. "A Munc13/RIM/Rab3 tripartite complex: from priming to plasticity?" *EMBO J* 24 (16):2839-50. doi: 10.1038/sj.emboj.7600753.

Dulubova, I., S. Sugita, S. Hill, M. Hosaka, I. Fernandez, T. C. Sudhof, and J. Rizo. 1999. "A conformational switch in syntaxin during exocytosis: role of munc18." *EMBO J* 18 (16):4372-82. doi: 10.1093/emboj/18.16.4372.

Dulubova, I., T. Yamaguchi, Y. Wang, T. C. Sudhof, and J. Rizo. 2001. "Vam3p structure reveals conserved and divergent properties of syntaxins." *Nat Struct Biol* 8 (3):258-64. doi: 10.1038/85012.

Fasshauer, D., R. B. Sutton, A. T. Brunger, and R. Jahn. 1998. "Conserved structural features of the synaptic fusion complex: SNARE proteins reclassified as Q- and R-SNAREs." *Proceedings of the National Academy of Sciences of the United States of America* 95 (26):15781-15786. doi: DOI 10.1073/pnas.95.26.15781.

Fernandez-Chacon, R., A. Konigstorfer, S. H. Gerber, J. Garcia, M. F. Matos, C. F. Stevens, N. Brose, J. Rizo, C. Rosenmund, and T. C. Sudhof. 2001. "Synaptotagmin I functions as a calcium regulator of release probability." *Nature* 410 (6824):41-9. doi: 10.1038/35065004.

Fernandez, I., D. Arac, J. Ubach, S. H. Gerber, O. H. Shin, Y. Gao, R. G. W. Anderson, T. C. Sudhof, and J. Rizo. 2001. "Three-dimensional structure of the synaptotagmin 1 C2B-domain: Synaptotagmin 1 as a phospholipid binding machine." *Neuron* 32 (6):1057-1069. doi: Doi 10.1016/S0896-6273(01)00548-7.

Fernandez, I., J. Ubach, I. Dulubova, X. Zhang, T. C. Sudhof, and J. Rizo. 1998. "Three-dimensional structure of an evolutionarily conserved N-terminal domain of syntaxin 1A." *Cell* 94 (6):841-9. doi: 10.1016/S0092-8674(00)81742-0.

Galvani, Luigi. 1791. "De viribus Electricitatis in Moto Musculari: Commentarius." *Ex Typographia Instituti Scientarium*.

Gao, Y., S. Zorman, G. Gundersen, Z. Xi, L. Ma, G. Sirinakis, J. E. Rothman, and Y. Zhang. 2012. "Single reconstituted neuronal SNARE complexes zipper in three distinct stages." *Science* 337 (6100):1340-3. doi: 10.1126/science.1224492.

Geppert, M., Y. Goda, R. E. Hammer, C. Li, T. W. Rosahl, C. F. Stevens, and T. C. Sudhof. 1994. "Synaptotagmin I: a major Ca2+ sensor for transmitter release at a central synapse." *Cell* 79 (4):717-27.

Gerst, J. E. 2003. "SNARE regulators: matchmakers and matchbreakers." *Biochim Biophys Acta* 1641 (2-3):99-110. doi: 10.1016/S0167-4889(03)00096-X.

Gipson, P., Y. Fukuda, R. Danev, Y. Lai, D. H. Chen, W. Baumeister, and A. T. Brunger. 2017. "Morphologies of synaptic protein membrane fusion interfaces." *Proc Natl Acad Sci U S A* 114 (34):9110-9115. doi: 10.1073/pnas.1708492114.

Giraudo, C. G., W. S. Eng, T. J. Melia, and J. E. Rothman. 2006. "A clamping mechanism involved in SNARE-dependent exocytosis." *Science* 313 (5787):676-80. doi: 10.1126/science.1129450.

Giraudo, C. G., A. Garcia-Diaz, W. S. Eng, Y. Chen, W. A. Hendrickson, T. J. Melia, and J. E. Rothman. 2009. "Alternative zippering as an on-off switch for SNARE-mediated fusion." *Science* 323 (5913):512-6. doi: 10.1126/science.1166500.

Gong, J., Y. Lai, X. Li, M. Wang, J. Leitz, Y. Hu, Y. Zhang, U. B. Choi, D. Cipriano, R. A. Pfuetzner, T. C. Sudhof, X. Yang, A. T. Brunger, and J. Diao. 2016. "C-terminal domain of mammalian complexin-1 localizes to highly curved membranes." *Proc Natl Acad Sci U S A* 113 (47):E7590-E7599. doi: 10.1073/pnas.1609917113.

Guan, R., H. Dai, and J. Rizo. 2008. "Binding of the Munc13-1 MUN domain to membrane-anchored SNARE complexes." *Biochemistry* 47 (6):1474-81. doi: 10.1021/bi702345m.

Hanson, P. I., R. Roth, H. Morisaki, R. Jahn, and J. E. Heuser. 1997. "Structure and conformational changes in NSF and its membrane receptor complexes visualized by quick-freeze/deep-etch electron microscopy." *Cell* 90 (3):523-35.

Hata, Y., C. A. Slaughter, and T. C. Sudhof. 1993. "Synaptic vesicle fusion complex contains unc-18 homologue bound to syntaxin." *Nature* 366 (6453):347-51. doi: 10.1038/366347a0.

Hayashi, T., S. Yamasaki, S. Nauenburg, T. Binz, and H. Niemann. 1995. "Disassembly of the reconstituted synaptic vesicle membrane fusion complex in vitro." *EMBO J* 14 (10):2317-25.

He, E., K. Wierda, R. van Westen, J. H. Broeke, R. F. Toonen, L. N. Cornelisse, and M. Verhage. 2017. "Munc13-1 and Munc18-1 together prevent NSF-dependent de-priming of synaptic vesicles." *Nat Commun* 8:15915. doi: 10.1038/ncomms15915.

Hobson, R. J., Q. Liu, S. Watanabe, and E. M. Jorgensen. 2011. "Complexin maintains vesicles in the primed state in C. elegans." *Curr Biol* 21 (2):106-13. doi: 10.1016/j.cub.2010.12.015.

Huntwork, S., and J. T. Littleton. 2007. "A complexin fusion clamp regulates spontaneous neurotransmitter release and synaptic growth." *Nat Neurosci* 10 (10):1235-7. doi: 10.1038/nn1980.

Ishizuka, T., H. Saisu, S. Odani, and T. Abe. 1995. "Synaphin: a protein associated with the docking/fusion complex in presynaptic terminals." *Biochem Biophys Res Commun* 213 (3):1107-14. doi: 10.1006/bbrc.1995.2241.

Jahn, R., and D. Fasshauer. 2012. "Molecular machines governing exocytosis of synaptic vesicles." *Nature* 490 (7419):201-7. doi: 10.1038/nature11320.

Jahn, R., J. Hell, and P. R. Maycox. 1990. "Synaptic vesicles: key organelles involved in neurotransmission." *J Physiol (Paris)* 84 (1):128-33.

Jahn, R., T. Lang, and T. C. Sudhof. 2003. "Membrane fusion." *Cell* 112 (4):519-33.

Jahn, R., and R. H. Scheller. 2006. "SNAREs--engines for membrane fusion." *Nat Rev Mol Cell Biol* 7 (9):631-43. doi: 10.1038/nrm2002.

Jahn, R., and T. C. Sudhof. 1993. "Synaptic vesicle traffic: rush hour in the nerve terminal." *J Neurochem* 61 (1):12-21.

Johnson, B. A., and R. A. Blevins. 1994. "NMR View: A computer program for the visualization and analysis of NMR data." *J Biomol NMR* 4 (5):603-14. doi: 10.1007/BF00404272.

Kaeser-Woo, Y. J., X. Yang, and T. C. Sudhof. 2012. "C-terminal complexin sequence is selectively required for clamping and priming but not for Ca2+ triggering of synaptic exocytosis." *J Neurosci* 32 (8):2877-85. doi: 10.1523/JNEUROSCI.3360-11.2012.

Katz, Bernard. 1962. "The transmission of impulses from nerve to muscle and the subcellular unit of synaptic action." *Proc. R. Soc. London Ser. B* 155:455-477.

Kavalali, E. T. 2015. "The mechanisms and functions of spontaneous neurotransmitter release." *Nat Rev Neurosci* 16 (1):5-16. doi: 10.1038/nrn3875.

Keller, S., C. Vargas, H. Zhao, G. Piszczek, C. A. Brautigam, and P. Schuck. 2012. "High-precision isothermal titration calorimetry with automated peak-shape analysis." *Anal Chem* 84 (11):5066-73. doi: 10.1021/ac3007522.

Khuong, T. M., R. L. Habets, S. Kuenen, A. Witkowska, J. Kasprowicz, J. Swerts, R. Jahn, G. van den Bogaart, and P. Verstreken. 2013. "Synaptic PI(3,4,5)P3 is required for Syntaxin1A clustering and neurotransmitter release." *Neuron* 77 (6):1097-108. doi: 10.1016/j.neuron.2013.01.025.

Khvotchev, M., I. Dulubova, J. Sun, H. Dai, J. Rizo, and T. C. Sudhof. 2007. "Dual modes of Munc18-1/SNARE interactions are coupled by functionally critical binding to syntaxin-1 N terminus." *J Neurosci* 27 (45):12147-55. doi: 10.1523/JNEUROSCI.3655-07.2007.

Kim, J. Y., B. K. Choi, M. G. Choi, S. A. Kim, Y. Lai, Y. K. Shin, and N. K. Lee. 2012. "Solution single-vesicle assay reveals PIP2-mediated sequential actions of synaptotagmin-1 on SNAREs." *EMBO J* 31 (9):2144-55. doi: 10.1038/emboj.2012.57.

Koushika, S. P., J. E. Richmond, G. Hadwiger, R. M. Weimer, E. M. Jorgensen, and M. L. Nonet. 2001. "A post-docking role for active zone protein Rim." *Nat Neurosci* 4 (10):997-1005. doi: 10.1038/nn732.

Krishnakumar, S. S., F. Li, J. Coleman, C. M. Schauder, D. Kummel, F. Pincet, J. E. Rothman, and K. M. Reinisch. 2015. "Re-visiting the trans insertion model for complexin clamping." *Elife* 4. doi: 10.7554/eLife.04463.

Krishnakumar, S. S., D. T. Radoff, D. Kummel, C. G. Giraudo, F. Li, L. Khandan, S. W. Baguley, J. Coleman, K. M. Reinisch, F. Pincet, and J. E. Rothman. 2011. "A

conformational switch in complexin is required for synaptotagmin to trigger synaptic fusion." *Nat Struct Mol Biol* 18 (8):934-40. doi: 10.1038/nsmb.2103.

Kuhne, Willy. 1862. "Uber die peripherischen Endorgane der motorischen Nerven."

Kummel, D., S. S. Krishnakumar, D. T. Radoff, F. Li, C. G. Giraudo, F. Pincet, J. E. Rothman, and K. M. Reinisch. 2011. "Complexin cross-links prefusion SNAREs into a zigzag array." *Nat Struct Mol Biol* 18 (8):927-33. doi: 10.1038/nsmb.2101.

Kyoung, M., A. Srivastava, Y. Zhang, J. Diao, M. Vrljic, P. Grob, E. Nogales, S. Chu, and A. T. Brunger. 2011. "In vitro system capable of differentiating fast Ca2+-triggered content mixing from lipid exchange for mechanistic studies of neurotransmitter release." *Proc Natl Acad Sci U S A* 108 (29):E304-13. doi: 10.1073/pnas.1107900108.

Lai, Y., U. B. Choi, J. Leitz, H. J. Rhee, C. Lee, B. Altas, M. Zhao, R. A. Pfuetzner, A. L. Wang, N. Brose, J. Rhee, and A. T. Brunger. 2017. "Molecular Mechanisms of Synaptic Vesicle Priming by Munc13 and Munc18." *Neuron* 95 (3):591-607 e10. doi: 10.1016/j.neuron.2017.07.004.

Lai, Y., U. B. Choi, Y. Zhang, M. Zhao, R. A. Pfuetzner, A. L. Wang, J. Diao, and A. T. Brunger. 2016. "N-terminal domain of complexin independently activates calcium-triggered fusion." *Proc Natl Acad Sci U S A* 113 (32):E4698-707. doi: 10.1073/pnas.1604348113.

Langley, J. N. 1905. "On the reaction of cells and of nerve endings to certain poisons, chiefly as regards the reaction of striated muscle to nicotine and to curari." *Journal of Physiology-London* 33 (4/5):374-413.

Lee, H. K., Y. Yang, Z. Su, C. Hyeon, T. S. Lee, H. W. Lee, D. H. Kweon, Y. K. Shin, and T. Y. Yoon. 2010. "Dynamic Ca2+-dependent stimulation of vesicle fusion by membrane-anchored synaptotagmin 1." *Science* 328 (5979):760-3. doi: 10.1126/science.1187722.

Li, F., F. Pincet, E. Perez, W. S. Eng, T. J. Melia, J. E. Rothman, and D. Tareste. 2007. "Energetics and dynamics of SNAREpin folding across lipid bilayers." *Nat Struct Mol Biol* 14 (10):890-6. doi: 10.1038/nsmb1310.

Li, F., F. Pincet, E. Perez, C. G. Giraudo, D. Tareste, and J. E. Rothman. 2011. "Complexin activates and clamps SNAREpins by a common mechanism involving an intermediate energetic state." *Nat Struct Mol Biol* 18 (8):941-6. doi: 10.1038/nsmb.2102.

Li, L., O. H. Shin, J. S. Rhee, D. Arac, J. C. Rah, J. Rizo, T. Sudhof, and C. Rosenmund. 2006. "Phosphatidylinositol phosphates as co-activators of Ca2+ binding to C2

domains of synaptotagmin 1." *J Biol Chem* 281 (23):15845-52. doi: 10.1074/jbc.M600888200.

Li, Y., S. Wang, T. Li, L. Zhu, Y. Xu, and C. Ma. 2017. "A Stimulation Function of Synaptotagmin-1 in Ternary SNARE Complex Formation Dependent on Munc18 and Munc13." *Front Mol Neurosci* 10:256. doi: 10.3389/fnmol.2017.00256.

Liang, B., V. Kiessling, and L. K. Tamm. 2013. "Prefusion structure of syntaxin-1A suggests pathway for folding into neuronal trans-SNARE complex fusion intermediate." *Proc Natl Acad Sci U S A* 110 (48):19384-9. doi: 10.1073/pnas.1314699110.

Liu, W., V. Montana, V. Parpura, and U. Mohideen. 2009. "Single Molecule Measurements of Interaction Free Energies Between the Proteins Within Binary and Ternary SNARE Complexes." *J Nanoneurosci* 1 (2):120-129. doi: 10.1166/jns.2009.1001.

Liu, X., A. B. Seven, M. Camacho, V. Esser, J. Xu, T. Trimbuch, B. Quade, L. Su, C. Ma, C. Rosenmund, and J. Rizo. 2016. "Functional synergy between the Munc13 C-terminal C1 and C2 domains." *Elife* 5. doi: 10.7554/eLife.13696.

Liu, X., A. B. Seven, J. Xu, V. Esser, L. Su, C. Ma, and J. Rizo. 2017. "Simultaneous lipid and content mixing assays for in vitro reconstitution studies of synaptic vesicle fusion." *Nat Protoc* 12 (9):2014-2028. doi: 10.1038/nprot.2017.068.

Lu, J., M. Machius, I. Dulubova, H. Dai, T. C. Sudhof, D. R. Tomchick, and J. Rizo. 2006. "Structural basis for a Munc13-1 homodimer to Munc13-1/RIM heterodimer switch." *PLoS Biol* 4 (7):e192. doi: 10.1371/journal.pbio.0040192.

Ma, C., W. Li, Y. Xu, and J. Rizo. 2011. "Munc13 mediates the transition from the closed syntaxin-Munc18 complex to the SNARE complex." *Nat Struct Mol Biol* 18 (5):542-9. doi: 10.1038/nsmb.2047.

Ma, C., L. Su, A. B. Seven, Y. Xu, and J. Rizo. 2013. "Reconstitution of the vital functions of Munc18 and Munc13 in neurotransmitter release." *Science* 339 (6118):421-5. doi: 10.1126/science.1230473.

Mahal, L. K., S. M. Sequeira, J. M. Gureasko, and T. H. Sollner. 2002. "Calcium-independent stimulation of membrane fusion and SNAREpin formation by synaptotagmin I." *J Cell Biol* 158 (2):273-82. doi: 10.1083/jcb.200203135.

Malhotra, V., L. Orci, B. S. Glick, M. R. Block, and J. E. Rothman. 1988. "Role of an N-ethylmaleimide-sensitive transport component in promoting fusion of transport vesicles with cisternae of the Golgi stack." *Cell* 54 (2):221-7.

Malsam, J., F. Seiler, Y. Schollmeier, P. Rusu, J. M. Krause, and T. H. Sollner. 2009. "The carboxy-terminal domain of complexin I stimulates liposome fusion." *Proc Natl Acad Sci U S A* 106 (6):2001-6. doi: 10.1073/pnas.0812813106.

Martens, S., M. M. Kozlov, and H. T. McMahon. 2007. "How synaptotagmin promotes membrane fusion." *Science* 316 (5828):1205-8. doi: 10.1126/science.1142614.

Martin, J. A., Z. Hu, K. M. Fenz, J. Fernandez, and J. S. Dittman. 2011. "Complexin has opposite effects on two modes of synaptic vesicle fusion." *Curr Biol* 21 (2):97-105. doi: 10.1016/j.cub.2010.12.014.

Maximov, A., J. Tang, X. Yang, Z. P. Pang, and T. C. Sudhof. 2009. "Complexin controls the force transfer from SNARE complexes to membranes in fusion." *Science* 323 (5913):516-21. doi: 10.1126/science.1166505.

Mayer, A., W. Wickner, and A. Haas. 1996. "Sec18p (NSF)-driven release of Sec17p (alpha-SNAP) can precede docking and fusion of yeast vacuoles." *Cell* 85 (1):83-94.

McMahon, H. T., M. Missler, C. Li, and T. C. Sudhof. 1995. "Complexins: cytosolic proteins that regulate SNAP receptor function." *Cell* 83 (1):111-9.

Michelassi, F., H. Liu, Z. Hu, and J. S. Dittman. 2017. "A C1-C2 Module in Munc13 Inhibits Calcium-Dependent Neurotransmitter Release." *Neuron* 95 (3):577-590 e5. doi: 10.1016/j.neuron.2017.07.015.

Mima, J., C. M. Hickey, H. Xu, Y. Jun, and W. Wickner. 2008. "Reconstituted membrane fusion requires regulatory lipids, SNAREs and synergistic SNARE chaperones." *EMBO J* 27 (15):2031-42. doi: 10.1038/emboj.2008.139.

Misura, K. M., R. H. Scheller, and W. I. Weis. 2000. "Three-dimensional structure of the neuronal-Sec1-syntaxin 1a complex." *Nature* 404 (6776):355-62. doi: 10.1038/35006120.

Pabst, S., J. W. Hazzard, W. Antonin, T. C. Sudhof, R. Jahn, J. Rizo, and D. Fasshauer. 2000. "Selective interaction of complexin with the neuronal SNARE complex. Determination of the binding regions." *J Biol Chem* 275 (26):19808-18. doi: 10.1074/jbc.M002571200.

Pabst, S., M. Margittai, D. Vainius, R. Langen, R. Jahn, and D. Fasshauer. 2002. "Rapid and selective binding to the synaptic SNARE complex suggests a modulatory role of complexins in neuroexocytosis." *J Biol Chem* 277 (10):7838-48. doi: 10.1074/jbc.M109507200.

Palay, S. L., and G. E. Palade. 1955. "The fine structure of neurons." *J Biophys Biochem Cytol* 1 (1):69-88.

Parisotto, D., M. Pfau, A. Scheutzow, K. Wild, M. P. Mayer, J. Malsam, I. Sinning, and T. H. Sollner. 2014. "An extended helical conformation in domain 3a of Munc18-1 provides a template for SNARE (soluble N-ethylmaleimide-sensitive factor attachment protein receptor) complex assembly." *J Biol Chem* 289 (14):9639-50. doi: 10.1074/jbc.M113.514273.

Pei, J., C. Ma, J. Rizo, and N. V. Grishin. 2009. "Remote homology between Munc13 MUN domain and vesicle tethering complexes." *J Mol Biol* 391 (3):509-17. doi: 10.1016/j.jmb.2009.06.054.

Peng, L., S. Ryazantsev, R. Sun, and Z. H. Zhou. 2010. "Three-dimensional visualization of gammaherpesvirus life cycle in host cells by electron tomography." *Structure* 18 (1):47-58. doi: 10.1016/j.str.2009.10.017.

Peters, Alan, Sanford L. Palay, and Henry deF Webster. 1991. *The fine structure of the nervous system : neurons and their supporting cells*. 3rd ed. New York: Oxford University Press.

Pobbati, A. V., A. Stein, and D. Fasshauer. 2006. "N- to C-terminal SNARE complex assembly promotes rapid membrane fusion." *Science* 313 (5787):673-6. doi: 10.1126/science.1129486.

Poirier, M. A., W. Xiao, J. C. Macosko, C. Chan, Y. K. Shin, and M. K. Bennett. 1998. "The synaptic SNARE complex is a parallel four-stranded helical bundle." *Nat Struct Biol* 5 (9):765-9. doi: 10.1038/1799.

Primakoff, P., and D. G. Myles. 2007. "Cell-cell membrane fusion during mammalian fertilization." *FEBS Lett* 581 (11):2174-80. doi: 10.1016/j.febslet.2007.02.021.

Radoff, D. T., Y. Dong, D. Snead, J. Bai, D. Eliezer, and J. S. Dittman. 2014. "The accessory helix of complexin functions by stabilizing central helix secondary structure." *Elife* 3. doi: 10.7554/eLife.04553.

Reim, K., M. Mansour, F. Varoqueaux, H. T. McMahon, T. C. Sudhof, N. Brose, and C. Rosenmund. 2001. "Complexins regulate a late step in Ca2+-dependent neurotransmitter release." *Cell* 104 (1):71-81.

Rhee, J. S., A. Betz, S. Pyott, K. Reim, F. Varoqueaux, I. Augustin, D. Hesse, T. C. Sudhof, M. Takahashi, C. Rosenmund, and N. Brose. 2002. "Beta phorbol ester- and diacylglycerol-induced augmentation of transmitter release is mediated by Munc13s and not by PKCs." *Cell* 108 (1):121-33.

Rhee, J. S., L. Y. Li, O. H. Shin, J. C. Rah, J. Rizo, T. C. Sudhof, and C. Rosenmund. 2005. "Augmenting neurotransmitter release by enhancing the apparent Ca2+ affinity of synaptotagmin 1." *Proc Natl Acad Sci U S A* 102 (51):18664-9. doi: 10.1073/pnas.0509153102.

Richmond, J. E., R. M. Weimer, and E. M. Jorgensen. 2001. "An open form of syntaxin bypasses the requirement for UNC-13 in vesicle priming." *Nature* 412 (6844):338-41. doi: 10.1038/35085583.

Rizo, J. 2018. "Mechanism of neurotransmitter release coming into focus." *Protein Sci*. doi: 10.1002/pro.3445.

Rizo, J., M. K. Rosen, and K. H. Gardner. 2012a. "Enlightening molecular mechanisms through study of protein interactions." *J Mol Cell Biol* 4 (5):270-83. doi: 10.1093/jmcb/mjs036.

Rizo, J., and T. C. Sudhof. 2012b. "The membrane fusion enigma: SNAREs, Sec1/Munc18 proteins, and their accomplices--guilty as charged?" *Annu Rev Cell Dev Biol* 28 (1):279-308. doi: 10.1146/annurev-cellbio-101011-155818.

Rizo, J., and J. Xu. 2015. "The Synaptic Vesicle Release Machinery." *Annu Rev Biophys* 44 (1):339-67. doi: 10.1146/annurev-biophys-060414-034057.

Rosenmund, C., A. Sigler, I. Augustin, K. Reim, N. Brose, and J. S. Rhee. 2002. "Differential control of vesicle priming and short-term plasticity by Munc13 isoforms." *Neuron* 33 (3):411-24.

Rothman, J. E. 1994. "Mechanisms of intracellular protein transport." *Nature* 372 (6501):55-63. doi: 10.1038/372055a0.

Sabatini, B. L., and W. G. Regehr. 1999. "Timing of synaptic transmission." *Annu Rev Physiol* 61:521-42. doi: 10.1146/annurev.physiol.61.1.521.

Schaub, J. R., X. Lu, B. Doneske, Y. K. Shin, and J. A. McNew. 2006. "Hemifusion arrest by complexin is relieved by Ca2+-synaptotagmin I." *Nat Struct Mol Biol* 13 (8):748-50. doi: 10.1038/nsmb1124.

Schoch, S., P. E. Castillo, T. Jo, K. Mukherjee, M. Geppert, Y. Wang, F. Schmitz, R. C. Malenka, and T. C. Sudhof. 2002. "RIM1alpha forms a protein scaffold for regulating neurotransmitter release at the active zone." *Nature* 415 (6869):321-6. doi: 10.1038/415321a.

Schuske, K., A. A. Beg, and E. M. Jorgensen. 2004. "The GABA nervous system in C. elegans." *Trends Neurosci* 27 (7):407-14. doi: 10.1016/j.tins.2004.05.005.

Seiler, F., J. Malsam, J. M. Krause, and T. H. Sollner. 2009. "A role of complexin-lipid interactions in membrane fusion." *FEBS Lett* 583 (14):2343-8. doi: 10.1016/j.febslet.2009.06.025.

Seven, A. B., K. D. Brewer, L. Shi, Q. X. Jiang, and J. Rizo. 2013. "Prevalent mechanism of membrane bridging by synaptotagmin-1." *Proc Natl Acad Sci U S A* 110 (34):E3243-52. doi: 10.1073/pnas.1310327110.

Shao, X., I. Fernandez, T. C. Sudhof, and J. Rizo. 1998. "Solution structures of the Ca2+-free and Ca2+-bound C2A domain of synaptotagmin I: does Ca2+ induce a conformational change?" *Biochemistry* 37 (46):16106-15. doi: 10.1021/bi981789h.

Shao, X., C. Li, I. Fernandez, X. Zhang, T. C. Sudhof, and J. Rizo. 1997. "Synaptotagmin-syntaxin interaction: the C2 domain as a Ca2+-dependent electrostatic switch." *Neuron* 18 (1):133-42.

Shen, J., D. C. Tareste, F. Paumet, J. E. Rothman, and T. J. Melia. 2007. "Selective activation of cognate SNAREpins by Sec1/Munc18 proteins." *Cell* 128 (1):183-95. doi: 10.1016/j.cell.2006.12.016.

Sherrington, Charles. 1897. "The central nervous system." *A Textbook of Physiology* 7 (3).

Shin, O. H., J. Lu, J. S. Rhee, D. R. Tomchick, Z. P. Pang, S. M. Wojcik, M. Camacho-Perez, N. Brose, M. Machius, J. Rizo, C. Rosenmund, and T. C. Sudhof. 2010. "Munc13 C2B domain is an activity-dependent Ca2+ regulator of synaptic exocytosis." *Nat Struct Mol Biol* 17 (3):280-8. doi: 10.1038/nsmb.1758.

Shin, O. H., J. Xu, J. Rizo, and T. C. Sudhof. 2009. "Differential but convergent functions of Ca2+ binding to synaptotagmin-1 C2 domains mediate neurotransmitter release." *Proc Natl Acad Sci U S A* 106 (38):16469-74. doi: 10.1073/pnas.0908798106.

Shon, M. J., H. Kim, and T. Y. Yoon. 2018. "Focused clamping of a single neuronal SNARE complex by complexin under high mechanical tension." *Nat Commun* 9 (1):3639. doi: 10.1038/s41467-018-06122-3.

Sitarska, E., J. Xu, S. Park, X. Liu, B. Quade, K. Stepien, K. Sugita, C. A. Brautigam, S. Sugita, and J. Rizo. 2017. "Autoinhibition of Munc18-1 modulates synaptobrevin binding and helps to enable Munc13-dependent regulation of membrane fusion." *Elife* 6. doi: 10.7554/eLife.24278.

Snead, D., R. T. Wragg, J. S. Dittman, and D. Eliezer. 2014. "Membrane curvature sensing by the C-terminal domain of complexin." *Nat Commun* 5:4955. doi: 10.1038/ncomms5955.

Sollner, T., M. K. Bennett, S. W. Whiteheart, R. H. Scheller, and J. E. Rothman. 1993a. "A protein assembly-disassembly pathway in vitro that may correspond to sequential steps of synaptic vesicle docking, activation, and fusion." *Cell* 75 (3):409-18.

Sollner, T., S. W. Whiteheart, M. Brunner, H. Erdjument-Bromage, S. Geromanos, P. Tempst, and J. E. Rothman. 1993b. "SNAP receptors implicated in vesicle targeting and fusion." *Nature* 362 (6418):318-24. doi: 10.1038/362318a0.

Sorensen, J. B., K. Wiederhold, E. M. Muller, I. Milosevic, G. Nagy, B. L. de Groot, H. Grubmuller, and D. Fasshauer. 2006. "Sequential N- to C-terminal SNARE complex assembly drives priming and fusion of secretory vesicles." *EMBO J* 25 (5):955-66. doi: 10.1038/sj.emboj.7601003.

Sudhof, T. C. 2002. "Synaptotagmins: why so many?" *J Biol Chem* 277 (10):7629-32. doi: 10.1074/jbc.R100052200.

Sudhof, T. C. 2004. "The synaptic vesicle cycle." *Annu Rev Neurosci* 27 (1):509-47. doi: 10.1146/annurev.neuro.26.041002.131412.

Sudhof, T. C. 2013. "Neurotransmitter release: the last millisecond in the life of a synaptic vesicle." *Neuron* 80 (3):675-90. doi: 10.1016/j.neuron.2013.10.022.

Sudhof, T. C., and J. E. Rothman. 2009. "Membrane fusion: grappling with SNARE and SM proteins." *Science* 323 (5913):474-7. doi: 10.1126/science.1161748.

Sutton, R. B., B. A. Davletov, A. M. Berghuis, T. C. Sudhof, and S. R. Sprang. 1995. "Structure of the first C2 domain of synaptotagmin I: a novel Ca2+/phospholipid-binding fold." *Cell* 80 (6):929-38.

Sutton, R. B., D. Fasshauer, R. Jahn, and A. T. Brunger. 1998. "Crystal structure of a SNARE complex involved in synaptic exocytosis at 2.4 A resolution." *Nature* 395 (6700):347-53. doi: 10.1038/26412.

Takahashi, S., H. Yamamoto, Z. Matsuda, M. Ogawa, K. Yagyu, T. Taniguchi, T. Miyata, H. Kaba, T. Higuchi, F. Okutani, and et al. 1995. "Identification of two highly homologous presynaptic proteins distinctly localized at the dendritic and somatic synapses." *FEBS Lett* 368 (3):455-60.

Takamori, S., M. Holt, K. Stenius, E. A. Lemke, M. Gronborg, D. Riedel, H. Urlaub, S. Schenck, B. Brugger, P. Ringler, S. A. Muller, B. Rammner, F. Grater, J. S. Hub,

B. L. De Groot, G. Mieskes, Y. Moriyama, J. Klingauf, H. Grubmuller, J. Heuser, F. Wieland, and R. Jahn. 2006. "Molecular anatomy of a trafficking organelle." *Cell* 127 (4):831-46. doi: 10.1016/j.cell.2006.10.030.

Tang, J., A. Maximov, O. H. Shin, H. Dai, J. Rizo, and T. C. Sudhof. 2006. "A complexin/synaptotagmin 1 switch controls fast synaptic vesicle exocytosis." *Cell* 126 (6):1175-87. doi: 10.1016/j.cell.2006.08.030.

Trimbuch, T., and C. Rosenmund. 2016. "Should I stop or should I go? The role of complexin in neurotransmitter release." *Nat Rev Neurosci* 17 (2):118-25. doi: 10.1038/nrn.2015.16.

Trimbuch, T., J. Xu, D. Flaherty, D. R. Tomchick, J. Rizo, and C. Rosenmund. 2014. "Re-examining how complexin inhibits neurotransmitter release." *Elife* 3:e02391. doi: 10.7554/eLife.02391.

Tucker, W. C., T. Weber, and E. R. Chapman. 2004. "Reconstitution of Ca2+-regulated membrane fusion by synaptotagmin and SNAREs." *Science* 304 (5669):435-8. doi: 10.1126/science.1097196.

Ubach, J., X. Zhang, X. Shao, T. C. Sudhof, and J. Rizo. 1998. "Ca2+ binding to synaptotagmin: how many Ca2+ ions bind to the tip of a C2-domain?" *EMBO J* 17 (14):3921-30. doi: 10.1093/emboj/17.14.3921.

Ungermann, C., and W. Wickner. 1998. "Vam7p, a vacuolar SNAP-25 homolog, is required for SNARE complex integrity and vacuole docking and fusion." *EMBO J* 17 (12):3269-76. doi: 10.1093/emboj/17.12.3269.

Varoqueaux, F., A. Sigler, J. S. Rhee, N. Brose, C. Enk, K. Reim, and C. Rosenmund. 2002. "Total arrest of spontaneous and evoked synaptic transmission but normal synaptogenesis in the absence of Munc13-mediated vesicle priming." *Proc Natl Acad Sci U S A* 99 (13):9037-42. doi: 10.1073/pnas.122623799.

Verhage, M., A. S. Maia, J. J. Plomp, A. B. Brussaard, J. H. Heeroma, H. Vermeer, R. F. Toonen, R. E. Hammer, T. K. van den Berg, M. Missler, H. J. Geuze, and T. C. Sudhof. 2000. "Synaptic assembly of the brain in the absence of neurotransmitter secretion." *Science* 287 (5454):864-9.

Voleti, R., D. R. Tomchick, T. C. Sudhof, and J. Rizo. 2017. "Exceptionally tight membrane-binding may explain the key role of the synaptotagmin-7 C2A domain in asynchronous neurotransmitter release." *Proc Natl Acad Sci U S A* 114 (40):E8518-E8527. doi: 10.1073/pnas.1710708114.

Volta, Alessandro. 1792. "Memoria prima sull-electricita." *Pavia: Giorancale Fisico-Medico, L. Brugnatell*.

Waldeyer-Hartz, Heinrich Wilhelm Gottfried von. 1891. "Uber einige neuere Forschungen im Gebiete der Anatomie des Centralnervensystems." *Dtsch. Med. Wochenschr.* 17:1213-1289.

Walter, A. M., K. Wiederhold, D. Bruns, D. Fasshauer, and J. B. Sorensen. 2010. "Synaptobrevin N-terminally bound to syntaxin-SNAP-25 defines the primed vesicle state in regulated exocytosis." *J Cell Biol* 188 (3):401-13. doi: 10.1083/jcb.200907018.

Weber, T., F. Parlati, J. A. McNew, R. J. Johnston, B. Westermann, T. H. Sollner, and J. E. Rothman. 2000. "SNAREpins are functionally resistant to disruption by NSF and alphaSNAP." *J Cell Biol* 149 (5):1063-72.

Weber, T., B. V. Zemelman, J. A. McNew, B. Westermann, M. Gmachl, F. Parlati, T. H. Sollner, and J. E. Rothman. 1998. "SNAREpins: minimal machinery for membrane fusion." *Cell* 92 (6):759-72. doi: 10.1016/S0092-8674(00)81404-X.

Weidman, P. J., P. Melancon, M. R. Block, and J. E. Rothman. 1989. "Binding of an N-ethylmaleimide-sensitive fusion protein to Golgi membranes requires both a soluble protein(s) and an integral membrane receptor." *J Cell Biol* 108 (5):1589-96.

Weninger, K., M. E. Bowen, U. B. Choi, S. Chu, and A. T. Brunger. 2008. "Accessory proteins stabilize the acceptor complex for synaptobrevin, the 1:1 syntaxin/SNAP-25 complex." *Structure* 16 (2):308-20. doi: 10.1016/j.str.2007.12.010.

Wilhelm, Krause. 1863. "Uber die Endigung der Muskelnerven." *Z. Rat. med.* 18:136-160.

Winter, U., X. Chen, and D. Fasshauer. 2009. "A conserved membrane attachment site in alpha-SNAP facilitates N-ethylmaleimide-sensitive factor (NSF)-driven SNARE complex disassembly." *J Biol Chem* 284 (46):31817-26. doi: 10.1074/jbc.M109.045286.

Wragg, R. T., D. A. Parisotto, Z. Li, M. S. Terakawa, D. Snead, I. Basu, H. Weinstein, D. Eliezer, and J. S. Dittman. 2017. "Evolutionary Divergence of the C-terminal Domain of Complexin Accounts for Functional Disparities between Vertebrate and Invertebrate Complexins." *Front Mol Neurosci* 10:146. doi: 10.3389/fnmol.2017.00146.

Wragg, R. T., D. Snead, Y. Dong, T. F. Ramlall, I. Menon, J. Bai, D. Eliezer, and J. S. Dittman. 2013. "Synaptic vesicles position complexin to block spontaneous fusion." *Neuron* 77 (2):323-34. doi: 10.1016/j.neuron.2012.11.005.

Wu, D., T. Bacaj, W. Morishita, D. Goswami, K. L. Arendt, W. Xu, L. Chen, R. C. Malenka, and T. C. Sudhof. 2017. "Postsynaptic synaptotagmins mediate AMPA receptor exocytosis during LTP." *Nature* 544 (7650):316-321. doi: 10.1038/nature21720.

Xiao, W., M. A. Poirier, M. K. Bennett, and Y. K. Shin. 2001. "The neuronal t-SNARE complex is a parallel four-helix bundle." *Nat Struct Biol* 8 (4):308-11. doi: 10.1038/86174.

Xu, H., Y. Jun, J. Thompson, J. Yates, and W. Wickner. 2010. "HOPS prevents the disassembly of trans-SNARE complexes by Sec17p/Sec18p during membrane fusion." *EMBO J* 29 (12):1948-60. doi: 10.1038/emboj.2010.97.

Xu, J., K. D. Brewer, R. Perez-Castillejos, and J. Rizo. 2013. "Subtle Interplay between synaptotagmin and complexin binding to the SNARE complex." *J Mol Biol* 425 (18):3461-75. doi: 10.1016/j.jmb.2013.07.001.

Xu, J., M. Camacho, Y. Xu, V. Esser, X. Liu, T. Trimbuch, Y. Z. Pan, C. Ma, D. R. Tomchick, C. Rosenmund, and J. Rizo. 2017. "Mechanistic insights into neurotransmitter release and presynaptic plasticity from the crystal structure of Munc13-1 C1C2BMUN." *Elife* 6. doi: 10.7554/eLife.22567.

Xue, M., T. K. Craig, O. H. Shin, L. Li, C. A. Brautigam, D. R. Tomchick, T. C. Sudhof, C. Rosenmund, and J. Rizo. 2010a. "Structural and mutational analysis of functional differentiation between synaptotagmins-1 and -7." *PLoS One* 5 (9). doi: 10.1371/journal.pone.0012544.

Xue, M., T. K. Craig, J. Xu, H. T. Chao, J. Rizo, and C. Rosenmund. 2010b. "Binding of the complexin N terminus to the SNARE complex potentiates synaptic-vesicle fusogenicity." *Nat Struct Mol Biol* 17 (5):568-75. doi: 10.1038/nsmb.1791.

Xue, M., Y. Q. Lin, H. Pan, K. Reim, H. Deng, H. J. Bellen, and C. Rosenmund. 2009. "Tilting the balance between facilitatory and inhibitory functions of mammalian and Drosophila Complexins orchestrates synaptic vesicle exocytosis." *Neuron* 64 (3):367-80. doi: 10.1016/j.neuron.2009.09.043.

Xue, M., C. Ma, T. K. Craig, C. Rosenmund, and J. Rizo. 2008a. "The Janus-faced nature of the C(2)B domain is fundamental for synaptotagmin-1 function." *Nat Struct Mol Biol* 15 (11):1160-8. doi: 10.1038/nsmb.1508.

Xue, M., K. Reim, X. Chen, H. T. Chao, H. Deng, J. Rizo, N. Brose, and C. Rosenmund. 2007. "Distinct domains of complexin I differentially regulate neurotransmitter release." *Nat Struct Mol Biol* 14 (10):949-58. doi: 10.1038/nsmb1292.

Xue, M., A. Stradomska, H. Chen, N. Brose, W. Zhang, C. Rosenmund, and K. Reim. 2008b. "Complexins facilitate neurotransmitter release at excitatory and inhibitory synapses in mammalian central nervous system." *Proc Natl Acad Sci U S A* 105 (22):7875-80. doi: 10.1073/pnas.0803012105.

Yang, X., P. Cao, and T. C. Sudhof. 2013. "Deconstructing complexin function in activating and clamping Ca2+-triggered exocytosis by comparing knockout and knockdown phenotypes." *Proc Natl Acad Sci U S A* 110 (51):20777-82. doi: 10.1073/pnas.1321367110.

Yang, X., Y. J. Kaeser-Woo, Z. P. Pang, W. Xu, and T. C. Sudhof. 2010. "Complexin clamps asynchronous release by blocking a secondary Ca(2+) sensor via its accessory alpha helix." *Neuron* 68 (5):907-20. doi: 10.1016/j.neuron.2010.11.001.

Yang, X., J. Pei, Y. J. Kaeser-Woo, T. Bacaj, N. V. Grishin, and T. C. Sudhof. 2015a. "Evolutionary conservation of complexins: from choanoflagellates to mice." *EMBO Rep* 16 (10):1308-17. doi: 10.15252/embr.201540305.

Yang, X., S. Wang, Y. Sheng, M. Zhang, W. Zou, L. Wu, L. Kang, J. Rizo, R. Zhang, T. Xu, and C. Ma. 2015b. "Syntaxin opening by the MUN domain underlies the function of Munc13 in synaptic-vesicle priming." *Nat Struct Mol Biol* 22 (7):547-54. doi: 10.1038/nsmb.3038.

Yavuz, H., I. Kattan, J. M. Hernandez, O. Hofnagel, A. Witkowska, S. Raunser, P. J. Walla, and R. Jahn. 2018. "Arrest of trans-SNARE zippering uncovers loosely and tightly docked intermediates in membrane fusion." *J Biol Chem* 293 (22):8645-8655. doi: 10.1074/jbc.RA118.003313.

Yoon, T. Y., X. Lu, J. Diao, S. M. Lee, T. Ha, and Y. K. Shin. 2008. "Complexin and Ca2+ stimulate SNARE-mediated membrane fusion." *Nat Struct Mol Biol* 15 (7):707-13. doi: 10.1038/nsmb.1446.

Zdanowicz, R., A. Kreutzberger, B. Liang, V. Kiessling, L. K. Tamm, and D. S. Cafiso. 2017. "Complexin Binding to Membranes and Acceptor t-SNAREs Explains Its Clamping Effect on Fusion." *Biophys J* 113 (6):1235-1250. doi: 10.1016/j.bpj.2017.04.002.

Zhang, X., J. Rizo, and T. C. Sudhof. 1998. "Mechanism of phospholipid binding by the C2A-domain of synaptotagmin I." *Biochemistry* 37 (36):12395-403. doi: 10.1021/bi9807512.

Zhao, M., S. Wu, Q. Zhou, S. Vivona, D. J. Cipriano, Y. Cheng, and A. T. Brunger. 2015. "Mechanistic insights into the recycling machine of the SNARE complex." *Nature* 518 (7537):61-7. doi: 10.1038/nature14148.

Zhou, Q., Y. Lai, T. Bacaj, M. Zhao, A. Y. Lyubimov, M. Uervirojnangkoorn, O. B. Zeldin, A. S. Brewster, N. K. Sauter, A. E. Cohen, S. M. Soltis, R. Alonso-Mori, M. Chollet, H. T. Lemke, R. A. Pfuetzner, U. B. Choi, W. I. Weis, J. Diao, T. C. Sudhof, and A. T. Brunger. 2015. "Architecture of the synaptotagmin-SNARE machinery for neuronal exocytosis." *Nature* 525 (7567):62-7. doi: 10.1038/nature14975.

Zhou, Q., P. Zhou, A. L. Wang, D. Wu, M. Zhao, T. C. Sudhof, and A. T. Brunger. 2017. "The primed SNARE-complexin-synaptotagmin complex for neuronal exocytosis." *Nature* 548 (7668):420-425. doi: 10.1038/nature23484.

Zorman, S., A. A. Rebane, L. Ma, G. Yang, M. A. Molski, J. Coleman, F. Pincet, J. E. Rothman, and Y. Zhang. 2014. "Common intermediates and kinetics, but different energetics, in the assembly of SNARE proteins." *Elife* 3:e03348. doi: 10.7554/eLife.03348.